Photoelectronic effects in Cadium Selenide

I.E. Ture

PHOTOELECTRONIC EFFECTS IN CADMIUM SELENIDE

by

I. E. TÜRE

Presented in candidature for the degree of

Doctor of Philosophy

in the

University of Durham

September 1984

To my parents

ACKNOWLEDGEMENTS

I would like to express my gratitude to my supervisor, Dr. J. Woods, for his continuous guidance and encouragement throughout the course of the research. I am particularly indebted to Dr. A. W. Brinkman for invaluable discussions and his constant help in the preparation of this thesis. I am also indebted to G. J. Russell for constructive discussions and help in the use of the transmission electron microscope.

I would like to thank Professor G. G. Roberts for the use of the facilities of the Department, and the workshop staff, headed by Mr. F. Spence for their skill and advice. I would like to extend my thanks to Dr. M. C. Petty and Dr. R. A. Abram for their valuable suggestions.

I am grateful to Mr. N. F. Thomson for the crystal growth, technical assistance, and for the drawing of the diagrams used in this thesis. I am also indebted to Mrs. P. Morrell for her patience and her proficiency in typing.

The financial support provided by the Middle East Technical University (Gaziantep extension campus) is greatfully acknowledged.

Finally, special thanks are due to my parents for their constant encouragement and support over the years.

ABSTRACT

Donor and acceptor type defect and impurity centres in CdSe single crystals have been investigated using photoconductivity and space-charge capacitance techniques, such as photocapacitance (PHCAP), infrared quenching of PHCAP, PHCAP transients, deep level transient spectroscopy (DLTS) and optical DLTS. Highly resistive ($\rho > 10^6$ Ω cm) photoconductive samples and medium resistivity (1 - 1000) Ω cm material for Schottky barrier formation have been prepared from the very conducting ($\sim 10^{-2}$ Ω cm) as-grown crystals, either by annealing in selenium vapour or by copper doping.

Samples annealed in selenium vapour had an acceptor level 0.62-0.64eV above the valence band, with a hole capture cross-section of 1.10^{-14} cm^2 which indicated that it is the main sensitising centre for photoconductivity in CdSe. There was also a well defined donor level $\sim$ 0.12eV below the conduction band and an acceptor level $\sim$0.22eV above the valence band. Similar measurements on CdSe crystals intentionally doped with copper revealed that the copper centre lies $\sim$1.0eV above the valence band and has capture cross-sections of $\sim 4.10^{-12}$ cm^2 and 7.10^{-18} cm^2 for holes and electrons respectively, clearly demonstrating that copper behaves as a sensitising centre in CdSe, as it does in most of the II-VI compounds.

Oxygen played an important role in controlling the electrical characteristics of the Schottky devices associated with the conversion of the surface structure of CdSe from a hexagonal to cubic phase. This phenomenon can be reproduced by mechanically polishing a hexagonal crystal. The cubic surface layers produced in this way have much higher resistivities than the underlying hexagonal base material and they give rise to photoconductive effects. Measurements on such surfaces revealed an additional acceptor level $\sim$ 0.38eV above the valence band.

The barrier height of the CdSe-Au Schottky contact has proved to be dependent on the work function of the metal, the thickness and nature of interfacial layers, and the amount of charge stored in the interface states.

CONTENTS

		Page
CHAPTER 1 - PROPERTIES OF CdSe		
1.1	Introduction	1
1.2	Structural Aspects	2
1.3	Optical Properties	3
1.4	Electrical Properties	4
1.5	Scope of the Present Study	5
	References	8
CHAPTER 2 - PHOTOCONDUCTIVITY AND RELATED SUBJECTS		
2.1	Introduction	10
2.2	Photoconductivity	10
2.3	Photoconductive Gain	12
2.4	Imperfection Centres	14
2.5	Response Time	15
2.6	Demarcation Levels	16
2.7	Sensitising Centres	18
2.8	Kinetics of Photoconductivity	20
2.9	Simple Recombination Kinetics	22
	References	25
CHAPTER 3 - SPACE-CHARGE METHODS AND RELATED PHENOMENA		
3.1	Introduction	26
3.2	Defect and Impurity Centres	26
3.2.1	Introduction	26
3.2.2	Shallow levels	27
3.2.3	Deep levels	28
3.2.4	Theoretical models	29
3.2.5	Lattice relaxation	31

Page

3.3 Metal-Semiconductor Junctions 32

3.3.1 Schottky-Mott theory 32
3.3.2 Schottky barriers on etched surfaces 34
3.3.3 Surface states and the Bardeen model 35
3.3.4 Schottky effect 38
3.3.5 Current transport mechanisms 41
(a) Forward bias 41
(b) Reverse bias 43
3.3.6 The capacitance of a Schottky barrier 44
3.3.7 Measurement of barrier heights 45
(a) I-V measurements 45
(b) Photoelectric method 46
(c) C-V measurements 47
3.3.8 The effect of an interfacial layer 48
(a) Effect on I-V characteristics 48
(b) Effect on C-V characteristics 49
3.3.9 The effect of deep levels 54

3.4 Space-Charge Capacitance Methods for the Detection of Deep Levels 56

3.4.1 Introduction 56
3.4.2 Steady-State Methods 57
(a) Photocapacitance 57
(b) Infrared quenching of photocapacitance 59
3.4.3 Transient Methods 59
(a) Photocapacitance transient 59
(b) Infrared quenching of photocapitance transient 62
(c) Deep level transient spectroscopy (DLTS) 63
(d) Optical DLTS 66

References 67

CHAPTER 4 - EXPERIMENTAL METHODS

4.1 Introduction 70

4.2 Crystal Growth 70

4.3 X-Ray Powder Photography 71

4.4 Resistivity Control Techniques 71

4.4.1 Annealing in selenium vapour 72
4.4.2 Copper doping 72
(a) Copper evaporation 73
(b) Plating solution 73
(c) Dilute plating solution 73
(d) Copper-Sulphate bath 73
4.4.3 Annealing in Cadmium vapour 74

4.5 Sample Preparation as Photoconductors 74

4.5.1 Ohmic contacts 74

Page

4.6 Reflection High Energy Electron Diffraction (RHEED) 75

4.7 Electrical and Optical Measurements 77

4.7.1 Current-voltage measurements 78
4.7.2 Capacitance-voltage measurements 78
4.7.3 The spectral response of photoconductivity and infrared quenching 79
4.7.4 Steady state and transient photocapacitance, infrared quenching of photocapacitance 80

4.8 Deep Level Transient Spectroscopy (DLTS) 80

References 82

CHAPTER 5 - EXPERIMENTAL RESULTS ON PHOTOCONDUCTIVITY AND INFRARED QUENCHING SPECTRAL RESPONSE

5.1 Introduction 83

5.2 Flow-run Platelets 84

5.3 Discussion 85

5.4 Samples annealed in Selenium 87

5.5 Discussion 88

5.6 Crystals with mechanically polished surfaces 89

5.7 Discussion 90

5.8 Samples Heavily Doped with Copper 91

5.9 Discussion 92

5.10 Samples Lightly Doped with Copper 94

5.11 Discussion 95

5.12 Copper Doping by Diffusion from Surface Layers of Metal 96

5.13 Discussion 97

5.14 General discussion of Photoconductivity Measurements 98

References 100

Page

CHAPTER 6 - CHARACTERISATION OF CdSe SCHOTTKY BARRIERS

6.1 Introduction 102

6.2 Schottky Barriers on Samples Annealed in Selenium for 3-days 103

6.2.1 Introduction 103
6.2.2 Electrical characteristics 103
6.2.3 Measurements of barrier height 104
(a) Photoelectric 104
(b) Forward I-V characteristics 105
6.2.4 RHEED Studies 106
6.2.5 Surface Effects 106
6.2.6 Energy Band Scheme 111
6.2.7 Discussion 112

6.3 Schottky Barriers on Samples Annealed in Selenium for 1-month 116

6.3.1 Introduction 116
6.3.2 Electrical characteristics 117
6.3.3 Measurements of barrier height 117
(a) Photoelectric 117
(b) Forward I-V characteristics 118
6.3.4 RHEED studies 118
6.3.5 Surface Effects 118
6.3.6 Discussion 118

6.4 Schottky Barriers Formed on Polished Cubic (Sphalerite) Layers 119

6.4.1 Introduction 119
6.4.2 Electrical characteristics 120
6.4.3 Measurements of barrier height 120
(a) Photoelectric 120
(b) Forward I-V characteristics 120
6.4.4 RHEED studies 121
6.4.5 Surface effects 122
6.4.6 Energy Band Scheme 123
6.4.7 Discussion 123

6.5 Schottky Barriers Formed on Cu-doped Samples 125

6.5.1 Introduction 125
6.5.2 Electrical characteristics 126
6.5.3 Measurements of barrier height 126
(a) Photoelectric 126
(b) Forward I-V characteristics 126
6.5.4 RHEED studies 126
6.5.4 Surface effects 127
6.5.6 Discussion 127

Page

6.6 Summary and Conclusions 128

References 129

CHAPTER 7 - DEFECT AND IMPURITY LEVELS MEASURED BY SPACE-CHARGE TECHNIQUES

7.1 Introduction 131

7.2 Measurement on Schottky Devices prepared on Se-annealed Samples 132

7.2.1 Introduction 132
7.2.2 Steady-state photocapacitance 132
7.2.3 Steady-state infrared quenching of photocapacitance 134
7.2.4 Transient photocapacitance measurements 135
(a) Photoionisation cross-section of holes 135
(b) Photoionisation cross-section of electrons 136
7.2.5 DLTS and ODLTS measurements 138
(a) DLTS measurements for electron-traps 138
(b) ODLTS measurements for hole-traps 138

7.3 Discussion 139

7.4 Schottky devices prepared on Cu-doped samples 143

7.4.1 Introduction 143
7.4.2 Steady-state PHCAP measurements 143
7.4.3 Steady-state IRQ-PHCAP measurements 145
7.4.4 PHCAP and IRQ-PHCAP transient measurements 145
(a) Photionisation cross-section of holes 145
(b) Photoionisation cross-section of electrons 146
7.4.5 DLTS and ODLTS Measurements 146
(a) DLTS measurements 147
(b) ODLTS measurements 147

7.5 Discussion 147

7.6 Schottky Devices prepared on Mechanically Polished Surfaces 152

7.6.1 Introduction 152
7.6.2 Steady-state PHCAP measurements 152

7.7 Discussion 153

7.8 Summary and Conclusions 154

References 155

Page

CHAPTER 8 - CONCLUSIONS

8.1 Summary of results 157

8.1.1 Material preparation 157
8.1.2 Schottky barriers 157
8.1.3 Deep levels 160

8.2 Suggestions for the Future Work 162

References 164

CHAPTER 1

PROPERTIES OF CdSe

1.1 INTRODUCTION

CdSe is a semiconductive material which belongs to the group known as II-VI compounds, together with other materials such as CdS, ZnSe, etc. The compounds formed from Zn or Cd, and S, Se or Te crystallise either in the wurtzite (hexagonal) or the zincblende (cubic) form, both of which are characterised by tetrahedral lattice sites. II-VI compounds have been studied fairly extensively over the last 40 years mainly because of their interesting luminescent and photoconductive properties. CdSe has many potential applications in a wide range of fields such as thin film transistors[1,2], image intensifiers[3], infrared and γ-ray detectors[4], solar cells[5,6,7] and ultrasonic amplification[8] but nevertheless less attention has been paid to this material than to most other II-VI compounds. This is attributable to a variety of factors:(a) the fundamental absorption edge lies beyond the visible region, (b) the difficulty of growing good stoichiometric single crystals, (c) the difficulty of obtaining moderate resistivity for device making, and (d) the more sensitive surface behaviour of CdSe. However, the growth of reasonable quality single crystals has been reported and some of their structural, optical and electrical properties have been investigated[9,10,11]. In this chapter a brief summary of these properties and the scope of the present investigation will be reviewed.

1.2 Structural Aspects

Although CdSe generally crystallises in the wurtzite form, the zincblende structure has also been reported in the literature[12,13]. The wurtzite structure (Figure 1.1) consists of two interpenetrating hexagonal lattices displaced with respect to one other by a distance of 3 c/8 along the c-axis. The nearest neighbour distance, with ideal tetrahedral sites, is 3 c/8 or $\sqrt{3}/8a$ where a = 4.2985Å and c = 7.0150Å are the lattice parameters[14] of the hexagonal CdSe crystal. The zincblende structure is derived from the diamond structure and is composed of two interpenetrating face-centred cubic lattices translated with respect to each other by 1/4 of the body diagonal of the unit cell (Figure 1.2). In this case the nearest neighbour distance is $\sqrt{3}/4$ a where a = 6.05Å is the lattice parameter[13] of the cubic CdSe.

In fact there is also a close relationship between the wurtzite and zincblende structures. The lattice parameters of the hexagonal unit cell are almost exactly related to the cubic parameter of the same compound by $a_{hex} = \frac{1}{2}\sqrt{2}\ A_{cub}$ and $c_{hex} = 2/3\sqrt{3}\ A_{cub}$. A useful description for the structural relations is based on the stacking sequence along the lowest indices for polar directions i.e. <111> and $\langle\bar{1}\bar{1}\bar{1}\rangle$. For zincblende structures the sequence along these directions is of the form

$$A\ \alpha\ B\ \beta\ C\ \gamma\ A\ \alpha\ B\ \beta\ C\ \gamma\ A\ \alpha \qquad (1.1)$$

where A, B, C and α, β, γ represent i.e. cadmium and selenium layers respectively. Using the same notation, the stacking of atomic layers in the wurtzite structure is of the form

$$A\ \alpha\ B\ \beta\ A\ \alpha\ B\ \beta\ A\ \alpha\ B\ \beta\ A\ \alpha \qquad (1.2)$$

The stacking sequence of the close-packed planes in wurtzite is

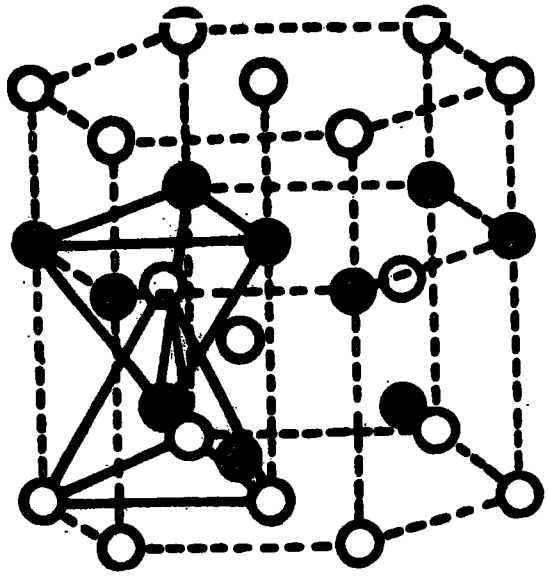

FIGURE 1.1 Wurtzite structure

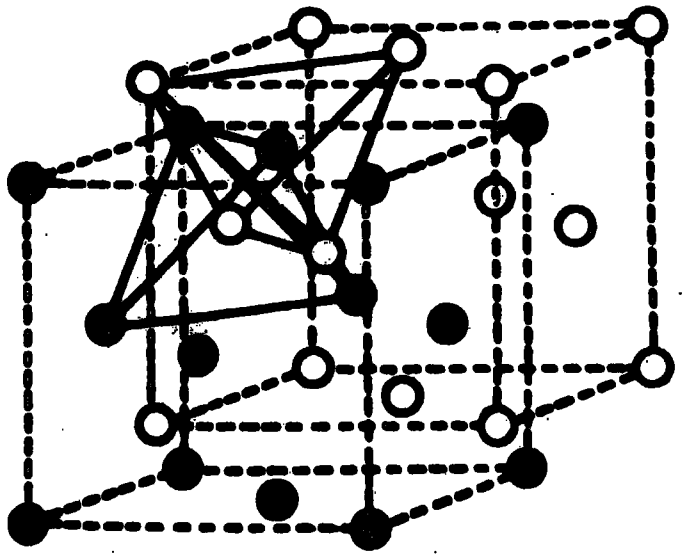

FIGURE 1.2 Zincblende structure

different from that in zincblende in that the positions of the atoms are repeated after every second double atomic layer instead of every third.

A transformation between cubic and hexagonal structures is also possible at some characteristic temperature. This involves the shearing of close-packed atomic planes in such a way as to change the stacking sequence from A α B β A α B β ----- in hexagonal to A α B β C γ A α B β C γ ---- in cubic[15].

The type of bonding in CdSe is a mixture of ionic and covalent. The ionic contribution is 19% (following Pauling's criterion) and the electronegativity difference is 0.9 in Pauling's units[9].

Perfect single crystals of CdSe have not yet been grown and as-grown crystals usually contain native defects such as cadmium interstitials. Because of its importance the crystal growth process used is described in chapter 4 while native defects are reviewed in chapter 3.

1.3 Optical Properties

The interaction of optical photons with a semiconductor is determined by its electronic structure. Since CdSe has a direct bandgap of about 1.84eV at 90K[10], the optical absorption coefficient varies as the square of the incident photon energy, and has a very large magnitude ($> 10^6$ cm^{-1}) for photon energies greater than the energy gap. The energy band structures of wurtzite and zincblende are given in figure 1.3 a, b. The energy values separating these bands, which are indicated on the same diagrams, were derived by Wheeler and Dimmock[16] from a study of absorption and reflection spectra, and the Zeeman splitting of free excition lines. They also obtained values of the effective masses of electrons ($m_e^*/m_o \simeq 0.13$ both parallel and perpendicular to the c-axis) and holes ($m_p^*/m_o \simeq$ 0.45 perpendicular and > 1 parallel to the c-axis).

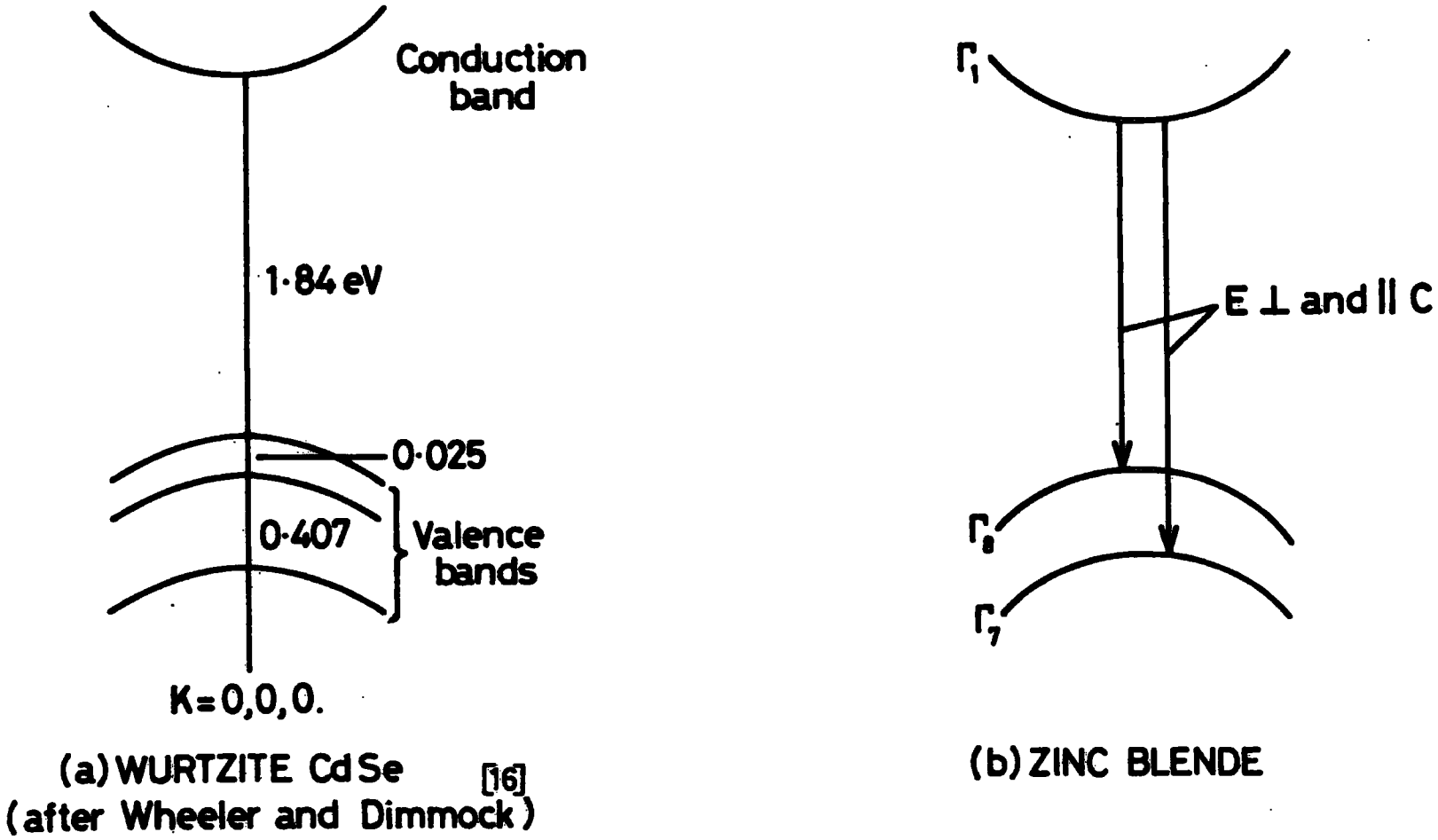

FIGURE 1.3 Energy band structures

The temperature dependence of the bandgap derived from measurements of the photosensitivity as a function of wavelength revealed that Eg decreases linearly at the rate of $dE_g/dT \approx -4.6.10^{-4}$eV/K[17]. Extrapolation to 300K gives Eg = 1.74eV, in rather good agreement with the values obtained using other experimental techniques[10]. The other optical properties of CdSe, such as the dielectric constant and the refractive index, are included in table 1.1 which summarizes a variety of the more important parameters of the compound.

1.4 Electrical Properties

The electrical properties of semiconductors are limited by their electronic band structure and lattice dynamics. These determine the intrinsic carrier concentration (n_i) of the material and the values of electron and hole mobility. (For mobilities of CdSe see table 1.1). The intrinsic carrier concentration of a semiconductor is determined by its energy bandgap Eg, and the effective masses of electrons and holes. When the room temperature values of the bandgap $\sim$ 1.74eV and of the effective density of states in the conduction band $\sim 1.14.10^{18}$ cm^{-3} are used, the intrinsic carrier concentration should be of the order of 10^3 cm^{-3}. Since the as-grown crystals of CdSe have a free carrier concentration of (0.3-1) 10^{18} cm^{-3}, they obviously contain shallow donors and must be considered as extrinsic semiconductors. The shallow donors are undoubtedly associated with a non-stoichiometric excess of cadmium.

Earlier investigations of CdSe and other II-VI compounds have shown that native crystalline imperfections probably play a substantial role in determining the electrical properties of these materials. The high electrical conduction in as-grown CdSe may be due to the presence of Cd-interstitials (or Se-vacancies). This implies that the CdSe crystals obtained from a melt of stoichiometric composition contain an excess of cadmium. This is in agreement with the suggestion that chalcogenide

Parameters	CdSe	Reference
Relative density	5.66 g /cm^3	10
Molecular Weight	191.36	10
Lattice parameters	Wurtzite a = 4.2985 Å c = 7.0150Å Cubic 6.05Å	14, 13
Direct bandgap (E_g)	1.84eV at 90K	10
Temperature dependence of E_g	$-4.6.10^{-4}$ eV/K	17
Effective mass of electrons (m_e^*)	0.13	16
Effective mass of holes (m_p^*)	0.45	16
Thermal conductivity at 300K	0.043 W.K^{-1} cm^{-1}	10
Dielectric constant	$\varepsilon \parallel c$ 9.25 $\varepsilon \perp c$ 8.75	9
Refractive index	2.55 (λ = 0.86μm)	9
Electron mobility	$\sim$650 cm^{2}V^{-1}s^{-1}	11
Hole mobility	$\sim$50 cm^{2}V^{-1}s^{-1}	11
Electron affinity	4.95eV	20
Melting point	1239°C	10

Table 1.1 Some Properties of CdSe

compounds will contain an excess of the element with the higher boiling point. It is assumed that the excess cadmium is present in interstitial positions as neutral atoms which can act as donors by giving up their outer electrons.

It is well known that the electrical and transport properties of semiconductors can be altered by various heat treatments. For example, heating CdSe in an atmosphere of Cd or Se is a widely used method for varying the resistivity by many orders of magnitude. Hung et al[18] have shown that the resistivity of Se-treated CdSe specimens may be as high as 10^9 to 10^{12} Ω cm. With decreasing Se vapour pressure the resistivity decreases slowly at first, then dramatically to <1 Ω cm then more slowly again (see figure 1.4). However heating in the vapour of the non-metallic component does not produce p-type conductivity. The ratio of cation radius (r_c) to anion (r_a) radius has been invoked to explain the experimentally observed limitations. If (r_c/r_a) > 1, then n-type conductivity occurs and if r_c/r_a < 1 p-type conductivity arises. It was realised long ago that it was difficult to obtain both n- and p-type conduction in wide bandgap semiconductors even when large amounts of impurities are introduced. This is attributed to self compensation which is common to all wide gap materials, and has been extensively studied in the highly ionic alkali halides and in the partly covalent II-VI compounds. Most of the current understanding derives from work initiated by Kröger[19] and co-workers in which the basic assumption is that intrinsic defects play a major role in the electronic doping of these materials.

1.5 Scope of the Present Study

During the past three decades wide bandgap II-VI compound semiconductors have received a great deal of attention, because of their

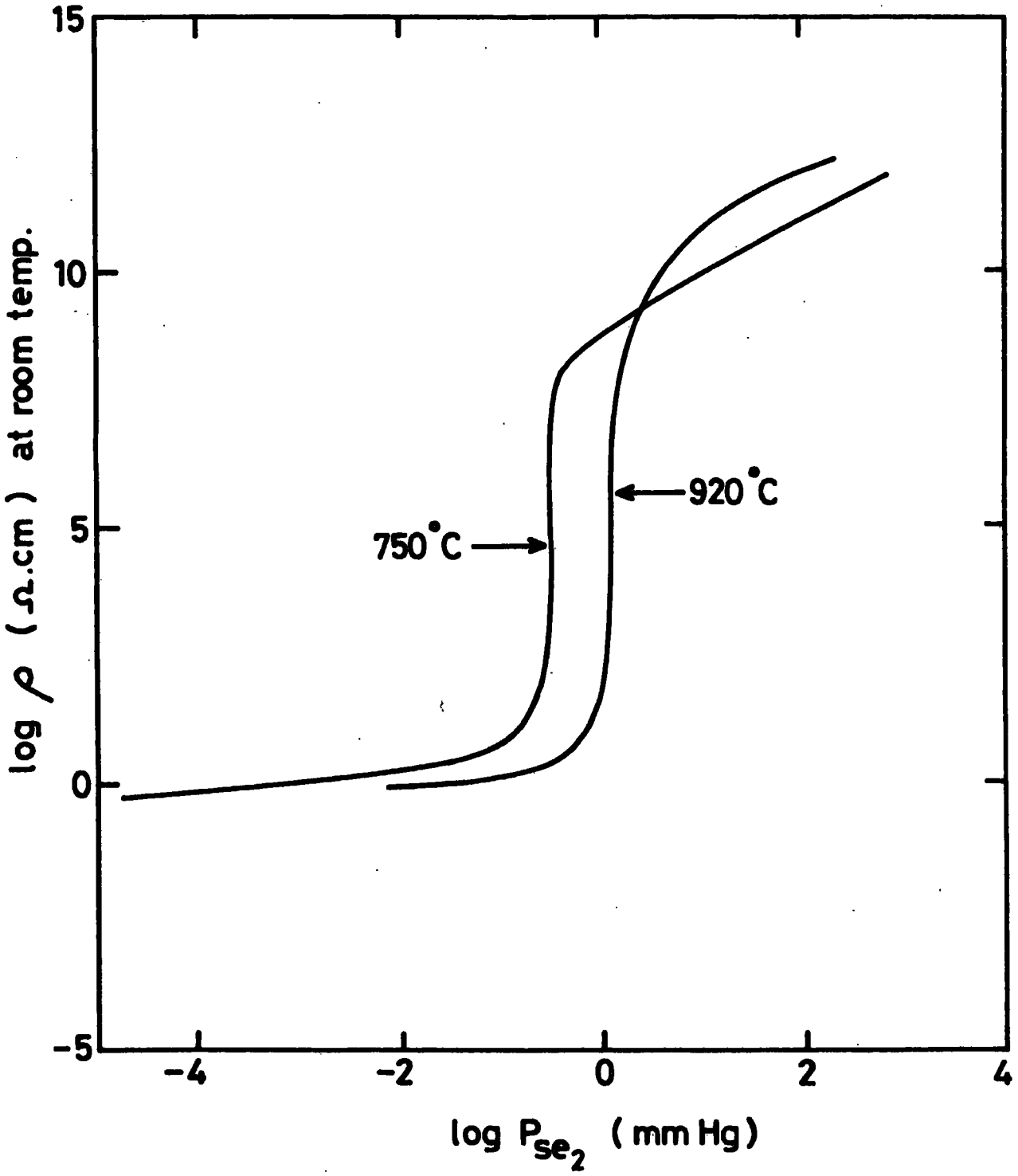

FIGURE 1.4 Dependence of room temperature resistivity on selenium vapour pressure for two annealing temperatures(750 and 920°C) (After Hung et al[18]).

potential in various fields, but as yet this potential has not been fully realised. CdSe shows particular promise as a material for solar cells and infrared detectors, since it possesses an appropriate bandgap for such applications. Since the electrical properties of these materials are strongly affected by crystalline imperfections, it is important to characterise the native defect and impurity centres, before reliable devices can be prepared. Therefore the work presented in this thesis was concentrated mainly on the identification and characterisation of such centres. In order to avoid the complications inherent in thin film structures (i.e. intergranular boundaries etc.), the present work was carried out entirely on single crystal CdSe.

The experimental methods for the characterisation of defect centres fall into two groups depending whether the bulk or space-charge regions are explored. The highly photoconductive crystals used to investigate bulk properties were prepared either by annealing CdSe crystals in Se-vapour or by doping with copper impurity. For the investigation of space charge regions Schottky devices were chosen because of their relatively simple structure. However, it proved to be very difficult to obtain the moderate resistivity (1-1000) Ω cm CdSe required for the preparation of satisfactory Schottky devices. Details of the experimental solution of this problem are given in chapter 4.4. The electrical characteristics of the Schottky devices, prepared on both Se-annealed and intentionally Cu-doped substrates were measured with emphasis on transient capacitance techniques. Drastic changes in the electrical characteristics of these devices occurred on ageing and this led to an extensive investigation of the surface properties of CdSe crystals. Finally a wide range of space-charge techniques were applied in order to obtain more quantitative results for the defect and impurity centres in this material.

The background theory of photoconductivity and the analysis of experimental data are described in chapters 2 and 5 respectively. Because of the importance of the topic chapter 6 is entirely devoted to the characterisation of the Schottky devices prepared on different surfaces. The results of the analysis using the space-charge techniques are given in chapter 7. The underlying theory of Schottky diodes and of the space-charge methods for the analysis of defect centres are reviewed in chapter 3. A summary of all the results is presented in chapter 8 together with some suggestions for the future work.

REFERENCES - CHAPTER 1

1. L. J. Brillson, F. Luo, and J. Wysocki, J. Appl. Phys. 52 (1981) 5250.
2. P. K. Weimer, G. Sadasiv, L. Meray-Horvath, and W. S. Homa, Proc. IEEE 54 (1966) 354.
3. F. H. Nicoll, "Photoelectronic materials and devices", pp.313-373. Van Nostand, New-Jersey 1965.
4. G. Dearnaley and D. C. Northrop, "Semiconductor counters for nuclear radiation", E. and F. N. Spon Ltd. London (1966).
5. D. Bonnet, Proc. of the 2nd pkhotovoltaic energy conf. 1979 p.387.
6. F. Buch, A. L. Fahrenbruch, and R. H. Bube, J. Appl. Phys. 48 (1977) 1596.
7. V. N. Komashchenko and G. A. Fedorus, Soviet Phys. Semicond. 1 (1967) 411.
8. T. A. Midford, J. Appl.Phys. 35 (1964) 3423.
9. M. Aven and J. S. Prener, "Physics and Chemistry of II-VI Compounds" North-Holland Publishing Co. Amsterdam (1967).
10. B. Ray, "II-VI Compounds" Pergamon Press Oxford (1969).
11. E. Kaldis, "Current topics in materials science", North-Holland Publishing Co. Amsterdam (1982).
12. A. D. Stuckes and G. Farrell, J. Phys. Chem. Solids 25 (1964) 477.
13. A. S. Pashinkin and R. A. Sapozhnikov, Sov. Phys. Cryst. 7 (1962) 501.
14. R. S. Title, Phys. Rev. 130 (1963) 17.
15. See, for example, C. S. Barrett and T. B. Massalki, "Structure of Metals", McGraw-Hill Inc. New York (1966) 486-534.
16. R. G. Wheeler and J. C. Dimmock, Phys. Rev. 125 (1962) 1805.

17. R. H. Bube, Phys. Rev. 98 (1955) 431.

18. M. P. Hung, N. Ohashi and K. Igaki, Japanese J. Appl. Phys. 8 (1969) 652.

19. F. A. Kröger, "The Chemistry of Imperfect Crystals", North-Holland Publication, Amsterdam (1964).

20. R. K. Swank, Phys. Rev. 153 (1967) 844.

CHAPTER 2

PHOTOCONDUCTIVITY AND RELATED SUBJECTS

2.1 INTRODUCTION

Measurements of photoconductivity provide powerful methods for investigating impurity and defect levels in semiconductors. With highly photosensitive materials such as CdSe, the importance of photoconductive measurements becomes even more significant. It is also well known that, evaluating the quality of semiconductors and improving the characteristics of devices based on them depends strongly on an accurate knowledge of defects and impurities in these materials. This thesis is concerned with the study of defects in CdSe and some part will be devoted to photoconductivity measurements as a means of determining the bulk properties of the material. As background therefore, the following sections are concerned with a review of theoretical aspects of photoconductivity.

2.2. PHOTOCONDUCTIVITY

The increase in conductivity of a material under illumination is known as photoconductivity and was first observed by W. Smith in 1873[1]. The theory of photoconductivity has been developed over a century by many authors[2-5].

The dark conductivity of a semiconductor is generally defined as:

$$\sigma = n q \mu_n + p q \mu_p \qquad (2.1)$$

where n and p are the densities of the free electrons and holes, and μ_n and μ_p are their mobilities, q is the electronic charge. In CdSe the

free electron lifetime is (10^{-4} - 10^{-2}) s usually several orders of magnitude larger than the free hole lifetime (10^{-7} - 10^{-8}) s . Hence the conductivity is controlled by one type of carrier only, namely the electrons, so that equation 2.1 reduces to

$$\sigma = n\ q\ \mu_n \tag{2.2}$$

Under illumination the change in conductivity will be given by

$$\Delta\sigma = \Delta n\ q\ \mu_n + n\ q\ \Delta\mu_n \tag{2.3}$$

Eqn. 2.3 shows that the photoconductivity also depends on the change in mobility ($\Delta\mu$) of the free carriers following illumination. The possible processes under which the mobility can be a function of photoexcitation are (a) excitation of carriers from a low mobility band to a high mobility band. In this particular case it is possible to produce photoconductivity even though $\Delta n=0$, (b) change in scattering of free carriers by a modification of the cross sections of impurity states.
The change in carrier density is dependent on both the rate of excitation of electrons f, and free electron lifetime τ_n. The fundamental relationship between these parameters can be expressed as:

$$\Delta n = f.\ \tau_n \tag{2.4}$$

A change in Δn can also be written in terms of changes in both parameters.

$$\delta\Delta_n = \tau_n\ \delta f + f\ \delta\tau_n \tag{2.5}$$

If τ_n is considered constant then the lifetime is independent of f, and photoconductivity varies linearly with f. If τ_n is not constant and related to changes in f, the relationship between Δn and f will be either sublinear or superlinear according to:

$$\tau_n \propto f^{-a} \qquad (0 < a < 1) \qquad (2.6a)$$

or

$$\tau_n \propto f^{a} \qquad (a > 1) \qquad (2.6b)$$

respectively. These relations will be discussed later, along with the kinetics of photoconductivity.

Substitution of eqn. 2.4 in eqn. 2.3 gives

$$\Delta\sigma = f \tau_n q \mu_n + n q \Delta\mu_n \qquad (2.7)$$

Since the first term on the right hand side of eq. 2.7 almost always dominates, the magnitude of the photoconductivity for a given excitation intensity will be proportional to the product $\tau_n \mu_n$.

2.3 PHOTOCONDUCTIVE GAIN

The gain of a photoconductor is defined as the number of free charge carriers passing between the electrodes per photon absorbed.

$$G = \frac{I}{qP} \qquad (2.8)$$

where I is the photocurrent generated and P is the total number of photons absorbed per second producing electron-hole pairs. The gain can also be expressed in a more microscopic way as the ratio of the free carrier lifetime to transit time between electrodes.

$$G = \frac{\tau_n}{t_r} \tag{2.9}$$

If L is the separation of the electrodes and V is the applied potential, the transit time is given by;

$$t_r = \frac{L^2}{\mu V} \tag{2.10}$$

Substituting eq. 2.10 in eq. 2.9.

$$G = \frac{\tau_n \mu_n V}{L^2} \tag{2.11}$$

Equation 2.11 shows that the gain factor depends on the applied voltage and the separation between electrodes as well as on the $\mu_n \tau_n$ product. High values of gain can be achieved by decreasing the spacing between the electrodes and increasing the voltage applied to the photoconductor. But the available gain is limited to some maximum value by the requirement of a minimum thickness of the material for optical absorption and by the fact that as the bias is increased, space charge limited current begins to flow. For some level of bias this current will become comparable to the photocurrent. When this happens the transit time will be equal to the dielectric relaxation time ($t_r = \tau_r$). Using this identity in eq. 2.9 the maximum value of gain can be expressed as:

$$G_{max} = \frac{\tau_n}{\tau_r} \tag{2.12}$$

2.4 IMPERFECTION CENTRES

Ideally a perfect crystalline material has no energy levels in its forbidden gap. But in a real semiconductor there are always some imperfections associated with impurities or native crystallographic defects. In general the exact nature of these centres is not well known and it is usual to classify these imperfections in terms of their observed behaviour i.e. as donor or acceptor levels, recombination and sensitising centres, majority or minority traps, etc. However, the important parameters of any centre are the capture cross sections and activation energies.

Levels are usually described as shallow or deep within the forbidden gap. (Although there is no very distinct difference between the levels, shallow ones are considered to be hydrogenic because they are well described by a simple hydrogenic model). Deep levels cannot be characterised in this simple way and models of these levels will be described in sections 3.2.3 and 3.2.4.

Deep centres in a semiconductor material can act either as traps or recombination centres and consequently influence the properties of the material. In general shallow centres act only as traps but play an important part in the characterisation of a semiconductor. If there are N empty centres per unit volume, then the rate of capture of free carriers (i.e electrons) is

$$\text{Capture rate} = N S_n v_n \qquad (2.13)$$

Where S_n is the capture cross section of a centre for electrons and v_n is the thermal velocity of electrons. Under these conditions the electron lifetime can be defined as:

$$\tau_n = (N S_n v_n)^{-1} \qquad (2.14)$$

If the centres lie at a depth E_t below the conduction band edge, then the probability of a captured electron being thermally released is

$$P = \nu \exp\left(- E_{t/kT}\right) \qquad (2.15)$$

Where ν is the attempt-to-escape frequency and T is the absolute temperature. On the other hand by making use of the simple Fermi level analysis[2] of conductivity, it can be shown that:

$$\nu = N_c \cdot v_n S_n \qquad (2.16)$$

Here N_c is the effective density of states in the conduction band. Equation 2.16 indicates that at a given temperature the attempt-to-escape frequency from a particular centre is directly proportional to the cross section for capture by that centre. This statement is generally valid and does not depend on any particular model.

2.5 RESPONSE TIME

The response time of a photoconductor is usually defined as the time for the photocurrent to decay to 1/e of its initial steady state value after the removal of the exciting illumination. In the absence

of traps the response time is equal to the free carrier lifetime, which is the time an excited electron spends in the conduction band. In the presence of traps the response time is much longer than the free carrier lifetime. This is because the density of trapped electrons usually exceeds the density of free electrons ($n_t >> n$) so that the decay of the photocurrent is limited by the thermal release of electrons from the traps. Only at high intensities where ($n >> n_t$) does the response time approach the free carrier lifetime.

If there are a considerable number of traps in a material, the free carrier lifetime has to be replaced by the response time τ_o, and the maximum gain becomes:

$$G = \frac{\tau_o}{\tau_r} \qquad (2.17)$$

In the presence of deep levels only, the maximum gain is reached for applied voltages below that required to give space-charge limited currents. Although in many cases the observed response cannot exceed the relaxation time and this limits the gain (eq. 2.17) to unity, there are some exceptions such as the incorporation of impurities as sensitising centres. Under these circumstances eq. 2.17 can be modified as follows:

$$G_{max} = \frac{\tau_o}{\tau_r} M \qquad (2.18)$$

Where M is the ratio of traps filled by the field to those filled by the light[2].

Experimentally the values of M can be as large as several hundred.

2.6 DEMARCATION LEVELS

In order to distinguish a trapping centre from a recombination centre the concept of the demarcation level is very helpful. In fact

the distinction between the centres is not rigid. For different conditions of temperature and illumination a trapping centre may act as a recombination centre. If the probability for an electron being thermally freed from a centre to the conduction band is greater than that of recombining with a hole, the centre is considered to be an electron trap. If the recombination probability is greater than that of the electron being thermally freed than the levels are recombination centres. Similar definitions can be made for hole traps.

The demarcation level is defined as the level at which the probability of a trapped electron being thermally released is equal to that of its recombining with a hole. The demarcation levels for electrons E_{dn} and holes E_{dp} are shown together with the steady state Fermi levels (E_{fn} and E_{fp}) in fig. 2.1 for an insulating semiconductor such as CdSe.

If n_t is the density of such electron-occupied levels lying E_t below the conduction band, and if the electron demarcation level coincides with these levels then by definition:

$$n_t \, C_n \exp(- E_{dn}/kT) = n_t \, p \, C_p \qquad (2.19)$$

Where p is the density of holes. The product of the capture cross-section and the thermal velocity of the free carriers is called the capture coefficient, so that $C_n = S_n v_n$ and $C_p = S_p . v_p$ are capture coefficients for electrons and holes respectively. The demarcation levels are related to the steady state Fermi levels in the following way.

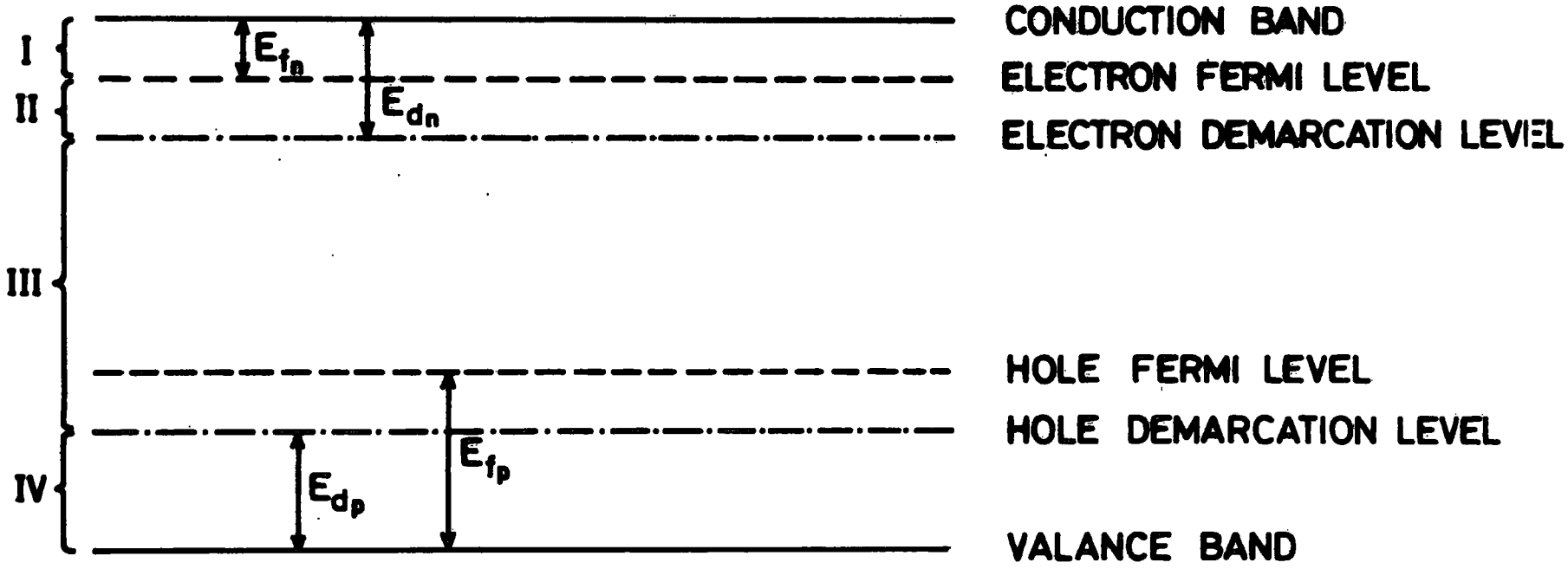

FIGURE 2.1 Fermi and demarcation levels for an insulator-like semiconductor.

$$E_{dn} = E_{fn} + kT \ln (N_n/N_p) \qquad (2.20a)$$

$$E_{dp} = E_{pf} - kT \ln (N_n/N_p) \qquad (2.20b)$$

Where N_n and N_p are the available densities for holes (i.e. the density of electron-occupied centres) and electrons (i.e. the density of hole occupied centres) respectively. As indicated in fig. 2.1 the bandgap of such a material can be divided into four regions with the help of demarcation levels in order to distinguish the traps from recombination centres. Centres located in region I act as electron traps while those in region IV act as hole traps. Although the centres in region II are above the electron demarcation level they are below the electron Fermi level so they will have a high degree of electron occupancy and will take part in recombination with free holes. Finally, centres located in region III act as recombination centres. The positions of the demarcation levels change with temperature and intensity of illumination. A decrease in temperature or an increase in the light intensity result in both demarcation levels moving towards their respective band edges.

2.7 SENSITISING CENTRES

Recombination centres defined in the previous section, can also be classified into two groups as class I and class II centres. Class I centres have a large capture cross section for both electrons and holes ($\sim 10^{-15}$ cm^2 or greater), while class II centres have a small capture cross section for electrons ($\sim 10^{-20}$ cm^2). The ratio of electron and hole capture cross sections for class II centres may be several orders of magnitude, in which case the electron lifetime will be much longer

than for holes and the photosensitivity will be increased. Pure crystals usually have class I centres only and are of very low sensitivity, but they can be made more sensitive photoconductors by the incorporation of appropriate impurities as class II or sensitising centres. In an n-type semiconductor, sensitising centres are formed by the introduction of compensated acceptor centres which can be either impurities or native defects. The process of sensitisation is shown in fig. 2.2 (a, b and c).

Figure 2.2a illustrates an unsensitised material with class I centres only. If class II centres are present as shown in fig. 2.2b, but lie below the hole demarcation level, they will act as hole traps and will not make any contribution to the sensitivity of the material. If the sensitising centres lie above the hole demarcation level as illustrated in fig. 2.2c they will increase the sensitivity. Because holes captured by class II centres have a longer life before recombination than holes captured by class I centres, class II centres become mainly occupied by holes and class I centres by electrons. Since free electrons can now only recombine with holes at centres whose cross sections for electrons are much smaller than the class I centre the free electron lifetime will be increased thus enhancing the photosensitivity. These processes become important if the concentration of class I and II centres is much greater than the density of free carriers. Recombination centres which have small cross-sections for both electrons and holes can be described as photoconductivity centres since the direct excitation of electrons from these to the conduction band would contribute to the photocurrent.

It can also be seen from fig. 2.2 that if the hole demarcation level is lowered through the class II levels by increasing the intensity

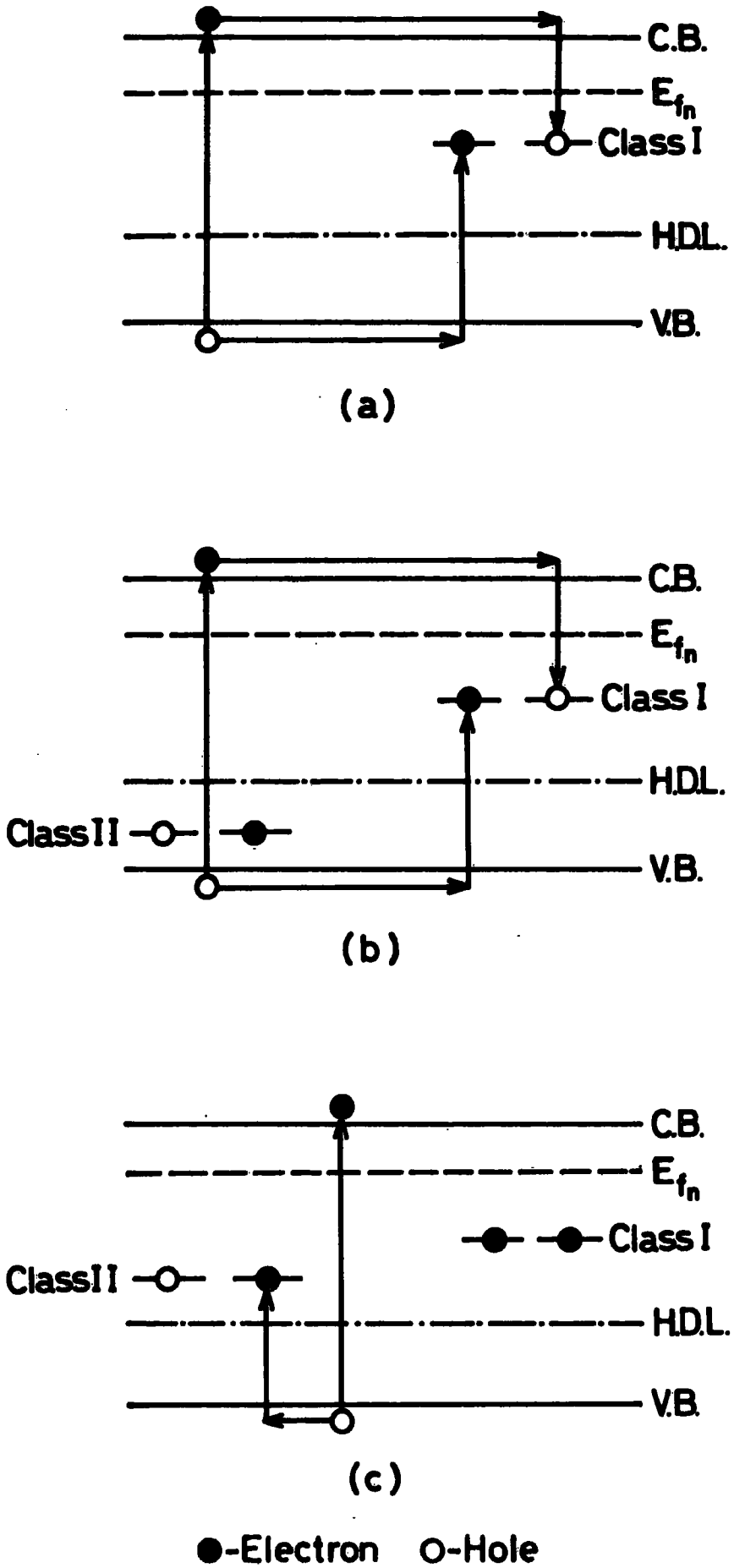

FIGURE 2.2 Process of sensitisation

of illumination at constant temperature then the sensitivity increases with light intensity and the measured photocurrent varies superlinearly with the intensity of light. On the other hand if the hole demarcation level is raised through class II levels by increasing temperature at fixed illumination the sensitivity decreases with temperature. This process is called thermal quenching of photosensitivity. When the hole demarcation level is below the level of the sensitising centres, a second light source can excite electrons optically from the valence band to the hole-occupied sensitising centres, releasing holes to be captured by the class I centres. This process will result in a decrease in photoconductivity and is called optical (infra-red) quenching. The exploitation of superlinearity, thermal and optical quenching will be discussed in more detail in chapter 3 on experimental methods.

2.8 KINETICS OF PHOTOCONDUCTIVITY

With intrinsic semiconductors electrons are thermally excited from the valence band to the conduction band and when thermal equilibrium is reached, without illumination;

$$g = n_o p_o Sv \qquad (2.21)$$

where g is thermal excitation rate, S is the capture cross section for free electron-hole recombination, v is thermal velocity of electrons and n_o and p_o are the thermal equilibrium density of electrons and holes respectively. If f is the photoexcitation rate of electron-hole pairs per unit volume per second, the total steady state generation rate under illumination is

$$g + f = (n_o + \Delta n)\ (p_o + \Delta p)\ C \qquad (2.22)$$

Where C is the recombination coefficient and is given by the product Sv. Because of the requirements of charge neutrality $n_o = p_o$ and $\Delta n = \Delta p$ eq. 2.22 becomes;

$$f = 2 \Delta n \, n_o \, C + \Delta n^2 \, C \qquad (2.23)$$

If $\Delta n \ll n_o$, which is usually the case in rather insensitive photoconductors, then from eq. 2.23

$$n = \frac{f}{2 n_o C} \qquad (2.24)$$

Substituting eq. 2.4 in eq. 2.24

$$\tau_n = (2 \, n_o \, C)^{-1} \qquad (2.25)$$

In this case the lifetime is constant and depends only on the density of electrons in thermal equilibrium in the dark and as shown before, the photoconductivity varies linearly with f. The second case is for $\Delta n \gg n_o$ and this occurs in highly sensitive insulator-like photoconductors. Eq. 2.23 can be rewritten as

$$\Delta n = (f/C)^{\frac{1}{2}} \qquad (2.26)$$

and now the lifetime is

$$\tau_n = (1/Cf)^{\frac{1}{2}} \qquad (2.27)$$

Using the relationship 2.6a, it can be seen that the lifetime varies inversely as the square root of the excitation intensity and the proportionality factor is the inverse square root of the capture coefficient. This corresponds to the sublinear relationship between photoconductivity and light intensity. The existence of impurities and other imperfections may cause the lifetime to depart from the relation 2.27. But if the excitation intensity is high enough eq. 2.27 is again valid when the recombination of free electrons and holes begins to dominate the situation.

2.9 SIMPLE RECOMBINATION KINETICS

In the one-centre trap free model, recombination centres sufficiently close to the Fermi level will be partly occupied by electrons or holes. When both the densities of occupied (n_R) and unoccupied ($N_R - n_R$) recombination centres are much greater than the free carrier density, there will be no significant change in the occupancy of these centres under illumination. The corresponding electron and hole lifetimes are then independent but not equal.

$$\tau_n = \frac{1}{C_n (N_R - n_R)} \tag{2.28}$$

$$\tau_p = \frac{1}{C_p n_R} \tag{2.29}$$

Where N_R is the total number of recombination centres. If the density of free carriers is much greater than n_R or $(N_R - n_R)$ then because of charge neutrality $\tau_n = \tau_p$. This situation occurs with high excitation intensities. Under these conditions if n_R^* represents the density of

electron-occupied imperfections and $(N_R - n_R)^*$ empty centres eqs. 2.28 and 2.29 become

$$\frac{1}{C_n (N_R - n_R)^*} = \frac{1}{C_p n_R^*} \tag{2.30}$$

or

$$\frac{n_R^*}{N_R} = \frac{C_n}{C_n + C_p} \tag{2.31}$$

Then the lifetime of electrons and holes is :

$$\tau_n = \tau_p = \frac{1}{N_R\left[\frac{C_p C_n}{C_p + C_n}\right]} \tag{2.32}$$

If $C_n \ll C_p$ eq. 2.32 reduces to $1/N_R C_n$ and if $C_p \ll C_n$ it becomes $1/N_R C_p$. This means that the rate of recombination is limited by the smallest capture coefficient.

Although certain features of photoconductivity can be explained by the simple one-centre model, more complex phenomena such as imperfection sensitisation, superlinearity, thermal and optical quenching of photo-sensitivity cannot. These phenomena can only be explained in terms of the interaction of at least two centres, as was implicity assumed in the earlier discussion of sensitising centres in sec. 2.7. Detailed mathematical analysis of these phenomena is beyond the scope of the present study, but it can be found in the literature[6].

As mentioned at the beginning of this chapter, photoconductivity measurements can be used to reveal the presence of impurity levels such as sensitising centres. A measurement of the photoconductive response as a function of photon energy gives direct information about the presence of deep level centres from various thresholds observed in the spectrum. In practice the interpretation of this data is usually very difficult for several reasons. For example the photoexcited non-equilibrium carrier density is a complicated non-linear function of the optical emission and capture rates of the energy levels in the bandgap.

CHAPTER 2 - REFERENCES

1. W. Smith, Nature 7 (1873) 303.

2. R. H. Bube, Photoconductivity of Solids. Wiley New-York (1960).

3. A. Rose, Concepts in photoconductivity and allied problems - Wiley New York (1963).

4. R. H. Bube, Electronic properties of crystalline solids - Academic Press (1974).

5. B. Gudden and R. Pohl, Physik Z, 23 (1922) 417.

6. G. A. Dussel and R. H. Bube, J. Appl. Phys. 37 (1966) 13.

CHAPTER 3

SPACE CHARGE METHODS AND RELATED PHENOMENA

3.1 INTRODUCTION

The study of defect and impurity levels in CdSe is the major concern of this thesis. In addition to the photoconductivity methods described in Chapter 2, the investigation of these levels has also been carried out using the space-charge region of a junction device. Because of their relatively simple structure Schottky diodes have been employed for this purpose.

The background theory of imperfections and their detection by space charge capacitance methods are revived in this chapter, together with the Schottky barrier devices.

3.2 Defect and Impurity Centres

3.2.1 Introduction. When the periodicity of the perfect crystal potential is interrupted by a native defect or an impurity atom, new energy levels become possible in a localised region of the crystal near the disturbance. These levels usually lie within the forbidden gap of a semiconductor and they have important effects on crystal properties. In semiconductor terminology many different names, such as, electron or hole traps, recombination centres, optical absorption centres, donor or acceptor centres etc., have been assigned to these localised energy states. These names do not correspond to different physical species but reflect the behaviour of the energy levels in differing circumstances (e.g. the behaviour of a trap as a recombination centre depending on the location of the demarcation level) (see chapter 2.6).

In fact in order to give a complete description for an energy level, several parameters, such as the ionisation energy, the density, thermal and optical capture and emission constants for electrons and holes have to be determined. However, the characterisation of defect and impurity levels by all these parameters is not easily realised and hence a certain degree of classification is usually required. For example, one very commonly used method is to classify the energy levels as either shallow or deep states according to their ionisation energies.

3.2.2 Shallow Levels. The impurity or defect levels located near to the allowed bands, with an ionisation energy comparable to kT, are considered to be shallow centres. These centres can be classified as either donors (positively charged when ionised) or acceptors (negatively charged when ionised). Since these levels are usually ionised at room temperature they play the dominant role in the determination of the conductivity type (n or p) of the semiconductor.

The simple hydrogen atom model can be used for the calculation of these small ionisation energies with appropriate correction for the dielectric constant of the crystal and the effective mass of the carrier. This theory, known as the effective mass theory, was first introduced by Kohn (1957)[1] and was successfully applied to many semiconductors for the calculation of shallow levels[2,3,4]. According to this model a hydrogenic system is embedded within the dielectric medium of a crystal, and the coulombic potential V of the ionised atom is considered to be a self-consistent one-electron potential. Because of the small effective mass (of the order of $\sim 0.1\ m_o$) and the relatively large dielectric constants of II-VI compounds, the binding energy between the ionised atom and the bound electron is much less than in the free hydrogen atom. This indicates that the bound

electron is in a large orbit and the wave function describing the electron is spread out over many lattice atoms and thus only the long range coulombic interactions are effective.

3.2.3 Deep Levels. The energy levels which lie further into the forbidden gap cannot be described by the hydrogenic model and are classified as deep levels. Deep centres are present in all semiconductors and even in small concentrations have a very important role in controlling the carrier lifetime[5]. Other undesirable effects of these centres are trapping and non-radiative recombination processes which can affect the efficiency of such devices as light-emitting diodes. On the other hand these effects are sometimes desirable, as with the fast recombination required in silicon switching devices, achieved by the incorporation of deep gold centres.

Deep impurity levels may be introduced into semiconductors by several different means, i.e. transition metal impurities (e.g. copper), vacancies and by subsitution of elements from columns of the periodic table adjacent to those of the host lattice. It is well known that native defects in II-VI compounds always seem to exist independently of any impurities added intentionally. With particular reference to CdSe, the native defects are cadmium interstitials or selenium vacancies which act as donors, and cadmium vacancies or selenium interstitials which act as acceptors. These defects can be neutral, singly or doubly charged states. The introduction of any electrically active defect into a crystal lattice implies that some form of compensation must occur in order to maintain the charge neutrality. As an example of this process consider the case where iodine (I) from group 7 of the periodic table is an impurity in CdSe. When the I is substitutionally introduced in place of Se, because of the different charge states of Se and I, there will be

a weakly bound electron in the vicinity of this impurity. This electron can easily be ionised at sufficiently high temperatures leaving behind a positively charged donor ion. When an acceptor-like native defect such as a cadmium vacancy exists simultaneously in the material then the ionised electron may compensate the vacancy. Alternatively if the energy difference for an electron to be transferred between the impurity donor level and cadmium vacancy acceptor level, is larger than the energy required for cadmium vacancy formation, a self-compensation mechanism may occur. This process leads to formation of cadmium vacancies to compensate the incorporated I donors[6]. This requires that:

$$2Se^{o} + Cd^{o} + 2I \rightarrow 2I^{+} + V_{cd}^{--} + 2Se + Cd \qquad (3.1)$$

in order to maintain the charge neutrality in the crystal. From a practical standpoint the formation of cadmium vacancies can either be encouraged by performing the impurity incorporation under high Se-pressure or prevented by performing the process in a Cd ambient.

3.2.4 Theoretical Models As the ionisation energies of deep centres are relatively large, there is a resulting strong potential which gives rise to the localisation of the carrier wave function near the site of the defect. Under these circumstances the short-range potentials will be more effective than the long-range ones and hence significant deviations from the hydrogenic model are expected and observed. The development of more appropriate models has proved to be very difficult[7] and, it is still not possible to calculate the exact binding energy of a deep level impurity in a semiconductor. Consequently most of the understanding in this field depends heavily on empirical ideas. Nevertheless, several models have been deveoped for

the characterisation of these levels and some of them have shown reasonable agreement with experiment[8,9,10]. Among these the Lucovsky model[11], for the energy dependence of the photoionisation cross-section, has been one of the more successful. According to this model the optical cross-section is derived from the Fermi golden rule[2] by inserting the solution of the ground state wave function, at a given ionisation energy E_i, for the delta-function potential well. The expression for the photoionisation cross-section (σ^o), then becomes

$$\sigma_L^{\,o}(h\nu) = \frac{1}{n}\left(\frac{E_{eff}}{E_o}\right)^2 \frac{16\pi e^2 \hbar\, (\Delta E_i^{\,o})^{\frac{1}{2}}\,(h\nu-\Delta E_i)^{3/2}}{3m^*c\,(h\nu)^3} \qquad (3.2)$$

where:

- n = the index of refraction for the material
- E_{eff}/E_o = the effective field ratio for the radiation inducing the transition
- c = velocity of light
- m^* = effective mass

The normalised cross-section ($\sigma_L^{\,o}$) for a state at E_i is shown together with the calculated ($\sigma_H^{\,o}$) curve for the hydrogenic formula in figure 3.1. As can be seen from this figure, $\sigma_H^{\,o}$ has a sharp peak at $h\nu = 2\Delta E_i^{\,o}$, whereas $\sigma_L^{\,o}$ shows the maximum to be at about $h\nu - 2\Delta E_i^{\,o}$ and falls off approximately as $h\nu^{-3/2}$ for $h\nu >> \Delta E_i^{\,o}$.

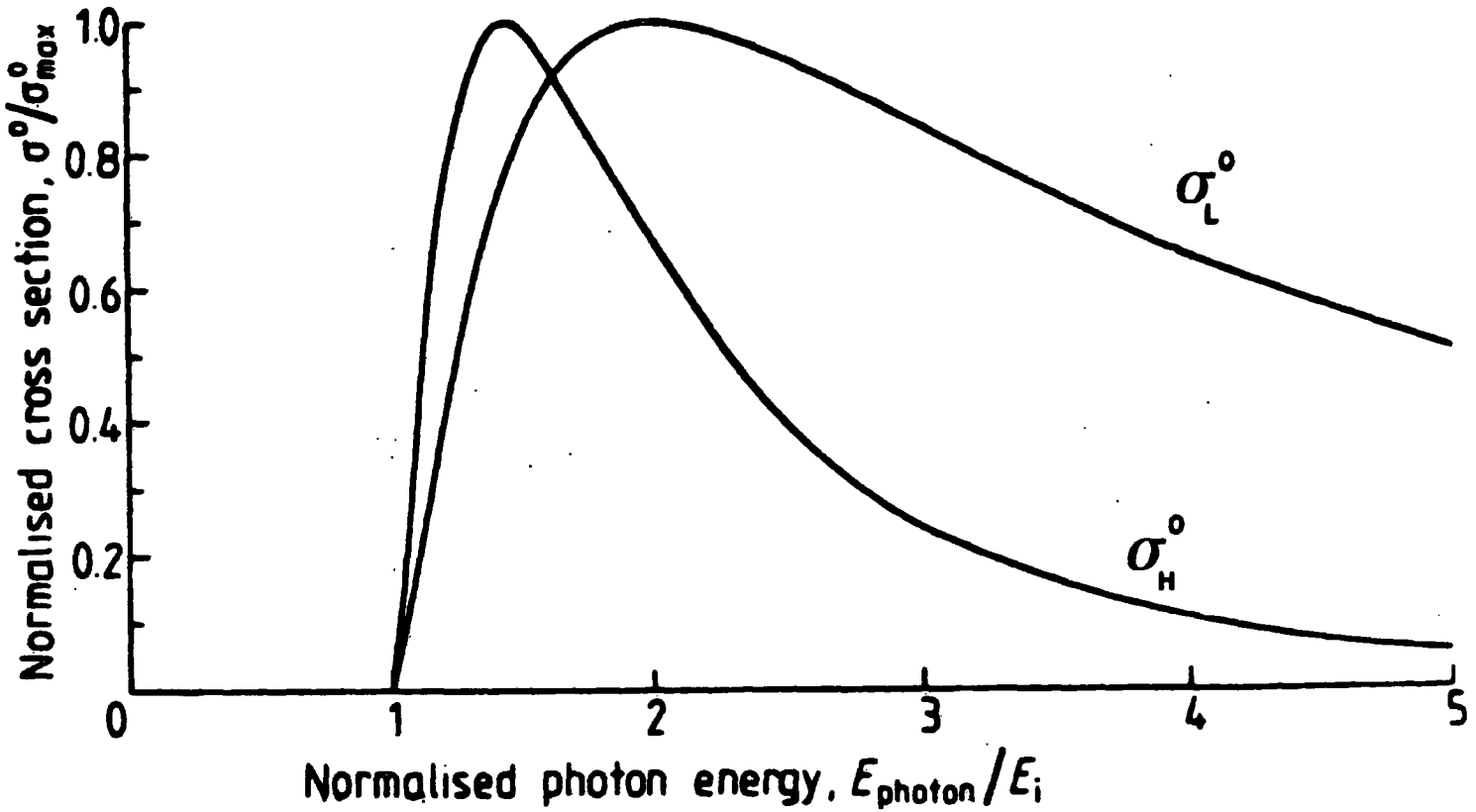

FIGURE 3.1 Normalised photoionisation cross-section σ^o as a function of normalised photon energy. (curves σ^o_H and σ^o_L are for the hydrogenic and Lucovsky models respectively[11]).

Following Lucovsky, several models [12,13] have been developed to improve the agreement between theory and experiment. More recently Grimmeiss et al[14] have modified eq. 3.2 as

$$\sigma^{0} \alpha (h\nu - \Delta E_i^{o})^{3/2} \left\{ h\nu \left[h\nu + \Delta E_i^{o} \left(\frac{m_o}{m^*} - 1 \right) \right]^2 \right\}^{-1} \qquad (3.3)$$

and have successfully applied it to O_2 doped GaP and GaAs. This modified version of the Lucovsky model has also been used in the present study to determine the threshold values of the ionisation energies by curve fitting techniques.

3.2.5 Lattice relaxation All the above models have been derived in the absence of electron-phonon coupling. However, one of the consequences of the short-range potential would be the modification of the electron wave function in the vicinity of the deep lying centre. This implies that when the localisation of the bound particle increases so does the coupling to phonons. In such a strongly coupled system, when the charge distribution of the defect atom changes, (i.e. its electron is excited into the conduction band), the bonding with the nearest neighbours in the lattice will be affected. The equilibrium configuration of neighbouring ions becomes unstable, and since the motion of the ion cores is much slower than that of the electrons the new equilibrium will not be achieved immediately. This process is called lattice relaxation and it gives rise to different emission and absorption spectra. Part of the excitation energy is transferred to the lattice and thus the electron recombination energy will be less than the excitation energy. This also implies that the optical ionisation energies may be different from the thermal ones. The difference between the optical and thermal ionisation energies is characterised by the

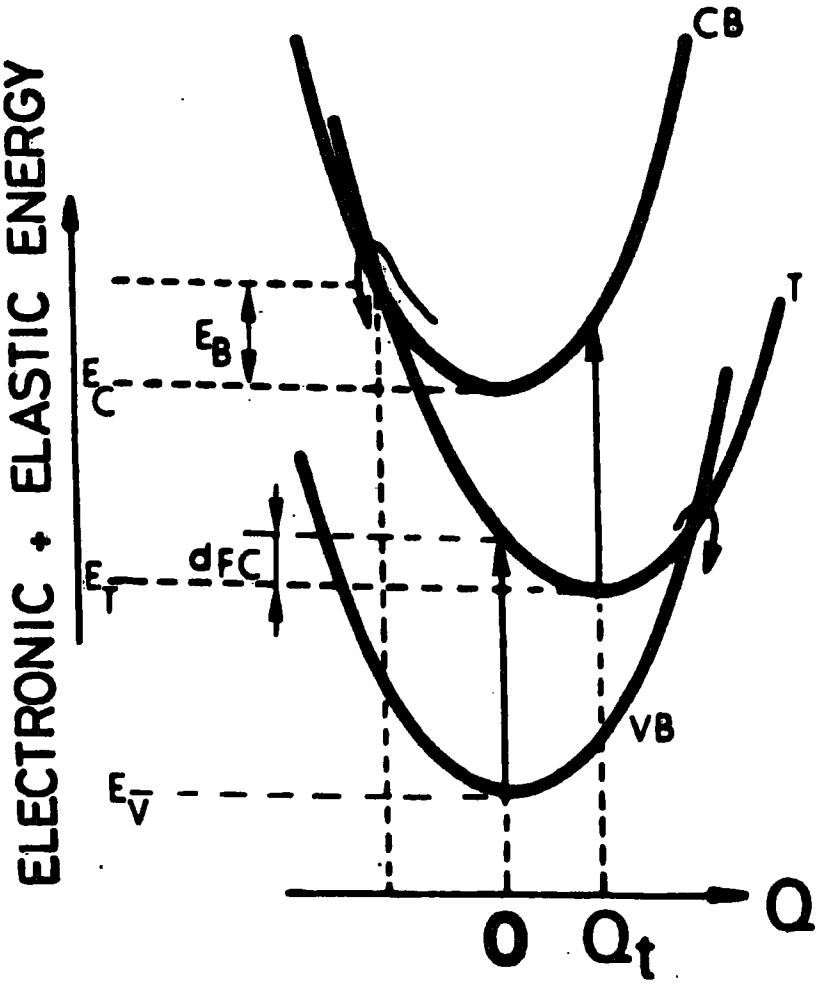

FIGURE 3.2 Configurational-coordinate diagram for a deep level[15].

Franck-Condon [7,15] shift, whereas the difference between the optical emission and absorption spectra is described as phonon broadening[7,16]. The concept of configuration coordinates is usually employed to illustrate this state of affairs. Figure 3.2 shows the configurational diagram for these processes.

It is clear that such a strongly coupled system would exhibit a high degree of dependence on temperature, resulting in optical broadening with increasing temperature. In addition to this, the strong coupling also increases the probability of a "multiphonon" capture mechanism[17]. This is a process of phonon-aided recombination in which it can be shown that the capture cross-section (σ) is thermally activated.

$$\sigma_n \doteq \sigma_n(\infty) \exp(-E_{B/kT}) \tag{3.4}$$

where E_B is defined in fig. 3.2. Henry and Lang[17] have demonstrated that with $T \to \infty, \sigma_n \to \sigma_n(\infty)$ which is of the order of $\sim 10^{-15}$ cm^2. Such large cross-sections which increase exponentially are commonly observed in semiconductors[18].

3.3 Metal-Semiconductor Junctions

3.3.1 Schottky-Mott Theory If an intimate contact is made between a metal and n-type semiconductor for which the work function of the metal (Φ_m) is greater than that of the semiconductor (Φ_s), transfer of electrons from the semiconductor to the metal occurs until the Fermi levels are in equilibrium. In consequence the energy bands in the bulk semiconductor are lowered by $\Phi_m - \Phi_s$, and a potential barrier is formed at the surface. The height of this barrier on the semiconductor side is thus $qV_{dif} = \Phi_m - \Phi_s$; where V_{dif} is the potential in the interior of the

semiconductor, with respect to the metal surface and is known as the diffusion potential. The height of the barrier on the metal side is given by

$$\Phi_{bn} = (\Phi_m - \Phi_s) + (\Phi_s - \chi_s) = \Phi_m - \chi_s \qquad (3.5)$$

or

$$\Phi_{bn} = V_{dif} + (E_c - E_F)$$

where χ_s is the electron affinity of the semiconductor. The band diagram of an ideal metal-semiconductor (MS) structure is shown in figure 3.3. Since the ionised impurity donors are immobile the positive space charge is distributed over a volume extending a distance W from the MS junction, and is known as the space-charge region or depletion region.

The first understanding of the nature of the electrostatic potential barrier and the rectifying mechanism was described by Schottky and independently by Mott in 1938. The main difference between the models is in the shape of the potential barrier. According to Schottky the density of charged impurities is constant in the barrier region, so that the electric field increases linearly and the potential quadratically as the metal is approached. The resulting parabolic shaped band bending is known as the Schottky barrier. On the other hand in the model proposed by Mott, the barrier region contains no impurities, so that the electric field is constant and the potential varies linearly. This type of barrier is known as the Mott barrier and is rarely encountered in practice. The early studies of MS contacts have been extensively reviewed by Henisch (1957)[19].

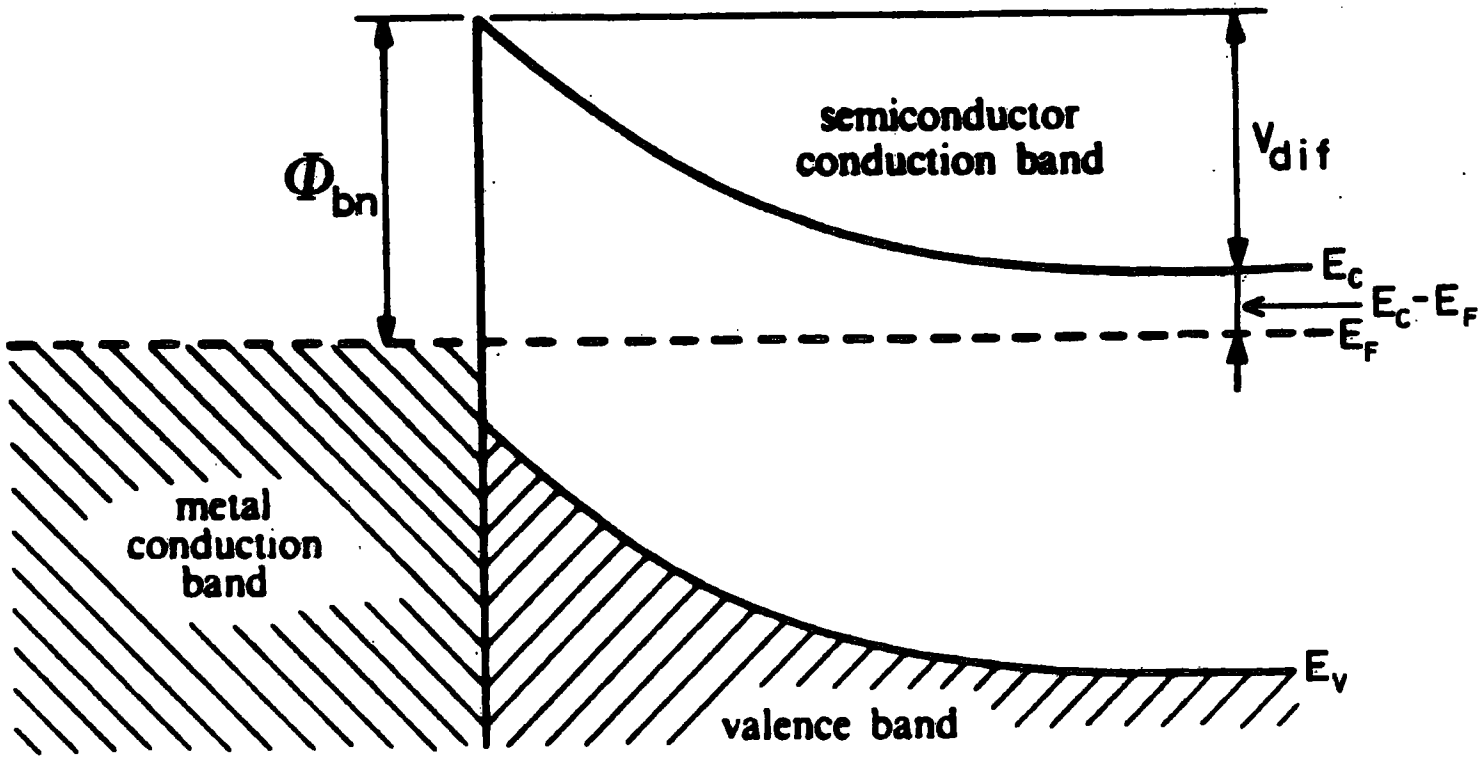

FIGURE 3.3 Energy band diagram of an ideal metal n-type semiconductor contact(Schottky barrier).

3.3.2 Schottky Barriers on Etched (Real) Surfaces. Since real surfaces are usually prepared by mechanical polishing followed by chemical etching, such a surface inevitably is covered by chemiadsorbed material, generally an oxide. As a result many Schottky barriers built on these surfaces are not ideal MS contacts but are instead metal-interfacial layer-semiconductor (MIS) structures. Schottky barriers built on clean (i.e. cleaved in ultra-high-vacuum) surfaces are not practical devices and are generally used only for research purposes. Furthermore, they have been found to be more difficult to analyse than Schottky barriers on real surfaces because of various interdiffusion effects[20].

The detailed energy band diagram of a metal n-type semiconductor contact with a thin interfacial layer (of the order of lattice parameters) is given in figure 3.4.

Here the symbols have the following meanings:

Φ_{bn} barrier height of MS barrier

Φ_{bo} asymptotic value of Φ_{bn} at zero electric field

ψ_o the energy level at the surface

V_{dif} built-in potential

$\Delta\Phi_{bn}$ image force barrier lowering

Δ the potential across the interfacial layer

ε_s permittivity of the semiconductor

ε_i permittivity of the interfacial layer

δ thickness of the interfacial layer

Q_d space-charge density in the semiconductor

Q_{ss} surface state density on the semiconductor

Q_m surface charge density on the metal

According to the Schottky-Mott approximation ($\Phi_{bn} = \Phi_m - \Phi_s$) the barrier height is linearly dependent on the metal work function.

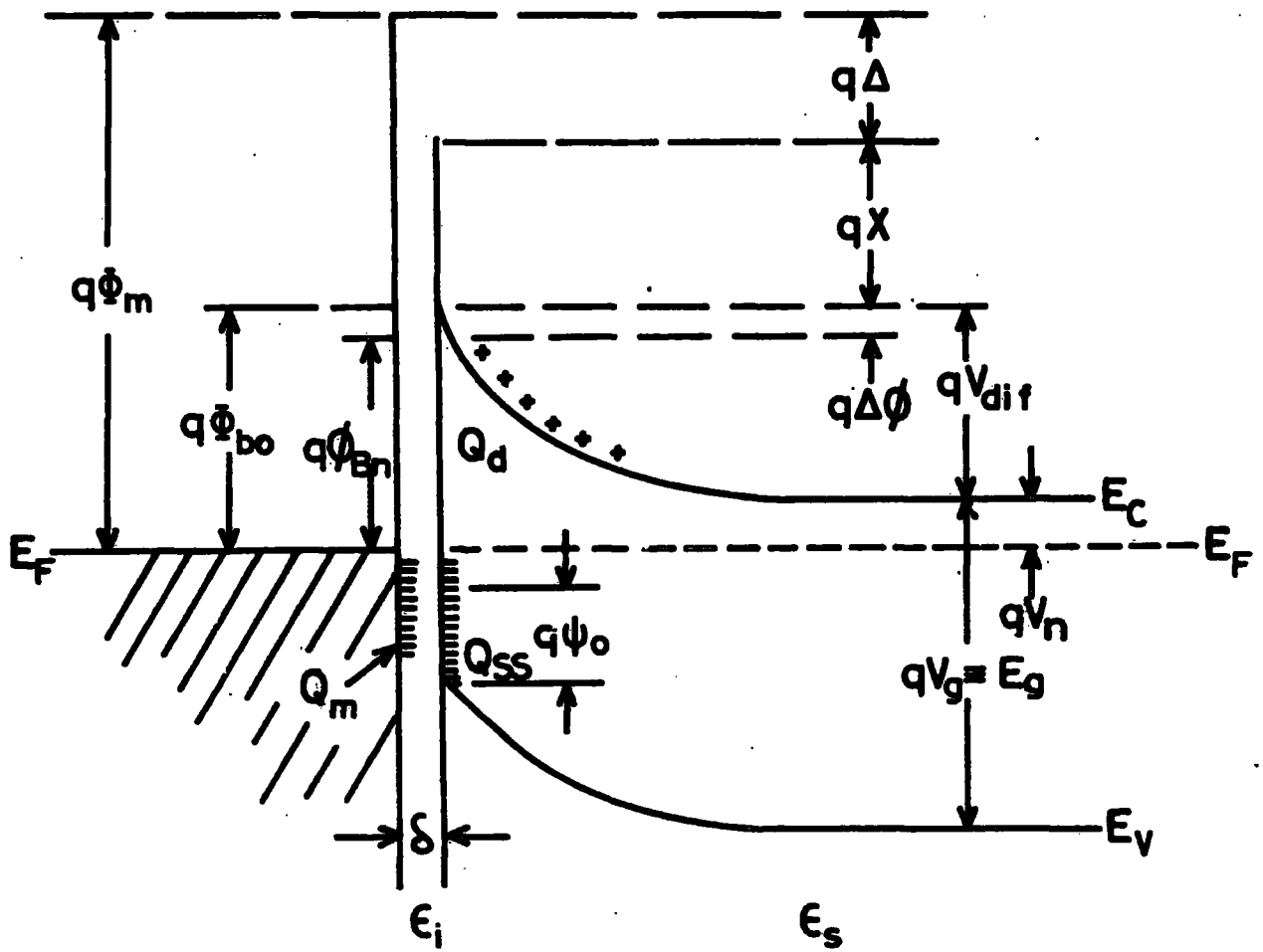

FIGURE 3.4 Detailed energy band diagram of a metal n-type semiconductor contact with a thin interfacial layer.(After Cowley and Sze[24]).

However, in practice it is found that the barrier height can be nearly independent of the work function of the metal. This led Bardeen[21] to propose a model in which surface states, located in the semiconductor energy gap, played the key role.

3.3.3 Surface states and the Bardeen Model One of the most obvious interruptions of the perfect periodicity of the crystalline solid occurs because of the surface, and as a result of this discontinuity there would be, in principle, broken bonds at the surface. The unsaturated valence electrons of the surface ("dangling bonds") can easily bind foreign atoms and are the cause of the strong adsorption of impurities on initially pure surfaces. The occurrence of discrete states arising from the surface boundary of a crystal was first shown by Tamm[22], and later the theory was expanded by Shockley[23].

The corresponding ionisation energies of these states lie in the forbidden gap and are localised at the surface. Those states which are entirely associated with the dangling bonds of the perfect crystal surfaces are called Tamm states. The density of these states is of the same order as the density of the surface atoms ($\sim 10^{14}$ cm^{2}).

The binding of impurity atoms to the crystal surface also gives rise to surface states, whose properties may differ from Tamm states. These are called extrinsic surface states. Since the extrinsic surface states can act either in donor or acceptor-like ways, the carrier concentrations near the surface may be affected and become position dependent. The surface will then have a positive or negative charge which is compensated by an equal, but opposite space-charge near the surface. As a result, in thermal equilibrium the energy bands bend either downwards (donor-like surface states in n-type), or upwards (acceptor-like surface states in n-type).

In fact in a metal semiconductor contact, according to Bardeen, if the density of these states is sufficiently high, the band bending may be dominated by the charge localised in the interface rather than the metal work function. Bardeen also introduced the concept of a neutral level, ψ_o, for these states, defined as a demarcation level below which the states must be filled in order to achieve an electrically neutral surface. In the absence of surface states the negative charge Q_m on the surface of the metal must be equal to the positive space-charge in the semiconductor (Q_d). This neutrality condition will certainly be affected by the existence of surface states and the condition becomes $Q_m = -(Q_{ss} + Q_d)$ where Q_{ss} is the charge in the surface states.

Since the occupancy of the surface states is also determined by the Fermi level of the semiconductor, states are assumed to be filled up to the Fermi level and empty above it (absolute-zero approximation). Now, if the neutral level ψ_o happens to be above the Fermi level, according to this approximation, states between the neutrality and Fermi level will remain empty. This gives rise to a net positive charge and in order to maintain the charge neutrality, Q_d therefore will be smaller than if the neutrality level coincided with the Fermi level, or surface states were absent altogether. This indicates that the width of the depletion (space-charge) region will be correspondingly reduced, and the amount of the band bending will also be decreased. On the other hand if the neutrality level ψ_o lies below the Fermi level, the net negative charge associated with the filled states between the neutrality and Fermi levels gives rise to an increase in band bending. This negative charge would result in a degree of band bending even if the metal-semiconductor contact were not formed.

When the density of surface states is sufficiently high the charge

associated with the electric field developed across the metal-semiconductor interface can be accommodated by these states without significantly altering the position of the Fermi level. The height of the MS barrier is then determined mainly by the occupancy of the surface states rather than the metal work function and the Fermi level is said to be pinned by the high density of surface states. This extreme case is called the Bardeen limit and the barrier height is given by

$$\Phi_{bn} = E_g - \psi_o \qquad (3.5)^a$$

where E_g is the energy gap of the semiconductor.

However, in general, the barrier height is usually a function of both the charge in the interface states and the metal work function. This has been demonstrated by Cowley and Sze[24] in a more general expression for the barrier height at zero bias which is given by

$$\Phi_{bn} = \beta(\Phi_m - \chi_s) + (1 - \beta)(E_g - \psi_o) \qquad (3.6)$$

where

$$\beta = \frac{\varepsilon_i}{\varepsilon_i + \delta q D_s} \qquad (3.7)$$

D_s is the density of surface states, ε_i and δ are the permittivity and thickness of the interfacial layer respectively. If $D_s \rightarrow 0$, it can easily be shown that equation 3.6 reduces to the Schottky-Mott theory given in equation 3.5. However if the density of surface states is not

constant, but strongly peaked about an average ψ_t which differs from the neutral level ψ_o equation 3.6 can be given by [20]

$$\Phi_{bn} = \beta(\Phi_m - \chi_s - \frac{\delta Q_t}{\varepsilon_i}) + (1 - \beta)(E_g - \psi_t) \qquad (3.8)$$

where Q_t is the charge in the surface states when they are filled up to ψ_t. In the Bardeen limit ($D_s \rightarrow \infty$). the barrier height will be pinned to the value $(E_g - \psi_t)$ and the Fermi level will be close to the peak in the surface state distribution.

3.3.4 Schottky Effect

The Schottky effect can be described as the lowering of the potential barrier by an amount $\Delta\Phi_{bn}$ due to the image forces between an electron and its induced positive charge on the metal surface. The barrier lowering is due to a combination of the electric field in the depletion region and the potential arising from the image force. This force is given by

$$F = - q^2/16 \pi \varepsilon_s x^2 \qquad (3.9)$$

where ε_s is the permittivity of the semiconductor and x is the distance between the electron and its induced positive charge. The potential energy due to the image force is represented by the dashed line in figure 3.5, and this superimposed on the potential energy due to the Schottky barrier gives the resulting potential barrier as shown. The

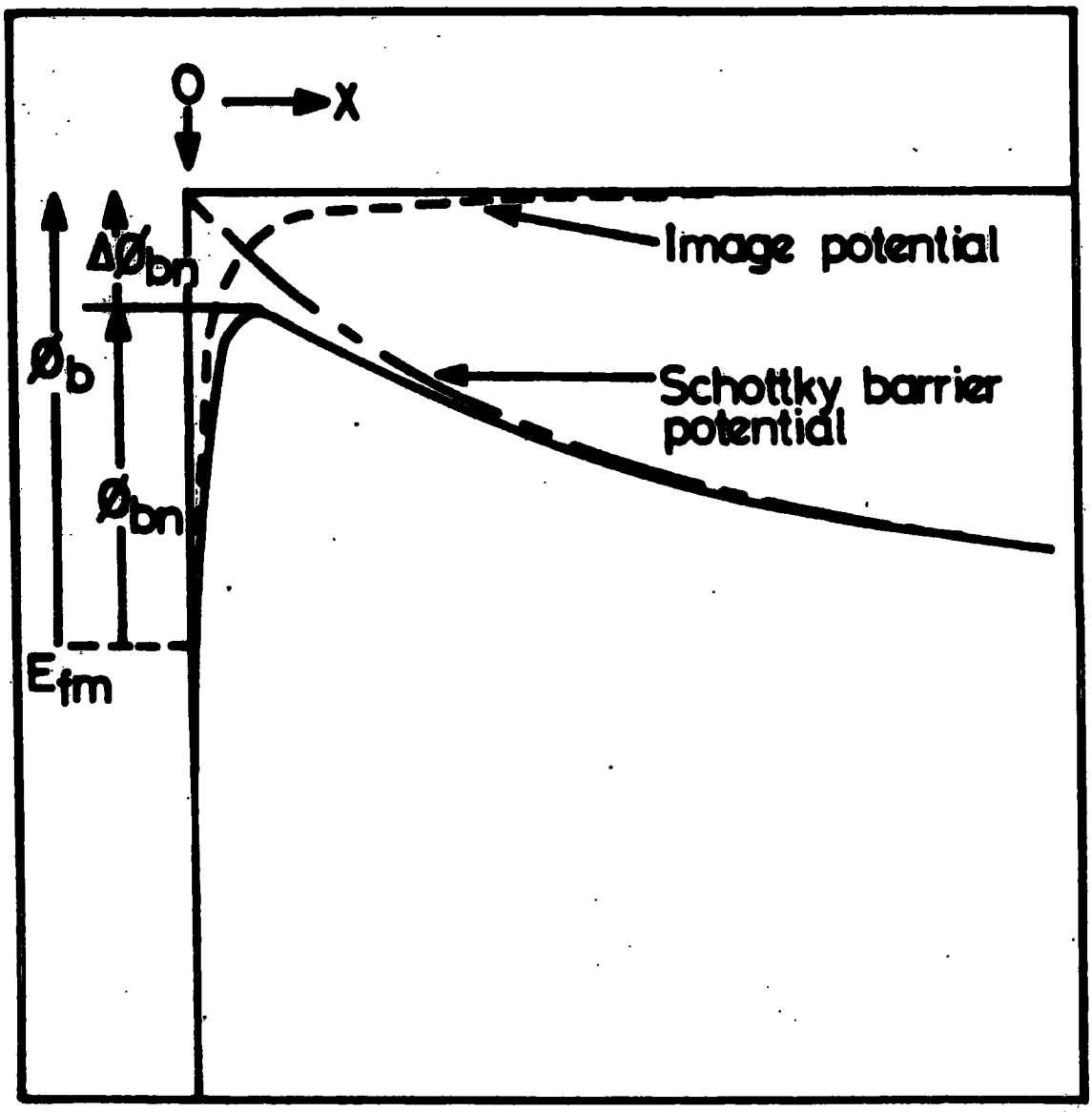

FIGURE 3.5 Image force lowering in a Schottky barrier.

potential energy $\psi(x)$ of an electron at a distance x from the metal surface is

$$\psi(x) = -q^2/16\pi\varepsilon_s x \tag{3.10}$$

when an external field E is applied the potential energy of the electron becomes

$$\psi(x) = -q^2/16\pi\varepsilon_s x - qEx \tag{3.11}$$

which has a maximum value

$$\psi_{max} = -q\left(q E_{max}/4\pi\varepsilon_s\right)^{\frac{1}{2}} \quad \text{at } x = x_{max} = \left(\frac{q}{16\pi\varepsilon_s E_{max}}\right)^{\frac{1}{2}} \tag{3.12}$$

This maximum value is less than that of the initial potential maximum without the field (see fig.3.5)and the difference is given by

$$\Delta\Phi_{bn} = \Phi_b - \Phi_{bn} = \left(q E_{max}/4\pi\varepsilon_s\right)^{\frac{1}{2}} \tag{3.13}$$

Now, assuming that the charge density rises abruptly from zero to the value qN_d at the edge of the depletion region, (depletion approximation), and N_d (donor density) is constant, the electric field strength will increase linearly with distance from the edge of this

region in accordance with Gauss's theorem. In this case the field strength at the surface will be given by

$$E_{max} = qN_d W/\varepsilon_s \tag{3.14}$$

where W is the width of the depletion region. The difference in potential across the depletion region (diffusion potential) will be equal to the product of the average field strength ($\frac{1}{2} E_{max}$) and the depletion width. When an external bias is applied, equation 3.5 can be written as

$$V_{dif} = \phi_{bn} - V - (E_c - E_F) \tag{3.15}$$

and hence

$$E_{max} = (2qN_d/\varepsilon_s)^{\frac{1}{2}} (\phi_{bn} - V - (E_c - E_F) - kT/q)^{\frac{1}{2}} \tag{3.16}$$

Substituting equation 3.16 in eq. 3.13, the image force barrier lowering is given by

$$\Delta\phi_{bn} = q^3 N_d/8\pi^2\varepsilon_s^3 \; [\phi_{bn} - V - (E_c - E_F) - kT/q]^{\frac{1}{4}} \tag{3.17}$$

Although the magnitude of the image force lowering is usually small ($\sim$ 0.03 eV) it can have a significant effect on the Schottky properties, particularly in the current transport mechanism since the current depends exponentially on ϕ_{bn}.

3.3.5 Current Transport Mechanisms

(a) Forward Bias

In Schottky barrier diodes there are several current transport processes when an external bias is applied. These are: (a) Thermionic emission of electrons over the top of the barrier, (b) quantum mechanical tunnelling through the barrier, (c) recombination in the depletion region, (d) minority carrier injection. These are illustrated in figure 3.6 for an n-type semiconductor-metal junction in which the metal electrode is positively biased (forward bias). In most cases the major contribution to the current transport is provided by the first process. The processes (b), (c) and (d) usually arise from non-ideal behaviour.

For the thermionic process, electrons must be transported first through the depletion region of the semiconductor. This occurs by the normal processes of diffusion and drift which take place in this region. Schottky and Spenke[25] proposed that the current flow is limited by diffusion processes, whereas Bethe[26] proposed that thermionic emission was the limiting mechanism. In fact, it has been shown that, in many cases, the current-voltage (I-V) characteristics are best described by the latter.

If the width of the space-charge region is less than the diffusion length of the electrons, according to thermionic emission theory, the forward biased current density can be expressed by

$$J_F = J_s \cdot [\exp(qV/kT) - 1] \qquad (3.18)$$

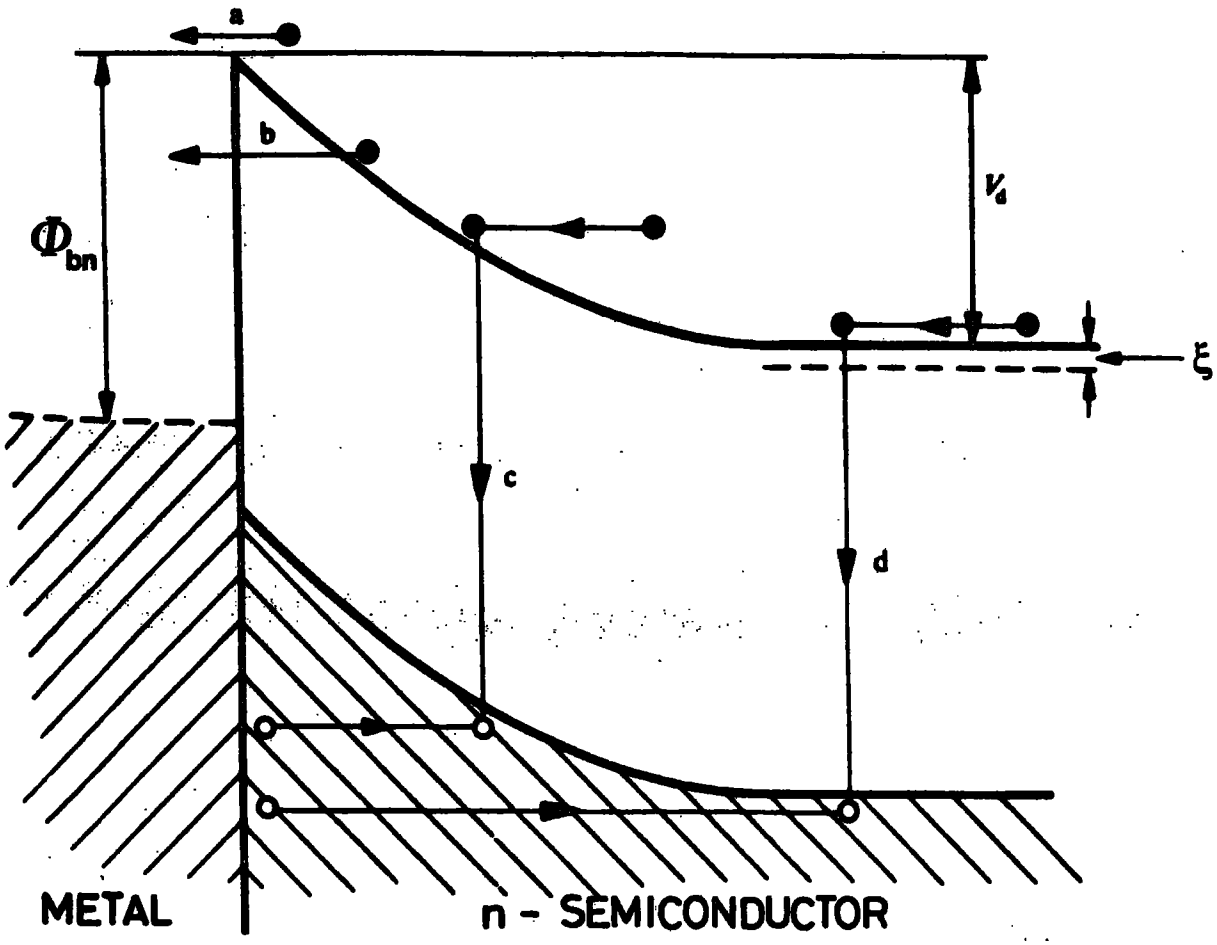

FIGURE 3.6 Current transport processes in a forward-biased Schottky barrier.

where J_s is the reverse saturation current density

$$J_s = R^* T^2 \exp\ (-\phi_{bn}/kT) \qquad (3.19)$$

Here $R^* = 4\ \pi m^* q\ k^2/h^3 \simeq 120\ m^*/m_o$ amp/cm^2.K^2 is the modified Richardson constant corresponding to the electron effective mass (m^*).(i.e. $R^* \simeq 15.6$ amp/cm^2.K^2 for CdSe since $m^*/m_o \simeq 0.13$)[27].

Conversely, if the space-charge region is greater than the diffusion length, the forward current is limited by the diffusion mechanism, and the current-voltage relationship becomes

$$J_F = q\ N_c \mu_e\ E_{max}.\ \exp\left(\frac{-q\phi_{bn}}{kT}\right)\left[\exp(qV/kT) - 1\right] \qquad (3,20)$$

Here E_{max} is the maximum electric field at the junction, μ_e the electron mobility and N_c is the effective density of states in the conduction band which is given by

$$N_c = 2(2\ \pi m^* kT/\hbar^2)^{3/2} \qquad (3.21)$$

In the most general case, the I-V relationship is usually given by a combination of these two mechanisms. Such a combination has been derived by Crowell and Sze[28] in which the current density is given by the expression

$$J_F = (q\ N_c v_r/1 + \frac{v_r}{v_d})\ \exp\ (-\ q\ \phi_{bn}/kT)\ [\exp\ (q\ V/kT) - 1\ ] \qquad (3.22)$$

where v_r is an effective recombination velocity at the potential energy

maximum, and v_d is an effective diffusion velocity for the transport of electrons from the edge of the depletion region to the potential energy maximum.

However, Schottky barriers prepared on etched surfaces inevitably deviate from the ideal behaviour and in particular, plots of lnJ versus V do not exhibit the predicted slope of q/kT. In this case the J-V relationship according to thermionic emission theory, can be described by the relation[29]

$$J_F = J_s \exp (qV/nkT) \qquad (3.23)$$

for bias voltages $V \geq 3kT/q$. The parameter "n" is known as the ideality (quality) factor and is normally greater than unity. This is usually attributed to the bias dependence of the barrier height which results from non-ideal interface conditions. This will be discussed more fully in sec 3.3.8. However, even with an ideal junction, the barrier height would be slightly bias-dependent because of the Schottky effect, which itself depends on the applied bias.

(b) Reverse bias

The reverse bias saturation current will also be affected by any dependence of the barrier height on applied bias. According to equation 3.16 when E_{max} increases with reverse bias (V_R), Φ_{bn} decreases with increasing V_R, and the reverse current J_R does not saturate but increases due to the image force barrier lowering.

$$J_R = J_s \exp (q \Delta\Phi_{bn}/kT) \qquad (3.24)$$

Since $\Delta\Phi_{bn}$ is proportional to $V^{\frac{1}{4}}$ (see eq. 3.17), for large values of V_R,

a plot of lnJ against $V^{\frac{1}{4}}$ should give a straight line the intercept of which on the lnJ axis gives J_s. In practice, the field dependence of the barrier height is usually greater than that predicted by the image force and the difference is very often due to the existence of an interfacial layer (see sec. 3.3.8).

Quantum mechanical tunnelling through the barrier, generation of electron-hole pairs in the depletion region, and transient effects are all mechanisms which may prevent the reverse current from saturating. Tunnelling becomes particularly important near the edges of the metal contact because of the increasing density of electric field lines. The increased field near the contact edges would give rise to greater image force lowering in any case. Tunnelling becomes much more pronounced if the surface of the semiconductor is accumulated due to the presence of positive surface charges which makes the barrier at the edge even thinner[30]. In consequence reverse bias characteristics often deviate considerabley from simple theory and this in turn results in relatively high reverse leakage currents.

3.3.6 The Capacitance of a Schottky Barrier The capacitance of a Schottky barrier arises from the charge due to ionised donors in the depletion region of the semiconductor, and an equal but opposite charge on the metal surface. The differential capacitance ($C = dQ/dV$) of this system is usually measured by superimposing a small alternating voltage onto the D.C. bias. An increase in reverse bias repels the electrons in the conduction band of the semiconductor giving rise to a wider depletion width and reducing the capacitance. When the depletion approximation is employed and the effect of minority carriers (holes) is neglected the charge due to the uncompensated donors in the depletion region, Q_d, is given by Gauss's law as

$$Q_d = \varepsilon_s E_{max} = (2 \varepsilon_s q N_d)^{\frac{1}{2}} (V_{dif} + V_R - kT/q)^{\frac{1}{2}} \qquad (3.25)$$

Substituting Q_d in the differential capacitance $C = \frac{\partial Q_d}{\partial V_{dif}}$ and solving gives

$$C = (q \varepsilon_s N_d/2)^{\frac{1}{2}} (V_{dif} + V_R - kT/q)^{-\frac{1}{2}} \qquad (3.26)$$

$$\text{or} \quad d(1/C^2) = 2/q \varepsilon_s N_d \cdot d(V_R) \qquad (3.27)$$

The graph of C^{-2} as a function of V_R should give a straight line with a slope of $2/q \varepsilon_s N_d$ and an intercept $-V_I$ on the V_R axis equal to $-V_{dif} + kT/q$. In practice the capacitance of Schottky diodes is usually affected by the existence of interfacial layers and deep traps due to native defects or impurities.

3.3.7 Measurement of Barrier Heights The barrier height of a Schottky barrier can be measured by various methods, including primarily J-V, photoelectric, and capacitance measurements.

(a) Current-Voltage Measurements

The forward bias current density-voltage characteristic of a near ideal Schottky diode is given by equation 3.23. As a result, a plot of lnJ against V can be used to determine both the ideality factor and the Schottky barrier height. The appropriate relations derived from equation 3.23, for these calculations are given below

$$\text{(ideality factor)} \quad n = \left(\frac{d(\ln J)}{dV}\right)^{-1} \frac{q}{kT} \qquad (3.28)$$

from the slope and

$$\Phi_{bn} = \frac{kT}{q} \ln \left(\frac{R^* T^2}{J_s} \right) \qquad (3.29)$$

from the intercept.

The value of J_s determined from the intercept, can only be accurate if the ideality factor is equal to unity. From a practical point of view the condition $n \leqslant 1.5$ is often taken as the requirement for a reasonably accurate calculation of Φ_{bn}.

The barrier height may also be determined from reverse bias measurements using the saturation current density J_s, as predicted by the thermionic emission theory. In this case Φ_{bn} can be calculated using J_s, which may be deduced from the intercept of the plot of lnJ against V and then substituting this in equation 3.24. However, since the saturation of the reverse current is usually affected by one of the mechanisms discussed in section 3.3.5(b), the use of this technique is very limited.

(b) <u>The Photoelectric Method</u>

When sufficiently energetic monochromatic light is incident upon the metal surface, some of the electrons excited from the Fermi level of the metal may cross into the semiconductor and contribute to the short circuit photocurrent. Fowler[31] has shown that the photocurrent per absorbed photon, R, is given by

$$R \simeq \frac{T^2}{(E_s - h\nu)} \left[\frac{x^2}{2} + \frac{\pi^2}{6} - \left(e^{-x} - \frac{e^{-2x}}{4} + \frac{e^{-3x}}{9} \ldots \right) \right] \qquad (3.30)$$

$$\text{for } x \geq 0 \; ; \quad \text{where } x = h(\nu - \nu_o) / kT \tag{3.31}$$

The term $h\nu_o$ represents the Schottky barrier height, ϕ_{bn}, and E_s is equal to the sum of ϕ_{bn} and the Fermi energy (measured from the bottom of the metal conduction band). Provided $E_s >> h\nu$ (a condition which is generally valid) and $h\nu - h\nu_o \geq 3kT$, then to a good approximation equation 3.30 reduces to

$$R = c(h\nu - h\nu_o)^2 \tag{3.32}$$

where c is a constant. Thus a plot of $R^{\frac{1}{2}}$ against $h\nu$ is linear over a certain range of energy and the intersection of this linear region with the energy axis gives a direct measurement of the reduced (by image force lowering) barrier height. The photoelectric method is the most accurate and direct method for the determination of barrier height and it is generally regarded as the definitive measurement.

(c) Capacitance-Voltage Measurements

The differential capacitance associated with the depletion region of the Schottky barrier is given by equation 3.26. Thus, if N_d is constant in the depletion region, a plot of C^{-2} against V_R should be linear with an intercept $V_I = V_{dif} - kT/q$, on the voltage axis. The barrier height is then given by

$$\phi_{bn} = V_{dif} + (E_c - E_F) \tag{3.33}$$

$$\text{where } E_c - E_F = kT/q \ln (N_c/N_d) \tag{3.34}$$

The barrier heights deduced from C-V measurements do not include the effect of Schottky barrier lowering. (On the other hand, since J-V and photoelectric techniques involve processes in which the electrons actually surmount the barrier they do include the effect of lowering).

3.3.8 The Effect of an Interfacial Layer. The inclusion of an insulating layer on a semiconductor has an appreciable effect on the electrical properties of Schottky barriers. Then the metal-semiconductor approximates to a metal-insulator-semiconductor (MIS) structure and the "I" layer gives rise to a significant additional barrier for carrier transport. The band diagrams for an MIS diode (a) in equilibrium and (b) under forward bias are shown in figure 3.7 a & b.

(a) Effect on I-V Characteristics

The effect of such an interfacial layer on the I-V characteristics has been extensively studied by Card and Rhoderick[33]. They divided the interface states into two groups such that states in equilibrium with the metal formed one group (D_{sa}), while those in equilibrium with the semiconductor (D_{sb}) formed the second. Under certain assumptions they were able to show that the ideality factor of a diode is given by[33]

$$n = 1 + \frac{(\delta/\varepsilon_i)\,(\varepsilon_s/W + q\,D_{sb})}{1 + (\delta/\varepsilon_i)\,q\,D_{sa}} \qquad (3.35)$$

where ε_i and δ are the permittivity and the thickness of the insulating layer respectively. For very thin insulating layers $D_{sa} \gg D_{sb}$; and hence equation 3.35 reduces to

$$n = 1 + \frac{\delta\,\varepsilon_s}{W(\varepsilon_i + \delta q\,D_{sa})} \qquad (3.36)$$

Conversely, for thicker insulating layers $D_{sb} >> D_{sa}$, and n is given by

$$n = 1 + \delta/\varepsilon_i \, [\varepsilon_s/W + q D_{sb}] \qquad (3.37)$$

When the density of surface states of either group is very low then equation 3.35 becomes

$$n = 1 - \frac{\delta \varepsilon_s}{W \varepsilon_i} \qquad (3.38)$$

(b) Effect on C-V characteristics

The effect of the interfacial layer is particularly important in C-V characteristics since the capacitance of this layer is effectively in series with the capacitance of the depletion region. Studies by Cowley[34] and Goodman[35] have shown that if an interfacial layer is present, the barrier height deduced from C-V measurements usually exceeds that measured by I-V or photoelectric methods.

In the extensive study of Cowley[34] the effects of the insulator and the bias-dependent interface states were included. When an MIS structure is considered first without the interface states then ϕ_{bn} may be defined in terms of energies (shown in figure 3.7a)

$$\Phi_{bn} = \Phi_m - \chi_s + (E_c - E_F) \qquad (3.39)$$

$$\text{i.e. } \Phi_{bn} = V_{dif} + \Delta(o) \qquad (3.40)$$

Using Gauss's law to relate the charge in the depletion region, Q_d, to the potential, $\Delta(o)$, yields (according to the depletion approximation).

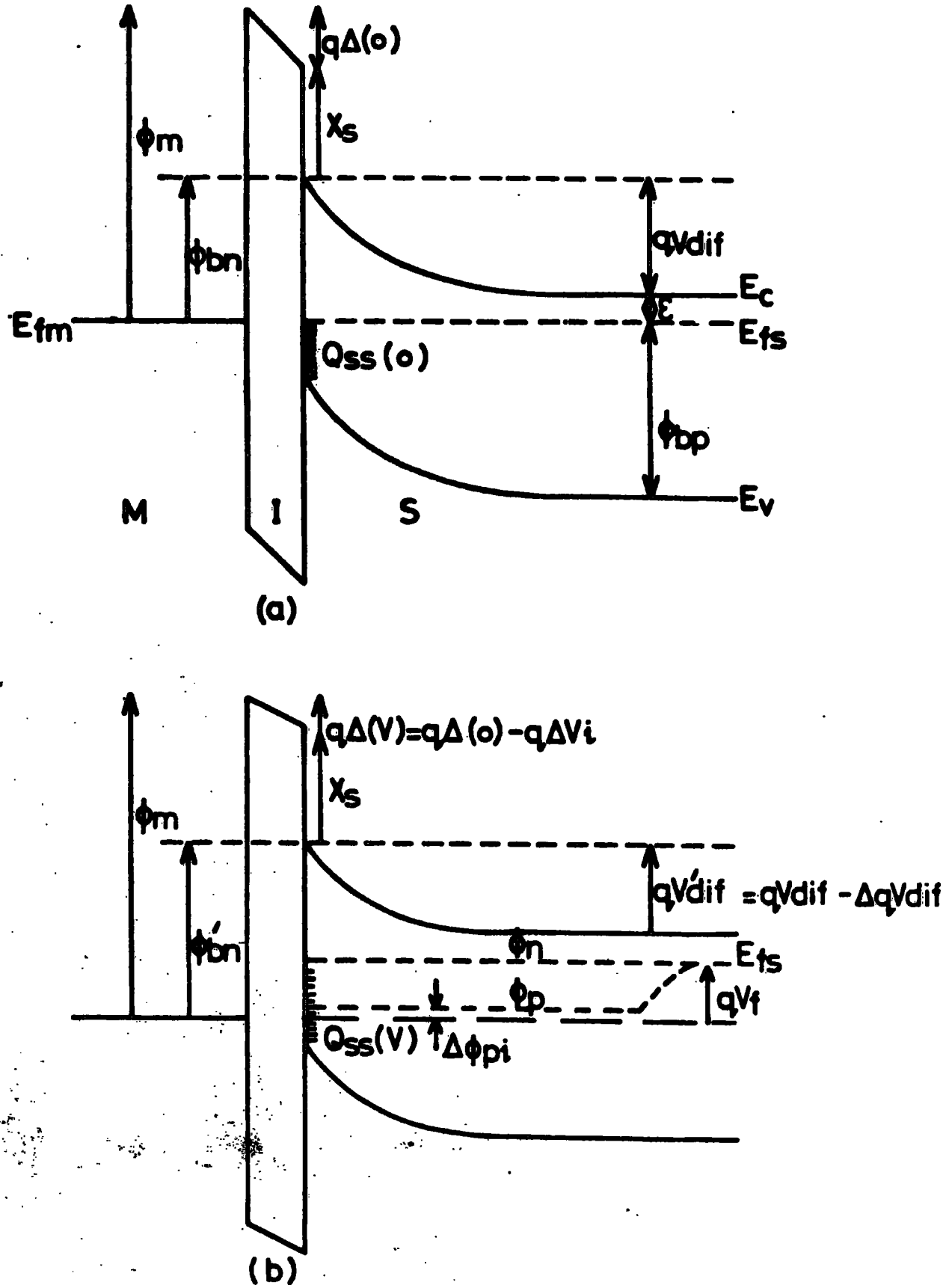

FIGURE 3.7 Energy band diagram of an MIS structure

(a) in equilibrium (b) under forward bias

$$\Delta(o) = (\delta/\epsilon_i)\ (2q\ \epsilon_s\ N_d\ V_{dif})^{\frac{1}{2}}$$

$$\text{or} \quad \Delta(o) = V_1^{\frac{1}{2}}\ V_{dif}^{\frac{1}{2}} \tag{3.41}$$

$$\text{where} \quad V_1 = 2q\ \epsilon_s\ N_d\ \delta^2/\epsilon_i^2 \tag{3.42}$$

Under the application of a reverse bias, $\Delta(V)$ replaces $\Delta(o)$ and V'_{dif} replaces V_{dif}. There equations 3.40 and 3.41 can be written as

$$\phi_{bn} + V = V'_{dif} + \Delta(V)$$

$$\text{and} \quad \Delta(V) = V_1^{\frac{1}{2}}\ V_{dif}'^{\frac{1}{2}}$$

Eliminating $\Delta(V)$ from these equations yields

$$\phi_{bn} + V = V'_{dif} + V_1^{\frac{1}{2}}\ V_{dif}'^{\frac{1}{2}} \tag{3.43}$$

The semiconductor space-charge is given by Gauss's law as $Q_d = (2q\ \epsilon_s N_d\ V'_{dif})^{\frac{1}{2}}$ and hence the differential capacitance is given by

$$C = \frac{dQ_d}{dV} = (2\ q\epsilon_s N_d)^{\frac{1}{2}} \left[\frac{d(V'^{\frac{1}{2}}_{dif})}{dV}\right] \tag{3.44}$$

The quadratic equation 3.43 can be solved and substituted into equation 3.44 to give

$$C = (2/q\ \varepsilon_s\ N_d)^{\frac{1}{2}} \left[\phi_{bn} + V + \frac{V_1}{4}\right]^{\frac{1}{2}}$$

$$\text{i.e. } C^{-2} = (2/q\ \varepsilon_s\ N_d)\ (V + V_{dif} + \frac{V_1}{4} + V_1^{\frac{1}{2}}\ V_{dif}^{\frac{1}{2}}) \qquad (3.45)$$

Thus a graph of C^{-2} against V is linear with a slope equal to that in the simple Schottky barrier case, but with an intercept which is significantly larger.

If the effect of interface states is included, the analysis is more complicated. Assuming that both type D_{sa} and D_{sb} states are uniformly distributed, then the change in the interface state charge under the application of a bias is

$$\Delta Q_{ss} = q\ D_{sb}\ V - q\ D_{sb}\ \Delta V_i - q\ D_{sa}\ \Delta V_i \qquad (3.46)$$

Also $\Delta(o)$ and $\Delta(V)$ are now given by the modified expressions

$$\Delta(o) = V_1^{\frac{1}{2}}\ V_{dif}^{\frac{1}{2}} + \delta/\varepsilon_i\ Q_{ss}(o)$$

$$\text{and} \quad \Delta(V) = V_1^{\frac{1}{2}}\ V_{dif}^{\frac{1}{2}} + \delta/\varepsilon_i\ Q_{ss}(V)$$

$$\text{i.e} \quad \Delta V_i = V_1^{\frac{1}{2}}\ (V_{dif}'^{\frac{1}{2}} - V_{dif}^{\frac{1}{2}}) + \delta/\varepsilon_i\ \Delta Q_{ss} \qquad (3.47)$$

Substituting equation 3.46 into 3.47, solving for $V_{dif}'^{\frac{1}{2}}$ and using in 3.44 yields

$$C^{-2} = \frac{2(1 + \alpha_1 + \alpha_2)}{q\,\varepsilon_s\,N_d(1 + \alpha_1)} \left[\frac{V_1 V_{dif}}{4\,(1 + \alpha_1 + \alpha_2)(1+ \alpha_1)} + \frac{V_1^{\frac{1}{2}} V_{dif}^{\frac{1}{2}}}{1 + \alpha_1} + \right.$$

$$\left. \frac{V_{dif}\,(1 + \alpha_1 + \alpha_2)}{(1 + \alpha_1)} + V \right] \qquad (3.48)$$

where $\alpha_1 = q\,D_{sa}\,\delta/\varepsilon_i$ and $\alpha_2 = q\,D_{sb}\,\delta/\varepsilon_i$

Very recently the more rigorous analysis of Fonash[36] on the basis of Cowley's study has revealed some discrepancies in the above calculations. His analysis concerns the use of equation 3.47 in the equation 3.44. If the charge in the interface states cannot respond to the high frequency measuring signal, then the quasistatic expression for V_{dif}', obtained from equation 3.44, does not accurately describe the variation of V_{dif}' in response to this signal. Fonash[36] has used the correct (a.c.) variation of V_{dif}' to analyse the various cases. The results of both Cowley's and Fonash's analyses are summarized below for some specific cases which are relevant to this study.

Case A $\delta < 30\text{Å}$, the occupation of the interface states is mainly determined by the Fermi level of the metal ($D_{sb} \simeq 0$, $D_{sa} \neq 0$ and interface states cannot follow an a.c. signal. In this case the interface states will be emptied or filled by the tunnelling of the

electrons from the metal, and according to Cowley the slope of C^{-2} against V_R will be the same as in the ideal case (i.e. eqn. 3.27). The intercept V_i on the voltage axis is given by

$$V_i = V_{dif} + \frac{V_1^{\frac{1}{2}}}{1 + \alpha_1} V_{dif}^{\frac{1}{2}} + \frac{V_1}{4(1 + \alpha_1)^2} \tag{3.49}$$

Fonash's analysis for the same case yields

$$\text{The slope } \frac{d\,(1/C^2)}{dV} = -\left[\frac{(1 + \alpha_1)(C_d + C_I)}{C_d + (1 + \alpha_1)\, C_I}\right] \frac{2}{\varepsilon_s\, q\, N_d} \tag{3.50}$$

and the intercept

$$V_i = V_{dif} + \left(\frac{1}{1+\alpha_1}\right) V_1^{\frac{1}{2}} V_{dif}^{\frac{1}{2}} + \left(\frac{1 - \alpha_1}{1 + \alpha_1}\right) \frac{V_1}{4} \tag{3.51}$$

Here C_I is the capacitance of the insulating layer.

Case B. $\delta > 30\text{Å}$. The interface states are mainly in equilibrium with the semiconductor ($D_{sa} \simeq 0$, $D_{sb} \neq 0$) and interface states can not follow the a.c. signal. Cowley's predictions are

$$\frac{d(1/C^2)}{dV} = -\,(1 + \alpha_2)\, \frac{2}{q\, \varepsilon_s\, N_d} \tag{3.52}$$

$$V_i = V_1^{\frac{1}{2}} V_{dif}^{\frac{1}{2}} + (1 + \alpha_2)\, V_{dif} + \frac{V_1}{4\,(1 + \alpha_2)} \tag{3.53}$$

while Fonash's analysis gives

$$\frac{d(1/C^2)}{dV} = -\left(\frac{C_d + C_I}{C_d + (1 + \alpha_2)\, C_I}\right) \frac{2}{q\, \varepsilon_s\, N_d} \qquad (3,54)$$

$$V_1 = V_1^{\frac{1}{2}} V_{dif}^{\frac{1}{2}} + (1 + \alpha_2)\, V_{dif} + (1 - \alpha_2)\, \frac{V_1}{4} \qquad (3.55)$$

In general the two approaches do not give radically different estimates for the diode parameters.

3.3.9 The Effect of Deep Levels The capacitance of a Schottky barrier will also be affected by the presence of deep traps in the semiconductor. This can be illustrated in figure 3.8 where the Schottky barrier contains a single type of deep trap with an activation energy E_T. In the absence of any external bias the traps lying below the Fermi level remain occupied by electrons, and those lying above the Fermi level will be empty. In general the occupation of the traps is determined by Shockley-Read-Hall statistics and the probability of a trap being occupied by an electron is given by

$$f = \frac{\sigma_n\, n\, \bar{v} + e_p}{\sigma_n\, n\, \bar{v} + e_n + \sigma_p\, p\, \bar{v} + e_p} \qquad (3.56)$$

Here σ_n, σ_p and e_n, e_p are the capture cross-sections and emission rates of the traps for electrons and holes respectively, and $\bar{v}$ is the average thermal velocity for both carriers. According to the principle of detailed balance e_n and e_p are related to σ_n and σ_p by

$$e_n = \sigma_n \langle v_n \rangle n_i \exp\left[q\,(E_T - E_i) / kT\right] \qquad (3.57)$$

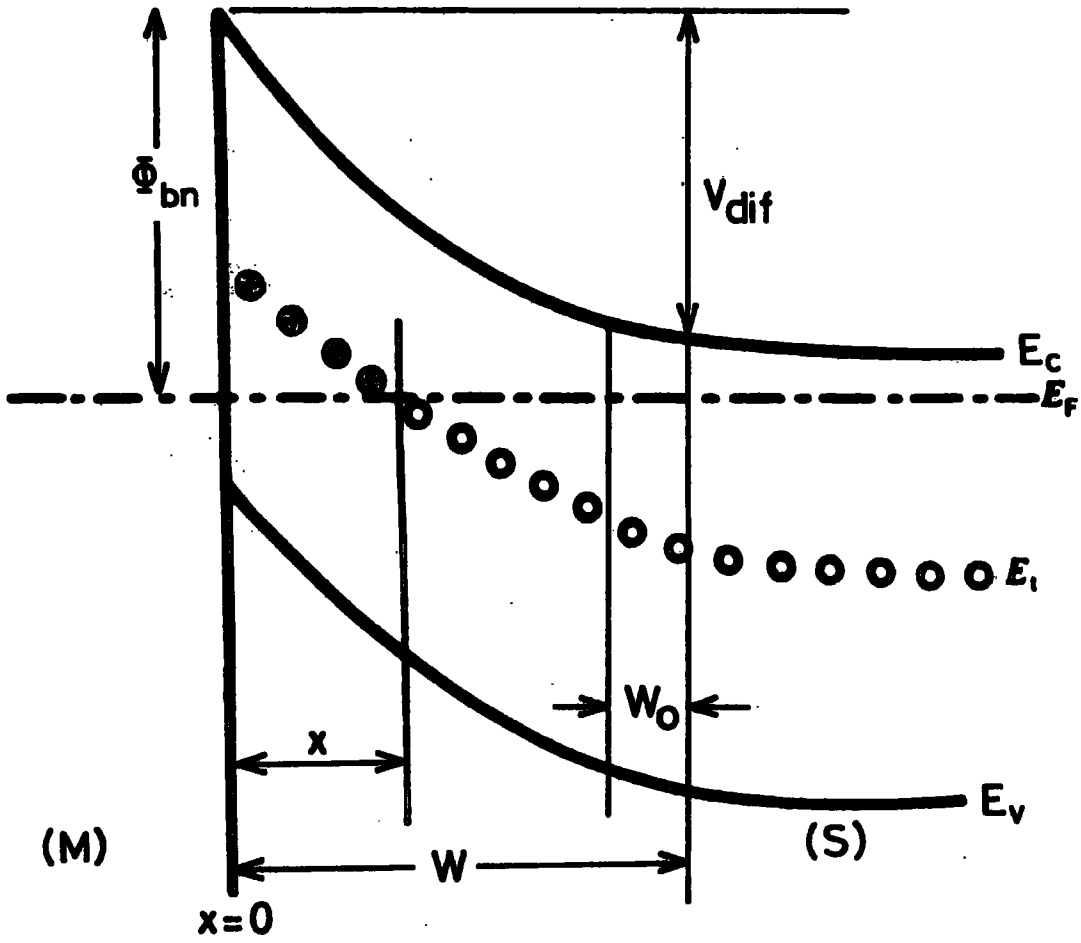

FIGURE 3.8 Energy band diagram of a Schottky barrier containing donor-like deep traps.

and

$$e_p = \sigma_p \langle v_p \rangle n_i \exp [q (E_i - E_T) / kT)] \tag{3.58}$$

where n_i and E_i are the intrinsic carrier concentration and Fermi level. It can easily be shown that for a case where $e_n >> e_p$ and $\sigma_n n >> \sigma_p p$ equation 3.56 reduces to

$$f \simeq \frac{\sigma_n n \bar{v}}{\sigma_p n \bar{v} + e_n} \tag{3.59}$$

On the other hand as mentioned earlier the capacitance of a diode is normally measured at some fixed voltage ΔV by superimposing a small oscillating voltage ΔV_{osc} on the applied bias. Figure 3.9 shows the effect of reverse bias on deep levels which are present in the depletion region. As seen from this figure ΔV_{osc} will uncover charge at both x and y. Free carriers are swept away from the point x while at y electrons are emitted from the traps (E_T) to the conduction band. If the frequency (ω_s) of the oscillating voltage is low, then the traps at y can follow the votage variations by emission and capture processes. This condition is given by

$$e_n > \omega_s \tag{3.60}$$

The emission rate of electrons (equation 3.57) is the limiting process since it is always slower than the capture process (when the Fermi level is above the trap level).

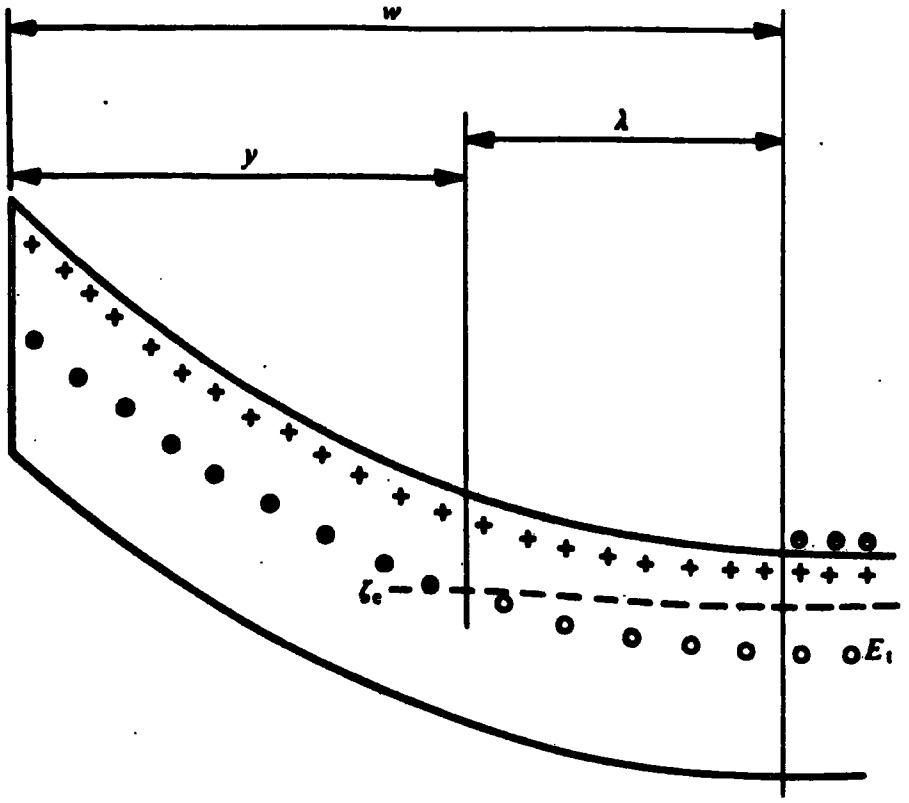

(a)

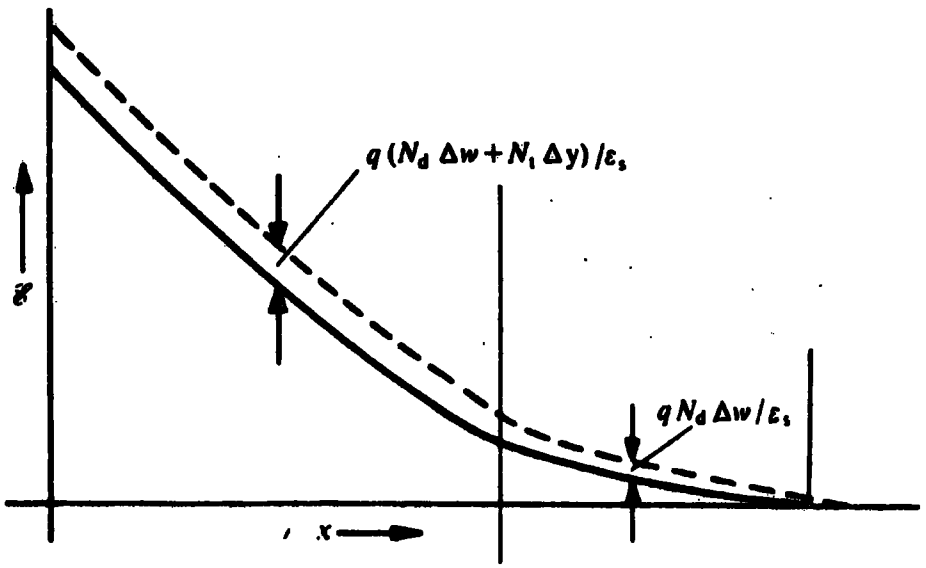

(b)

FIGURE 3.9 Effect of reverse bias on deep traps[20]

(a) charge state, (b) field distribution
- reverse bias V_R ----- reverse bias $V_R + \Delta V_R$

The general expression for the capacitance of the Schottky barrier, in the presence of deep traps, is given by[39]

$$C = A \left(\frac{\varepsilon_s q N_d^+}{2 (V_{dif} + V)} \right)^{\frac{1}{2}} \left(1 + \frac{N_T}{n} \frac{e_n^2}{e_n^2 + \omega_s^2} \right) \qquad (3.61)$$

where A is the area of the diode and N_T is the density of the deep levels, and N_d^+ is the total ionised donor density. It can easily be shown that when $\omega_s >> e_n$ equation 3.61 reduces to the normal Schottky capacitance (i.e. eqn. 3.26). The effects of deep traps on the junction capacitance (including response to both a.c. test signal and variations in D.C. bias) have been more fully discussed by Roberts and Crowell[40], Zohta[41], Kimmerling[42], and more recently by Noras[43].

3.4 Space-Charge Capacitance Methods for the Detection of Deep Levels

3.4.1 Introduction. Space-charge techniques have become a powerful tool for the characterisation of deep levels in semiconductors especially in the last decade[44,48]. The main reason for this interest is the recognition that space-charge methods provide sensitive and quantitative information about the electronic parameters of deep levels (i.e. capture and emission rates). Moreover, the detection of non-radiative centres has also become possible by junction capacitance methods.

However, there are some deficiencies of these methods, such as the requirement of a reliable junction device and the presence of a high electric field in the space charge region[49]. Considering that every method will have some limitations, it is always desirable to employ

several of these techniques simultaneously in order to provide a more comprehensive and reliable description of the deep levels. The background theory of the space-charge methods used in this study are briefly reviewed below.

3.4.2 Steady State Methods

(a) Photocapacitance

When the charge state of a deep level in the depletion region of a junction device is changed by the absorption of photons the capacitance of the junction is also changed. The steady state photocapacitance (PHCAP) technique entails the recording of the variation in the junction capacitance with wavelength. Although this method has been successfully applied to more shallow levels[52] (i.e. they have high emission rates) and their photoionisation threshold energies are easily determined, applications to deep levels has proved more difficult because of the longer time constants associated with these levels. Nevertheless, some of these problems can be overcome either by scanning the wavelength extremely slowly, or alternatively by recording the data manually point by point. The existence of several energy levels in the bandgap of a material also gives rise to complications in the analysis.

The capacitance of the depletion region of a Schottky barrier is given by (i.e. eq.3.26)

$$C = \left[\frac{q \varepsilon_s (N_d^+ - N_a^-)}{2 (V_{dif} + V_R)} \right]^{\frac{1}{2}} \qquad (3.62)$$

Where N_d^+ and N_a^- are the ionised donor and acceptor ion concentrations. With the application of a constant reverse bias the change in photocapacitance (ΔC) will be dependent only on $(N_d^+ - N_a^-)$. The

interpretation of photocapacitance (PHCAP) spectra can be summarized as follows:

Case A A donor level E_{T_1} in the upper half of the bandgap and $h\nu < Eg/2$.

When $h\nu > E_c - E_{T_1}$ electrons will be excited from the level into the conduction band leaving behind positively charged donor atoms (N_d^+). Thus the change in capacitance, ΔC, will be positive.

Case B An acceptor level E_{T_2} in the lower half of the bandgap and $h\nu < Eg/2$.

When $h\nu > E_{T_2} - E_v$ holes will be excited from the level into the valence band leaving behind negatively charged acceptor (N_a^-). Thus ΔC will be negative.

In the case where both levels (E_{T_1} and E_{T_2}) exist simultaneously and $E_c - E_{T_1} \simeq E_{T_2} - E_V$ then the processes are in competition and the interpretation will be complicated.

Case C Both E_{T_1} and E_{T_2} are present simultaneously but $E_c - E_{T_1} \neq E_{T_2} - E_v$ and $h\nu > Eg/2$.

In this situation Case A and Case B transitions will always occur. However, there will, in general, be other competing transitions which may be dominant (depending on σ^o and $h\nu$).

(i) $E_{T_1} - E_v > h\nu > E_c - E_{T_2}$, electrons from the E_{T_2} acceptor level will be excited to the conduction band. The resulting decrease in N_a^- will tend to make ΔC positive.

(ii) $E_c - E_{T_2} > h\nu > E_{T_1} - E_v$, the ionised donors will be filled by electrons excited from the valence band and this tends to reduce the N_d^+ concentration and hence ΔC will be negative.

(iii) $h\nu > E_c - E_{T_2}$ and $E_{T_1} - E_V$ and $E_c - E_{T_2} \neq E_{T_1} - E_v$.

In this case both (i) and (ii) will occur and the sign of $_{\Delta}C$ uniquely identifies which is the dominant level.

Case D. Two or more donor levels in the upper half and similarly several acceptor levels in the lower half of the bandgap. The situation can be treated as with Case C unless the activation energies of the individual donors and acceptors are very close to each other. In principle the different levels can be resolved.

Case E. A donor like level in the lower half and an acceptor like level in the upper half. This situation becomes quite complex because of the competition between filling and emptying processes. In these circumstances additional information from other measurements (such as infrared quenching and DLTS) would certainly be helpful in the analysis.

(b) Infrared Quenching of Photocapacitance (IRQ-PHCAP)

This is an analogous technique to the infrared quenching of photoconductivity which was described in the previous chapter (see Chapter 2.7). When a constant primary light of sub bandgap energy is employed, there would be a change in steady state $_{\Delta}C$. If the device is simultaneously illuminated by a secondary light source of variable wavelength (usually $h\nu \leqslant Eg/2$, in the infrared region), then the change in PHCAP (ΔC) may be quenched. Varying the wavelength of the secondary light will produce a quenching spectrum. The reduction in $_{\Delta}C$ arises because of the filling of the acceptor like levels from the valence band.

3.4.3 Transient Methods

(a) Photocapacitance Transient (PHCAP-TR)

Although the steady state methods provide valuable qualitative characteristics, quantitative values can only be realised by using transient methods. The spectral dependence of the cross-section for

photoionisation of electrons, σ_n^o from a deep level to the conduction band can be determined by this technique.

The rate equation for the electron occupancy of an energy level in the bandgap of a semiconductor can be written as

$$\frac{dn_T}{dt} = e_p\, p_T - C_p\, p.n_T - e_n n_T + C_n\, n\, p_T \qquad (3.63)$$

where $e_n = e_n^o + e_n^t$ and $e_p = e_p^o + e_p^t$ represent the total of both the thermal and optical emission rates of electrons and holes, similarly C_n and C_p denote the total capture constants for radiative and non-radiative recombination processes, n_T and p_T are the concentration of occupied and empty centres respectively. The total number of centres (N_T) is given by

$$N_T = p_T + n_T \qquad (3.64)$$

In the space-charge region of a reverse biased Schottky barrier the free carrier concentration is generally negligible so within the region $(w - w_o)$ n and p can be omitted (see figure 3.8). Furthermore if the experiment is performed at sufficiently low temperature ($e_n^t = e_p^t = 0$) the rate equation reduces to

$$\frac{dn_T}{dt} = e_p^o\,(N_T - n_T) - e_n^o\, n_T \qquad (3.65)$$

The solution of the above equation is given by

$$n_T(t) = \frac{e_p^o}{e_n^o + e_p^o}\, N_T - \left(\frac{e_p^o}{e_n^o + e_p^o}\, N_T - n_T(o) \right) \exp \left[-(e_n^o + e_p^o)\, t \right] \qquad (3.66)$$

Here $\frac{e_p^o}{e_n^o + e_n^o} N_T$ can be denoted by $n_T(\infty)$, because in the steady state equation 3.65 yields $e_p^o (N_T - n_T) = e_n^o n_T$. $\tau = \frac{1}{e_n^o + e_p^o}$ is defined as the time constant of the transient.

Equation 3.66 at $t = 0$ and $t > 0$ can be used for two different initial conditions, either with the level filled or empty. In the first case (with the level filled)

$$t = 0 \quad n_T(0) = N_T \qquad \text{(a)}$$

$$t > 0 \quad n_T(t) = \frac{e_p^o}{e_n^o + e_p^o} N_T + \frac{e_n^o}{e_n^o + e_p^o} N_T \exp(-t/\tau) \qquad \text{(b)} \qquad (3.67)$$

In the second case (with the level empty)

$$t = 0 \quad n_T(0) = 0 \qquad \text{(a)}$$

$$t > 0 \quad n_T(t) = \frac{e_p^o}{e_n^o + e_p^o} N_T [1 - \exp(-t/\tau)] \qquad \text{(b)} \qquad (3.68)$$

On the other hand the capacitance of a reverse-biased Schottky barrier is expressed as

$$C = \left(\frac{A^2 q \varepsilon_s}{2 (V_{dif} + V)} N_I \right)^{\frac{1}{2}} \qquad (3.69)$$

where N_I is the total concentration of the ionised impurity and/or defect levels in the transition region. If these levels are acceptor-like then N_I can be written.

$$N_I = N_d - n_T(t) \tag{3.70}$$

Using equations 3.66 and 3.70 in 3.69 the time dependence of the junction capacitance becomes

$$C^2(t) = \frac{A^2 q \varepsilon_s}{2(V_{dif}+V)} [N_d - n_t(\infty) - [n_T(o) - n_T(\infty)]e^{-t/\tau}] \tag{3.71}$$

Substituting $\frac{A^2 q \varepsilon_s}{2(V_{dif}+V)} [N_d - n_T(\infty)] = C^2(\infty)$ in equation 3.71 yields

$$\ln [C^2(\infty) - C^2(t)] = \ln [n_T(0) - n_T(\infty)] - t/\tau \tag{3.72}$$

thus if $\ln [c^2(\infty) - C^2(t)]$ is plotted against time, the sum of the optical emission rates is obtained from the slope. The absolute values of σ_n^o cannot be obtained from these measurements unless N_T is determined by some other means, and the photon flux, ϕ, is known. This is simply because of the involvement of both e_n^o and e_p^o in transient (emptying process) measurements.

(b) Infrared Quenching of the photocapacitance transient (IRQ-PHCAP-TR)

Initially emptying the levels with primary illumination with $h\nu > E_c - E_T$ will set the initial condition $n_T(o) = \frac{e_p^o}{e_n^o + e_p^o} N_T$ since both e_n^o and e_p^o are operative in the process. Now, illuminating the diode with a secondary irradiation with photon energy $E_c - E_T > h\nu_s > E_T - E_V$ some time after switching off the primary source, will also give rise to a transient change in PHCAP with a time constant $1/\tau \simeq e_p^o$ since this time $e_n^o \simeq 0$. Thus the absolute values of

σ_p^o can be directly obtained by plotting $\ln[C^2(\infty) - C^2(t)]$ against time. The slope of the plot will be

$$1/\tau = e_p^o = \sigma_p^o \phi \tag{3.73}$$

If the photon flux, ϕ is known the spectral distribution of the absolute values of photoionisation cross-section σ_p^o can be determined.

(c) Deep Level Transient Spectroscopy (DLTS)

DLTS can be described as a capacitance transient, thermal scanning method. It was first introduced by Lang[50] (1974). The technique has been proved to be very useful, particularly for the characterisation of relatively deep non-radiative centres in semiconductors.

The technique is based on the capacitance transient concept, where the time constant of the transient (a decay following an initial disturbance) is measured as a function of temperature. The activation energy of the level can then be obtained. The most important practical feature of the DLTS technique is the introduction of the concept of the emission rate window. In this way it is possible to detect only those transients within the range of the rate window as the emission rate varies due to the change in temperature. In consequence when the repetitive capacitance transient is observed through the rate window and the sample temperature is slowly scanned (which changes the thermal emission rate and hence the capacitance decay rate) a peak appears in the plot of capacitance change versus temperature. This peak identifies the temperature at which the emission rate happens to be the same as the rate window. Therefore replotting the spectrum for a number of different rate windows enables the dependence of the emission rate on temperature to be determined. The emission rates are thermally

activated giving, according to the principle of detailed balance $e_n^t = (\sigma_n^t < v_n > N_c) \exp (- \Delta E/kT)$ for electrons (i.e. eq. 3.57 section 3.3.9). A standard means of characterising the depth of an energy level is to construct a plot of ln e_n^t against 1/T and to report the slope of the resulting straight line as the activation energy of the trap. Since the pre-exponential terms in equation 3.57 such as <v> may also be temperature dependent, special care has to be taken in attributing this slope to the activation energy.

With this technique a dual-gated signal averager (double boxcar) has been introduced in order to determine the emission rate window accurately. It also provides a signal averaging capability to enhance the signal-to-noise ratio. Figure 3.10 shows how the double box-car is used to select the rate window. The left hand side of this figure represents the capacitance transients at various temperatures, which the right hand side shows the corresponding DLTS signal from the double boxcar. This signal is the difference between the capacitance at time t_1 and at time t_2 as a function of temperature. It can easily be seen from this figure that, $C(t_1) - C(t_2)$, goes through a maximum when the inverse of the transient rate constant (τ), is equal to the rate window.

The normalised DLTS signal, S(T), shown in figure 3.10 can be defined as:

$$S(T) = [C(t_1) - C(t_2)]/\Delta C(0) \qquad (3.74)$$

where $\Delta C(0)$ is the capacitance change due to the pulse at t = 0. For the exponential transients S(T) will be given by

$$S(T) = \exp (- t_1/\tau) \; [1 - \exp(-\Delta t/\tau])) \qquad (3.75)$$

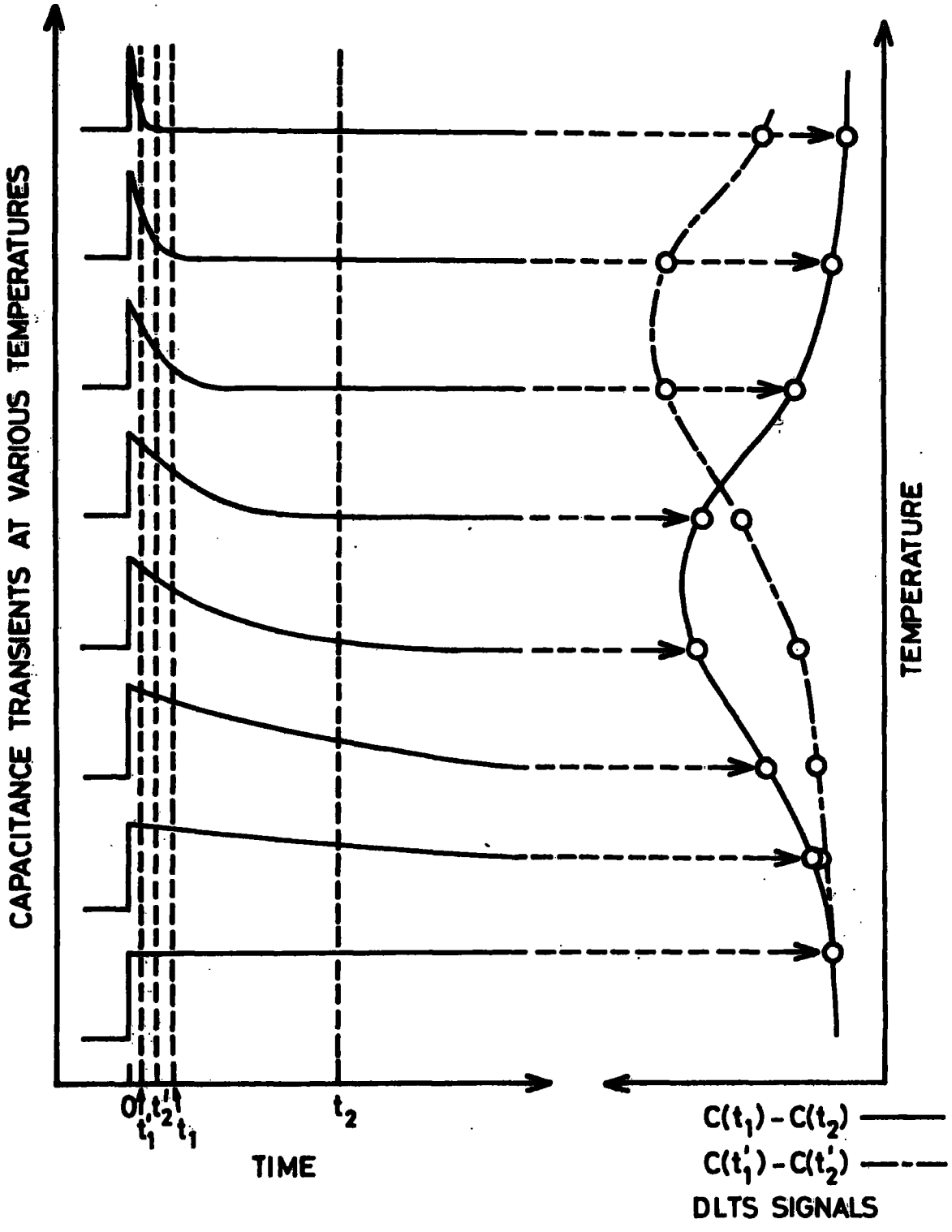

FIGURE 3.10 Implementation of a rate window by means of a double-boxcar integrator[50].

where $\Delta t = t_2 - t_1$ and the temperature dependence of τ is given by $\tau = 1/e^t$.

When a particular trap is considered, τ_{max} will be defined as the value of τ at the maximum of the $C(t_1) - C(t_2)$ versus T spectrum. The relationship between τ_{max} and t_1 and t_2 is given by

$$\tau_{max} = (t_1 - t_2)/[\ln(t_1/t_2)] \qquad (3.76)$$

The emission rate corresponding to the peak observed in a DLTS thermal scan is a precisely defined quantity. The time constant for electron emission for example can also be written in the form of $\tau_n = (N_c < v_n > \sigma_n)^{-1} \exp(\Delta E_T/kT)$. Where the pre-exponential coefficient (in SI units) is given by $\frac{2.8 \times 10^{-56}}{m_e^* T^2 \sigma_n}$. Thus by measuring the temperatures at the maxima of the DLTS signals and calculating τ_{max} from eq. 3.76 should give a straight line for the plot of $\ln(\tau t^2)$ against $1000/T$. The line yields the ionisation energy, ΔE_T, of the trap from the slope and the capture cross-section at infinite temperature $\sigma_n(\infty)$ from the intercept on the $\ln(\tau T^2)$ axis.

DLTS is a highly versatile and useful technique for detecting fast non-radiative recombination centres which cannot be easily identified by other methods. This can be done by simply biasing the specimen in favour of such fast capturing traps while suppressing the signal from the slower traps by using very short pulses. These pulses will be able to fill a fast trap but will be unable to fill slower traps sufficiently. Thus varying the pulse width is a very effective way of discriminating against signals from less interesting traps.

(d) Optical Deep Level Transient Spectroscopy (ODLTS)

If electric pulses are replaced by optical ones, the DLTS technique is referred to as optical DLTS (ODLTS)[51]. This mode of operation is very useful in the analysis of minority carrier traps in Schottky barriers or MIS devices. Since most of the II-VI compounds cannot be made p-type, minority carrier injection is not possible. Therefore recourse to ODLTS on MS structures is the only alternative for the characterisation of hole traps in these materials.

The principles of operation reviewed above for DLTS are valid for ODLTS. The details of the measuring techniques for both DLTS and ODLTS are described in Chapter 4.7.

REFERENCES - CHAPTER 3

1. W. Kohn, Solid State Phys. 5 (1957) 257.
2. T. H. Ning and C. T. Sah, Phys. Rev. B4 (1971) 3468.
3. D. M. Larson, Phys. Rev. 187 (1969) 1147.
4. H. H. Woodbury and M. Aven, Phys. Rev. B9, 12 (1974) 5195.
5. H. G. Grimmeiss, Ann. Rev. Mat. Sci. (1977) 341-376.
6. F. A. Kröger, The Chemistry of Imperfect Crystals, 1964 North-Holland Amsterdam.
7. M. Jaros, Deep Levels in Semiconductors, 1982, Adam Hilger Ltd. Bristol.
8. S. T. Pantelides and C. T. Sah, Phys. Rev. B10 (1974) 621.
9. S. T. Pantelides and C. T. Sah, Phys. Rev. B10 (1974) 638.
10. P. W. Anderson, Phys. Rev. 124 (1961) 41.
11. G. Lucovsky, Solid St. Commun. 3 (1965) 299.
12. H. B. Bebb and R. A. Chapman, Proc. 3rd Int. Conf. on Photocond. Pergamon Press, New York, 1971, p.245.
13. H. B. Bebb, Phys. Rev. 185 (1969) 1116.
14. H. G. Grimmeiss, C. Ovren, and J. W. Allen, J. Appl. Phys. 43 (1976) 1103.
15. De Bois, 'Deep level thermal and optical spectroscopy', Electronic structure of crystal defects and disordered systems, Les Editions de Physique, Aussois 1980.
16. H. Kukimoto, C. H. Henry and F. R. Meritt, Phys. Rev. B7 (1973) 2486.
17. C. H. Henry and D. V. Lang, Phys. Rev. B15 (1977) 989.
18. D. V. Lang and C. H. Henry, Phy. Rev. Lett. 35 (1975) 1525.
19. H. K. Henisch, Rectifying semiconductor contacts, Oxford Univ. Press 1957, Oxford.
20. E. H. Rhoderick, Metal-semiconductor contacts, Clarendon Press 1980, Oxford.

21. J. Bardeen, Phys. Rev. 71 (1947) 717.

22. C. G. Scott and C. E. Reed 'Surface of phosphors and semiconductors', Academic Press 1975, London.

23. W. Shockley, Phys. Rev. 56 (1939) 317.

24. A. M. Cowley and S. M. Sze, J. Appl. Phys. 36 (1965) 3212.

25. W. Schottky and E. Spenke, Wiss. Verof Siemens-Werken, 18 (1939) 225.

26. H. A. Bethe, M.I.T. Rad. Lab. Rep. 43-12 (1942).

27. R. G. Wheeler and J. O. Dimmock, Phys. Rev. 125 (1962) 1805.

28. C. R. Crowell and S. M. Sze, Sol. Stat. Elec. 9 (1966) 1035.

29. S. M. Sze, Physics of semiconductor devices, John Wiley and Sons, New York (1969).

30. A. Y. C. Yu and E. H. Snow, J. Appl. Phys. 39 (1968) 3008.

31. R. H. Fowler, Phys. Rev. 38 (1931) 45.

32. C. R. Crowell, W. G., Spitzer, L. E. Howarth and E. E. Labate, Phys. Rev, 127 (1962) 2006.

33. H. C. Card and E. H. Rhoderick, J. Phys. D : Appl. Phys. 4 (1971) 1589.

34. A. M. Cowley, J. Appl. Phys. 37 (1966) 3024.

35. A. M. Goodman, J. Appl. Phys. 34 (1963) 329.

36. S. J. Fonash, J. Appl. Phys. 54 (1983) 1966.

37. J. S. Blakemore, Semiconductor Statistics, Pergamon Press, Oxford (1962).

38. O. Engstrom and A. Alm, Solid-State Elec. 21 (1978) 1571.

39. G. Vincent, D. Bois and P. Pinard, J. Appl. Phys. 46 (1975) 5173.

40. G. I. Roberts and C. R. Crowell, J. Appl. Phys. 41 (1970) 1767.

41. Y. Zohta, Solid State Elec. 16 (1973) 1029.

42. L. C. Kimmerling, J. Appl. Phys. 45 (1974) 1839.

43. J. M. Noras, J. Phys. C : Solid State Phys. 14 (1981) 2341.

44. C. T. Sah, L. Forbes, L. L. Rosier and A. F. Tasch Jr. Sol. Stat. Elec. 13 (1970) 759.

45. G. L. Miller, D. V. Lang and L. C. Kimmerling, Ann. Rev. Mat. Sci. 1977, p.377.

46. H. G. Grimmeiss, Inst. Phys. Conf. Ser. 22 (1977) 187.

47. H. G. Grimmeiss and L. A. Ledebo, J. Appl. Phys. 46 (1975) 2155.

48. P. F. Lindquist and R. H. Bube, J. Appl. Phys 43 (1972) 2839.

49. B. Monemar and H. G. Grimmeiss, Prog. Cryst. Growth Charac. 5 (1982) 47.

50. D. V. Lang, J. Appl. Phys. 45 (1974) 3023.

51. A. Mitonneau, G. M. Martin and A. M. Mircea, Int. Symp. GaAs Edinburgh 1976.

CHAPTER 4

EXPERIMENTAL METHODS

4.1 INTRODUCTION

As explained earlier because CdSe is considerably less well researched than most II-VI compounds, a wide range of experimental methods have been employed here to obtain a broad characterisation. The present chapter describes the major experimental techniques used together with the methods of preparing photoconductive samples. The procedures for the preparation of the substrate materials for the fabrication of Schottky diodes are given in their respective sections.

4.2 CRYSTAL GROWTH

CdSe crystals used during the course of the present study were grown in this laboratory using a vapour phase technique originally developed here for CdS[1]. The technique is based on the sublimation method devised by Piper and Polich[2] which utilises a self-sealing technique to ensure that congruent evaporation is achieved. Starting material of polycrystalline CdSe powder was first sublimed in a stream of argon and then allowed to recrystallise as needles, rods and platelets. These were lightly ground and loaded directly into the specially constructed silica growth tubes, which were evacuated and sealed. In order to obtain good matter transport it was necessary to maintain the total pressure in the growth tube close to the P_{min} condition[3]. Consequently the growth tubes were connected to a small, independently heated reservoir containing either selenium or cadmium. The required P_{min} condition was then simply fulfilled by controlling the temperature of the reservoir as appropriate. The growth tube was

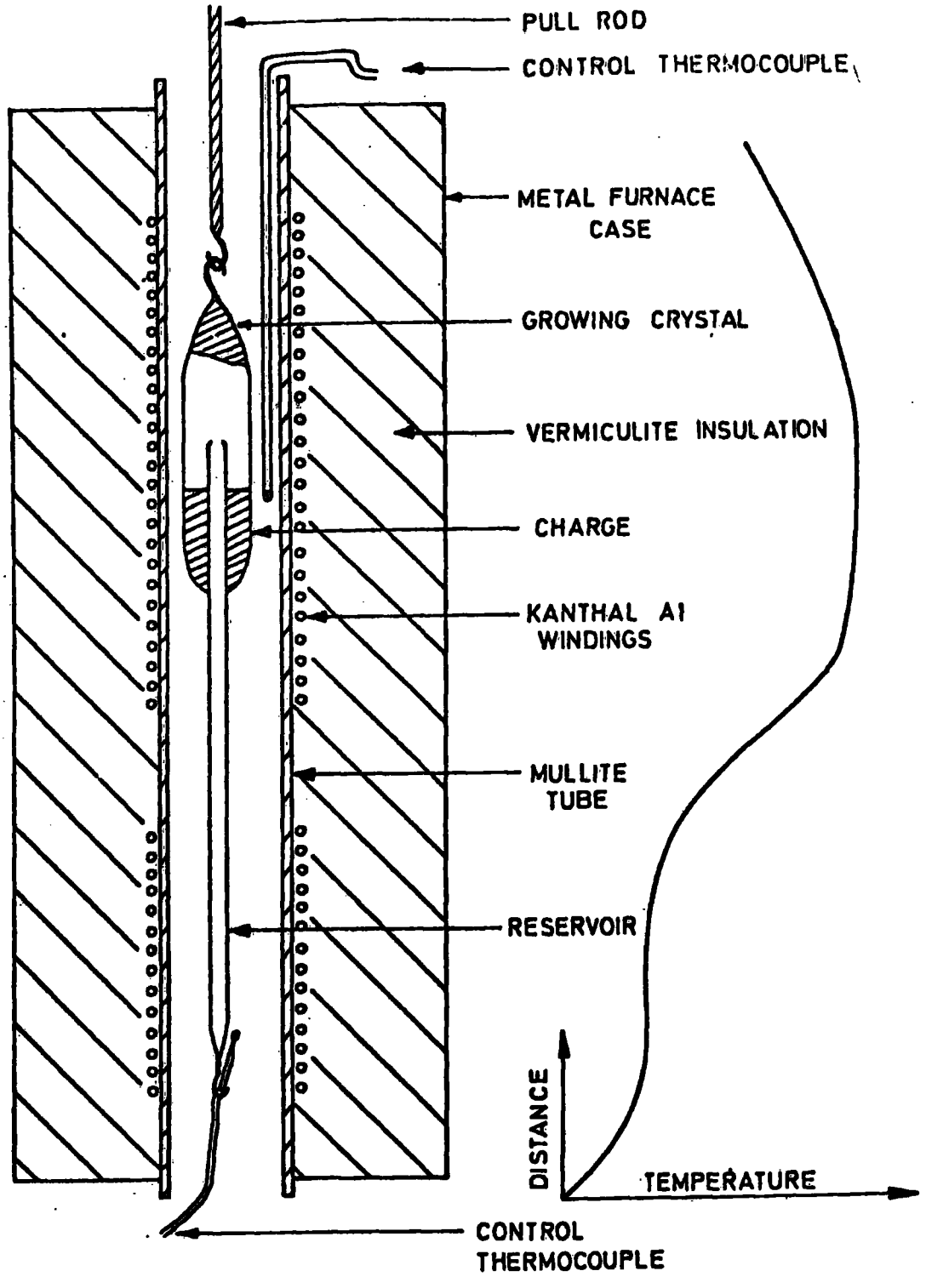

FIGURE 4.1 **Experimental arrangement for the growth of CdSe single crystals from the vapour phase.**

inserted into the furnace such that the charge was initially in a flat portion of the temperature profile (Fig. 4.1). The tube was then gradually withdrawn at a rate of between 0.5 and 1.5 mm/hour along the temperature gradient. Nucleation and growth proceeded from the cooler tip, producing after about 10 days, a cylindrical single crystal boule of CdSe about 1 cm in diameter and 3 c m in length. The boules were oriented using the Laue back-reflection technique and were then cut into dice with dimensions of 4 x 4 x 1 mm^3 so that the large area faces lay parallel with the (0001) basal plane.

4.3 X-RAY POWDER PHOTOGRAPHY

It was found that the hexagonal (wurtzite) structure of an as-grown CdSe crystal could be transformed to the cubic (sphalerite) phase by mechanical polishing and heat treatment. X-ray powder photography was used to investigate the phase transformation of CdSe. While powder produced from crushed single crystal material exhibited the hexagonal structure, ball-milled powder from the same single crystal boule displayed the cubic structure. Mechanical polishing of single crystals also led to work-damaged surface layers with the cubic structure. The lattice parameters of such layers were measured using reflection high energy electron diffraction (RHEED) with the electron beam in a JEOL JEM 120 electron microscope incident at grazing angle on the polished crystal surfaces. The X-ray and RHEED results are compared and described in Chapter 5.

4.4 RESISTIVITY CONTROL TECHNIQUES

Because the resistivities of the as-grown CdSe crystals were very low, of the order of (10^{-2} Ω cm), the material was not suitable either for fabrication into barrier layer devices, or for bulk photoconductors.

Consequently, several methods have been employed to increase the resistivity to an appropriate value. The techniques used are summarised below.

4.4.1 Annealing in Selenium Vapour

Annealing in selenium vapour was carried out in silica tubes divided into two parts by a small constriction. The dice were placed in one half and selenium in the other. After evacuation and sealing, the tube was placed in a two zone furnace which provided independent control of the selenium temperature and hence the Se-partial pressure over the dice (Fig. 4.2). To obtain moderate resistivity, (1-1000 Ω cm) substrate material for device making samples were heated at about 550°C in a partial pressure of selenium of 6×10^{-3}A. Higher temperatures and partial pressures of selenium were used to produce high resistivity crystals ($\rho > 10^6$ Ωcm) for photoconductors. The annealing period was also varied from 3 days to several months.

4.4.2 Copper Doping

Since copper acts as an acceptor impurity in CdSe, the low resistivity of the as-grown crystals could be increased by introducing copper into the material. After a layer containing copper had been deposited by some method, i.e. by evaporation of the metal or by the production of Cu_2Se by chemical exchange, the samples were held at 650°C for several hours in sealed silica tube filled with argon. Experiments showed that the diffusion of copper into CdSe was quite rapid; i.e. copper could be driven into a 1 mm thick CdSe crystal in about 2 hrs. On the other hand the different methods used to deposit the copper could give different results, presumably according to the different valence states of the copper. A summary of these methods is given below.

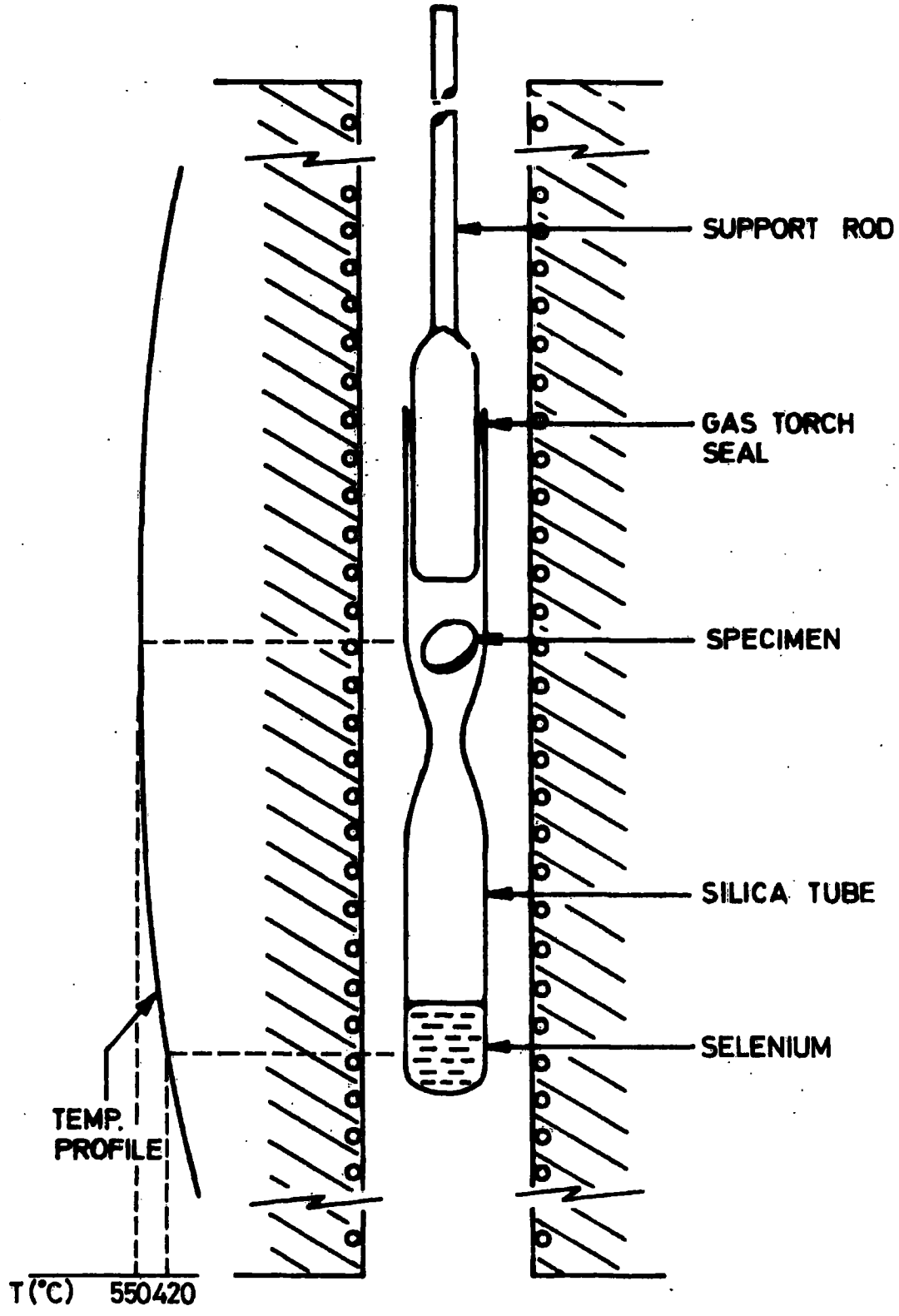

FIGURE 4.2 Experimental arrangement for annealing in selenium vapour

(a) Copper Evaporation

Metallic copper was evaporated onto the polished and concentrated HCl etched CdSe dice in a vacuum of 10^{-5} torr. The amount of copper for the evaporation was calculated according to the required resistivity of the samples. To obtain moderate resistivity (1-1000 Ω cm) the mass of copper required was usually in the range of ($\sim$5) mg.

(b) Plating Solution

The dice which were mounted onto a glass substrate with Lacomite, were dipped into an aqueous solution containing 1 g of cuprous chloride for about 20 s. This solution is comprised of 75ml of deionised water, 12ml of concentrated HCl and 7ml of hydrazine hydrate. The resistivity of the CdSe crystals could be increased to the very high values ($\rho > 10^6$ Ωcm) after the diffusion process and the resultant samples were used as photoconductors.

(c) Dilute Plating Solutions

Dilute plating solutions were prepared by dissolving 100 mg of CuCl in 25cc concentrated HCl and diluting a very small quantity of this solution with water. Dilute solutions of 1.10^{-5} g/cc to $2x10^{-3}$ g/cc were used to obtain moderate resistivity samples. Although the quantity of copper in the dilute solutions was reduced by some 10^6 times compared with the normal prepared plating solution, highly resistive (10^4-10^5)Ωcm samples were still sometimes obtained. These samples are referred to as low copper doped crystals in this thesis. In fact the results obtained from atomic absorption spectroscopy clearly identified the differences in the quantity of copper in the samples which were immersed in different strength plating solutions.

(d) Copper-Sulphate Bath

Some samples were dipped into an aqueous solution of $CuSO_4$ at 80°C and then were also found to be very highly resistive but less

photoconductive after the diffusion treatment. The electrical and optical characteristics of these samples were quite unstable.

4.4.3 Annealing in Cadmium Vapour

In an attempt to control the resistivity, some highly resistive Cu-doped samples were re-annealed in Cd-vapour to reduce their resistivity. This was done in similar silica tubes to those used for selenium annealing (Sec. 4.4.1), with the selenium charge replaced by cadmium and the temperature increased to 650°C.

4.5 SAMPLE PREPARATION AS PHOTOCONDUCTORS

The dice cut from the single crystal boule were first mechanically polished with alumina powder to remove the saw marks and damage produced by the diamond wheel. After polishing, the samples were etched in concentrated HCl for a few minutes and then washed in methanol. The dice were then subjected to their respective annealing or doping treatments as described in sec. 4.4 to raise the resistivity. The heat treated dice were again polished, etched and washed to provide clean, smooth surfaces on which to make ohmic contacts.

4.5.1 Ohmic Contacts

Ohmic contacts were made on freshly etched and cleaned surfaces of CdSe crystals using pure metallic indium wire applied two different ways. In the first method a short length of indium wire was lightly pressed on the surface of the dice which was then heated in argon at 240°C for a few minutes. After the indium had melted the samples were cooled to room temperature while still in the argon ambient. In the second method indium wire was applied to the samples simply with a special soldering iron to complete the contacts. Ohmic contacts made by these methods were found to be very similar and satisfactory.

4.6 REFLECTION HIGH ENERGY ELECTRON DIFFRACTION (RHEED)

A JEM 120 transmission electron microscope has been used in the reflection high energy electron diffraction (RHEED) mode to investigate the structure of the crystal surface and to follow the changes occurring in it during ageing, after mechanical polishing and after the growth of layers of Cu_2Se on it. The RHEED technique utilises Bragg's law of diffraction.

$$\lambda = 2 d_{hkl} \sin\theta \qquad (4.1)$$

where λ is the wavelength of the electrons, d_{hkl} is the interplanar spacing and θ is the Bragg angle between the electron beam and the diffracting atomic planes. In this work the accelerating voltage employed was 100 keV in all cases and the corresponding electron wavelength is 0.037Å. This, taken in conjunction with the fact that d_{hkl} is of the order of 2Å for most materials, leads to Bragg angles of less than 2°. In consequence only those crystal planes that are inclined at less than a few degrees to the surface of a specimen will give rise to electron diffraction. The conditions necessary to produce an electron diffraction pattern are illustrated in fig. 4.3. When the incident beam strikes the crystal plane (hkl) at the Bragg angle θ, then it is diffracted to form a diffraction spot at p on the fluorescent screen (or photographic film) at a distance L from the sample. Each plane (hkl) in real space produces a reciprocal lattice point which lies on a line perpendicular to the real space planes. In three dimensions the Bragg reflection condition can be determined using a geometrical model known as the Ewald sphere construction and this is illustrated in fig. 4.4. In this graphical representation of Bragg's law of

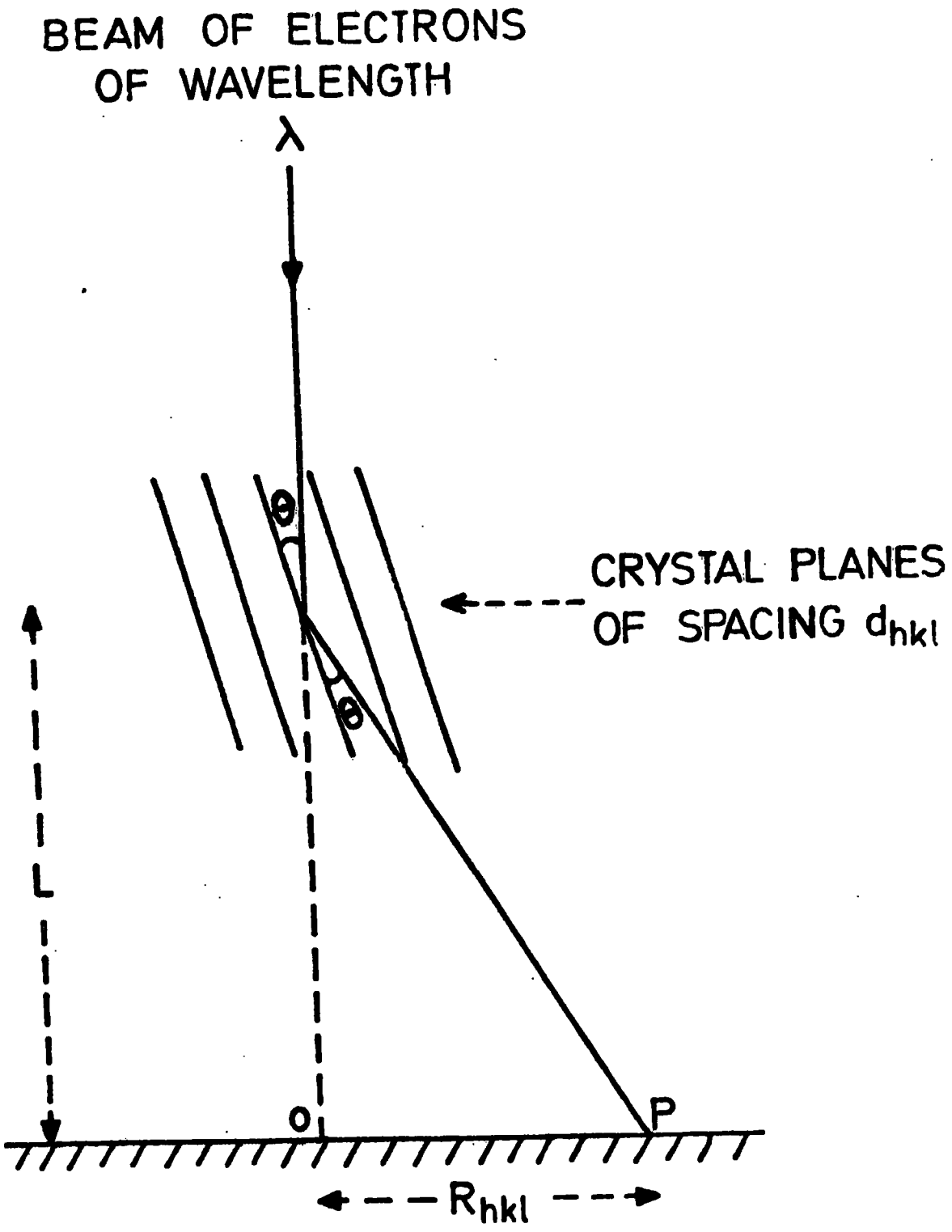

FIGURE 4.3: Schematic diagram illustrating the RHEED technique

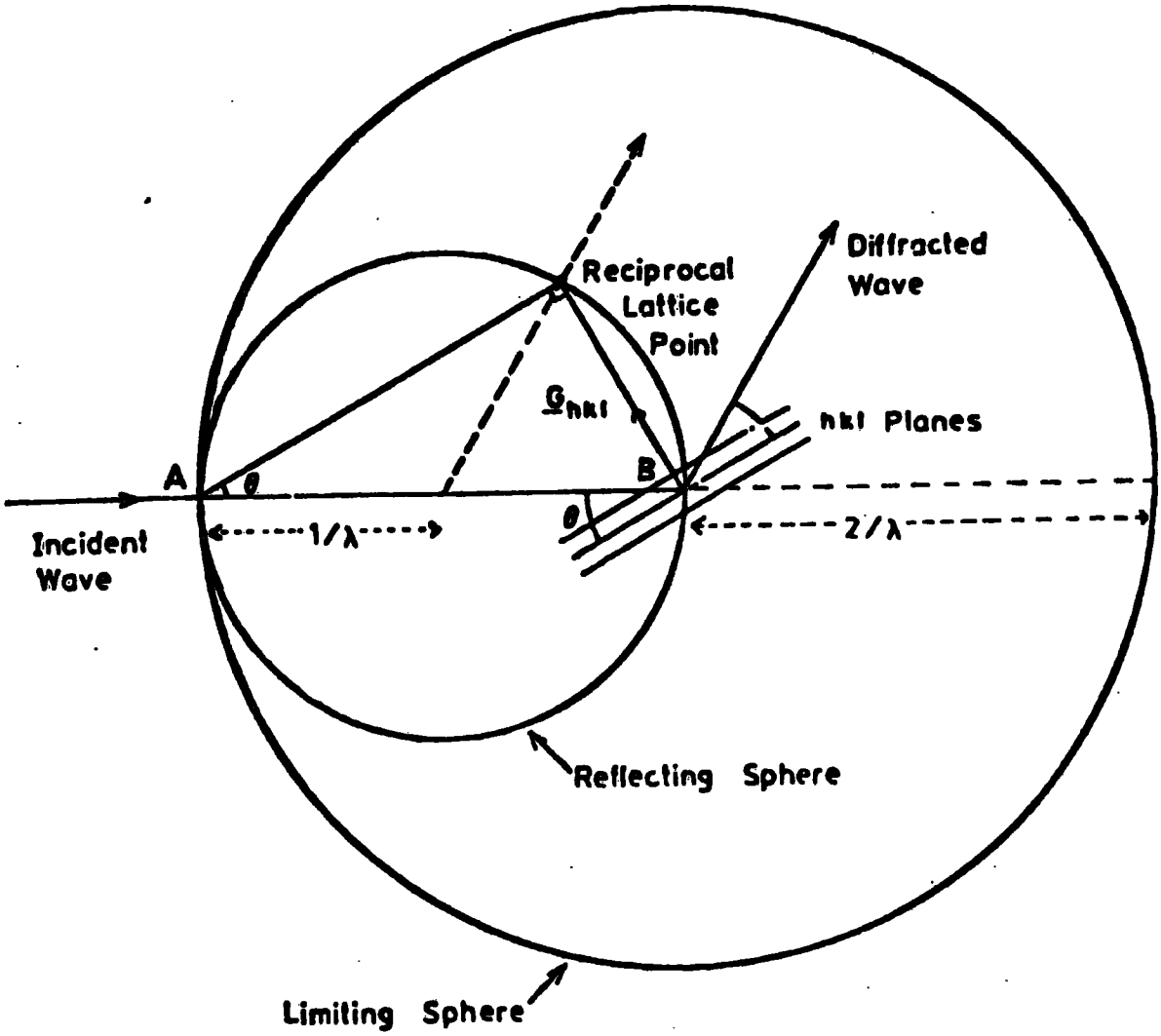

FIGURE 4.4: Ewald's sphere construction

diffraction, constructive interference occurs only when the reflection sphere intersects points in the reciprocal lattice. Since the radius of the sphere is $1/\lambda$, it is very large in comparison with the reciprocal lattice distances of $1/d_{hkl}$ for the diffraction of a beam of high energy electrons. In fact, at high energies, such as 100keV, the reflection sphere can be approximated to a plane section through the reciprocal lattice, and the RHEED pattern corresponds to this plane section lying perpendicular to the direction of the incident beam.

The advantages of the RHEED technique over other techniques such as X-ray diffraction can be summarised as follows[5]:

(a) The technique is easy to apply and the observations are straight forward to interpret.

(b) It is a non-destructive technique which requires minimal specimen preparation.

(c) It is particularly useful in the investigation of thin surface layers of the order of several microns or less whereas X-rays are not applicable.

(d) Changes in the complete diffraction pattern may be clearly observed on a fluorescent screen as the crystal orientation and diffraction conditions are changed. Again no such facility is possible with X-ray diffraction.

(e) The exposure time required for the photographic recording of the diffraction pattern is of the order of seconds, while it is tens of minutes or even hours for X-rays.

(f) The examination of materials with interplanar spacings larger than 10Å can be made possible by varying the effective camera length L, which is done by adjusting the strength of the intermediate lens.

(g) The transformation from real to reciprocal space is easier to visualise than it is with X-ray diffraction because the necessary condition for crystal planes to diffract high energy electrons is that they should lie approximately parallel to the incident beam.

(h) As the angle for Bragg diffraction of electrons by typical crystal planes is less than 2 degrees, a diffraction pattern covering a large number of reflections in reciprocal space can be recorded on a flat photographic plate. With X-ray diffraction or LEED a large angular spread of the patterns has to be covered.

4.7 ELECTRICAL AND OPTICAL MEASUREMENTS

In general, two types of cryostat systems were used for the electrical and optical measurements. The simpler first type, shown in figure 4.5, was used mainly for the measurement of spectral response of photoconductivity, infrared quenching of photoconductivity etc. at liquid nitrogen temperature. The second type, shown in figure 4.6, is a gas exchange type cryostat. It was used in those experiments which required intermediate values of temperatures between liquid nitrogen and room temperature. The cryostat consists of a copper specimen block, fitted with a heater, and connected via the gas exchange vessel to a liquid nitrogen reservoir. The temperature of the specimen can be controlled with the heater and by varying the pressure and hence the thermal conductivity of the gas in the exchange vessel between the liquid nitrogen container and the heat exchanger block.

In both types of cryostat system, the temperatures were measured using copper-constantan thermocouples.

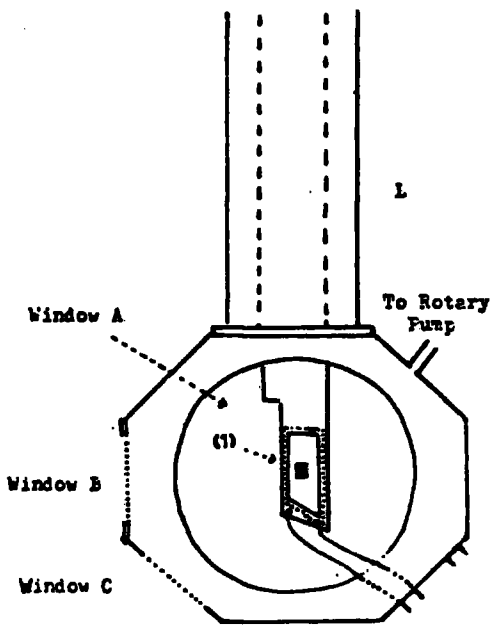

FIGURE 4.5 Cold-finger cryostat

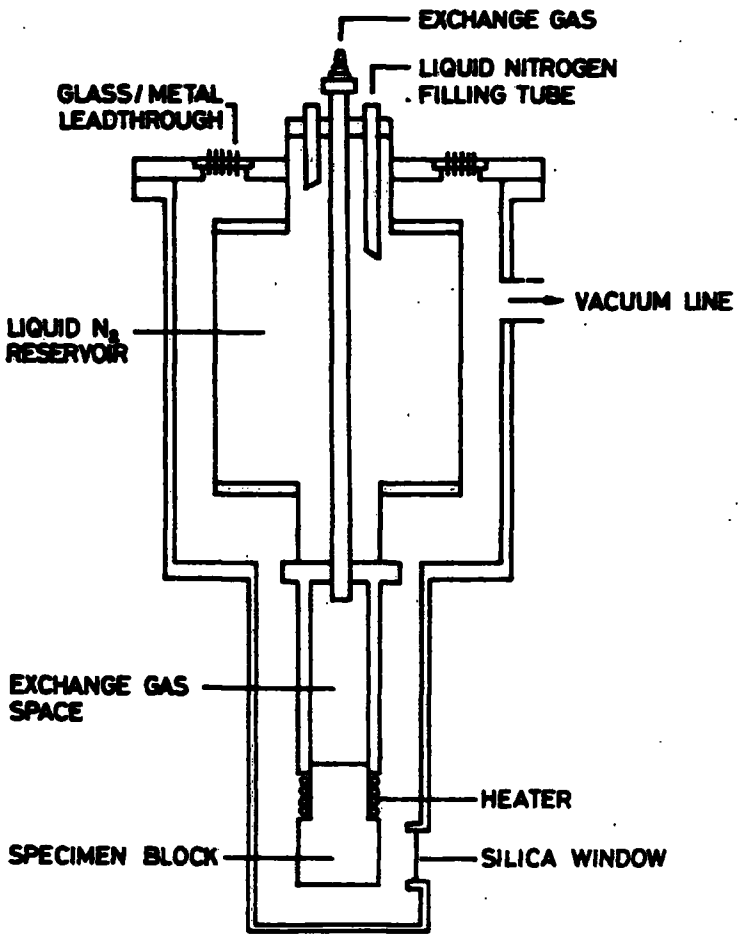

FIGURE 4.6 Gas-exchange cryostat

4.7.1 Current-Voltage Measurements

The current-voltage characteristics of the CdSe photoconductors and other devices were measured using Farnell (Type DM131) or Bradley (type 173B) voltmeters and low impedance Hewlett-Packard (type 3465B) or Keithley 602 electrometers. An automatic system consisting of a power supply, and Bryans model 21001 X-Y recorder was also used in the initial tests to monitor the change in characteristics with heat treatment or ageing.

A solar simulator of AM1 intensity with a 1.5KW quartz-halogen strip lamp was employed for the current-voltage characteristics recorded under illumination. A standard silicon PIN diode (type 10DF) was used in the calibration of the solar simulator by adjusting the distance of the sample platform from the source to provide 100 mW/cm^2 constant illumination. A 2 cm deep tray of flowing water was placed between the source and the sample platform to simulate atmospheric water vapour absorption.

4.7.2 Capacitance-Voltage Measurements

The capacitance of Schottky, MIS and heterojunction devices was measured as a function of bias voltage and frequency using an Ortec-Brookdeal Ortholoc model 9502 in the two-phase mode. The frequency in the range 5-240 KHz was monitored with a digital frequency meter Marconi TF 2430. The amplitude of the small A.C. signal voltage (usually 20-60mV peak-to-peak) was varied by an attenuator and was calibrated with an oscilloscope (telequipment type D1010). The block diagram of the capacitance-voltage measuring system for the high frequencies is shown in figure 4.7. The variable bias applied to the devices in this arrangement was provided by an integrated circuit voltage ramp, with an adjustable scan rate of 1 sec/volt to 1000

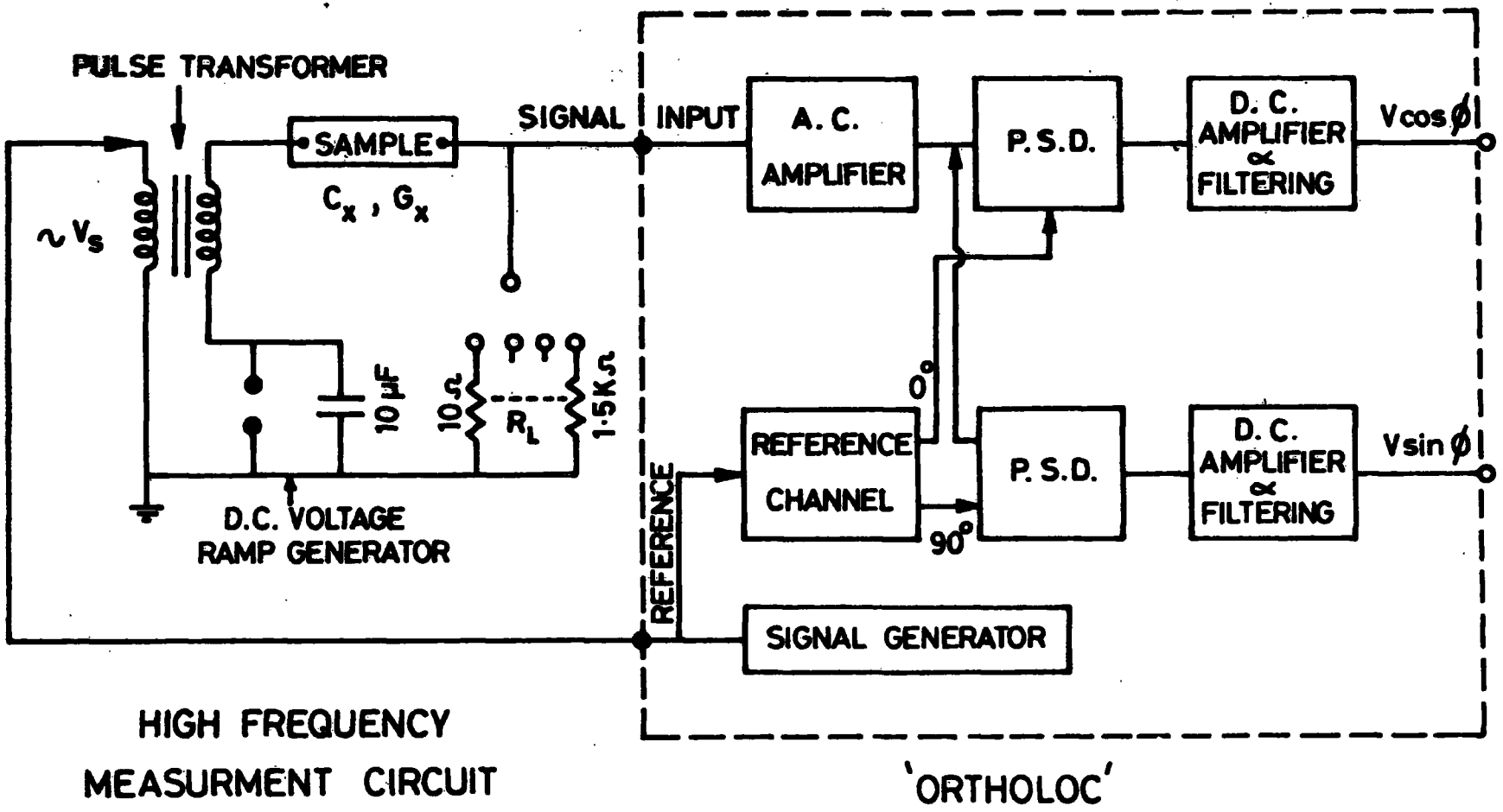

FIGURE 4.7 Block diagram of the capacitance-voltage measuring system

sec/volt. The ramp voltage was fed directly to the X input of a Hewlett-Packard X-Y-T recorder model 7041A. The Y input of this recorder was connected either to the in-phase or quadrature outputs of the Ortholoc, so that C-V or G-V characteristics could be plotted automatically. Standard silver-mica capacitors were used to calibrate the system before every measurement. Absolute values of device capacitance were determined by replacing it with a standard capacitor of a similar value to that estimated for the device. The other necessary condition to measure the correct values of capacitance and conductance with the circuit shown in fig. 4.7 is that $Y_{device} << Y_T$, where Y_T is the total admittance of the circuit. Variable resistances in the range 10Ω to 1.5KΩ provided the different ranges of device impedances.

In some experiments a Boonton model capacitance meter was used together with the automatic system instead of the Ortholoc.

4.7.3 The Spectral Response of Photoconductivity and Infra-Red Quenching

For the measurements of spectral response of photoconductivity and infra-red quenching, a Barr and Stroud double monochromator type VL2 with spectrosil "A" quality prisms was employed. A 250w, 24v quartz-halogen lamp with a variable power supply provided the light source at the input slit of the monochromator. The energy distribution of this light source together with the VL2 monochromator is shown in figure 4.8 This was measured using a Hilger and Watts thermopile FT 16301. The light source was chopped at 8Hz and the resulting thermopile output signal was recovered using a Brookdeal lock-in amplifier type 401 and a Brookdeal nanovolt preamplifier type 431.

Almost all of the spectral measurements were taken over the wavelength range from 0.6μm to 2μm. The experimental arrangement for

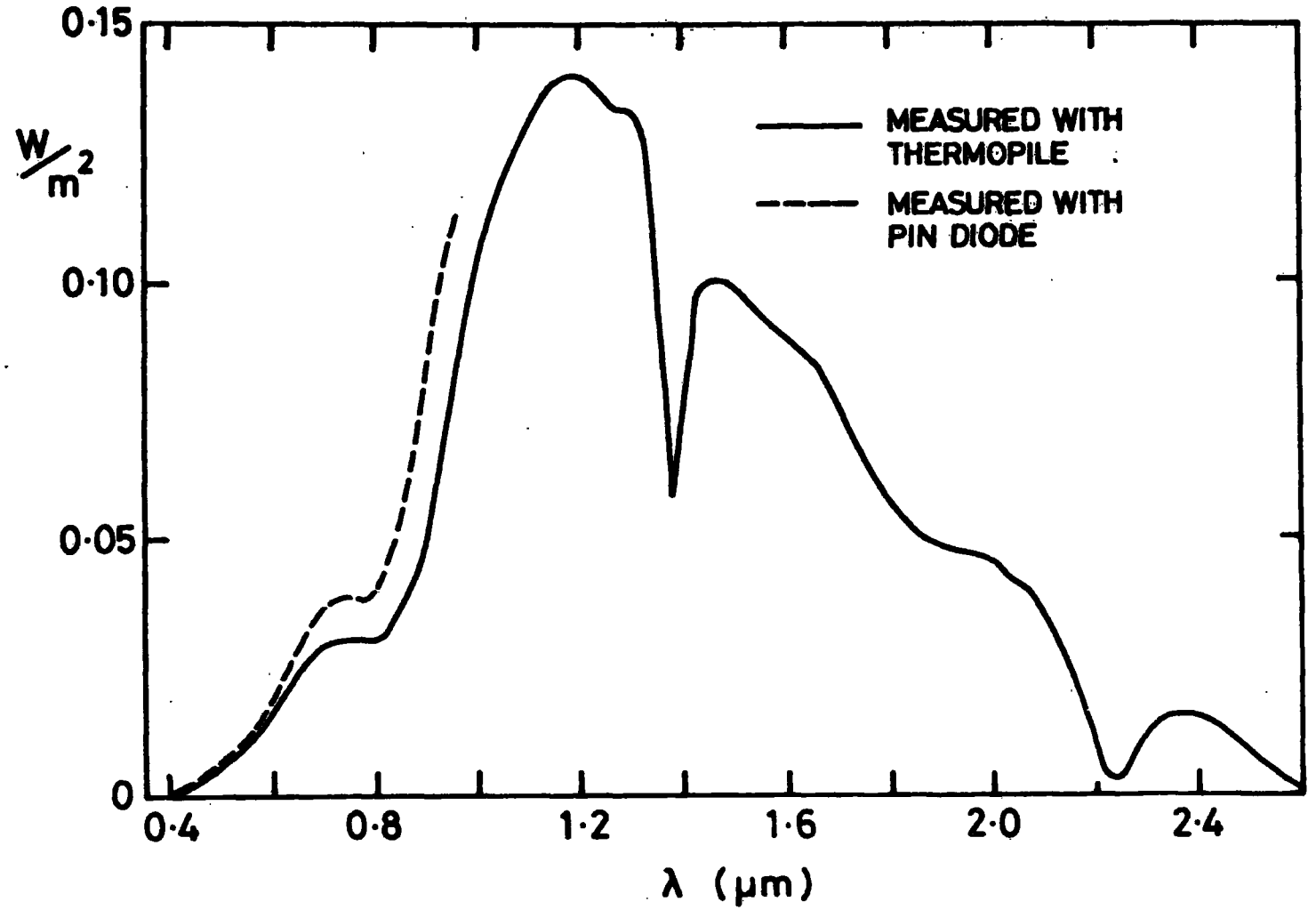

FIGURE 4.8 Energy distribution of light source and the monochromator

measurements of photoconductivity and infra-red quenching is shown in figure 4. 9 With infra-red quenching of photoconductivity the samples were exposed continuously to an additional constant light source through a combination of appropriate filters, while the samples were being scanned with monochromatic light from the monochromator.

The bias voltage applied across the sample was provided by a Farnell LT 30-1 power supply while the current was measured with a Keithley 602 electrometer and recorded on a Honeywell electronik 196 chart recorder.

4.7.4 Steady State and Transient Photocapacitance; Infra-red Quenching of Photocapacitance

Measurements of steady state and transient photocapacitance and infra-red quenching of photocapacitance were made using a combination of the experimental arrangements employed for the photoconductivity and capacitance work, see figure 4.10 Sometimes the Ortholoc was replaced with the Boonton capacitance meter, which operates at 1MHz, to verify the results and to eliminate any complication that might arise from the 200KHz maximum upper limit of the Ortholoc. These measurements were carried out in the gas exchange cryostat, since transient measurements were made normally and required a constant temperature to be maintained for relatively long periods of time. Comprehensive details about these photocapacitance techniques have been given by Sah et al[6].

4.8 DEEP LEVEL TRANSIENT SPECTROSCOPY (DLTS)

The block diagram of the DLTS system used is shown in fig. 4.11 The basic principles of the DLTS boxcar method have been established by Lang[7]. The main features of our system which differ from the boxcar method are; (1) computer control of the system, (2) data storage facility for offline analysis and (3) sampling DVM enabling many points on a simple transient to be sampled.

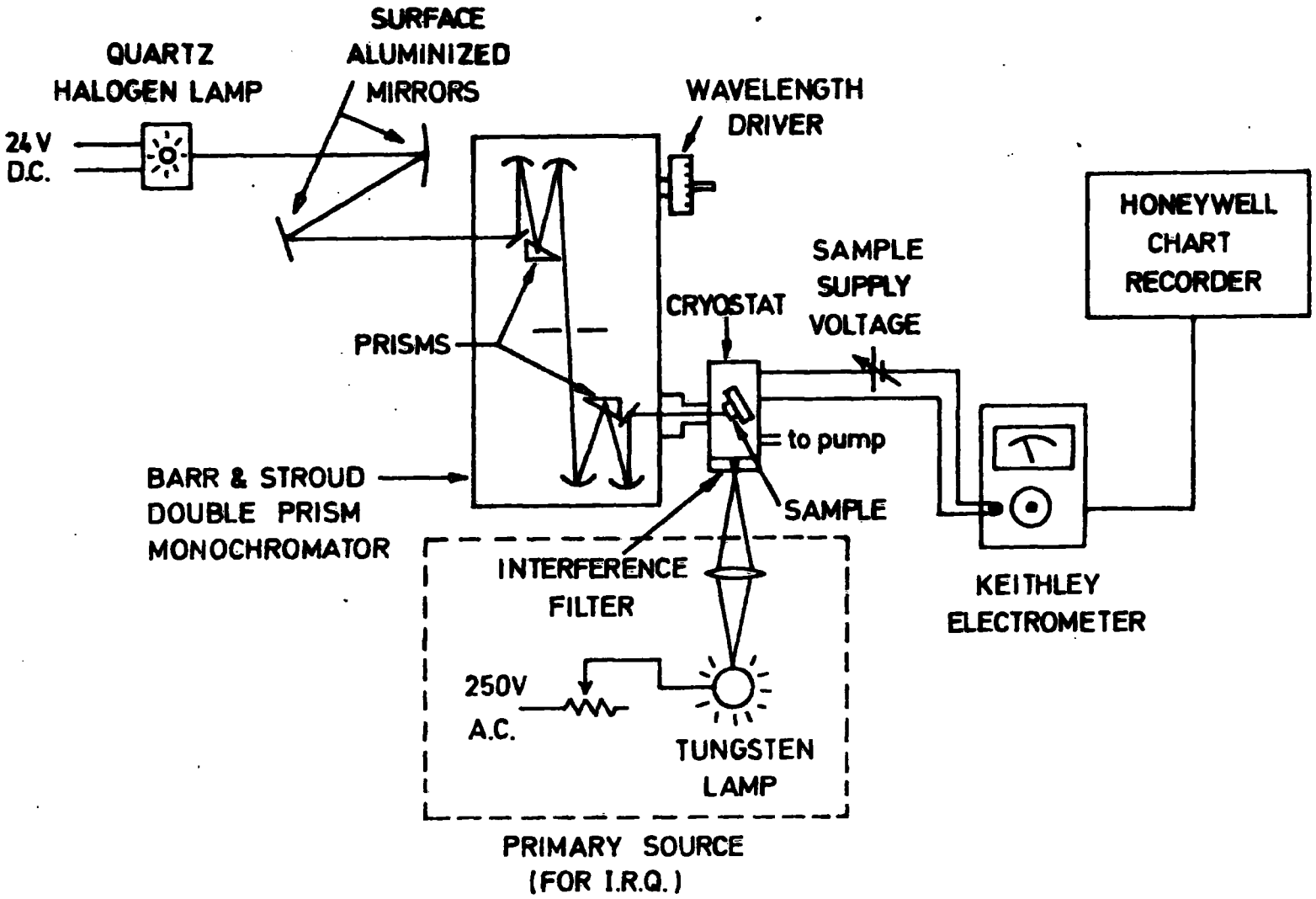

FIGURE 4.9 Experimental arrangement used for photoconductivity and infrared quenching measurements

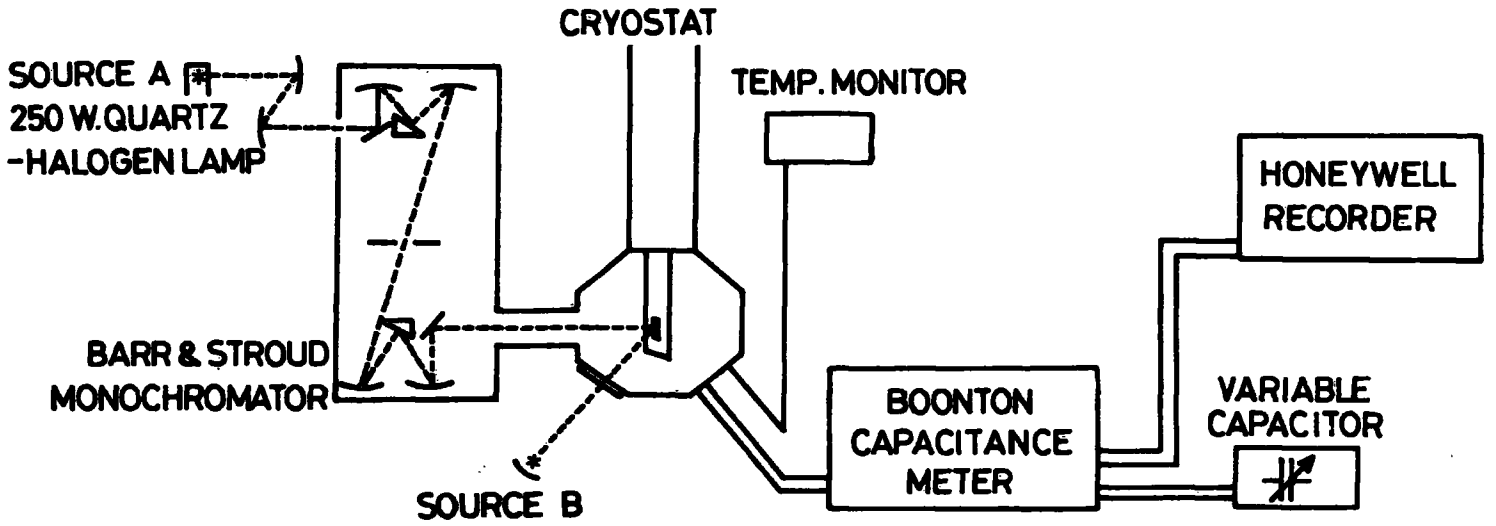

FIGURE 4.10 **Experimental arrangement used for photocapacitance measurements**

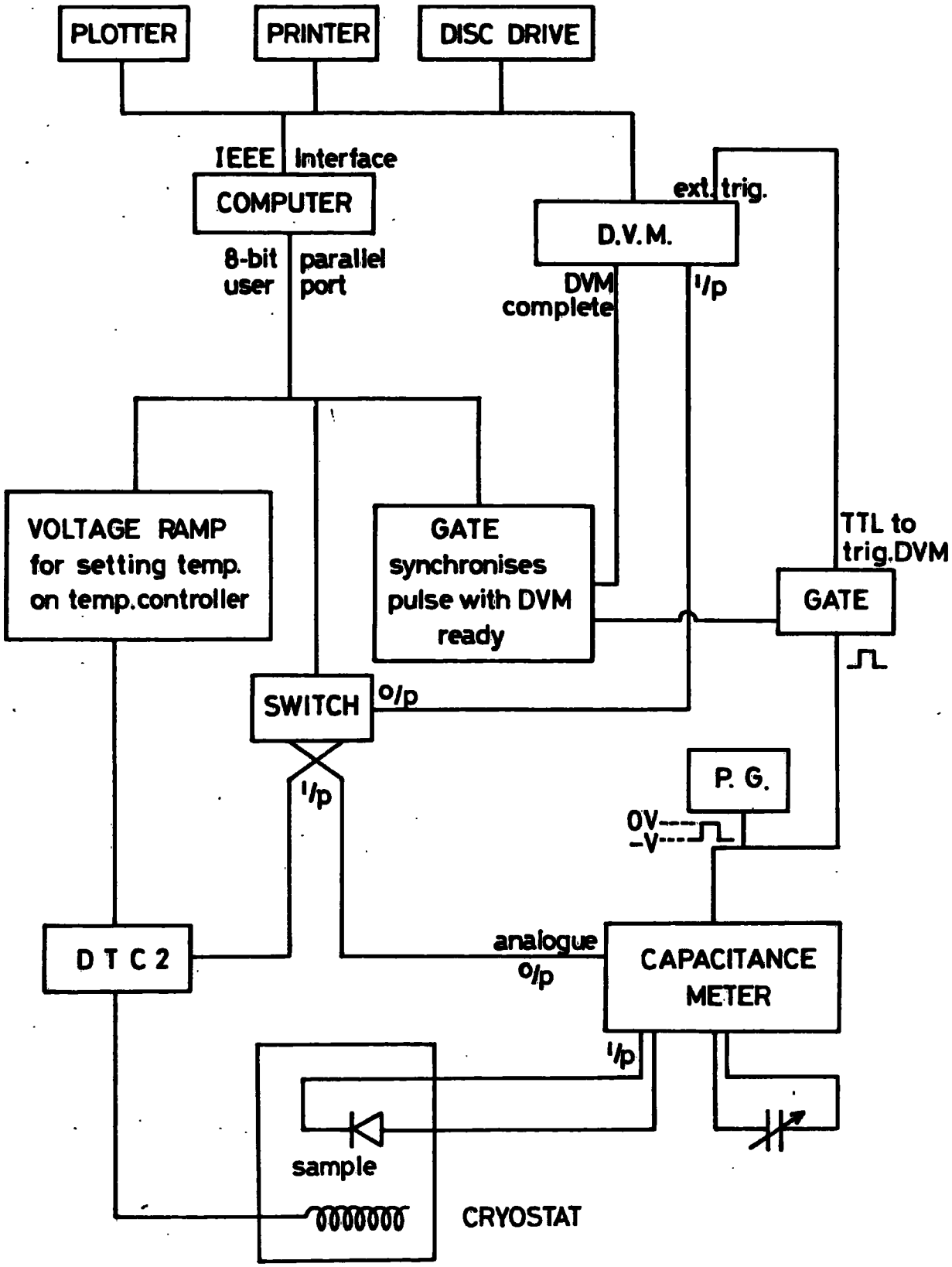

FIGURE 4.11 The block diagram of the DLTS system

The sample is mounted in the cryostat (Oxford Instrument DN704), which is then cooled down to liquid nitrogen temperature and left to stablise for at least ½ hour. Relevant information about each run (e.g. sample type, temperature range, heating rate, min/max gate delay, pulse repetition period, bias, Boonton scale etc.) is stored on a floppy disc during the stabilisation period. When the system is running the temperature controller ramps the temperature which is continually being monitored by the computer. When a set temperature has been reached, the DVM samples the transient at two fixed rates - 16 samples at 4.14 m sec/reading and 16 samples at 41.4 m sec/reading. This gives information about the traps with slow and fast time constants. The main limitation is the sampling rate of the DVM, with the fastest available being 4.14 m sec/reading so that traps with fast time constants (small ionisation energy/capture cross-section) cannot be studied. The data is subsequently sent to the computer which stores the collected information on the disc. A spectrum with a known time constant is plotted during the run to monitor the system as the run proceeds. Once the run has been completed, offline analysis of the data is carried out, and DLTS spectra and Arrenhius plots are made.

REFERENCES

1. L. Clark and J. Woods, J. Crystal Growth 3/4 (1968) 126.

2. W. W. Piper and S. J. Polich, J. Appl. Phys. 32 (1961) 1278.

3. M. R. Lorenz in Physics and Chemistry of II-VI Compounds, Eds. M.Aven and J. S. Prener, (North-Holland μ, Amsterdam 1967) 79.

4. B. D. Cullity, Elements of X-ray diffraction Addison-Wesley 1967.

5. G. J. Russell, Prog. Crystal Growth and Characterisation. 5 (1982) 291.

6. C. T. Sah, L. Forbes, L. L. Rosier and A. F. Tasch, Jr., Sol. State Elec. 13 (1970) 759.

7. D. V. Lang, J. Appl. Phys. 45 (1974) 3023.

CHAPER 5

EXPERIMENTAL RESULTS ON PHOTOCONDUCTIVITY AND INFRA-RED QUENCHING SPECTRAL RESPONSE

5.1 INTRODUCTION

Since CdSe is among the most sensitive of photoconductors its properties were investigated much earlier than those of most other photoconductive materials[1]. In general the study of photoconductivity in pure and intentionally doped CdSe has revealed energy levels associated with impurities and native defects which play very important roles in determining device characteristics. In contrast with the rather simple experimental arrangements used to investigate photoconductivity phenomena, the interpretation of the results is found to be very complex. This allows only a semiquantitative analysis of the localised energy levels within the bandgap to be made. More information about these localised energy levels can be obtained by using space-charge techniques which are discussed later together with junction device properties.

In this chapter four types of photoconductive samples are described. These are (1) flow run platelets (2) crystals heated in selenium vapour (3) crystals doped with copper and (4) crystals with mechanically polished surfaces. Copper incorporation in CdSe is of particular importance because it leads to a highly sensitive photoconductor and because of its role in Cu_2Se/CdSe heterojunction solar cells. Consequently three types of copper doping were investigated; high and low concentrations of copper were introduced by diffusion after plating Cu_2Se on to the surfaces of a crystal; low

concentrations were also obtained by heating crystals on to which a layer of metallic copper had been put down by vacuum deposition.

The basic theory and the experimental arrangements used for photoconductivity measurements have already been described in chapters 2 and 4. The spectral dependence of photoconductivity and infra-red quenching were measured at room temperature and liquid nitrogen temperature over a range of photonenergies from 0.59eV (2.08μm) to 1.95eV (0.64μm) and 0.54eV (2.28μm) to 1.2eV (1.02μm) respectively.

5.2 FLOW RUN PLATELETS

Platelets obtained at the first stage of the crystal growth process (chapter 4.2) were found to be more stoichiometric than the final single crystal boule grown from them. The resistivities of these platelets varied from 1 to 10^{10} Ω cm, whereas the single crystal material had a very low resistivity in the range 10^{-3} to 10^{-2} Ω cm. Indium contacts were made on selected high resistivity platelets using a special soldering iron. Some difficulty was often encountered because of the very brittle nature of the material. A linear I-V relationship was generally found for either polarity of applied bias indicating that the contacts were ohmic.

The spectral dependence of the photoconductivity of platelets measured at room and liquid nitrogen temperatures is shown in fig. 5.2.1 together with the lamp response curve. Threshold values (sudden increases in photocurrents as the wavelength is reduced) at 1.15, 1.31 and 1.48eV at room temperature suggested the presence of deep acceptor levels at 0.59, 0.43 and 0.26eV above the valence band edge. At liquid nitrogen temperature a single threshold at 1.22eV was observed corresponding to a level 0.62eV above the valence band. The peak at

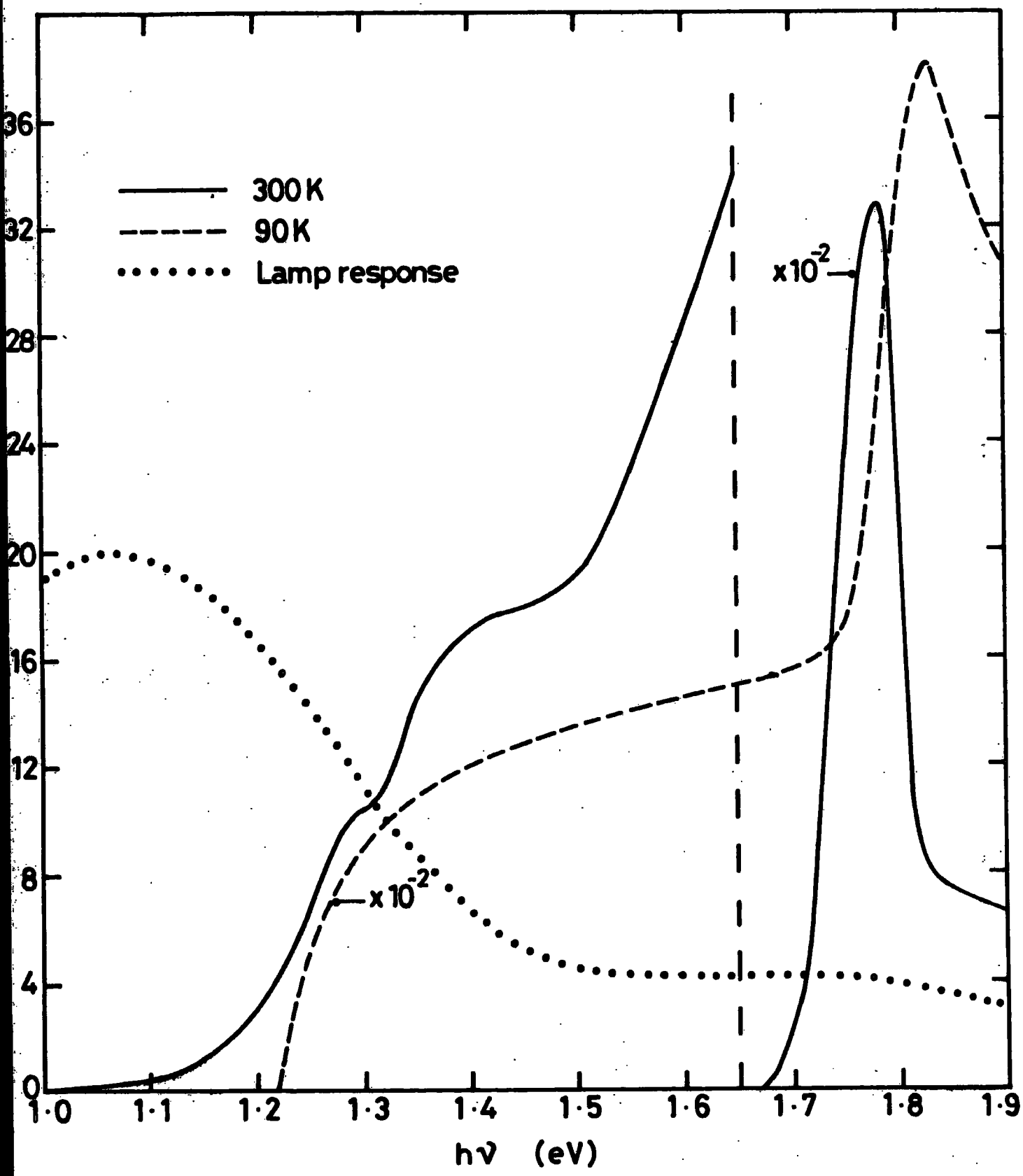

FIGURE 5.2.1 Spectral dependence of photocurrent at 90 and 300 K for as-grown platelets.

about 1.74eV at room temperature and 1.84eV at liquid nitrogen temperature is due to intrinsic photoconductivity i.e. band to band transitions. The ratio of intrinsic photoconductivity to extrinsic photoconductivity is small at liquid nitrogen temperature compared to that at room temperature.

Infra-red quenching of the photoconductivity of these samples was recorded at liquid nitrogen temperature by filtering the constant bias illumination with a combination of an infra-red absorption filter and a 0.7μm long pass filter. Fig. 5.2.2 shows the quenching spectrum of as grown CdSe platelets plotted as quenching percentages of the primary photocurrent. The well defined threshold at 0.64eV clearly locates the position of the main sensitising centre. The dip at about 0.9μm is attributable to the lamp response. Quenching did not occur at room temperature.

5.3 DISCUSSION

The photoconductivity of pure CdSe crystals has been extensively studied by Bube[2], Kindleysides and Woods[3] and Manfredotti et al[4]. According to the four-centre model[5] of photoconductivity, a large increase in photoconductive sensitivity occurs when the so called class II centres lie above their hole demarcation level. An approximate calculation of the hole demarcation level associated with these centres showed it to be about 0.8eV above the valence band edge at room temperature. (A value of $\sim 10^7$ for the ratio of the capture cross sections for these centres was taken from the literature). Under these circumstances the centres lie below the demarcation level and their occupancy would be determined by thermal exchange with the valence band rather than by recombination kinetics[2]. However, lowering the hole demarcation level, $E_{dp} < 0.35$eV by decreasing the temperature at the

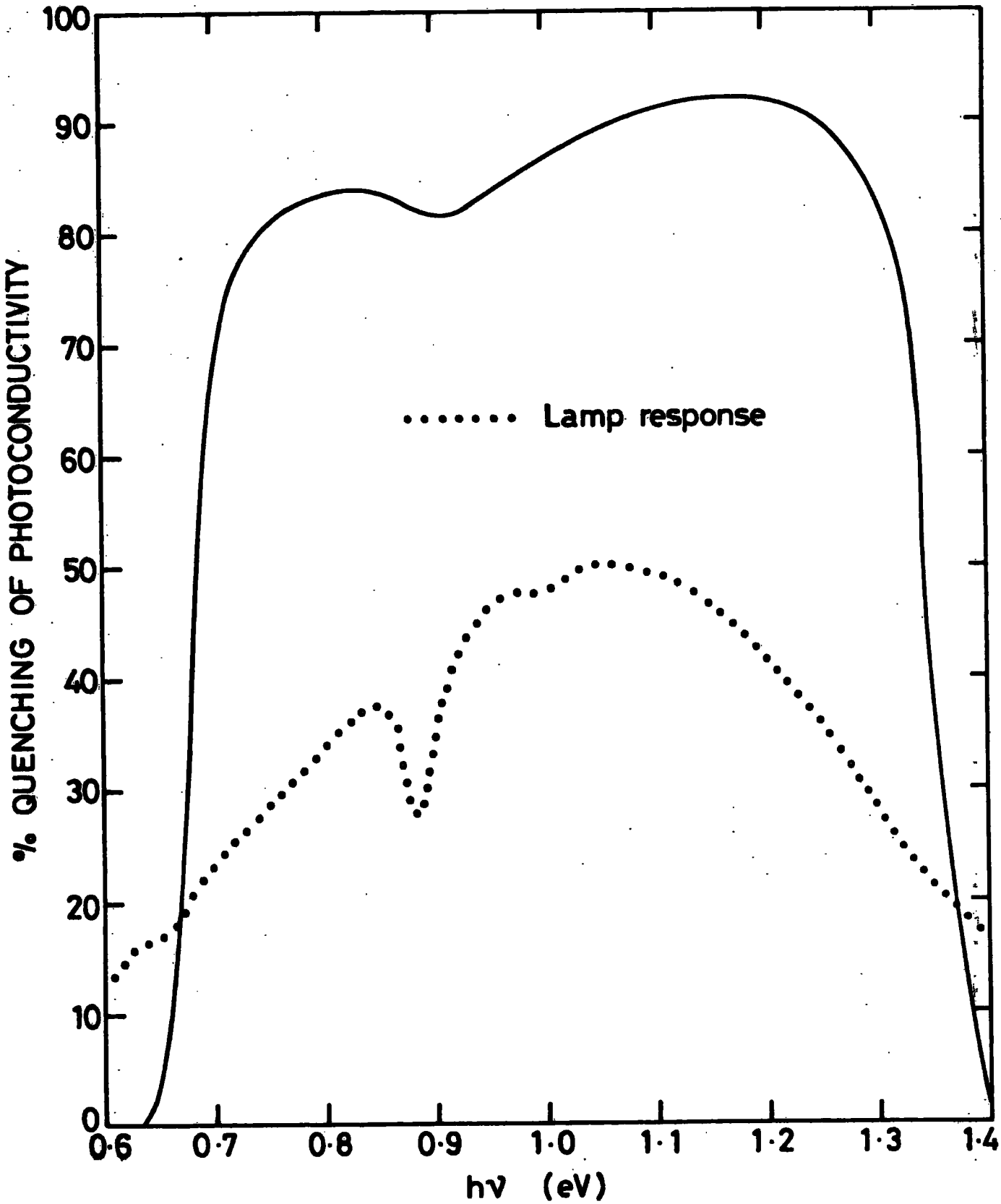

FIGURE 5.2.2 Infrared quenching of photocurrent at 90 K for as-grown platelets.

same light intensity would change the behaviour of these centres from hole traps to recombination centres, thus increasing the majority carrier lifetime and hence the photoconductivity. This explains the relatively large extrinsic photoconductivity response observed at liquid nitrogen temperature. The nature of the sensitising centres has been well established as doubly ionised cadmium vacancies[6.7.8]. The cross-section ratios of these coulomb repulsive type centres as large as $Sp/Sn = 10^8$ have been reported[9]. The infra-red quenching measurements not only confirm the existence of these centres but also provide a better estimate of their ionisation energy namely 0.64eV. This is in good agreement with the current literature describing the main sensitising centre in CdSe[10,11].

Similar calculations for the demarcation levels associated with 0.26 and 0.43 centres indicated that these centres lie below their demarcation levels at room temperature and behave as hole traps. At liquid nitrogen temperature their calculated demarcation levels would fall below the activation energies for both levels unless the 0.26eV level has a capture cross-section ratio greater than $S_p/S_n = 10^5$, (such a level in CdSe has been reported in several studies[12,13] and attributed to a singly ionised vacancy with a capture cross section ratio of $S_p/S_n \sim 10^3$ [4]). The disappearance of the 0.26 and 0.43eV levels in photocurrent spectra taken at liquid nitrogen temperature could be explained in one of two ways. They are either (a) singly ionised sensitising centres with small capture cross-section ratios $S_p/S_n < 10^2$ and in small densities or (b) class I centres which have opposing effects to the 0.64eV class II centres. In both cases the 0.26 and 0.43eV levels remain undetectable because of the large number of the

principal sensitising centres which dominate the photoconductive behaviour of the CdSe crystals.

5.4 SAMPLES ANNEALED IN SELENIUM

The non-stoichiometric growth of CdSe containing an excess of the cadmium component was first reported by Heinz and Banks[14]. As a result nearly degenerate CdSe crystals were produced i.e. they were very conductive and not photosensitive. It has been suggested that the shallow donors responsible for this behaviour are either selenium vacancies[15] or cadmium interstitials[16]. One well known method of obtaining photosensitive material is to anneal the highly conducting samples in selenium vapour to compensate these donors[16, 17]. The experimental procedure used to prepare photoconductive samples by annealing in selenium vapour was described in chapter 4.1.

The spectral dependence of photocurrent at 300K and 90K for an annealed crystal is shown in figure 5.4.1. Threshold values at photon energies of 0.87 and 1.55eV at 300K indicated the existence of a level near the middle of the bandgap and another some 0.19eV above the valence band edge. However at 90K threshold values of 1.03, 1.30 and 1.50eV were observed corresponding to energies 0.81, 0.54 and 0.34eV with respect to the top of the valence band. The ratio of the intrinsic to extrinsic photo response was found to be larger at 90K in contrast to the behaviour of the platelets. Measurements of the infra-red quenching of photocurrent were also made at liquid nitrogen temperature. A typical quenching spectrum of a selenium annealed sample is shown in figure 5.4.2 indicating possibly two different sensitising centres between 0.54 and 0.59 above the valence band.

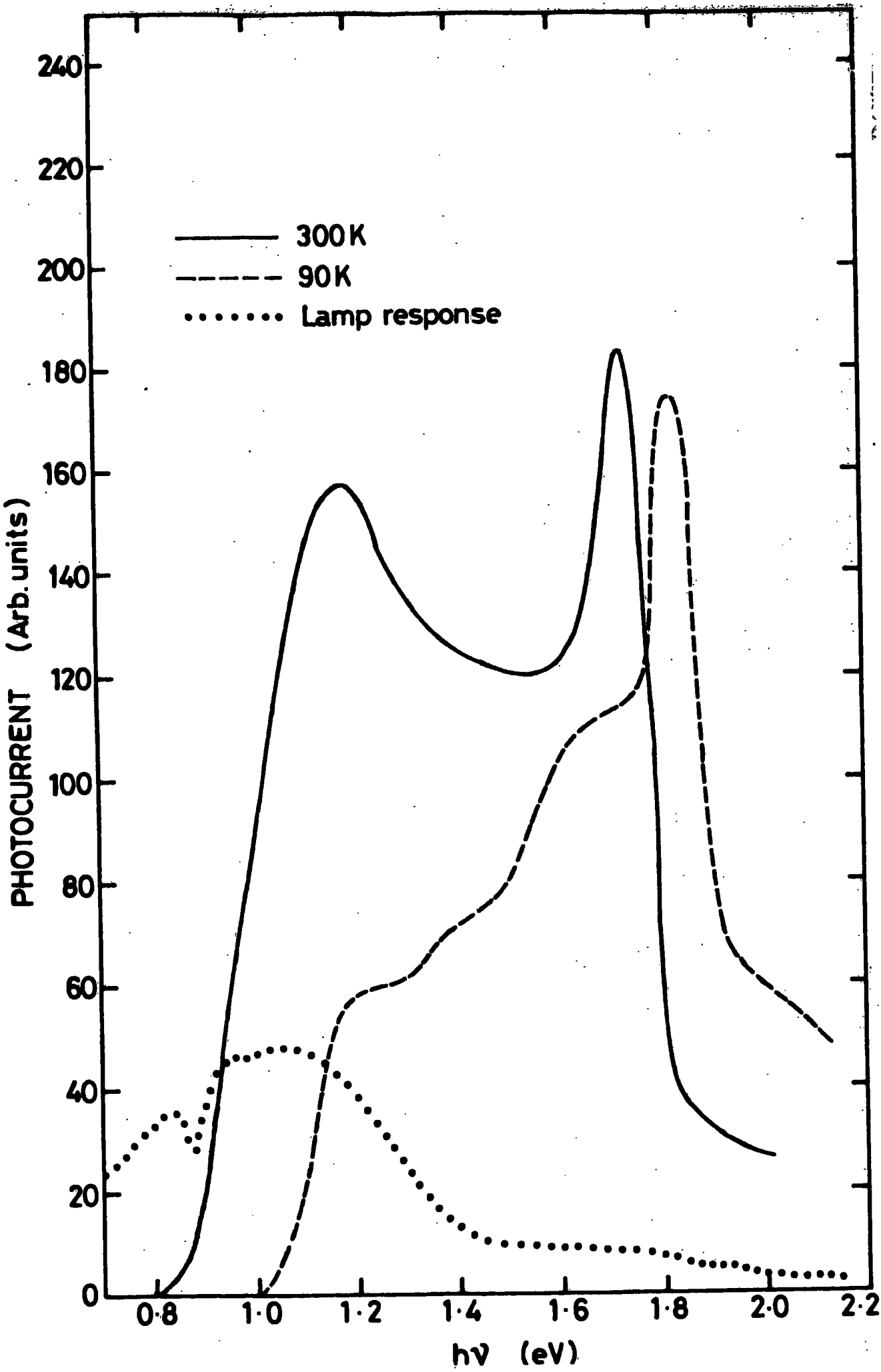

FIGURE 5.4.1 Spectral dependence of photocurrent at 90 and 300 K for samples annealed in selenium vapour.

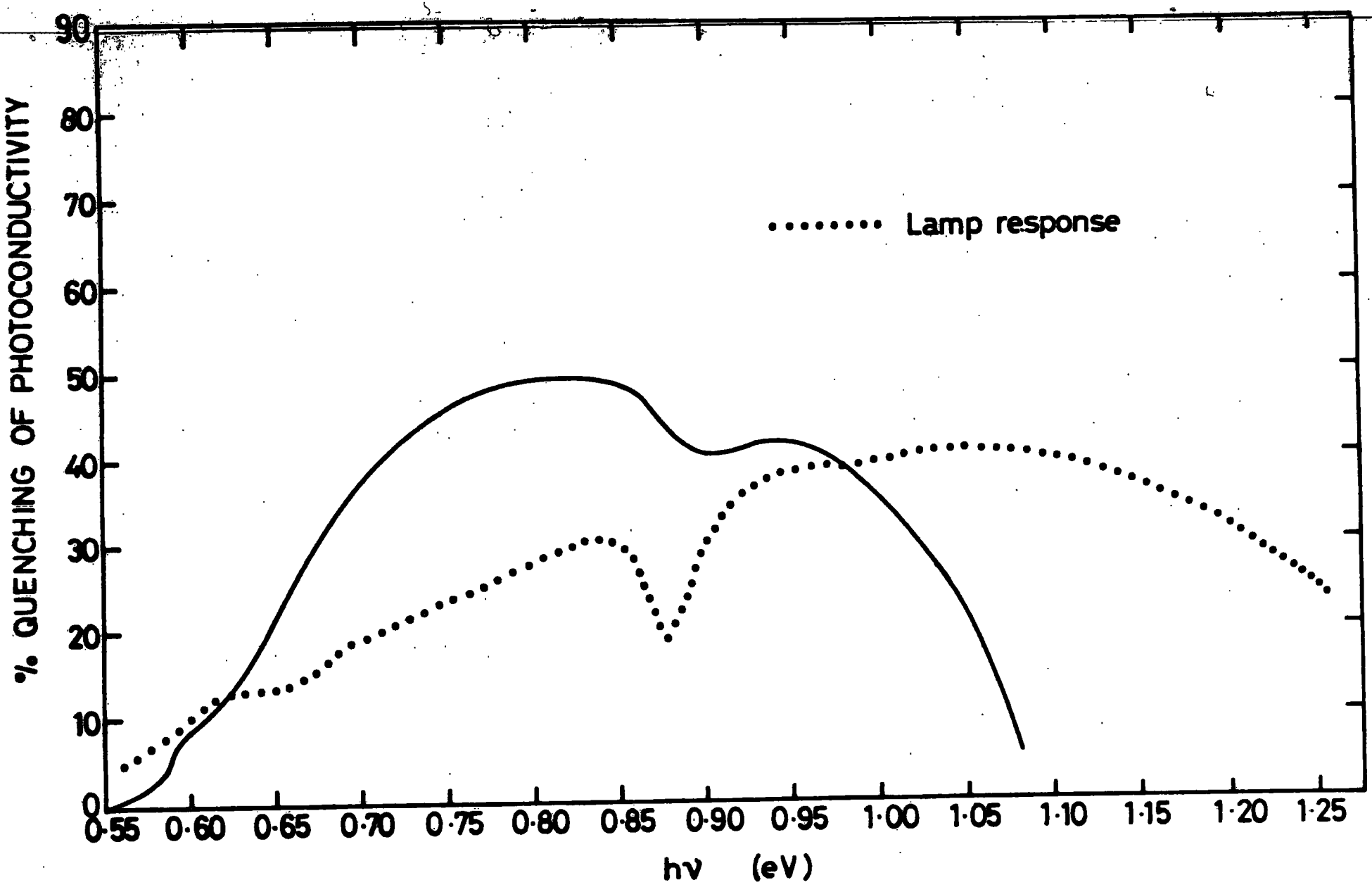

FIGURE 5.4.2 Infrared quenching of photocurrent at 90 K for samples annealed in selenium vapour.

5.5 DISCUSSION

In comparison with the as-grown platelets the photosensitivity of the annealed samples was reduced by at least two orders of magnitude and the 0.64eV sensitising centre was not clearly observed (compare for example the two quenching curves in fugures 5.2.2 and 5.4.2). This would imply that treatment in selenium vapour supresses the formation of doubly ionised cadmium vacancy (V_{Cd}^{--}) responsible for the 0.64eV level[4,9]. Initially the existence of numerous uncompensated cadmium interstitials (selenium vacancies) was responsible for the low resistivity. The ionisation of electrons to the conduction band can be represented either as $V_{se}^{\circ} \rightarrow V_{se}^{++} + 2e^{-}$ or as $Cd_i^{o} \rightarrow Cd_i^{++} + 2e^{-}$. In any event such shallow donors will provide many charge carriers for the conduction band. Annealing an insensitive crystal in vacuum has been shown to produce sensitive crystals[7,16] by promoting the formation of cadmium vacancy acceptors through a self compensation mechanism[18]. This can probably be represented as $Cd^{\circ} + Se^{\circ} \rightarrow Cd + V_{se} + Se\uparrow \rightarrow Cd^{\circ} + V_{se}^{++} + 2e^{-} \rightarrow V_{Cd}^{--} + Cd + V_{se}^{++}$ [19]. In the case of selenium annealing the removal of the selenium from lattice sites will be supressed by the partial pressure of selenium and this may be expressed as $Cd^{o} + V_{se}^{++} + 2e^{-} \xrightarrow{Se_2} Cd^{\circ} + Se^{\circ}$. This implies that annealing in selenium should increase the resistivity of the crystal, but not necessarily increase the photosensitivity. However a certain degree of sensitivity as observed in our experiments may be attributed to some singly ionised defect centres or complexes which could have been created during the annealing process.

Robinson and Bube[10] have reported several centres lying between 0.1 to 0.95eV above the valence band edge in CdSe crystals annealed at comparatively high temperatures in selenium. The results obtained from

the present study are in good agreement with their reported values (see Table 5.4.1). Similar deep levels have also been identified by Kindleysides and Woods[3] in annealed crystals. The level found in the middle of the bandgap (0.9eV) was attributed to either class I[3] or photoconductivity centres[10]. The shallower level of 0.19eV was described as an optical absorption centre (0.2eV) by the same authors. The several scattered threshold values of the spectral response of photoconductivity at liquid nitrogen temperature (fig. 5.4.1) could be interpreted as indicating the presence of several diffused levels within the bandgap. In fact this behaviour might well be expected in the absence of the main sensitising centre (0.64eV) which no longer dominates the spectral response. Calculation shows that the 0.19eV level remains below its demarcation level at low temperature and therefore cannot be resolved clearly.

These results will be discussed further in conjunction with the more quantitative data obtained from measurements of photocapacitance of Schottky devices (see Chapter 7).

5.6 CRYSTALS WITH MECHANICALLY POLISHED SURFACES

RHEED studies of mechanically polished CdSe crystals exhibited a polycrystalline sphalerite cubic layer at the surface, which was more resistive and photoconductive than the underlying hexagonal single crystal structure[20]. These investigations revealed a close relationship between the adsorption of oxygen and mechanical polishing which has not been previously reported[21]. Separate investigations of oxygen adsorption[22,23,24] and of the cubic phase of CdSe[25] have been made but have not been correlated. Generally oxygen has very important effects on all semiconductors and with CdSe in particular it gives rise to acceptor-like levels[26]. Since the mechanical polishing promotes

the chemiadsorption of oxygen, a study of such polished photoconductive surfaces should give some information about the effects of oxygen in CdSe. Polished surface samples were prepared on dice cut from highly conducting single crystal boules as described in chapter 4.5. For this purpose alumina powder with 1μm particle size was used in the final stages of polishing. To avoid the formation of short circuit paths to the underlying conducting hexagonal substrate, special care was taken when making indium contacts to these very thin layers of cubic phase material.

The spectral response of the photoconductivity of a polished sphalerite surface layer at 300 and 90K is shown in figure 5.6.1. At 300K threshold values occurred at 1.16, 1.36 and 1.46eV corresponding to deep acceptor levels at 0.58, 0.38 and 0.28eV respectively. At 90K a single threshold at about 1.47eV was observed corresponding to a level 0.37eV above the valence band edge. Despite the well defined intrinsic photoconductivity peak observed at 90K there was only a small shoulder for the corresponding peak at 300K and no infra-red quenching was detected at either temperture.

5.7 DISCUSSION

The difference between the intrinsic photoconductivity peaks at 300 and 90K was very pronounced. To interpret this behaviour one must take into consideration that the observed darker resistivity of these cubic surface layers was several orders of magnitude less than is usual in CdSe photoconductors. This means that a larger number of electrons were present in the conduction band which could probably verge upon the density of ionised donors at 300K. When the density of free carriers exceeds (i.e. by photoexcitation) the density of donors the photoconductivity mechanism may well be altered to another regime with

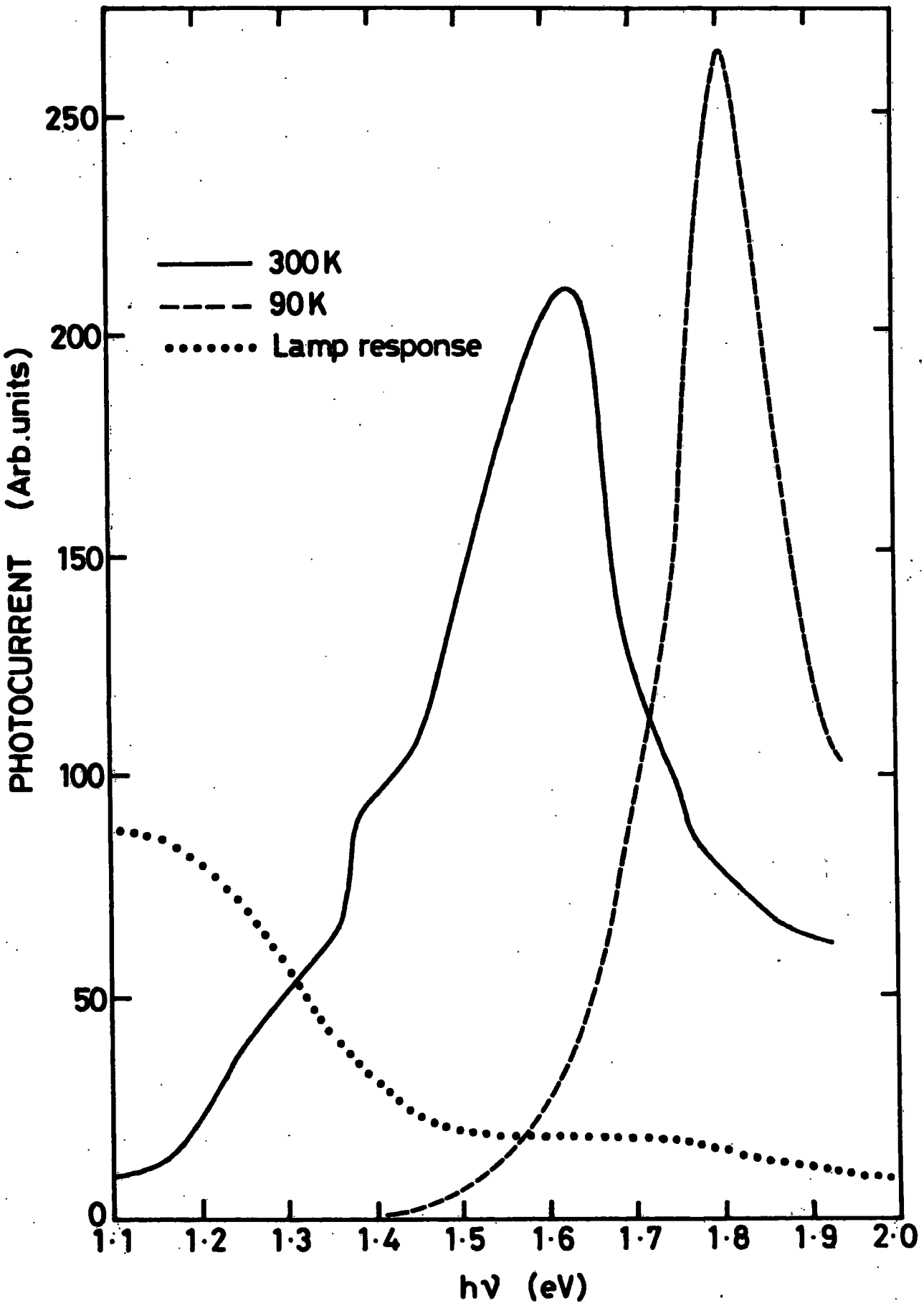

FIGURE 5.6.1 Spectral dependence of photocurrent at 90 and 300 K for mechanically polished(sphalerite) surface layers.

proportionately less photosensitivity. Assuming that the dominant donor levels are located at about 0.15eV below the conduction band (for which strong evidence was found from space-charge measurements[27]) then the calculation shows that their occupancy at 90K would be markedly changed and hence affect the photoconductivity. The acceptor levels at 0.58 and 0.28eV are thought to be intrinsic to CdSe since they have also been detected in pure crystals by other authors[4,6,7]. However, the level at 0.38eV could be associated with the adsorption of oxygen. Extensive studies of the surface properties of single crystal CdSe, particularly in connection with oxygen adsorption phenomena have been carried out by Brillson[27]. These have shown very similar results to those of the present study particularly for surfaces exposed to air or to oxygen. More recently Haak and Tench[28] have also reported similar results using electrochemical photocapacitance spectroscopy (EPS) with CdSe in aqueous solutions.

The non-appearance of the 0.28eV level at 90K might be explained by the influence of 0.38eV level but there is no simple explanation for the failure to observe the 0.58eV level at this temperature. Since the 0.28 and 0.38eV levels were beyond the experimental limitations of the infra-red quenching measurement, the absence of the 0.58eV level at 90K could also account for the quenching effect not being observed.

5.8 SAMPLES HEAVILY DOPED WITH COPPER

The alternative method of preparing high resistivity photosensitive samples of n-type CdSe is to counter-dope the crystal with copper[29]. Copper is known to act as a deep acceptor and to compensate the selenium vacancies (Cd interstitials) which are responsible for the high conductivity. In fact the diffusion of copper, even at low temperature, into CdSe leads to considerable changes in device characteristics. The

main reason for investigating the role of copper, introduced initially as a layer of Cu_2Se by the chemiplating method (wet method), is simply that this involves the same process by which Cu_2Se/CdSe heterojunction solar cells can be made. The details of the experimental techniques for the preparation of heavily doped samples has already been given in Chapter 4.2.

The spectral dependence of photocurrent at room and liquid nitrogen temperatures for a typical heavily copper doped crystal is shown in figure 5.8.1. Long wavelength threshold values of 0.74eV at room temperature and 0.80eV at liquid nitrogen temperature were observed which correspond to levels of 1.0 and 1.04eV above the valence band respectively.

A typical infra-red quenching spectrum for these samples at liquid nitrogen temperature is shown in figure 5.8.2 indicating a relatively smaller quenching effect and a sensitising level some 0.68eV above the valence band edge.

5.9 DISCUSSION

The steep increase of photocurrent at the long wave-length threshold of the spectral response can be attributed to copper-centres located about 1.0eV above the valence band. It is quite clear that the apparent second threshold (very close to the first one) coincides with the dip in the lamp response which is also shown on the same figure, and does not therefore indicate the presence of a second level. The sharp decrease in photocurrent at shorter wavelengths may also be partly associated with the corresponding decrease in the lamp response, but this would not have been sufficient, on its own to account for the observed behaviour. There are several other mechanisms which may contribute to the observed decrease and these fall into three groups:

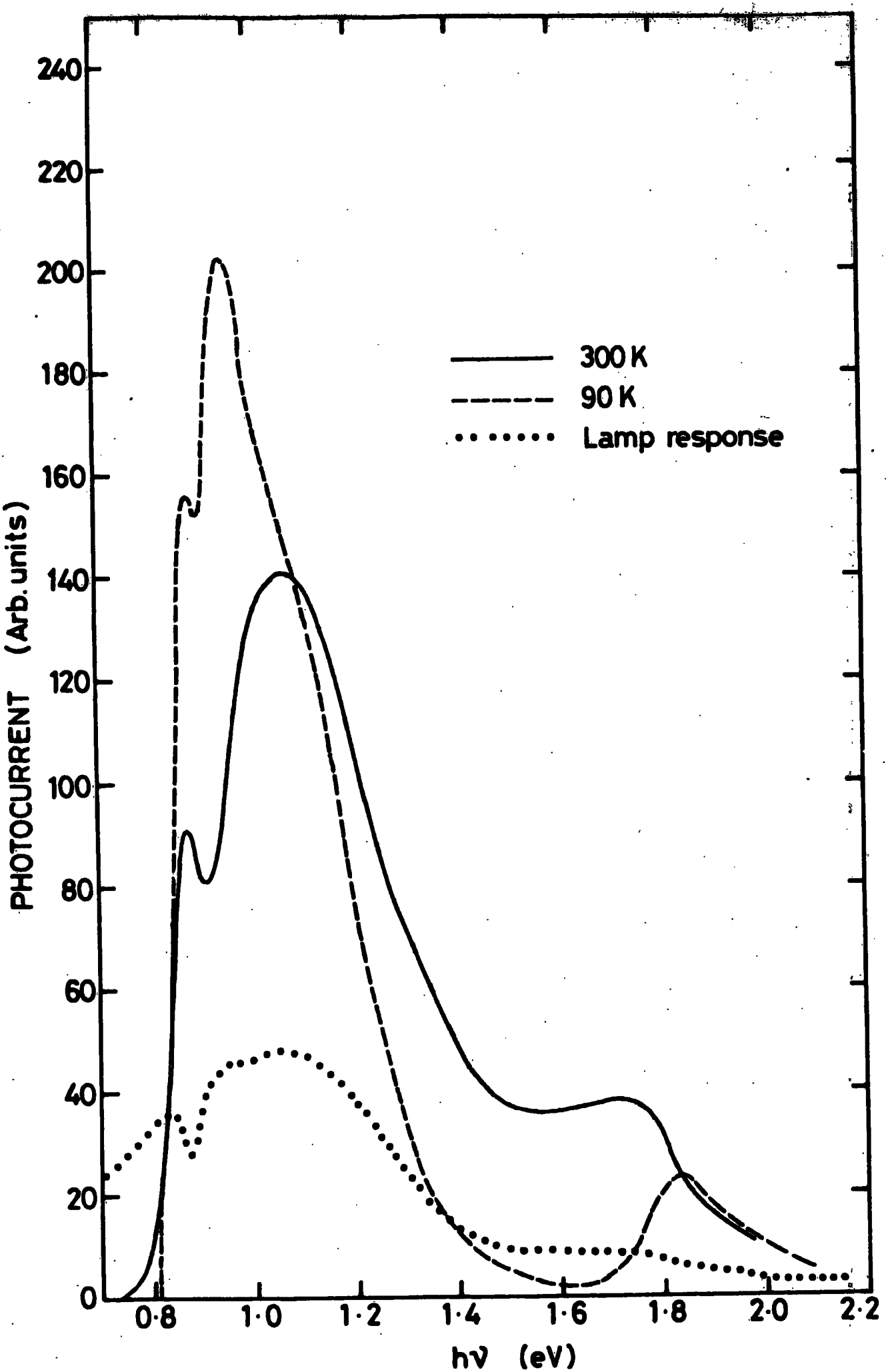

FIGURE 5.8.1 Spectral dependence of photocurrent at 90 and 300 K for heavily Cu-doped samples.

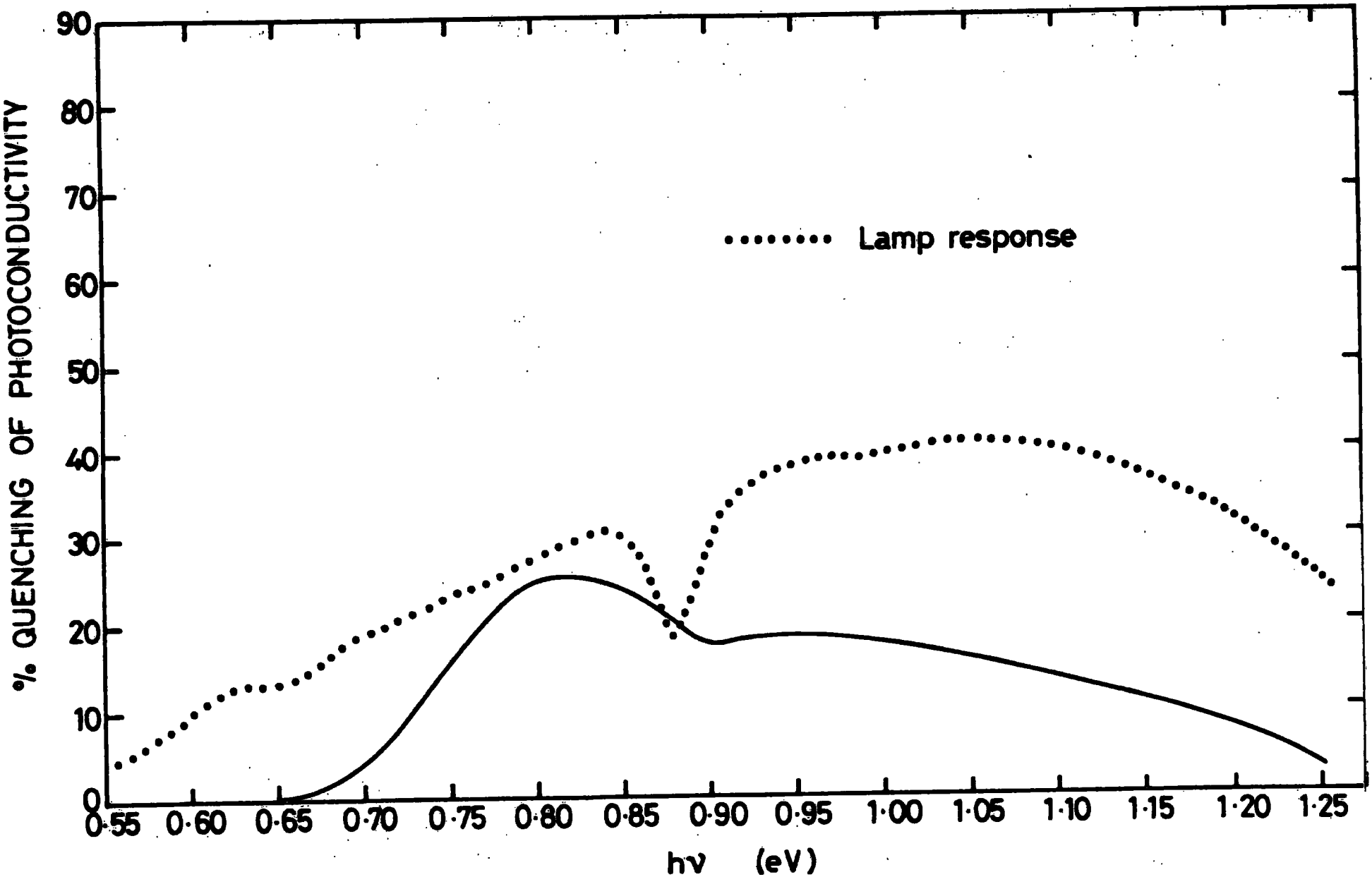

FIGURE 5.8.2 Infrared quenching of photocurrent at 90 K for heavily Cu-doped samples.

1. The very high density of copper impurity in the material could cause a substantial fraction of the light to be absorbed by these impurity centres thus effectively reducing the role of native defects in the spectral response. A similar effect has been reported by Bube and Young[30] for CdS:I:Cu crystals with different concentrations of copper impurity. Our results imply (as it will be shown below) that native defects may also coexist with the copper-centres in the crystal. This was in fact demonstrated in several measurements on heavily and lightly copper doped samples. In a further experiment the copper-diffused surface of the highly doped samples was removed mechanically and chemically. Assuming that some copper profile existed, this would have reduced the average level of doping. Repeating the photoconductivity measurements then revealed an increased response from the levels thought to be related to native defects. This is more fully discussed below.
2. A decrease in the photoionisation cross-section of the deep copper centres with increasing photon energy could also account for the fall in the photocurrent in figure 5.8.1. According to Lucovsky[31] the delta function associated with the photoionisation cross-section falls as $h\nu^{-3/2}$ for photon energies larger than the ionisation energy of the impurity level.
3. The presence of fast recombination centres close to the middle of the bandgap would also result in a decrease of photocurrent under certain conditions especially if they are present in high concentration, and/or their cross-sections for both electrons and holes are large.

The apparent lack of response in the IRQ spectra attributable to the 1.0eV Cu level is at first sight surprising. However, it should be noted that the expected position of the Cu-centre response in the quenching spectrum would coincide with the dip in the lamp response. More importantly the IRQ method is only really applicable to levels lying in the lower half of the bandgap and is thus not suited to the observation of a level lying 1.0eV above the valence band in CdSe. The nature and role of the Cu-related centre will be more fully discussed in Chapter 7 in the light of the space-charge region measurements reported there.

The threshold value of 0.68eV found in the quenching spectrum is almost certainly associated with the usual (V_{Cd}^{--}) sensitising centre in the material. This provides further evidence for the co-existence of both native defect and copper impurity levels.

5.10 SAMPLES LIGHTLY DOPED WITH COPPER

Attempts to obtain moderate resistivity (1-1000) Ω cm CdSe crystals suitable for Schottky diode fabrication led to the investigation of lightly copper doped samples. These were several orders of magnitude less resistive than the heavily doped crystals, dark resistivities achieved were in the range 10^4 - 10^6 Ω cm. which was in fact still too high for Schottky diodes, but the photoconductive properties of these lightly doped samples turned out to be particularly interesting and informative. The details for the sample preparation and experimental arrangements have already been described in Chapter 4.

The spectral dependence of photocurrent is shown in figure 5.10.1 at three different temperatures to illustrate the change in behaviour as the temperature was reduced from room to liquid nitrogen temperature. At 300K threshold values were found at 0.74 and 1.46eV corresponding to

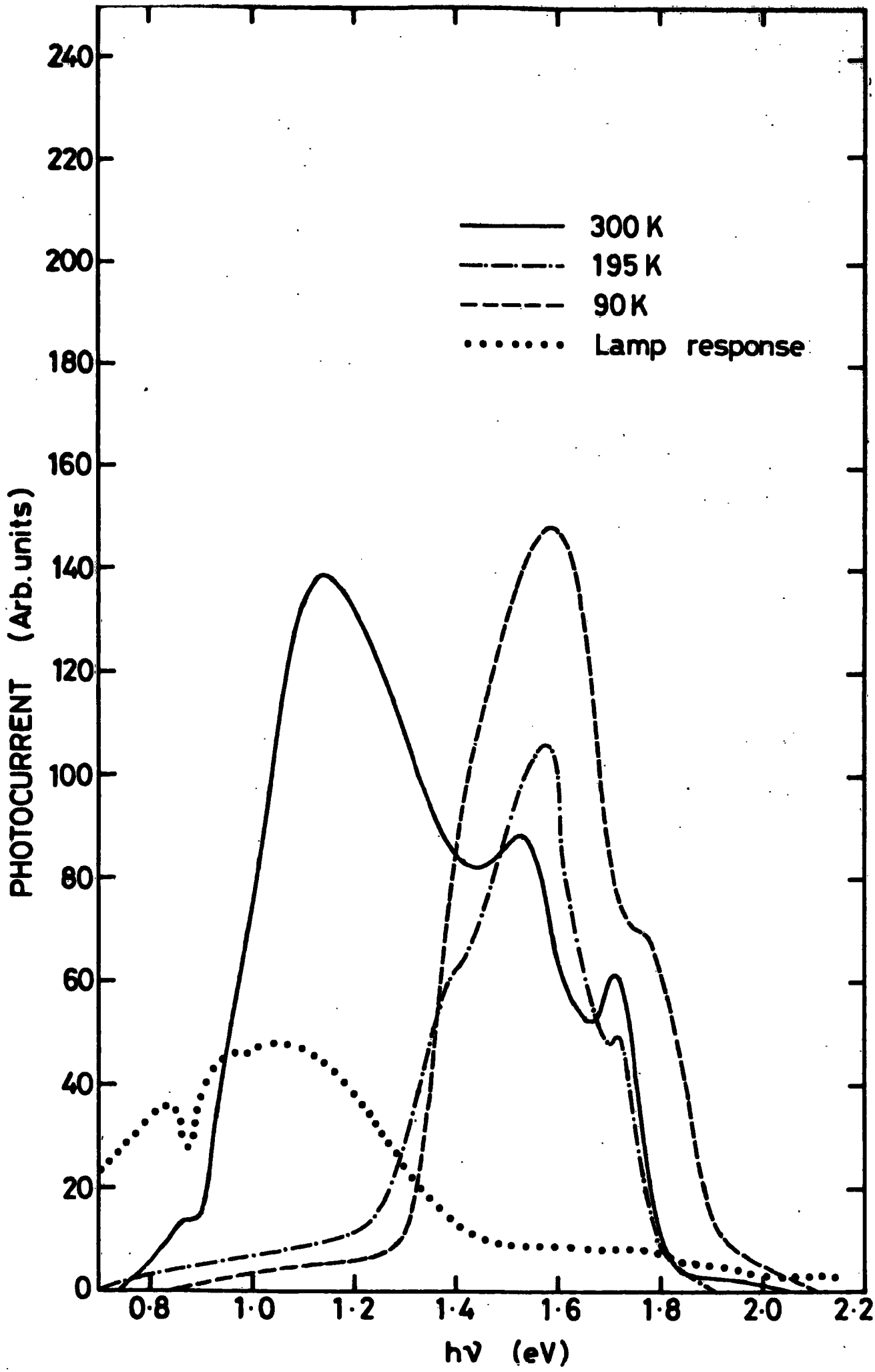

FIGURE 5.10.1 Spectral dependence of photocurrent at 90,195 and 300 K for lightly Cu-doped samples.

energies of 1.0 and 0.28eV with respect to the valence band edge. At 90K two threshold values at 0.83 and 1.31eV were observed corresponding to levels at 1.01 and 0.53eV respectively. At around 195K threshold values of 0.76, 1.24 and 1.43eV suggested there were three acceptor levels at 1.01, 0.53 and 0.33eV above the valence band. In spite of the fact that samples containing different concentrations of copper gave rise to a considerable variety of shapes in the photoconductivity spectra, the main threshold values remained the same. Figure 5.10.2 and 5.10.3 show the spectral dependence of the photocurrent for samples with different copper concentrations and present the extreme cases which reflect this behaviour. This is further evidence that native defects are still important in copper doped crystals.

The infra-red quenching spectra of these samples were usually very similar to that in Figure 5.10.4 which is for a lightly doped sample held at liquid nitrogen temperature. The threshold value of 0.65eV again reveals the main sensitising centre.

5.11 DISCUSSION

The appearance of the 0.28 and 0.53eV levels together with the 1.0eV level may be interpreted in the same way as that discussed in section 5.9. According to this argument the light energy is partially absorbed by copper centres and partially by the native defects. As a consequence of this the response from the native defects will also be evident in the overall spectra. Under these circumstances the fact that the 0.64eV level did not appear explicitly in the photoconductivity spectra could indicate these centres have a low optical absorption coefficient relative to the copper centres. In summary it is probable that the deep acceptor level 1.0eV above the valence band can be associated with copper impurity centres. The dominant role of the 0.53eV

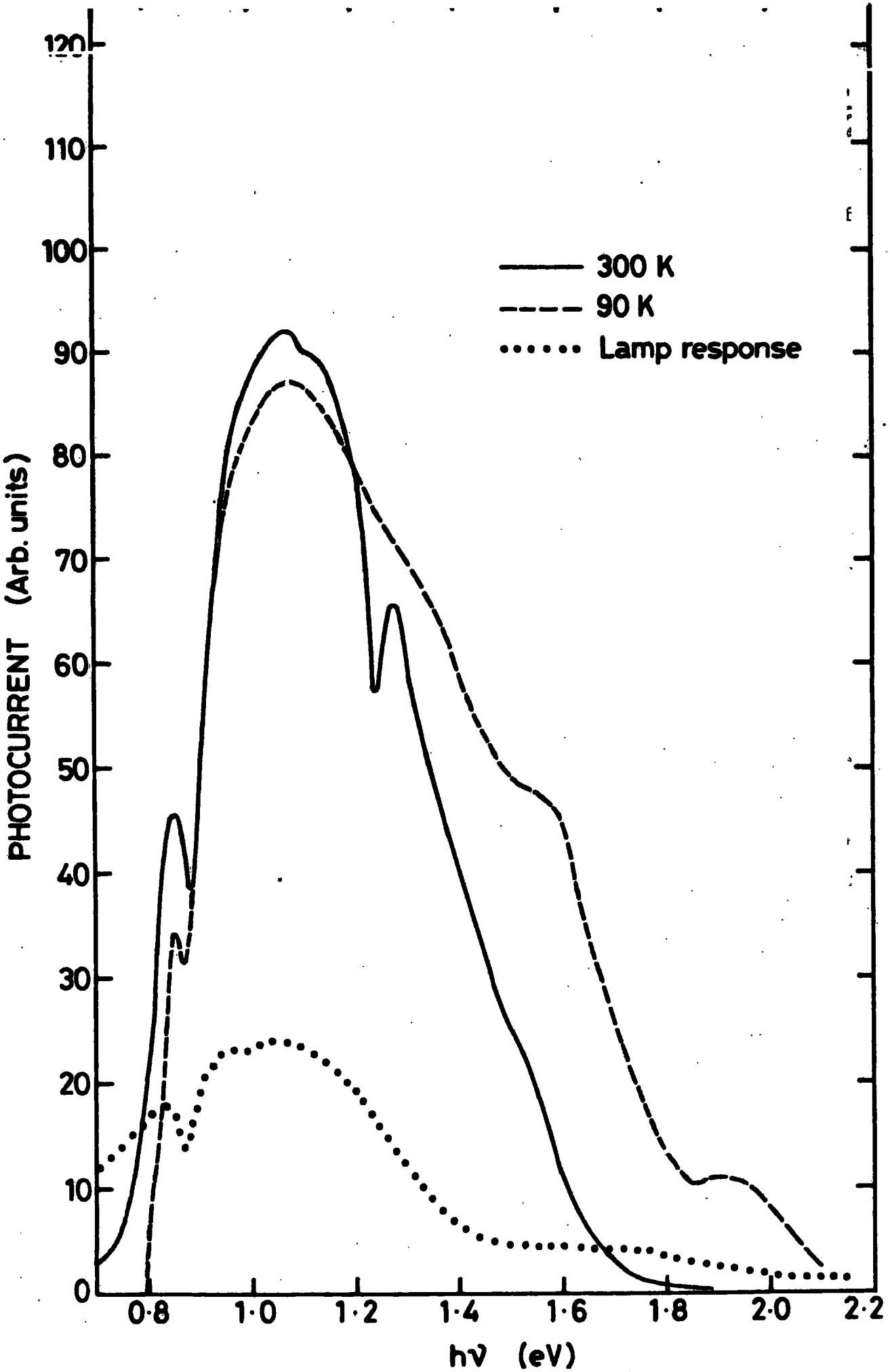

FIGURE 5.10.2 Spectral dependence of photocurrent at 90 and 300K for lightly Cu-doped samples

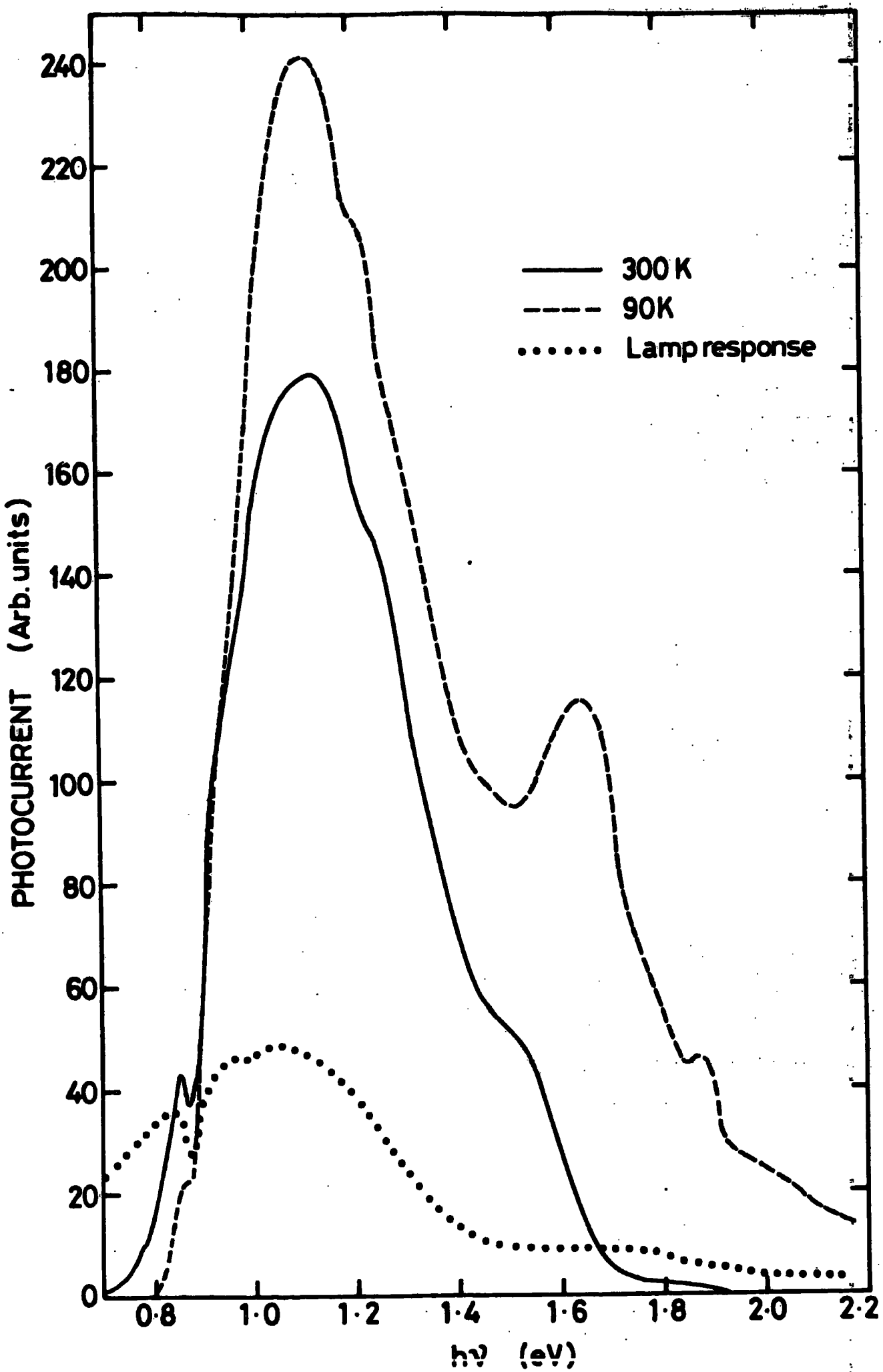

FIGURE 5.10.3 Spectral dependence of photocurrent at 90 and 300K for lightly Cu-doped samples

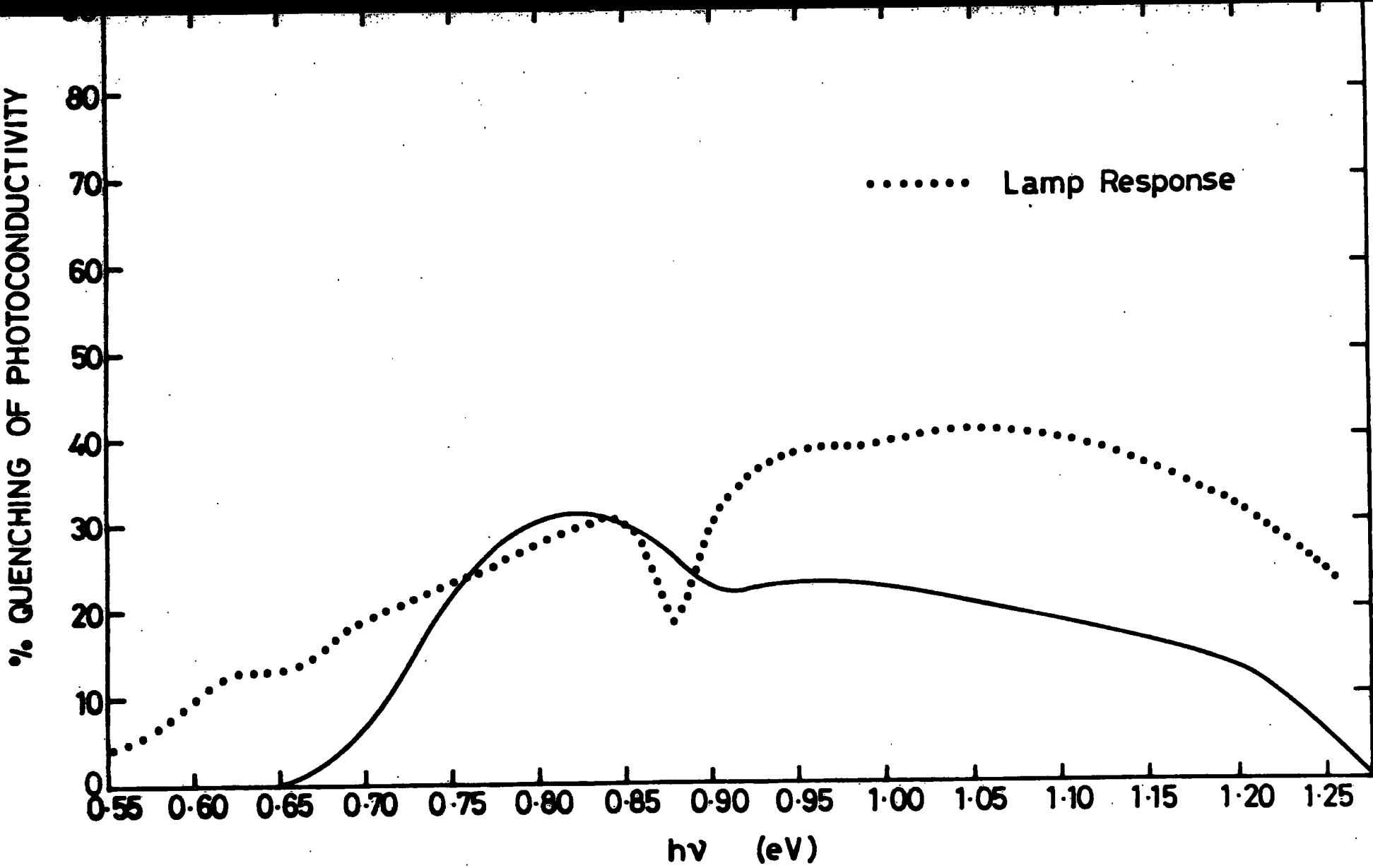

FIGURE 5.10.4 Infrared quenching of photocurrent at 90 K for lightly Cu-doped samples.

level at lower temperatures might either be interpreted to suggest that it acts as:

(1) a second sensitising centre (probably singly ionised) which is thermally quenched at room temperature and does not therefore make any significant contribution to the spectral response, or

(2) more likely as a photoconductivity centre.

In fact both interpretations have been offered by Robinson and Bube[10] for a level near 0.5eV, but without further evidence it is not clear which suggestion is correct.

5.12 COPPER DOPING BY DIFFUSION FROM SURFACE LAYERS OF METAL

A small amount of pure metallic copper was introduced into CdSe single crystals by diffusion following vacuum deposition for similar reasons to those mentioned in section 5.10. This time a low dark resistivity ($\rho < 10^3\ \Omega$ cm) was obtained and Schottky devices were successfully fabricated on these crystals. The one great advantage in examining the photoconductive properties of these crystals was that the capacitative techniques could also be applied, because of reduced resistivity, so that a comparison could be made between the results obtained from the different methods (see Chapter 7).

The spectral dependence of the photocurrent at a variety of temperatures for a sample doped with copper metal is shown in figure 5.12.1. The observed photoconductive threshold and their associated energies are collected together in Table 5.14.1. At 300K threshold values occurred at 0.98 and 1.59eV corresponding to levels at 0.76 and 0.15eV with respect to the valence band edge. At 90K threshold values of 1.16, 1.55 and 1.68eV were observed corresponding to energies of 0.68, 0.29 and 0.16eV above the valence band. At the intermediate

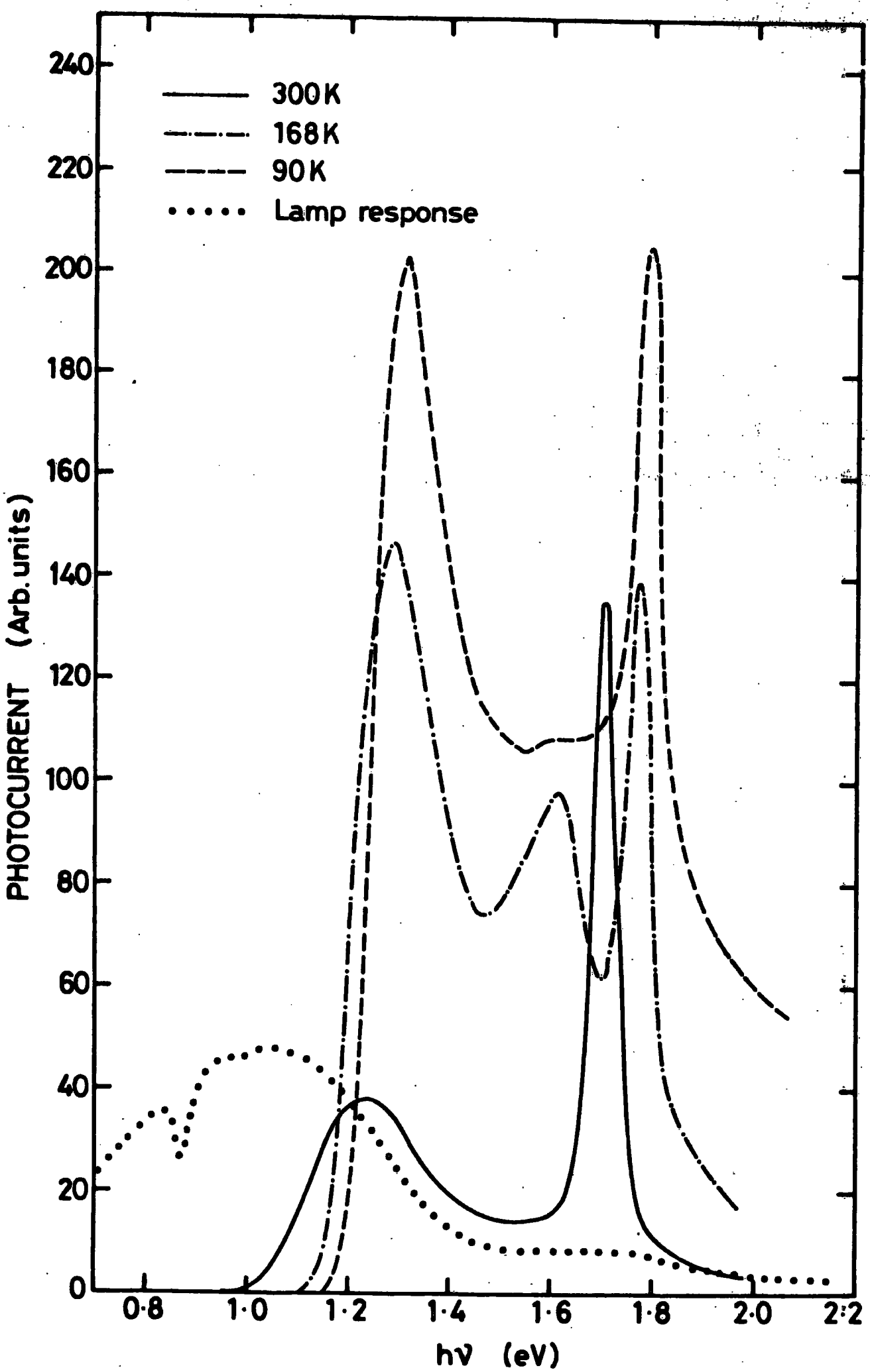

FIGURE 5.12.1 Spectral dependence of photocurrent at 90,168 and 300 K for samples lightly doped with Cu by evaporation of the metal.

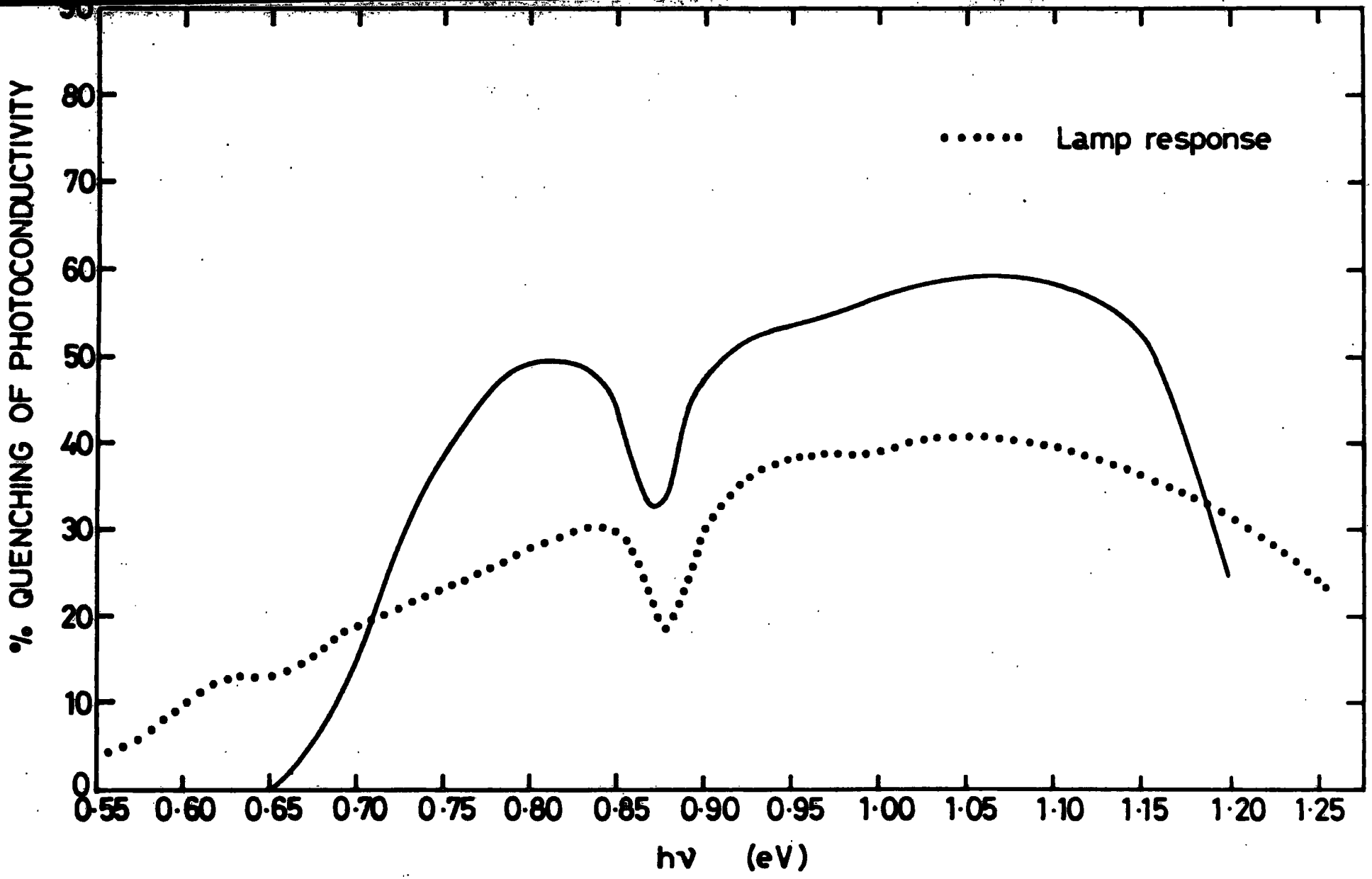

FIGURE 5.12.2 Infrared quenching of photocurrent at 90 K for samples lightly doped with Cu by evaporation of the metal.

temperature of 168K the corresponding energies for the acceptor levels were 0.64, 0.31 and 0.10eV.

The infra-red quenching spectrum shown in fig. 5.12.2 demonstrates that the percentage quenching was high and reveals the 0.65eV single threshold of the well known sensitising centre associated with cadmium vacancies.

5.13 DISCUSSION

With these lightly doped crystals the non-appearance of the 1.0eV level previously associated with copper makes the comparison between the spectral responses of the lightly copper doped samples difficult. Nevertheless it has been shown that heat treatment similar to that used during the copper diffusion process does not produce a sensitive CdSe crystal in the absence of copper impurity. This implies that the presence of a small quantity of copper impurity promotes the thermal generation of Cd-vacancies to increase the resistivity and sensitivity. On the other hand there must be a certain minimum copper content in the material in order for it to be detected.

Although a level at 0.76eV has also been reported as a sensitising centre[10], there is insufficient experimental evidence at this stage to confirm this. The levels at 0.68 and 0.29eV have already been discussed and are thought to be related to native defects, doubly and singly ionised acceptors respectively. The photoconductive peak corresponding to the 0.29eV level was thermally quenched at about240K (see fig. 5.13.1). There has also been a suggestion by Robinson and Bube[10] that a third sensitising centre exists at about 0.1eV above the valence band but this is beyond the experimental scope of one infra-red quenching measurement.

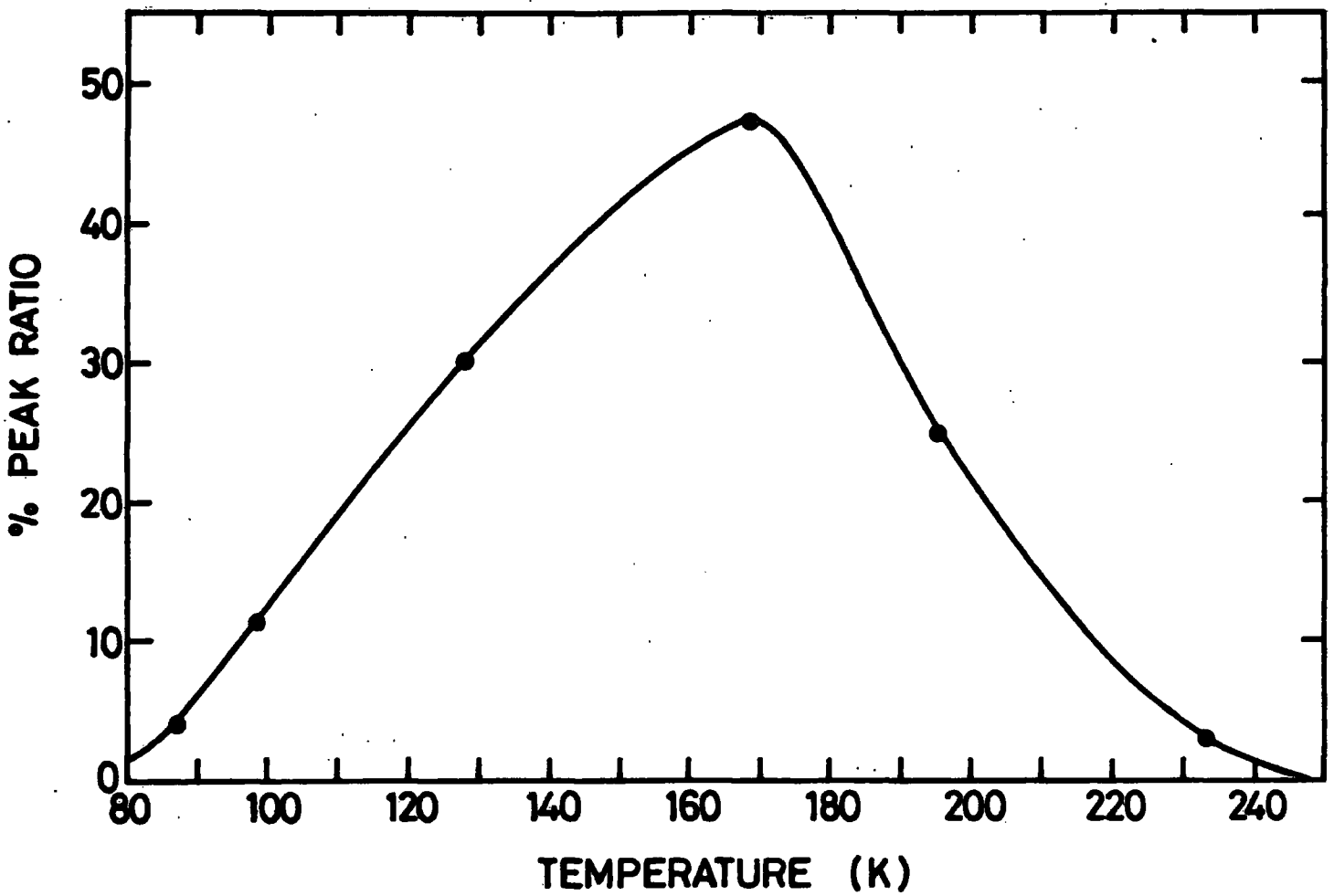

FIGURE 5.13.1 Temperature dependence of the 0.2 eV peak in the spectral response of the photocurrent (fig.5.12.1),for samples lightly doped with Cu by metal evaporation.

5.14 GENERAL DISCUSSION OF PHOTOCONDUCTIVITY MEASUREMENTS

A list of the observed thresholds for photoconductivity and infra-red quenching in platelets, selenium annealed and all three types of copper doped samples is given in table 5.14.1 together with the values available from the current literature.

It must be pointed out that the relationship between the photocurrent and the light intensity was in general non-linear so that it was difficult to correct the photoconductivity spectra for the lamp response. It was decided therefore to present uncorrected curves together with the lamp correction curve when necessary.

Chemical analysis by atomic absorption spectroscopy was useful in demonstrating that the level of possible contamination of the undoped crystals with copper was less than 0.5 ppm. It also provided a valuable means of comparing the concentrations in the various copper doped specimens. The quantitative values obtained from these measurements are given on the related figures and in table 5.14.1. Although in the lightly copper doped samples the initial quantity of copper put down was around 10^5 times less than with the wet plated samples for heavy doping (see Chapter 4.2), the measured copper concentration in the lightly doped samples was only two orders of magnitude smaller. This is attributed to interactions between the impurity and other defects which result in higher diffusion rates at lower impurity concentrations. Extensive studies by Clarke[23], Szeto and Somorjai[33], Woodbury[34], and Sullivan [35] on the diffusion particularly of Cu and Ag into II-VI compounds have generally shown very high diffusion constants for these impurities. With low impurity concentrations they have found even faster processes and much larger diffusion coefficients, suggesting different diffusion mechanisms at

TABLE 5.14.1 List of generally observed thresholds in photoconductivity and infra-red quenching measurements for various types of photoconductive CdSe samples.

SAMPLE	KINDLEYSIDES & WOODS [3]		ROBINSON & BUBE [6]		BUBE & BARTON [7]		MANFREDOTTI ET AL [4]		BRILLSON (SURFACE) [27]		PRESENT STUDY	
	LEVELS(eV)	REMARKS	LEVELS(eV)	REMARKS	LEVELS(eV)	REMARKS	LEVELS(eV)	REMARKS	LEVELS(eV)	REMARKS	LEVELS(eV)	REMARKS
FLOW-RUN PLATELETS	0.90 0.74 0.60 sensitising 0.26 ground state 0.15 ground state	class I luminescence			1.00 sensitising 0.64 sensitising 0.60 cu sensitising		0.74 sensitising 0.26 sensitising		0.29	(VACUUM CLEANED)	0.44 sensitising 0.43 0.26	
ANNEALED IN Se			0.85 0.75 0.60 0.45 0.30 0.20 0.10 sensitising	photocond. sensitising photocond. sensitising optical absor.							0.61 0.37 0.34 0.09	sensitising
CRYSTALS WITH MECHANICALLY POLISHED SURFACES									0.68 0.38	Air exposed Oxygen exposed	0.68 0.38 0.28	oxygen related
HEAVILY DOPED WITH Cu (Cu Conc. $\sim 4.10^3$ ppm)			1.05 0.85 0.50	Cu photo-conducting sensitising photocond.							1.00 Cu 0.68 sensitising	
LIGHTLY DOPED WITH Cu (Cu Conc. $\sim 10^2$ ppm)											1.01 Cu 0.85 sensitising 0.53 0.28	
LIGHTLY DOPED WITH Cu (METALLIC EVAP.) (Cu Conc. ~ 10 ppm)											0.76 0.64 sensitising	

different impurity concentrations. The diffusion and solubility of copper cannot be investigated in isolation since the copper diffusion always requires an annealing process. This in turn gives rise to some self-diffusion and thermal generation effects in the crystal which makes the problem more complicated.

All infra-red quenching measurements were made at liquid nitrogen temperature since class II centres do not contain holes at room temperature, i.e. the photoconductivity is thermally quenched at room temperature and no optical quenching effect could be detected as a result. Although infra-red quenching measurements are known to be more decisive and are easier to interpret than photoconductivity spectra, there are some limitations restricting the usefulness of the technique. For example, if the energy of the incident light is larger than half the bandgap energy, there will be simultaneous filling and emptying processes for the levels lying half-way between the conduction and valence bands. This makes it very difficult to detect levels near the middle of the bandgap (i.e. $\sim$1.0eV level above the valence band). Conversely, levels below 0.5eV could not be observed in quenching due to the lack of a suitable low energy light source and the low temperature limit of liquid nitrogen.

Finally it is reassuring that many of the energy values reported in the present study are in good agreement with the current literature. The small discrepancies which do exist are not unexpected, given the differences in crystal growth processes and sample preparation techniques employed.

CHAPTER 5 - REFERENCES

1. M. Aven, J. S. Prener, Phys. & Chem. of II-VI compounds, North-Holland Pub. Co., Amsterdam 1967.
2. R. H. Bube, J. Phys. Chem. Solids 1 (1957) 234.
3. L. Kindleysides & J. Woods, J. Phys. D. Appl. Phys. 3 (1970) 1049.
4. C.Manfredotti, R. Murri, E. Pepe & D. Semisa, Phys. Stat. Sol. (a) 20 (1973) 477.
5. G. A. Dussel & R. H. Bube, J. Appl. Phys. 37 (1966) 13.
6. R. H. Bube, Phys. Rev. 99 (1955) 1105.
7. R. H. Bube & L. A. Barton, J. Chem. Phys. 29 (1958) 128.
8. E. H. Stupp, J. Appl. Phys. 34 (1963) 163.
9. R. H. Bube, J. Appl. Phys. 32 (1961) 1707.
10. A. L. Robinson & R. H. Bube, J. Appl. Phys. 42 (1971) 5280.
11. R. H. Bube, J. Appl. Phys. 35 (1964) 586.
12. G. L. Belenkii & M. K. Sheinkman, Sov. Phys. Semicond. 2 (1969) 1280.
13. R. H. Bube, J. Chem. Phys. 30 (1959) 266.
14. D. M. Heinz & E. Banks, J. Chem. Phys. 24 (1956) 391.
15. H. Tubota, H. Suzuki & K. Hirakawa, J. Phys. Soc. Japan 15 (1960) 170.
16. R. A. Burmeister & D. A. Stevenson, Phys. Stat. Sol. 24 (1967) 683.
17. M. P. Hung, N. Ohashi & K. Igaki, Jap. J. Appl. Phys. 8 (1969) 652.
18. F. A. Kröger, The chemistry of imperfect crystals, North-Holland Pub. Co., Amsterdam 1964.
19. J. Varvas & T. Nirk, Phys. Stat. Sol (a) 33 (1976) 75.
20. G. J. Russell, A. T. Fellows, S. Oktik, E. Türe & J. Woods, J. Mat. Sci. Lett. 1 (1982) 176.

21. I. E. Türe, G. J. Russell & J. Woods, J. Cryst. Growth 59 (1982) 223.

22. E. Guesne, C. Sebenne & M. Balkanski, Surface Sci. 24 (1971) 18.

23. M. F. Chung & H. E. Farnsworth, Surface Sci. 25 (1972) 321.

24. M. J. Katz & K. J. Haas, Surface Sci. 19 (1970) 380.

25. L. Dümeritz, J. Cryst. Growth 23 (1974) 307.

26. R. H. Bube, J. Chem. Phys. 27 (1957) 496.

27. L. J. Brillson, Surface Sci. 69 (1977) 62.

28. R. Haak & D. Tench, J. Electrochem. Soc. 131 (1984) 275.

29. R. H. Bube, Photoconductivity of Solids, Robert E.Krieger, Pub. Comp. Huntington, New York 1978.

30. R. H. Bube & B. Young, J. Appl. Phys. 35 (1964) 462.

31. G. Lucovsky, Solid St. Communs. 3 (1965) 299.

32. R. L. Clarke, J. Appl. Phys. 30 (1959) 957.

33. W. Szeto & C. A. Somorjai, J. Phys. Chem. 44 (1966) 3490.

34. H. H. Woodbury, J. Appl. Phys. 36 (1965) 2287.

35. G. A. Sullivan, Phys. Rev. 184 (1969) 184.

CHAPTER 6

CHARACTERISATION OF CdSe SCHOTTKY BARRIERS

6.1 INTRODUCTION

In this chapter the properties of Schottky devices on differently prepared surfaces of CdSe single crystals are described. These devices were mainly fabricated so that space-charge techniques could be applied as an alternative to photoconductivity measurements for the characterisation of defect and impurity levels.

Although Schottky barriers were chosen for these applications because of their relatively simple structures compared to other junction devices such as Cu_2Se/CdSe heterojunctions, the variations in the electrical characteristics of the Schottky diodes with time required further investigation. These variations were found to be very much related to oxygen adsorption and associated surface structural transformations[1]. Therefore RHEED studies were also included in the analysis of these devices in order to provide a better understanding.

Since the diodes were made either on etched or mechanically polished surfaces of CdSe, they can be considered to be metal-interfacial layer-semiconductor (MIS) rather than metal-semiconductor (MS) structures. An attempt was made to deduce the parameters (i.e. thickness and surface state density) of the interfacial layers involved using the analyses of both Cowley[2] and Fonash[3] and to present a somewhat more conclusive energy band scheme for these devices.

6.2 SCHOTTKY BARRIERS ON SAMPLES ANNEALED IN SELENIUM FOR 3-DAYS

6.2.1 Introduction

As mentioned in Chapter 4.4, our as-grown CdSe usually had a very high conductivity and it was not possible to form rectifying contacts on these samples. The details of the annealing process in selenium vapour to obtain moderate resistivity crystals and subsequent sample preparation have been described in chapter 4.4.1 and 4.5. In this section the electrical characteristics of the Schottky diodes on substrates heated in Se vapour for 3 days are discussed. The changes in the electrical characteristics which occur on ageing in air are attributed to changes in surface properties largely related to oxygen adsorption.

Following the annealing process the dice were mechanically polished with alumina powder down to a grit size of 1μm, and etched first in 2% bromine methanol for 3 minutes, then in concentrated HCl for a further 2 minutes. In order to complete the Schottky diode structure a 2 mm diameter gold dot was evaporated onto one of the large area faces with the indium contact on the opposite face.

6.2.2 Electrical Characteristics

The current-voltage (I-V) characteristics of Schottky devices measured immediately after fabrication showed little rectification and a large reverse bias leakage current. I-V measurements of the same device taken after storage for 48 h and 2 months in the open laboratory at room temperature led to a considerable improvement in the characteristics (see Fig. 6.2.1). The same degree of improvement as that produced by the 2 months of ageing could also be achieved by heating in air at 100^{0}C for 16h.

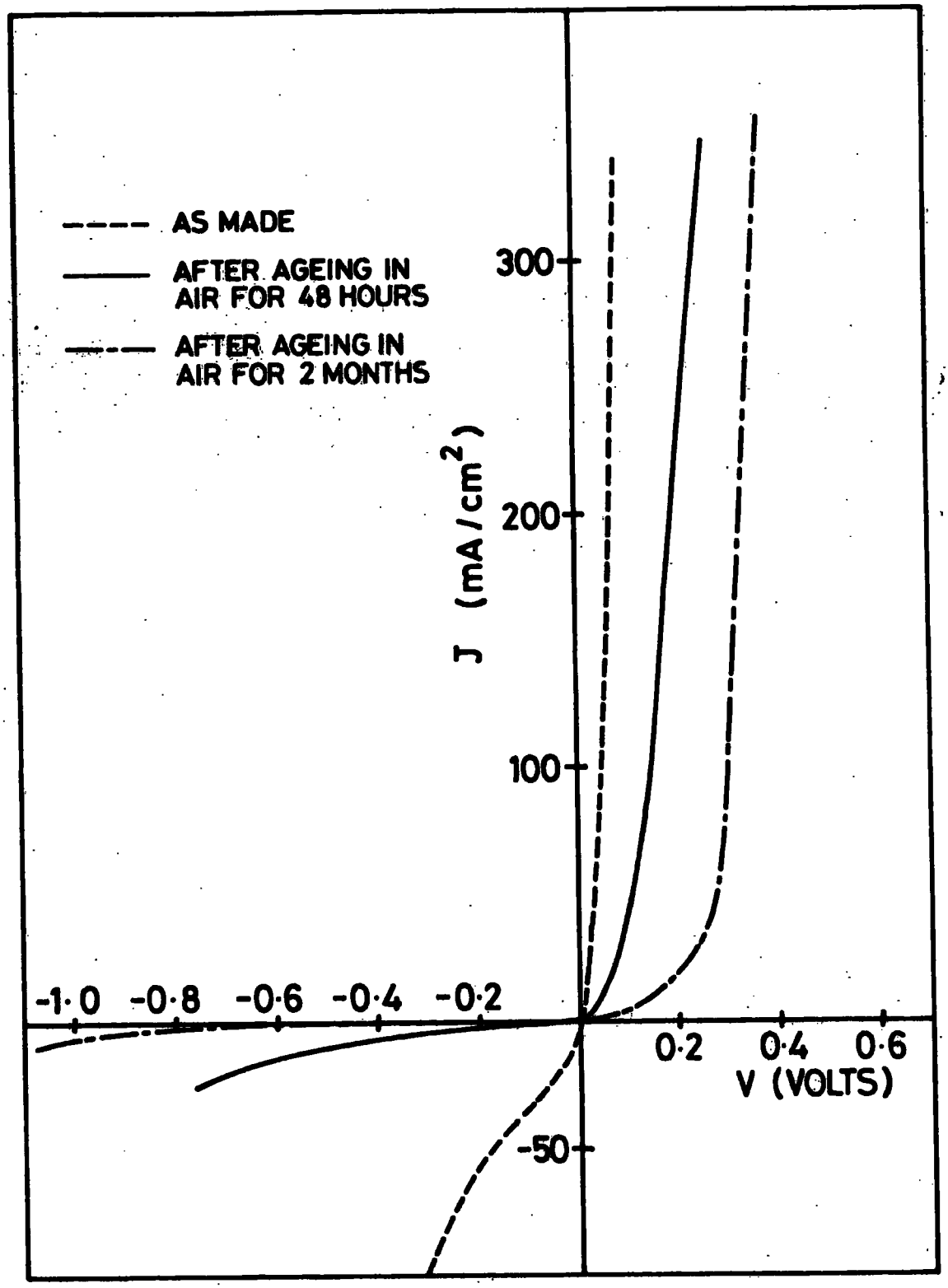

FIGURE 6.2.1 I.V. characteristics of a typical Schottky device formed on 3-day Se-annealed CdSe (before and after ageing).

The corresponding capacitance-voltage (C-V) characteristics measured at 1 MHz for the same device and at the same time intervals as in the previous figure are shown in figure 6.2.2, in the form of C^{-2} against V. From these plots values of the diffusion potential at zero bias V_{do} (i.e. $V_{do} = V_{dif} + kT/q$) and effective donor density (N_d) can be calculated using simple Schottky-Mott theory[4], if the effects of surface states and the interfacial layer are ignored. (These factors will be fully discussed later). Accordingly values of V_{do}, N_d, Fermi energy ($E_c - E_F$), barrier height (Φbn_{C-V}) and the depletion layer width (W_{C-V}) have been obtained and recorded in table 6.2.1) using equations $d(1/C^2)/d(V_{do} - kT/q + V_r) = 2/q\ \varepsilon_s N_d$ (3.12), $(E_c - E_F) = kT/q\ \ln N_c/N_d$ (3.7), $\Phi bn_{C-V} = V_{do} + (E_c - E_F)$ (2.14) and $W_{C-V} = [2\ (V_{do} + V_r)\varepsilon_s/qN_d]^{\frac{1}{2}}$ (3.16).

6.2.3 Barrier Height Measurements

(a) Photoelectric

The theory concerned with the determination of barrier heights by the photoelectric method was reviewed in Chapter 3.3.7. Because of the very small short-circuit current of the as-made Schottky diodes barrier heights could not be determined for these devices by this method. However, Schottky diodes which had been aged for long periods of time, did produce detectable short-circuit currents and barrier heights could then be determined. Figure 6.2.3 shows a Fowler plot of $I_{ph}^{\frac{1}{2}}$ versus $h\nu$ for an aged Schottky diode, indicating a value of $\Phi bn_{ph} = 0.64$eV for the barrier height from the intercept. This is in a reasonably good agreement with the value of $\sim$0.69eV determined from the C-V measurements. A more detailed discussion of the photoelectric method for determining barrrier height will be given in sect 6.2.5.

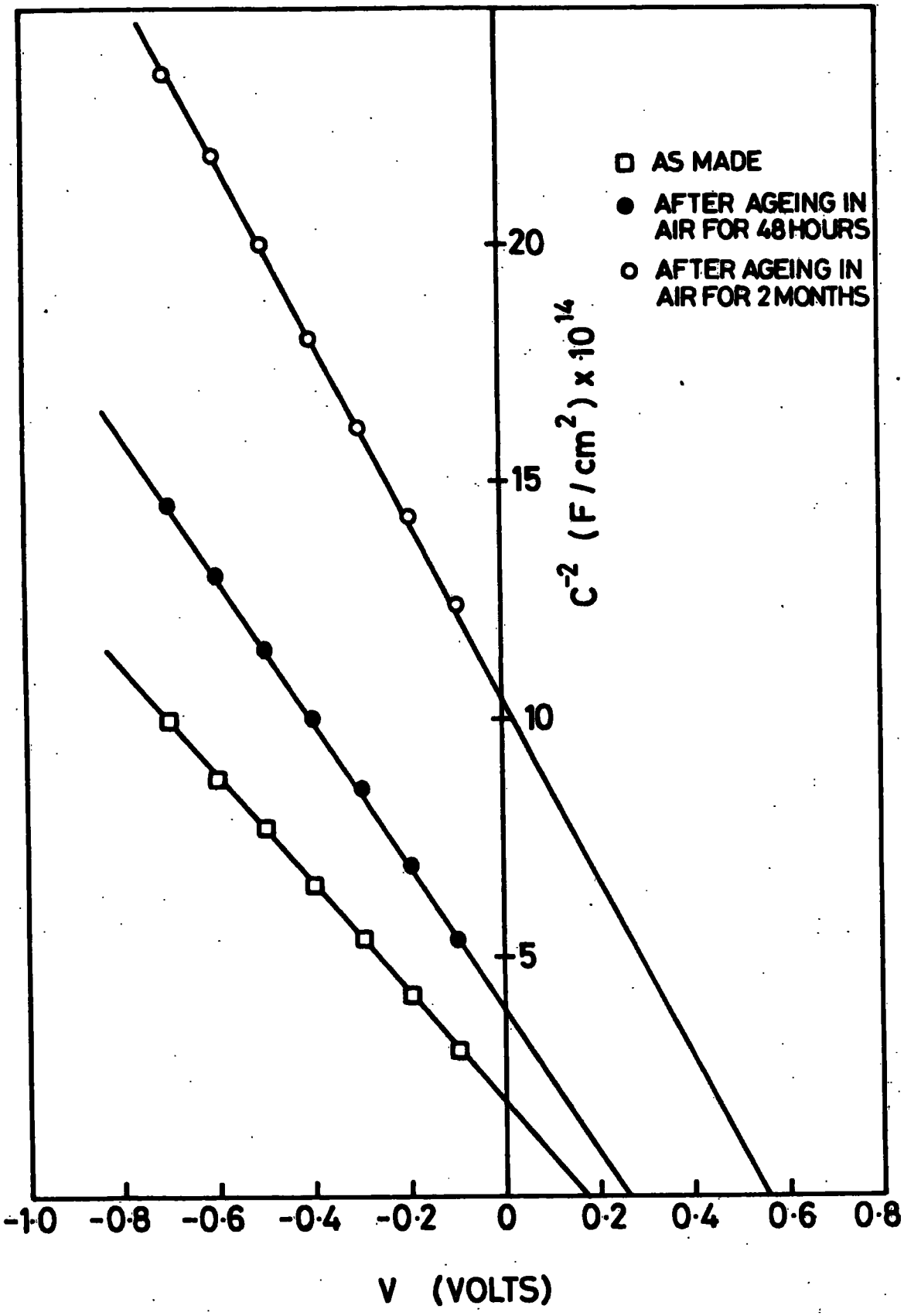

FIGURE 6.2.2 C^{-2}-V characteristics of the same Schottky device (fig. 6.2.1) measured before and after ageing

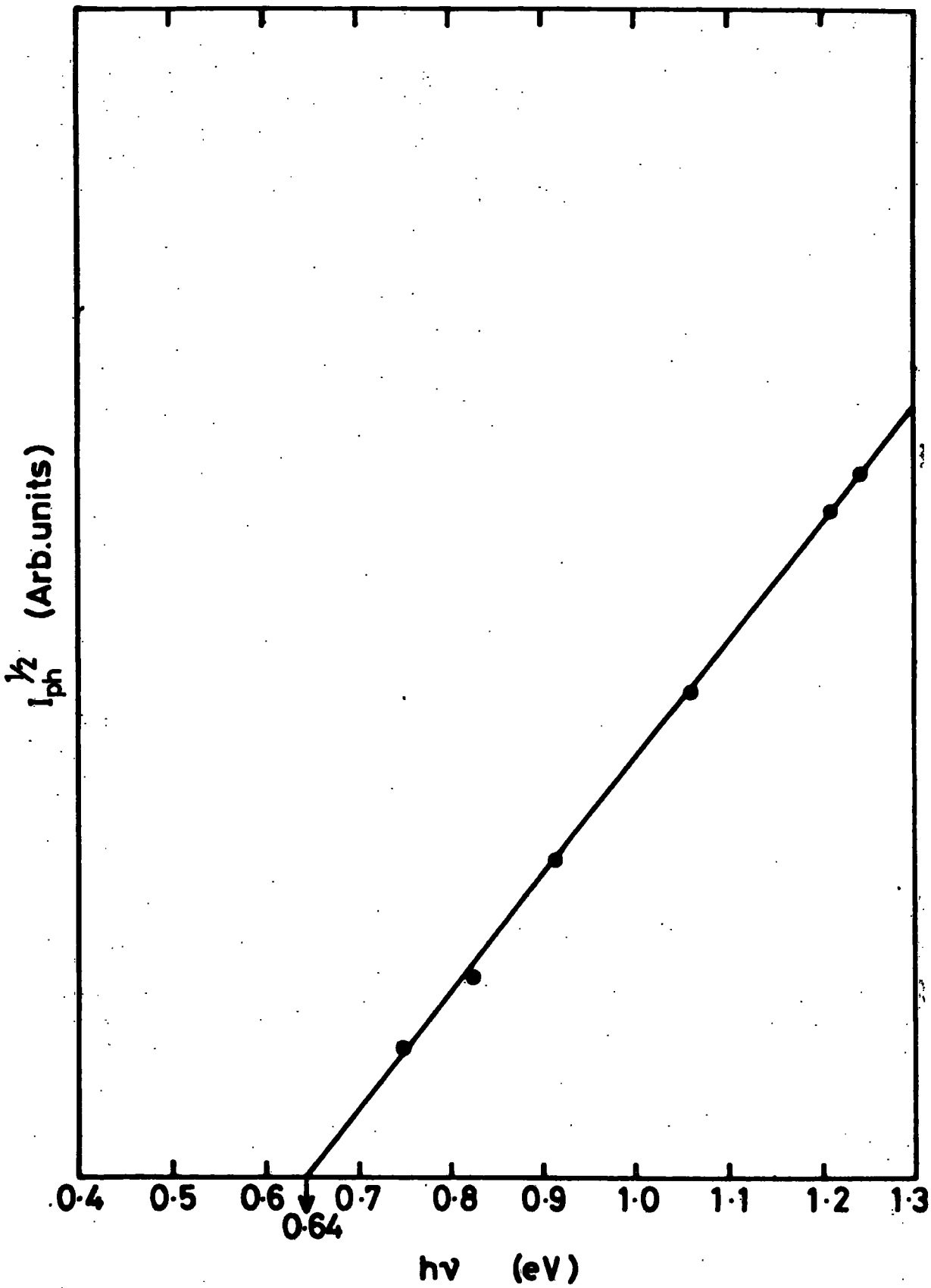

FIGURE 6.2.3 A Fowler plot of an aged Schottky diode prepared on 3-day Se-annealed CdSe

Description of Characteristics	V_{dif}(eV)	$N_d(10^{16})$ cm^{-3}	(E_c-E_F) eV	$\bar{\Phi}_{bn_{C-V}}$ (eV)	(W_{C-V}) μm zero bias
As-made	0.18	1.28	0.11	0.29	0.11
After ageing in air for 2 days	0.26	0.89	0.12	0.38	0.17
After ageing in air 2-months	0.56	0.69	0.13	0.69	0.29

TABLE 6.2.1 General characteristics of 3-days Se annealed Schottky devices

(b) Forward (I-V) Characteristics

The barrier height of a Schottky diode can also be determined from the forward bias I-V characteristics by using equation (3.18), $J = J_s \exp(qV/nkT)$ based on thermionic emission theory (see chap. 3.3.5). The saturation current density J_s, found from the intercept of lnJ against V (which is usually a straight line of slope greater than 3kT/q) is the key parameter in equation (3.18) $J_s = R^*T^2 \exp(-q\Phi_{bn}/kT)$. Since the ideality factors for the Schottky devices were generally larger than unity $1.8 \leqslant n < 3.5$, estimates of barrier height using this procedure would not be very accurate. In order to overcome this difficulty an attempt was made to determine the saturation current density from the reverse bias characteristics. The reverse bias characteristics of the aged Schottky devices were found to be most appropriate for this purpose since they were in a reasonable agreement with the simple image force barrier lowering effect (see Chap. 3.3.4).

The forward characteristic of an aged Schottky device is shown in figure 6.2.4. (while the reverse bias characteristic of the same device, plotted on axes of lnJ against $V^{1/4}$ is shown in figure 6.2.5. Saturation current densities of $J_{sF} \sim 1.65\ 10^{-4}$ Amp/cm^2 and $< J_{sR}$ $3.75\ 10^{-4}$ Amp/cm^2 were derived from figures 6.2.4 and 6.2.5 respectively. These values were in fact very similar and gave a difference of only 0.02 eV in the barrier height calculations. Since the equation 3.18 is not very sensitive to the choice of R^{**}, the substitution of the effective Richardson constant R^* for R^{**}, is a reasonable approximation[5]. With $R^* \simeq 15.6$ Amp cm^{-2} K^{-2} for CdSe (see Chap. 3.3.5) equation 3.18 yielded the barrier height of $\Phi_{bn_{I-V}} = 0.58$eV for the saturation current obtained from the forward characteristics.

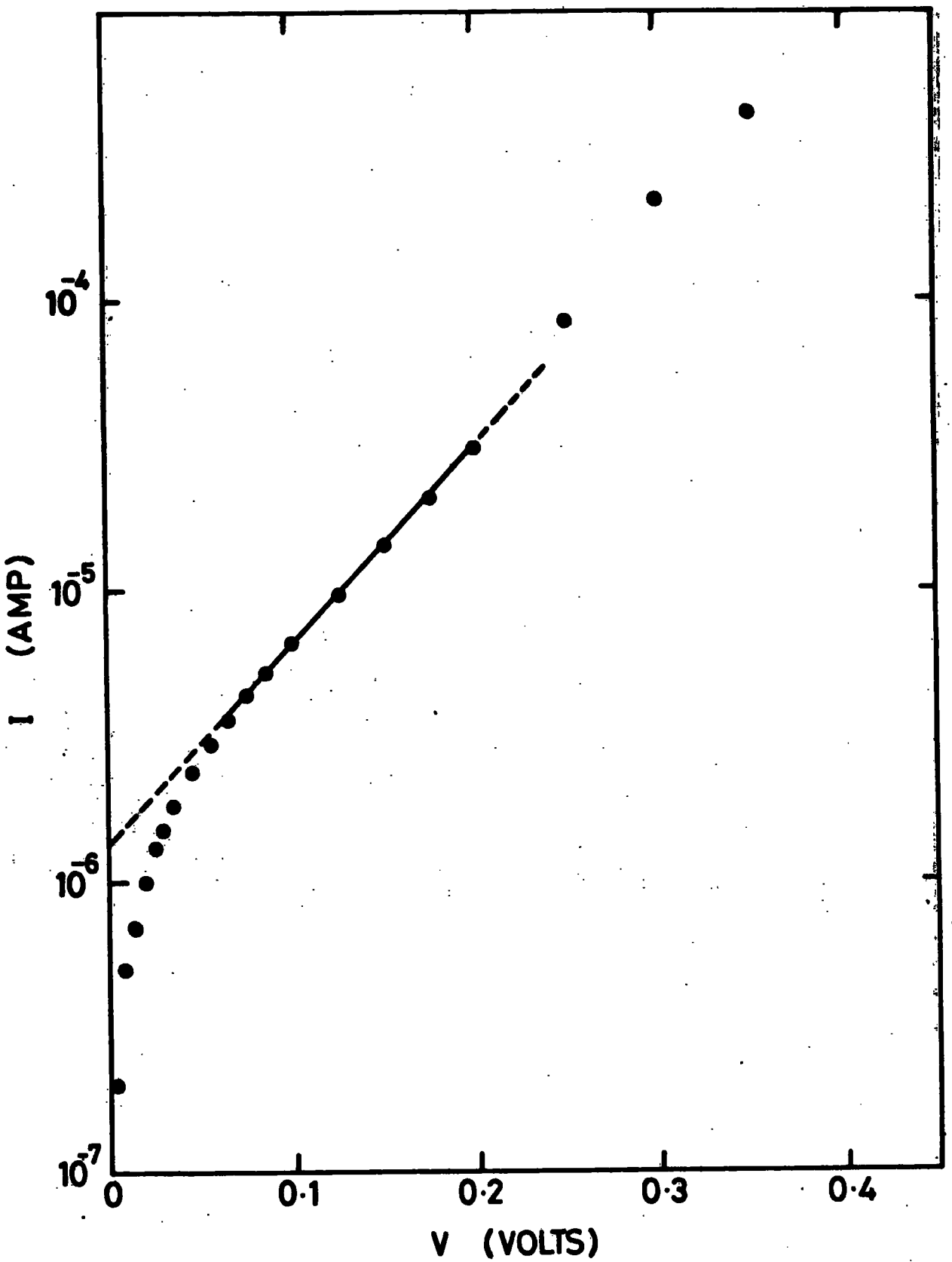

FIGURE 6.2.4 Semilog plot of forward I-V characteristics of an aged Schottky diode prepared on 3-day Se-annealed CdSe

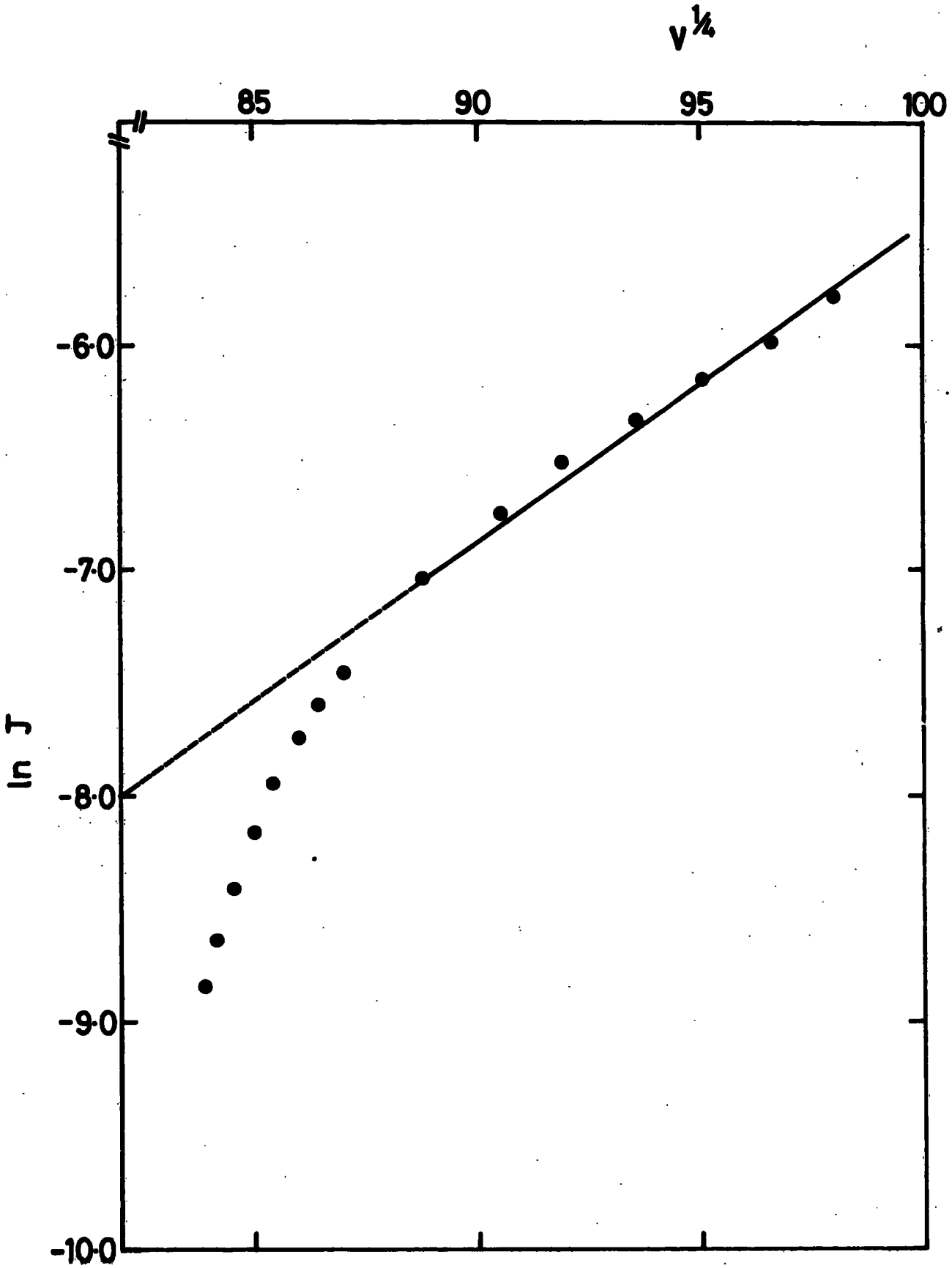

FIGURE 6.2.5 Reverse bias I-V characteristics of the diode in fig. 6.2.4 plotted on lnI vs $V^{1/4}$

6.2.4 RHEED Studies

In general the methods used in surface studies can be divided into two groups; (a) the chemistry and lattice structure of the surface, (b) electrical phenomena taking place at and near the surface. Although many studies have been reported in each of these groups and considerable progress has been achieved, very few attempts have been made to correlate the two types of measurement. The aim of the work reported here was to investigate the effects that the adsorption of oxygen has on CdSe surfaces both structurally and electrically. It is worth recording that wet or dry nitrogen, carbon dioxide, or argon do not have similar effects to oxygen.

The RHEED pattern obtained from the $(000\bar{1})$ basal plane of a freshly etched CdSe single crystal with the 100KeV beam lying parallel to the $(10\bar{1}0)$ direction is shown in figure 6.2.6. All Schottky devices fabricated on etched surfaces were formed on substrates which gave rise to diffraction patterns such as this. When a Schottky device was heated in air at 100°C for 16h, or alternatively was left in room conditions for about 2 months, re-examination of the same surface in RHEED yielded the diffraction pattern shown in figure 6.2.7. The three most intense diffraction rings in this pattern correspond to interplanar spacings of 3.49, 2.10 and 1.81 Å and can be indexed as arising from the sphalerite structure with a lattice parameter of about 6.00Å. The ageing effect was independent of crystal orientation.

6.2.5 Surface Effects

It is a well known fact that Schottky devices built on real (etched) surfaces of semiconductors are not ideal MS diodes but are metal-thin insulator-semiconductor (MIS) structures instead. This is

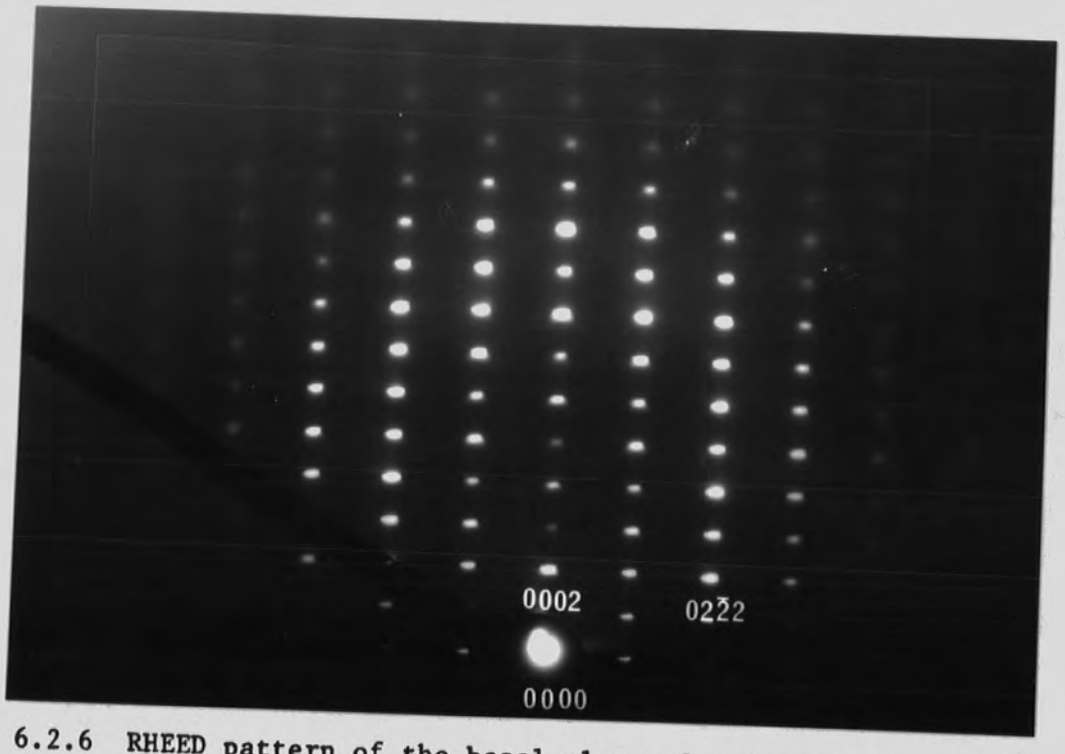

FIGURE 6.2.6 RHEED pattern of the basal plane of a freshly etched CdSe single crystal

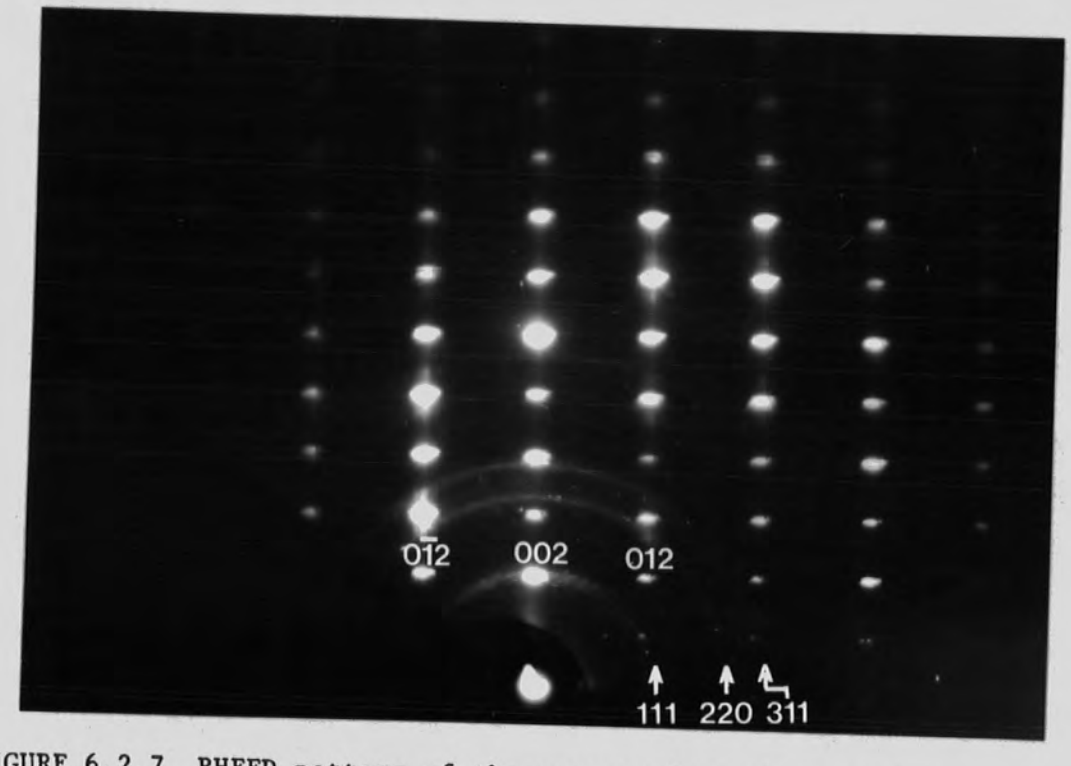

FIGURE 6.2.7 RHEED pattern of the same surface after ageing

usually due to a so-called 'oxide' layer formed by reaction with the etchant or by exposure to the atmosphere. In this particular study of CdSe, it is evident from the shifts in the plots of C^{-2} against V that the surface (interface) states and interfacial layer have a substantial effect on the C-V curves. Since the photoelectric technique is generally regarded as giving a more definitive measurement of the barrier height[7], (as long as the Fowler plot gives a good straight line), the thickness of the insulating layer and the density of the interfacial states can be estimated by using the difference in barrier heights measured by the C-V and photoelectric techniques. The value of the photoelectric barrier height $\Phi_{bn_{ph}}$, can be calculated by using equation[3.32], $\Phi_{bn_{ph}} = \Phi_{bn}' + \Delta\Phi_{bn}$. In figure 6.2.3 $\Phi_{bn}' \simeq 0.64$eV is the intercept of the Fowler plot and $\Delta\Phi_{bn} \simeq 0.027$eV is the Schottky barrier lowering at zero bias. A value of 0.667eV then results for $\Phi_{bn_{ph}}$.

The value of the barrier height from C-V measurements is given by $\Phi_{bn}'_{C-V} = \Phi_{bn_{C-V}} + kT/q$ and was found to be 0.701eV. When an insulating layer and associated surface states are present $\Phi_{bn}'_{C-V}$ can also be written as[4];

$$\Phi_{bn_{C-V}}' = V_{do} + (E_C - E_F) + \frac{\psi_1}{4} + \psi_1^{\frac{1}{2}} V_{dif}^{\frac{1}{2}} \qquad (3.35)$$

The first two terms on the right hand side correspond to the barrier measured by the photoelectric method $\Phi_{bn_{ph}}$. Therefore subsituting $\Phi_{bn_{ph}}$ for these gives;

$$(\Phi_{bn'_{C-V}} - \Phi_{bn_{ph}}) = \Delta\Phi_i = \frac{\psi_1}{4} + \psi_1^{\frac{1}{2}} V_{dif}^{\frac{1}{2}} \qquad (6.4)$$

where $\psi_1 = \gamma^2 q N_d/\varepsilon_s$ (6.4a)

and $\gamma = \delta\varepsilon_s/\varepsilon_i + q \delta D_s$ (6.4b)

Equation 6.4 may be re-arranged as

$$\psi_1^2 - 8(\Delta\Phi_i + 2 V_{dif}) \psi_1 + 16\Delta\Phi_i^2 = 0 \qquad (6.5)$$

and solving for ψ_1 gives a value of $\sim 1.9\ 10^{-3}$ eV.

Now under the assumptions that; (a) the surface states were too slow to follow the ac (1MHz) signal used in the C-V measurements, (b) the donor density in the bulk did not change much as a result of ageing, (c) the insulating interfacial layers in as prepared devices were thinner than 30Å so that the surface states were in equilibrium with the metal[4], (d) the interfacial layers in aged devices were more than 30Å thick so that surface states were then mostly in equilibrium with the semiconductor, (e) the permittivity of the interfacial layer was the same as that of the semiconductor ($\varepsilon_i \simeq \varepsilon_s$ and $\varepsilon_s \simeq 10\varepsilon_o$), Cowley's analysis[2] could be applied. This analysis shows that, if assumptions (a), and (c) are valid for the as-made devices the slope of $d(1/C^2)/dV$ will be given by the same equation as for an identical MS diode. Conversely, if the

assumptions of (a), (b), (d) and (e) are applicable to the aged devices the slope becomes

$$-(d(1/C^2)/dV) = (1 + \alpha_2)\ 2/q\,\varepsilon_s\,N_d \qquad (6.6)$$

where α_2 is defined as $\alpha_2 = q\,\delta\,D_{sb}/\varepsilon_i$ (6.7)

Here δ is the thickness of the interfacial layer, and D_{sb} the number of surface states which were in equilibrium with the semiconductor. The ratio of the corresponding slopes for the aged (2-months) and as-made devices taken from figure 6.2.2 is then just the term $(1 + \alpha_2)$ which was $\sim$1.86. From equation 6.7 the thickness of the interfacial layer can now be written in terms of the surface state density (D_{sb}),

$$\delta = (0.86\ \varepsilon_i)\ /\ qD_{sb} \qquad (6.8)$$

Substituting for δ in equations 6.4.b and 6.4.a together with the previously calculated value for $\psi_1 \simeq 1.9\ 10^{-3}$eV gives a surface state density of $D_{sb} \simeq 3.84.10^{12}\ cm^{-2}\ eV^{-1}$ and hence $\delta \simeq 124\text{Å}$.

A similar analysis using the more rigorous theory of Fonash[3] was also applied to the above results. The slopes for the as-made and aged devices then become

$$(1 + \alpha_1)\ (C_W + C_I)/C_W\ (1 + \alpha_1) \qquad (6.9)$$

and $C_W' + C_I'/C_W' + (1 + \alpha_2)\, C_I'$ (6.10)

Where C_W, C_W' and C_I, C_I' are the capacitances of the depletion regions and the interfacial layers for the as-made and aged devices respectively. Here,

$$\alpha_1 = q\,\delta D_{sa}/\varepsilon_i \tag{6.11}$$

represents the density of surface states (D_{sa}) in equilibrium with the metal. Following the same assumptions used above and inserting the values for the capacitances (except for C_I'), it can be shown that the prediction obtained by applying Cowley's analysis to the as-made diode is in fact a reasonably good approximation. The ratio of slopes can then be written in terms of α_2 which was

$$\alpha_2 \simeq 3.06\ 10^{-18} + 0.86\ C_I'/1.86\ C_I' \tag{6.12}$$

The capacitance of the implied interfacial layer for the aged devices (C_I') could not be estimated easily since there was no saturation of the C-V curves in the high accumulation region. However, when C_I' was calculated for different thicknesses of surface layers ranging from 30 to 200 Å, α_2 was found to vary by only 6% between the minimum and the maximum thicknesses. Inserting a representative value of 100 Å for the thickness, α_2 was then found to be 0.45. Then a density of surface states of $D_{sb} \simeq 2.15.10^{12}$ cm^{-2} eV^{-1} was estimated from equations 6.7.

Alternatively, if it can be assumed that ideality factors of $n \gg 1$ indicate the existence of an interfacial layer then the density of surface states may be estimated using the analysis of Card and Rhoderick[6]. This gives the ideality factor in terms of the density of surface states and the thickness of the interfacial layer:

$$n = 1 + \frac{(\delta/\epsilon_i)\left[(\epsilon_s/W) + q\,D_{sb}\right]}{1 + (\delta q\,D_{sa}/\epsilon_i)} \qquad \text{(i.e. eq.3.35)}$$

With aged devices, since the thickness of the interfacial layer exceeded 30Å, most of the states were considered to be in equilibrium with the semiconductor rather than with the metal[4]. Following the above analysis (eq. 3.35) using this assumption, and the predicted value of 124Å the surface state density for the aged devices was estimated to be $D_{sb} \simeq 6.7\ 10^{12}\ cm^{-2}\ eV^{-1}$ from the observed ideality factor of $n = 2.54$.

6.2.6 Energy Band Scheme

According to the simple Schottky-Mott theory (eq. 3.5) the barrier height for the Au:n (CdSe) system should be $\Phi_{bn} \simeq 0.15eV$ ($\Phi_m \simeq 5.1eV$) and $\chi_s \simeq 4.95eV$)[8].

The values of Φ_m and Φ_s given in last reference were obtained under UHV conditions. However such conditions did not prevail in these experiments where barrier heights ranging from 0.29 to 0.70eV have been measured. In the Bardeen model[9], the Schottky barrier height is determined by the charge localised at the semiconductor surface in the interface states. The surface state charge density can be obtained from $\Phi_{bn} = \beta(\Phi_m - \chi_s - \frac{\delta Q_t}{\epsilon_i}) + (1 - \beta)(Eg - \psi_t)$ (3.8) where $\beta = \epsilon_i/(\epsilon_i + \delta\, qDs)$ (which refers to a distribution of surface

states with a maximum at ψ_t, where Q_t is then the charge stored in the surface states when they filled up to ψ_t).

$$\frac{\varepsilon_i}{\delta\beta}\left[\Phi_{bn} - (1-\beta)(E_g - \psi_t) - \beta(\Phi_m - \chi_s)\right] = Q_t \qquad (6.12)$$

Brillson[10] has reported observing a set of surface state levels located ~ 0.4eV below the conduction band. Assuming this to be the appropriate value for $(E_g - \psi_t)$, application of equation 6.12 to both the aged and the as-made devices, using previously calculated values of the surface state density, allowed estimates of Q_t to be made. These are given in Table 6.2.2.

The relatively smaller negative value of the surface charge in as-made devices (Table 6.2.2) would be expected to produce a degree of band bending at the surface. This could be responsible for the observed barrier height which was larger than the conventional value predicted by the Schottky-Mott limit $(\Phi_m - \chi_s)$. This argument could also be extended to the aged devices where a larger negative value of surface charge was calculated indicating even more band bending and hence a much larger value for the barrier height. The apparent increase in the magnitude of the surface charge in aged devices would indicate a shift in the neutrality level (ψ_o) (see chap. 3.3.3) towards the valence band edge.

The resultant band diagrams for (non-ideal) as-made and aged diodes of Au:n(CdSe) are shown in figure 6.2.8 a, b.

6.2.7 Discussion

The poor rectification, and particularly the very large reverse

Description of Characteristics	D_{sb} cm^{-2} eV^{-1}	β	Q_t Coul/cm^2	No. of filled States D_{sa} cm^{-2} eV^{-1}	No. of filled States D_{sb} cm^{-2} eV^{-1}
As-made	—	0.83	$-3.08.10^{-7}$	$1.9\ 10^{12}$	—
Aged	$3.84.10^{12}$	0.54	-5.42.10-7	—	$3.4.10^{12}$

TABLE 6.2.2 Surface state characteistics for 3-days Se annealed Schottky devices.

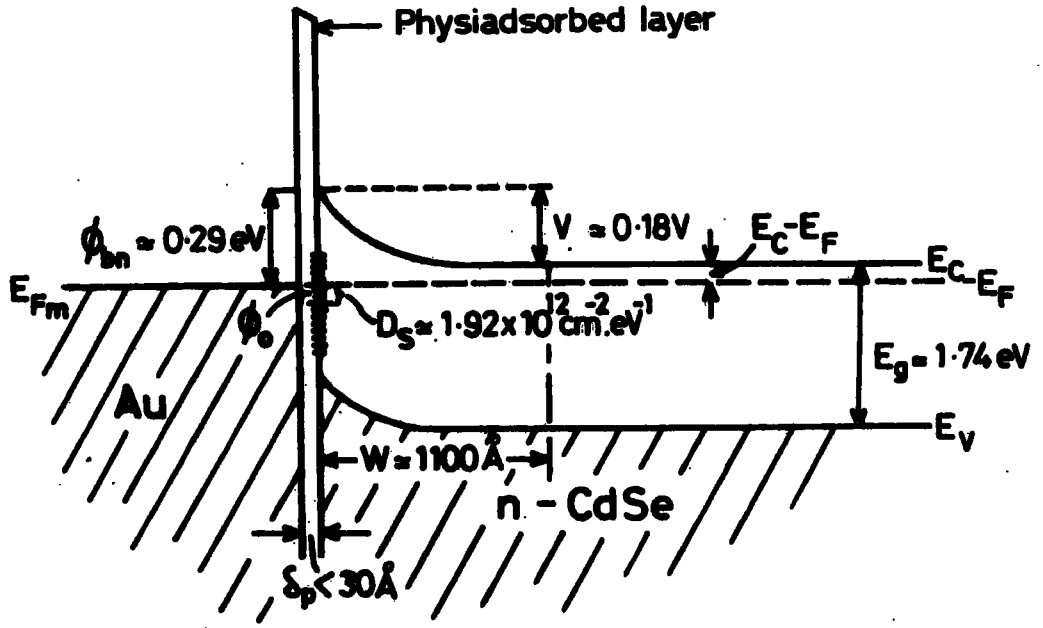

(a)

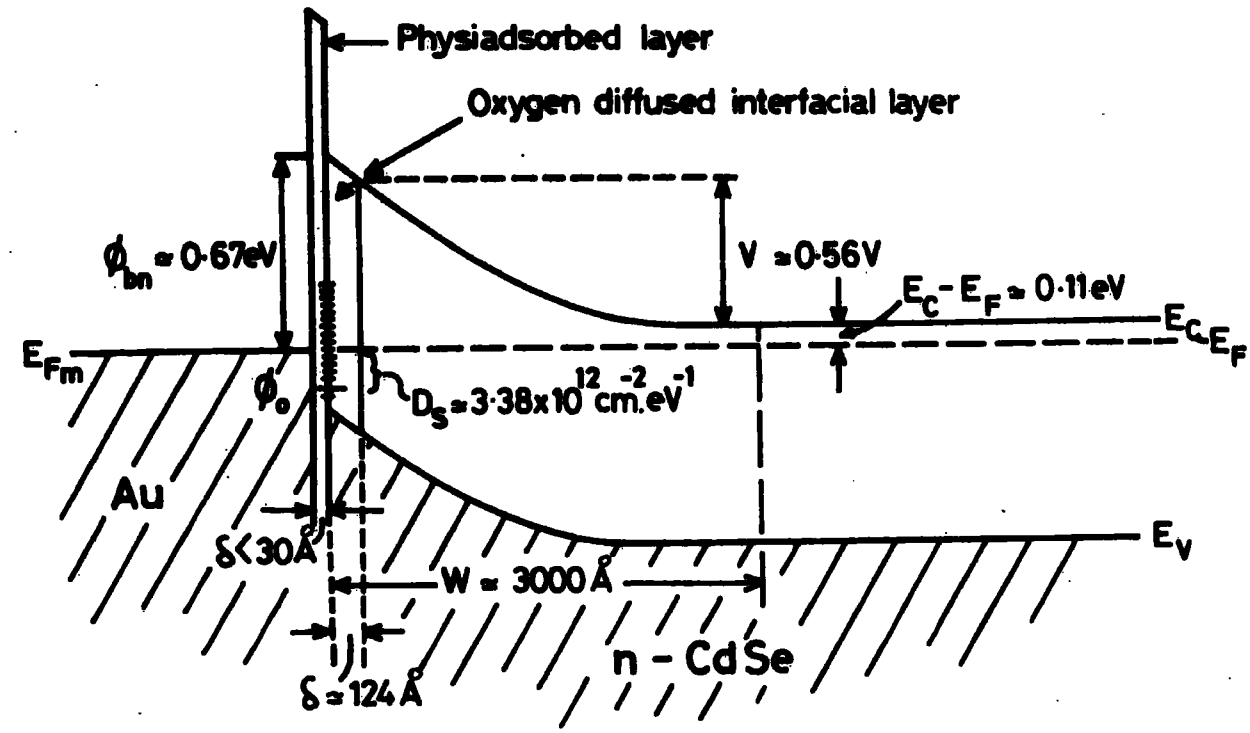

(b)

FIGURE 6.2.8 The band diagram of Au:n (CdSe) Schottky barriers (a) As made (b) Aged

bias leakage current of as-made diodes could be interpreted in terms of a highly conductive surface layer and physically adsorbed oxygen. Heinz and Banks[11] (1957) have reported that, in as-grown CdSe single crystals, there is an excess of Cd and that this excess is more pronounced at the surface. The surfaces are therefore more conductive than the bulk. Detailed studies by Bube[12] (1957) have shown that oxygen is adsorbed on these surfaces and that the adsorbed oxygen produces acceptor-like states thereby reducing surface conductivity. Somorjai[13] has also made extensive studies of the interaction of oxygen with highly conducting thin film CdSe surfaces. He found that the oxygen gave rise to both donor and acceptor-like surface states, in which the latter were important because of their permanence and quantity. A change in the surface layer, from accumulation into depletion has also been reported by other workers both on single crystals[14,15,16] and thin film[17,18] CdSe. The behaviour of a Schottky diode on such highly conducting (accumulated) surfaces has already been reported by Yu and Snow[19] (1968), Shannon[20] (1976) and Popovic[21] (1978).

When first made, the Schottky barriers used in the present study would have had physically adsorbed oxygen beneath the gold contact, and this would have contributed to the poor diode behaviour. This thin layer would reduce the effective barrier height thereby allowing a tunnelling current to flow[47]. The improvement in the rectification of the diode and particularly the drastic reduction of the reverse bias leakage current which occurs after ageing in air is attributed to a change in the role of the adsorbed layer of oxygen. With time, initially physi-adsorbed oxygen will diffuse into the surface region giving rise to acceptor-like surface states. First

the surface will become progressively less conductive and will eventually act as a guard-ring around the gold contact. Similar behaviour to this has been reported by Lepsetter and Sze[22] with devices prepared on silicon with a diffused p-type guard-ring to eliminate the surface accumulation effect. Secondly, adsorption evidently also occurs beneath the gold contact both by the chemi-adsorption of oxygen which was trapped at the surface before the deposition of the evaporated gold and by the diffusion of oxygen through and around the gold layer. Consequently, after ageing, the structure of these devices may be considered to be MIS rather than MS. The change in the region beneath the surface caused by the diffusion of oxygen was accompanied by the structural modification shown by RHEED patterns (Fig. 6.2.6, 6.2.7) coinciding with the variations in the electrical characteristics. Further evidence to support this conclusion will be given in sec. 6.4 by noting the similarity between the characteristics of the devices prepared on mechanically polished surfaces and those of diodes which were formed on etched surfaces and measured after 2-months of ageing in air.

In order to provide a better understanding of the effect of oxygen on the Au:n(CdSe) structures a semi-quantitative analysis of surface states was attempted making several inevitable assumptions. Among these, the barrier height determined by the photoelectric method was considered to be the best estimate and it was therefore used as a reference value in these calculations. Now it has been shown that the direct measurement of MS barrier heights can be affected by the presence of non-linearities in the Fowler plots due to (1) the photoexcitation of carriers from interface states[23,24] and (2) the presence of a thick insulating layer which gives rise to a

different slope corresponding to the metal-insulator barrier. However, the latter was clearly not the case since there was no evidence for a thick oxide layer (δ_{ox} > 30Å) from the RHEED investigations. Instead, in the aged devices there was an internal layer of polycrystalline, sphalerite CdSe which was more resistive so that there would be no discontinuity in the energy bands at the interface between the bulk and this interfacial layer. (See fig. 6.2.8b). Secondly the Fowler plots were linear implying that the contribution from the photoexcitation of carriers in surface states was negligible. By invoking an interfacial layer as shown in fig. 6.2.8(b), the semiconductor permittivity could also be used as the permittivity of the interfacial layer so that assumption (e) in Sec. 6.2.5 would be a good approximation.

The role of oxygen as an acceptor impurity in CdSe has already been reported[12,13]. If there was a large amount of diffused oxygen in the bulk semiconductor, the net donor density ($N_d = N_d^+ - N_a^-$) might have been reduced and the concentration gradient of the oxygen acceptors would cause a non-linearity in C^{-2} -V curves. Since there was no significant deviation from linearity in the curves presented in fig. 6.2.2 it follows that assumption (b) was also reasonable. The remaining assumptions (a), (c) and (d) were in fact very good approximations and have already been implicitly discussed earlier in this chapter.

As the results in table 6.2.2 show, the barrier heights were evidently less dependent on the work function of the metal contact, particularly in aged devices. Barrier heights which were nearly independent of the work function of the metal used, have been reported by Mead[25] and later by Consigny et al[26,27] for CdSe

single crystals. For this to occur the density of surface states should be of the order of 10^{13} cm^{-2} (9). The surface state densities of (3-7) 10^{11} cm^{-2} observed by Consigny(27) and co-workers were far too low to cause pinning the Fermi level. The detailed study by Brillson(10) of CdSe surfaces also revealed that the surface state densities never exceed $10^{12}cm^{-2}$. However, in the present work equation 6.12 and table 6.2.2 demonstrated that the barrier height was a combination of several parameters such as the thickness of the interfacial layer, the occupancy of the surface states and the difference $(\Phi_m - \chi_s)$ between the work function of the metal and the electron affinity of the semiconductor, particularly at the as-made stage. It has to be pointed out that recent studies by Frese(28) have shown that the lower values of electron affinity of 4.1eV reported by Shay and Spicer(29) for some CdSe surfaces could be significant. Equation 6.12 shows that a small increase (i.e. > 0.12eV) in the $(\Phi_m - \chi_s)$ term would give rise to a positive charge stored in interface states, suggesting that the surface was accumulated. An important implication of this situation would be the requirement of a smaller number of surface states to pin the Fermi level. In fact some preliminary experiments with $(SN)_x$ Schottky barriers on CdSe did show a dependence on the 'metal' work function with a barrier height of > 1eV for these devices and thus providing additional support for the above discussion.

6.3 SCHOTTKY BARRIERS ON SAMPLES ANNEALED IN SELENIUM FOR ONE-MONTH

6.3.1 Introduction

Large reversible changes in the resistivity of CdSe crystals on annealing in a partial pressure of one of the components have been reported by several workers(30,31,32). Since the diffusion of

selenium would have been very slow at the low annealing temperatures used to obtain moderate resistivity samples it was unlikely that a uniform bulk resistivity was obtained after 3-days treatment. As a result subsequent steps of mechanical polishing and etching necessary for the device fabrication could easily remove the moderate resistive layers. This was in fact demonstrated in the resistivity control experiments. To overcome this problem and to produce more homogenous substrate material longer periods of annealing in Se-vapour at 550°C (one month) were employed.

6.3.2 Electrical Characteristics

Schottky devices similar to those described in sec. 6.2 were formed on these substrates and the electrical characteristics were recorded immediately after fabrication and after ageing in air at 100°C for 16h. The I-V characteristics of a typical Schottky device in the as-made and aged conditions are shown in fig. 6.3.1. The leakage current of the as-made diode was much less than from as-made diodes on 3-day annealed material. After accelerated ageing in air at 100°C for 16h the I-V characteristics were very similar to the 3-day annealed devices treated in the same way.

The C-V characteristics measured in the same way as described in sec. 6.2 are shown in figure 6.3.2 and the diode parameters, N_d, V_{dif}, (E_c-E_F), $\Phi_{bn_{C-V}}$ and W_{C-V} (from Schottky-Mott theory) are tabulated in table 6.3.1. The longer treatment in selenium vapour gave rise as expected to a lower uncompensated donor density for these devices.

6.3.3 Measurements of Barrier Height

(a) Photoelectric

A Fowler plot derived from the spectral response of the

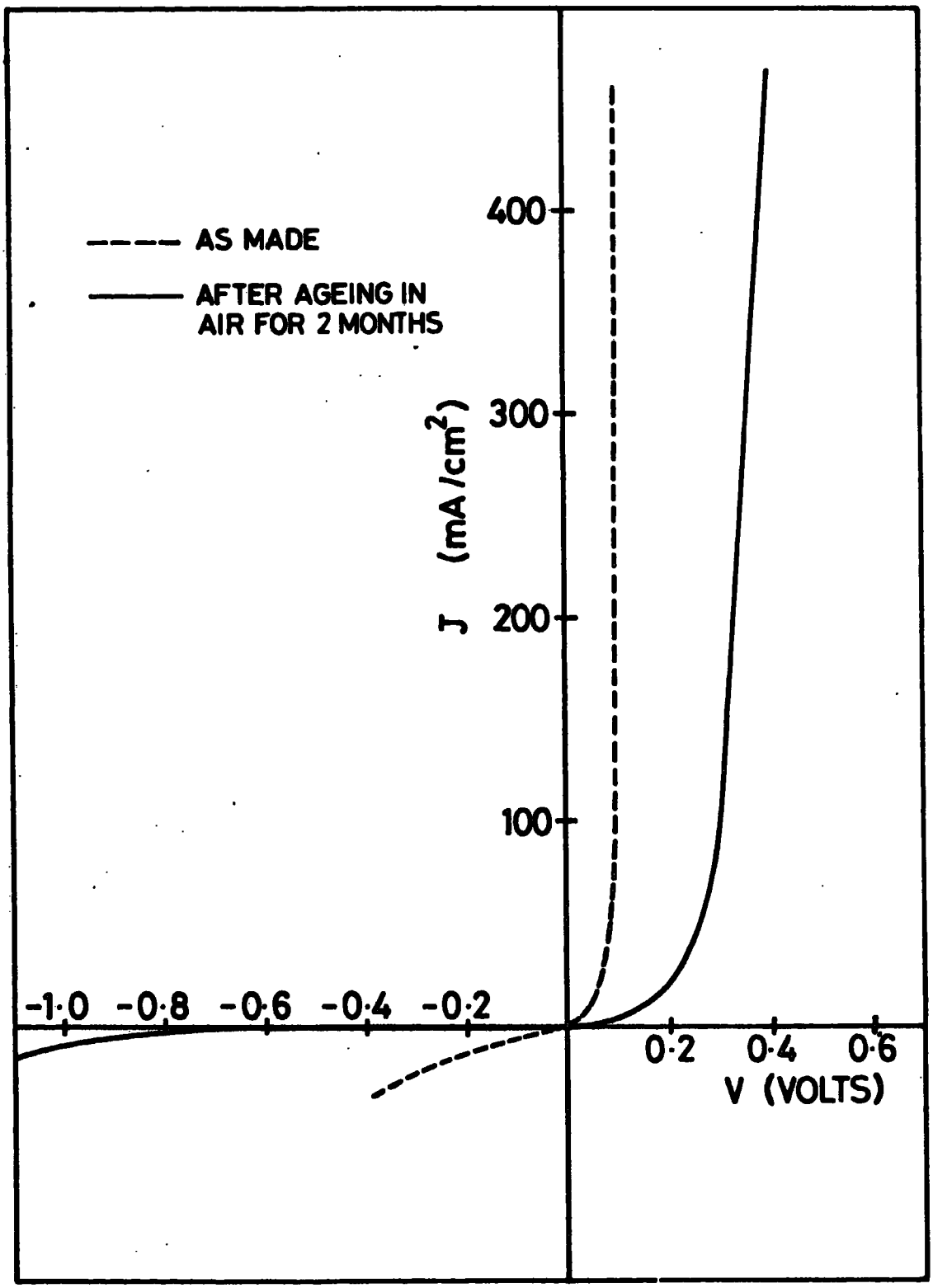

FIGURE 6.3.1 I-V characteristics of a typical Schottky device formed on 1-month Se-annealed CdSe (Before and after ageing)

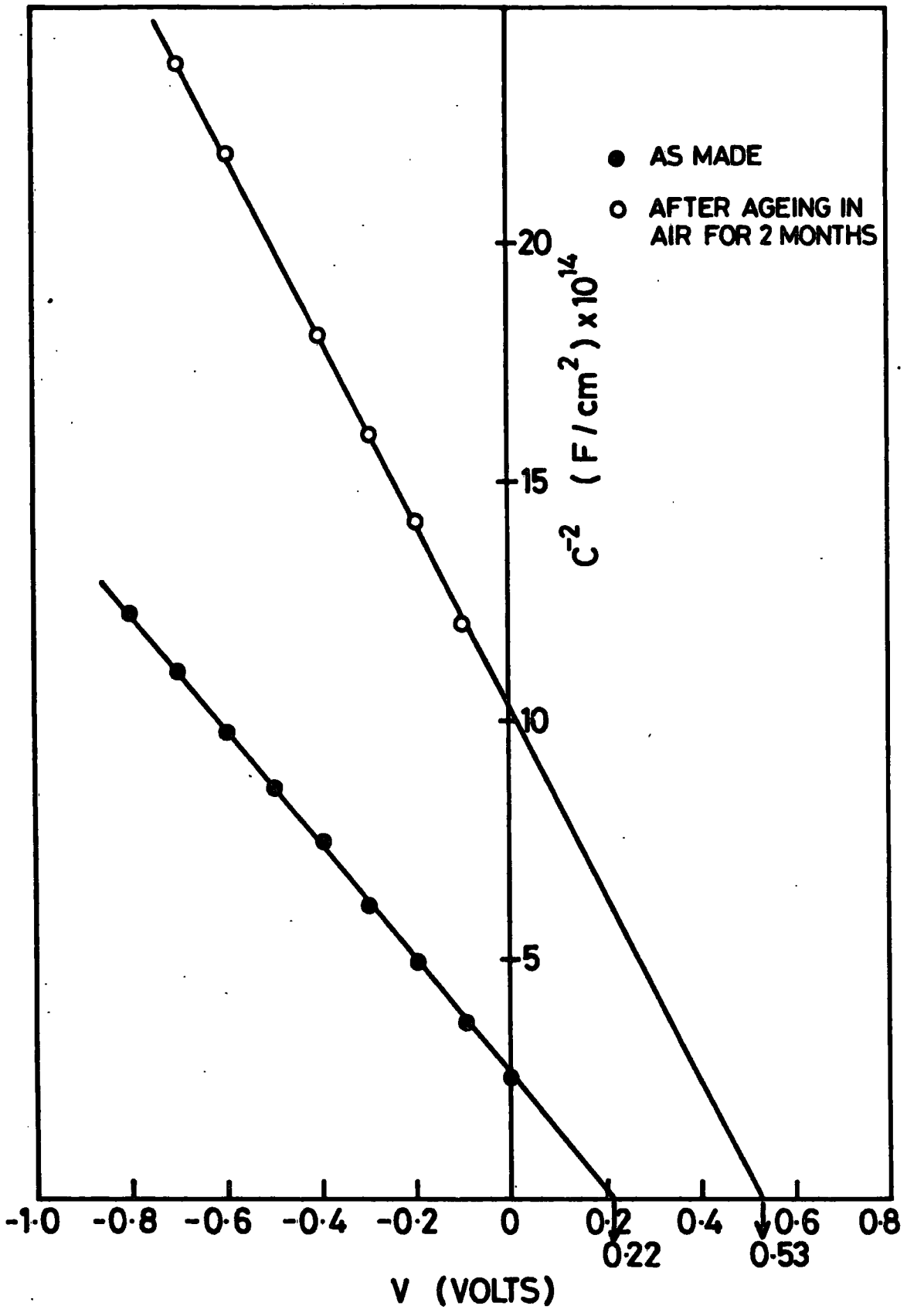

FIGURE 6.3.2 C^{-2}-V characteristics of the same Schottky device (fig. 6.3.1) measured before and after ageing

Description of Characteristics	V_{dif} (eV)	N_d $(10^{16})cm^{-3}$	(E_C-E_F) eV	$\Phi_{bn_{C-V}}$(eV)	W_{C-V} μm Zero bias
As-made	0.22	1.14	0.12	0.34	0.15
After ageing in air 100°C 16h.	0.53	0.74	0.13	0.66	0.28

TABLE 6.3.1 General characteristics of 1-month Se annealed Schottky devices.

short-circuit current of a typical aged Schottky device prepared on one-month Se-annealed CdSe substrate is shown in figure 6.3.3. A value of $\Phi bn_{ph} \simeq 0.63eV$ was obtained from the intercept of this plot.

(b) Forward I-V Characteristics

The plot of lnJ against V for the forward I-V characteristic for the same device is shown in fig. 6.3.4. Similar calculations to those described in sections 6.2.3 yielded a value of $\Phi_{bn} \simeq 0.57eV$ for the barrier height.

6.3.4 RHEED Studies

RHEED examination on the aged devices which were formed on one-month Se-annealed material gave almost identical diffraction patterns to that previously shown in fig. 6.2.7.

6.3.5 Surface Effects

Similar calculations to those described in section 6.2.5 for the interfacial layer and surface states following the theories of Cowley[2], Fonash[3] and Card and Rhoderick[6] (see sec. 6.25), yielded values of $\delta \simeq 85\text{Å}$, $D_{sb} \simeq 3.5 \times 10^{12}\ cm^{-2}\ eV^{-1}$; $D_{sb} \simeq 2.0 \times 10^{12}\ cm^{-2}\ eV^{-1}$; and $D_{sb} \simeq 6.5 \times 10^{12}\ cm^{-2}\ eV^{-1}$ respectively. These in turn lead to the values of β, surface charges and the number of filled surface states listed in Table 6.3.2. The band diagram in figure 6.2.8 a and b is also appropriate for the devices on one-month annealed material.

6.3.6 Discussion

The apparent improvement in the I-V characteristics of the as-made diodes compared to those prepared on 3-day annealed material

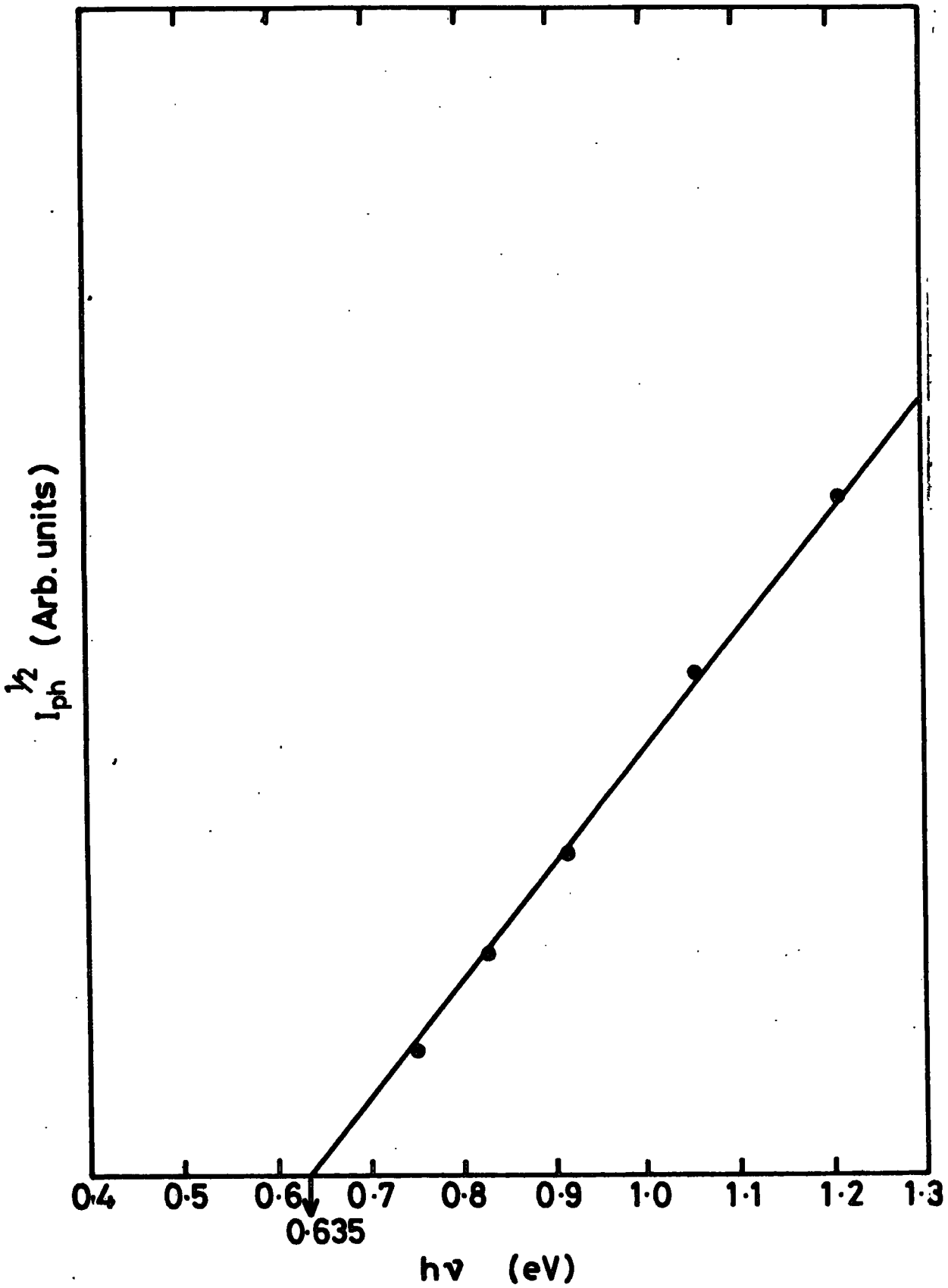

FIGURE 6.3.3 A Fowler plot of an aged Schottky diode prepared on 1-month Se-annealed CdSe

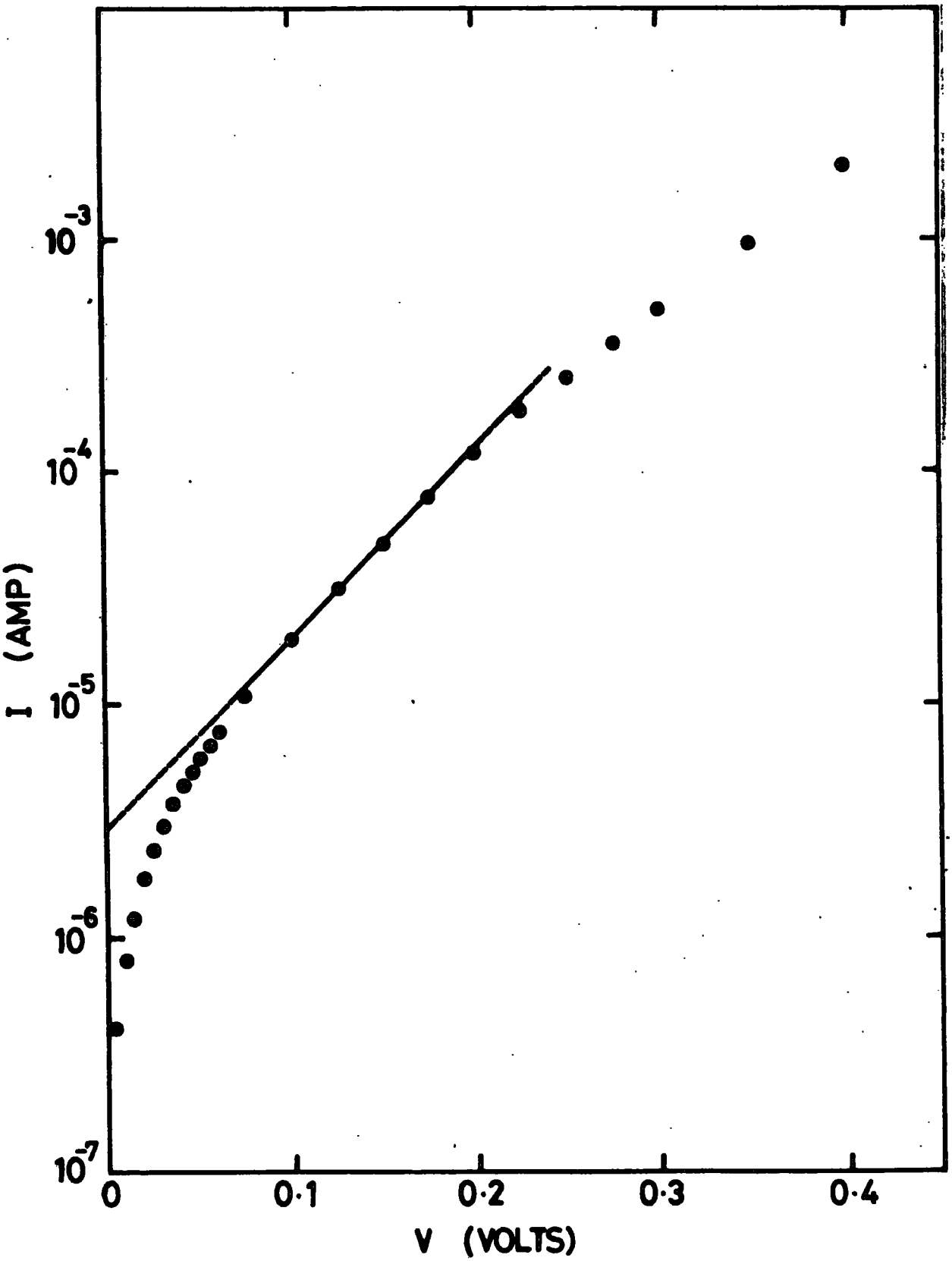

FIGURE 6.3.4 Semilog plot of forward I-V characteristics of an aged Schottky diode prepared on 1-month Se-annealed CdSe

Description of Characteristics	D_{sb} cm^{-2} eV^{-1}	β	Q_t Coul/cm^2	No. of filled States D_{sa} cm^{-2} eV^{-1}	No. of filled States D_{sb} cm^{-2} eV^{-1}
As-made	—	0.84	$-5/25\ 10^{-7}$	$3.28\ 10^{12}$	—
Aged	* $3.53\ 10^{12}$	0.64	$-6.83\ 10^{-7}$	—	$4.2.10^{12}$

TABLE 6.3.2 Surface state characteristics for 1-month Se annealed devices.

* From Cowley's analysis; given as a representative value.

may be interpreted in terms of the compensation of the surface accumulation layer by the introduction of selenium. This would lead to the formation of cadmium vacancies[31] which would act as acceptors in an analogous way to the oxygen introduced during this ageing process. The lower net donor concentration in devices on one-month annealed material is supporting evidence for this mechanism.

According to references (13), (15) and (16) dealing with Cd-rich surfaces of CdSe, the adsorption ofoxygen is strongly related to the number of available donor states at the surface. This implies that the occurrence of the polycrystalline cubic phase of CdSe which is associated with oxygen adsorption would be less pronounced if the surface were more resistive (i.e. less Cd-rich). However, after ageing no appreciable difference in the RHEED patterns of 3-day and one-month Se-annealed material was observed, probably because of the actual change in the resistivity was relatively very small. It is worth noting that RHEED investigations on highly resistive crystals displayed either no polycrystalline ring pattern or else a very weak one after they were heat treated in air at 100°C for even longer periods than 16h.

In other respects the one-month annealed material resembled to the 3-day annealed CdSe and much of the discussion in sec. 6.2.7 therefore applies.

6.4 SCHOTTKY BARRIERS FORMED ON POLISHED CUBIC (SPHALERITE) LAYERS

6.4.1 Introduction

As mentioned briefly in chapter 5.3 the polycrystalline cubic layers produced on single crystal CdSe by mechanical polishing had a higher resistivity than the underlying hexagonal base and displayed

photoconductive effects. Schottky devices have been prepared on these cubic layers and their properties investigated. The details of the preparation of the sphalerite layers were given in chapters 4 and 5.

6.4.2 Electrical Characteristics

The I-V characteristics of a Schottky device made on such a polished layer showed a smaller reverse bias leakage current than of any aged device on etched surfaces and did not change with ageing (see Fig. 6.4.1). The structure of these devices could more realistically be regarded as MIS even in the as-made stage because of the insulating property of the cubic layer.

The C-V characteristic for the same device is shown in Fig. 6.4.2 and the calculated parameters are summarised in Table 6.4.1. The higher value of donor concentration for these devices was entirely due to the use of a more conducting CdSe crystal which had not been heat treated in Se-vapour. As the values in Table 6.4.1 show, the barrier height was slightly larger than that of the device prepared on the etched surface which had been aged for 2 months. This is consistent with the similarity of the I-V characteristics of the two devices.

6.4.3 Measurements of Barrier Height

(a) Photoelectric

Since the short-circuit current of these devices was very small, a reliable measurement of the barrier height by the photoelectric method could not be made.

(b) Forward (I-V) Characteristics

The plot of LnJ against V for a typical device prepared on a mechanically polished surface is shown in Fig. 6.4.3. The

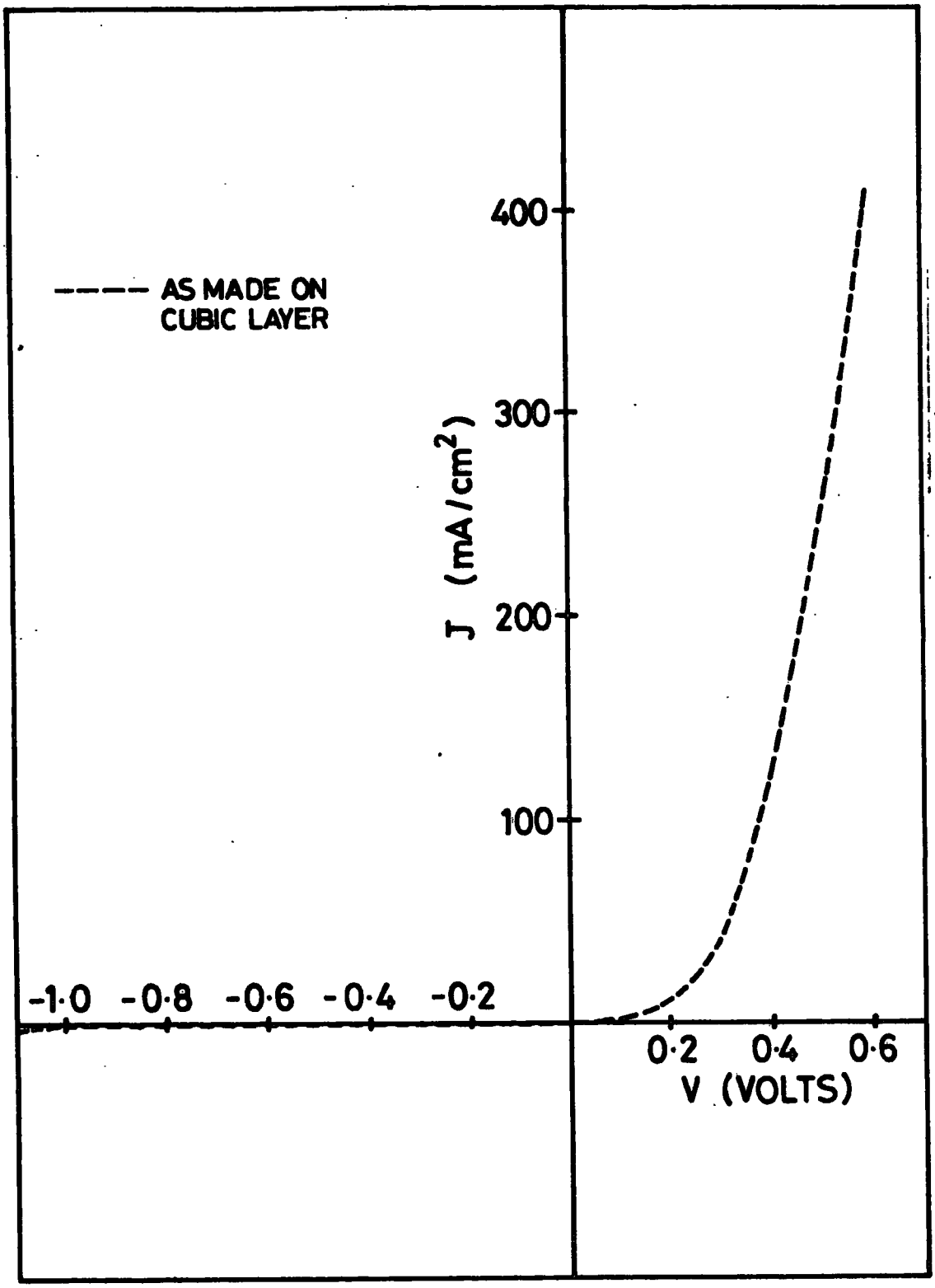

FIGURE 6.4.1 I-V characteristics of a typical Schottky device prepared on a mechanically polished surface of CdSe

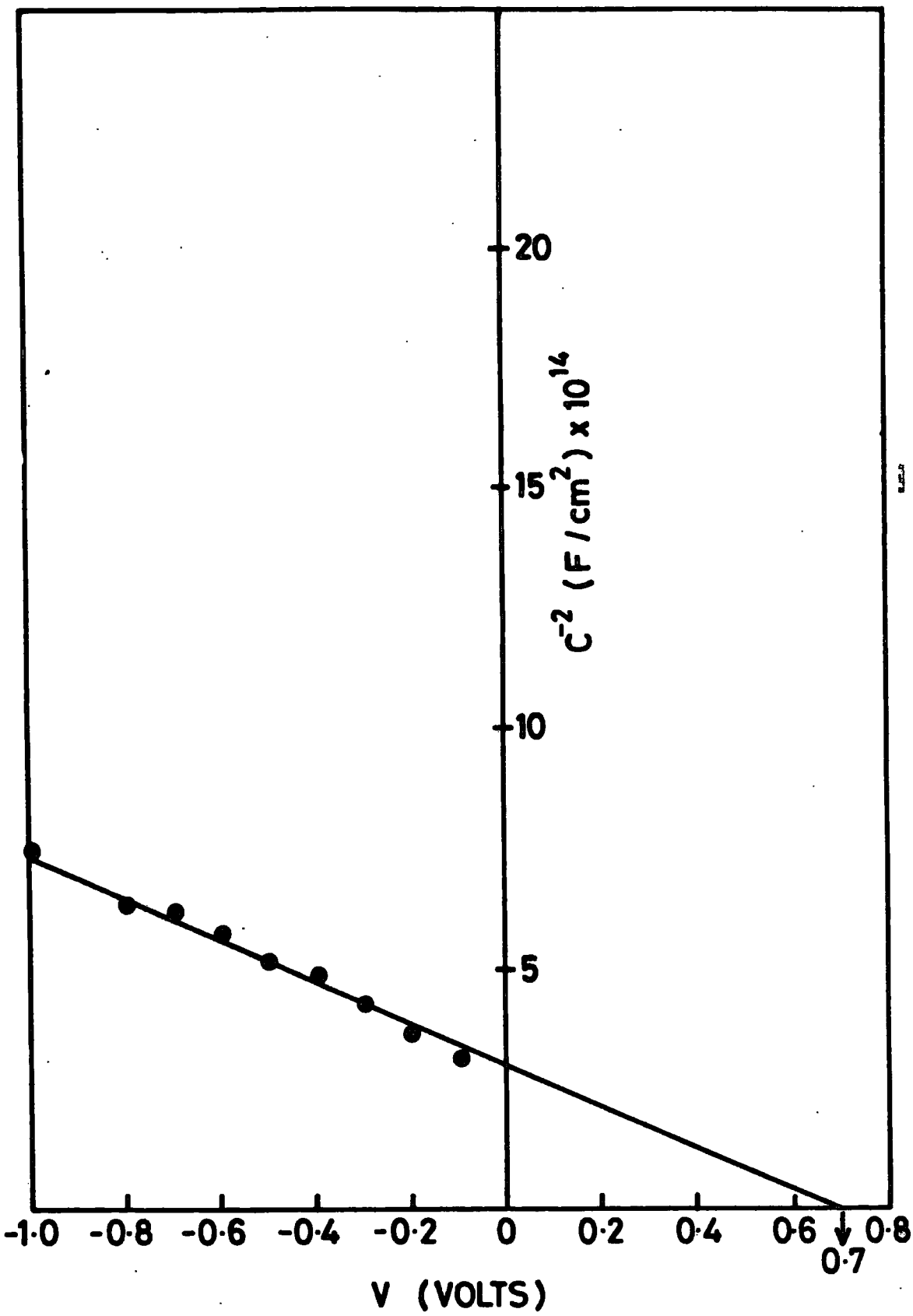

FIGURE 6.4.2 C^{-2}-V characteristics of the same device (fig. 6.4.1)

Description of Characteristics	V_{dif}(eV)	N_d (10^{16}cm^{-3})	(E_C-E_F)eV	$\Phi_{bn_{C-V}}$(eV)	W_{C-V} μm
As-made	0.7	3.29	0.09	0.79	0.16

TABLE 6.4.1 General characteristics of Schottky barrier devices formed on mechanically polished surfaces.

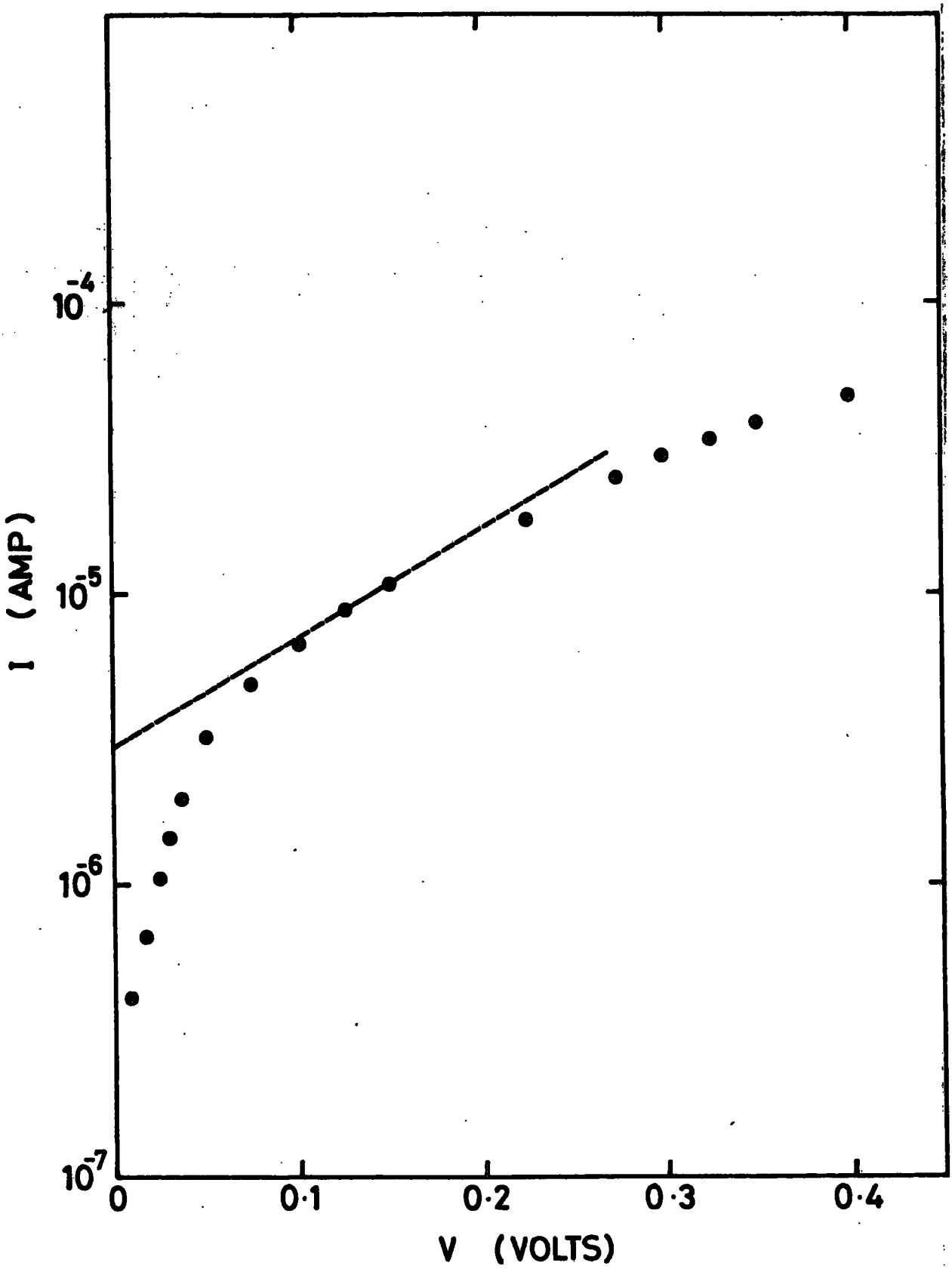

FIGURE 6.4.3 Semilog plot of forward I-V characteristics of the same device (fig. 6.4.1)

calculations for the barrier height using the intercept of this plot gave a smaller value of $\Phi bn_{I-V} \approx 0.56eV$ compared to that of 0.8eV obtained from C-V measurements. This is probably due to the even larger values of $n \geq 5$ ideality factors of these devices.

6.4.4 RHEED Studies

When a single crystal of CdSe was polished using alumina powder with a particle size of 1μm or less, the resulting surface, regardless of the orientation of the underlying crystal always gave rise to the RHEED pattern shown[33] in Fig. 6.4.4. The diffraction rings in this pattern indicated that the surface layer on this sample was entirely polycrystalline. The radii of the first three rings increased in the sequence $\sqrt{3}$, $\sqrt{8}$, $\sqrt{11}$ and were consequently indexed as the (111), (220) and (311) reflections of the cubic sphalerite phase of CdSe.

The nature of the interface between the single crystal hexagonal substrate and the polycrystalline cubic polished layer was studied by successively etching the crystal in concentrated HCl and re-examining it in RHEED as the damaged layer was progressively removed. The RHEED pattern in 6.4.5 represents the polished CdSe crystal after being etched for 15s. Etching for longer than this gave rise to the same diffraction pattern as shown in Fig. 6.2.6. The pattern in figure 6.4.5 contains features from both the polycrystalline layer and the underlying single crystal. In addition, there were arcs of intensity passing through many of the diffraction spots of the hexagonal structure.

When a CdSe crystal was ground to a powder in an agate mortar until the mean particle size was of the order of 20μm, X-ray powder photography studies showed that the grains were still hexagonal.

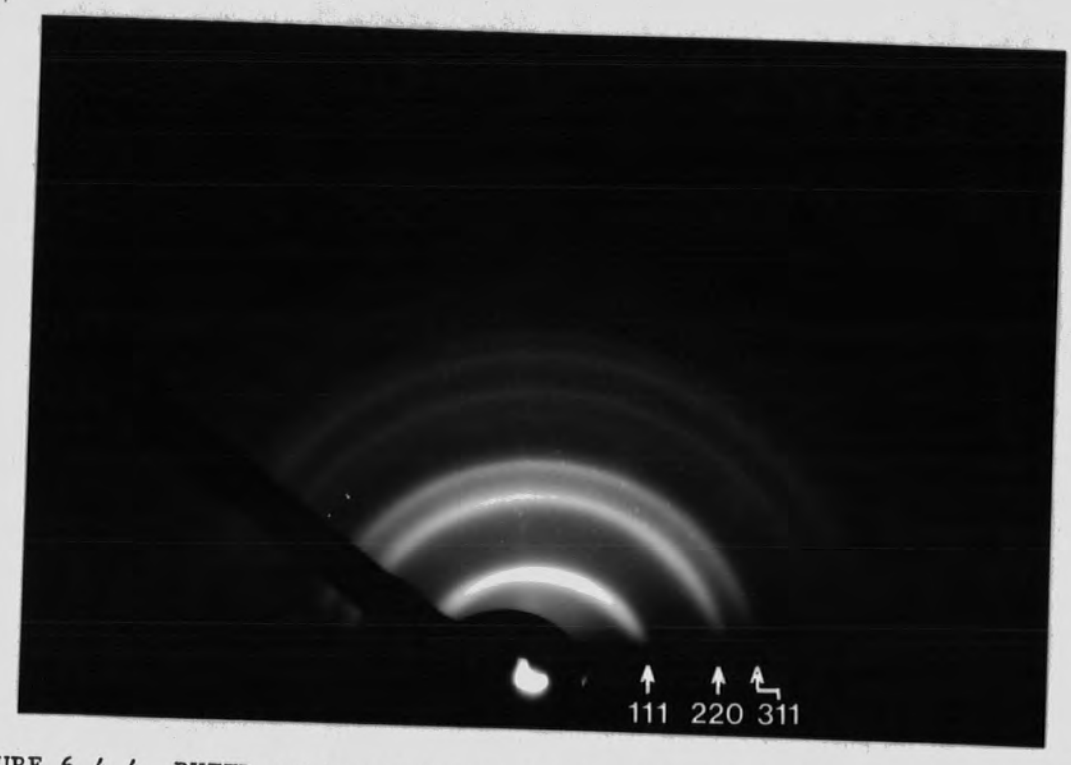

FIGURE 6.4.4 RHEED pattern of a mechanically polished surface of CdSe

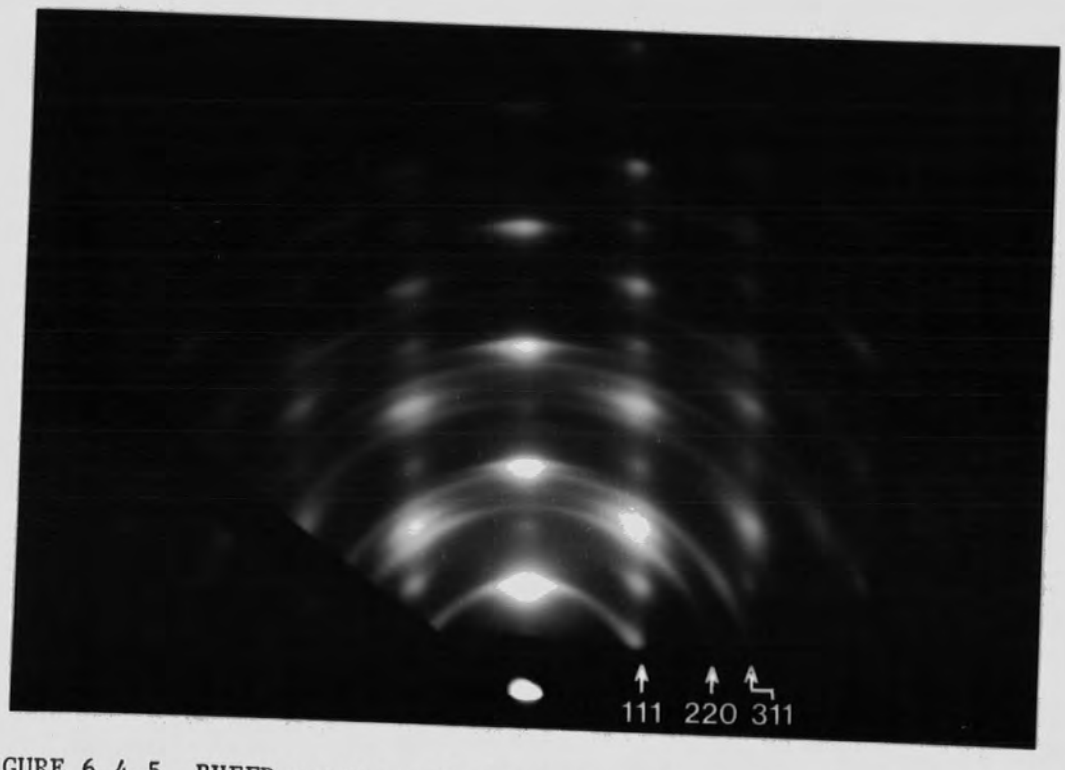

FIGURE 6.4.5 RHEED pattern of the same surface after 15s etch in HCl

However, after ball-milling which reduced the particle size to less than 2μm the grains were predominantly cubic. Here, Fig. 6.4.6 and 6.4.7 represent the powder photographs of hexagonal and cubic structures corresponding to samples with 20μm and ½μm particle sizes respectively.

6.4.5 Surface Effects

The method followed in sec. 6.2.5 for the calculations of the interfacial layer and surface states could not be applied to these devices. Even if the barrier height had been deduced by the photo-electric technique the measurements would certainly be affected by the deliberate introduction of the insulating layer between the metal and the semiconductor. With this type of device the capacitance value of $C \simeq 7.4.10^{-8} F/cm^2$ in the near accumulated region of the C-V characteristic was assumed to be due primarily to the interfacial layer. The thickness of this layer could then be estimated from ($C_I = \varepsilon_i / \delta_i$) as $\delta_i \simeq 1200Å$. Using the assumptions (a) (d) and (e) (see sec. 6.2.5) Fonash's analysis[3] was applied. According to this the extrapolated voltage intercept (V_i) can be written in terms of the diffusion potential (V_{dif}), the thickness (δ_i), and the surface state density (D_{sb}) of the insulating layer.

$$V_i = V_{dif}^{\frac{1}{2}} \cdot V_1^{\frac{1}{2}} + (1 + \alpha_2) V_{dif} + (1 - \alpha_2) V_1/4 \qquad (6.13)$$

Where $\alpha_2 = q \delta_i D_{sb}/\varepsilon_i$ i.e. eq. 3.48 and $V_1 = 2q N_d \delta^2/\varepsilon_i$, i.e. eq. 3.42 Fonash's analysis also gives the slope as

$$- d(1/C^2)/dV = (1 + \alpha_2) \frac{2}{q\varepsilon_s N_d} \qquad \text{(i.e. eq. 3.52)}$$

If the value of the donor density of ($N_d \simeq 1.125\ 10^{17}\ cm^{-3}$),

FIGURE 6.4.6 X-ray diffraction photograph of unmilled (hexagonal) CdSe

FIGURE 6.4.7 X-ray diffraction photograph of milled (cubic) CdSe

independently calculated from the resistivity measurement of the as-grown CdSe substrate, was substituted in eq. 3.42 and eq. 3.52 then values of $\alpha_2 \simeq 2.42$, $D_{sb} \simeq 1.3\ 10^{12}\ cm^{-2}\ eV^{-1}$, $V_1 \simeq 5.86$ V were obtained. Inserting those values and $V_i = 0.7$ V from figure 6.4.2 into eq. 6.12 yielded the value $V_{dif} \simeq 0.38$ V for the diffusion potential of the MIS structure.

6.4.6 Energy Band Scheme

When the equation $\Phi_{bn} = \beta(\Phi_m - \chi_s - \delta_i/\epsilon_i\ Q_t) + (1-\beta)\ (Eg - \psi_f)$ i.e. 6.12. was applied to these devices in the same way in which it was used in sec. 6.2.6, the stored charge in surface states and the corresponding number of filled states were found to be $Q_t = -\ 1.17\ 10^{-7}$ Coul. cm^{-2} and $D_{sb} \simeq 7.33\ 10^{11}\ cm^{-2}\ eV^{-1}$ respectively. (for this, values of $\beta = 0.26$, $\Phi_m - \chi_s = 0.15$eV, $(Eg - \psi_f) \simeq 0.4$eV, $(E_C - E_F) \simeq 0.05$eV and $\Phi_{bn} \simeq 0.75$eV were employed.)

The proposed band diagram for the MIS devices fabricated on polished surfaces of CdSe is shown in Fig. 6.4.8.

6.4.7 Discussion

The strong similarity between the electrical characteristics of the devices made on polished surfaces and those of the aged devices prepared on etched surfaces suggested a relationship between oxygen adsorption and mechanical polishing. The introduction of acceptor-type surface states by mechanical polishing has also been shown to have an effect similar to oxygen adsorption on Germanium (Clarke, 1953[34]. More conclusive support for this relationship came from RHEED studies of both types of surface which have shown identical diffraction patterns (i.e. diffraction rings corresponding to the sphalerite phase of CdSe with the same lattice constant of $\sim$6.00Å).

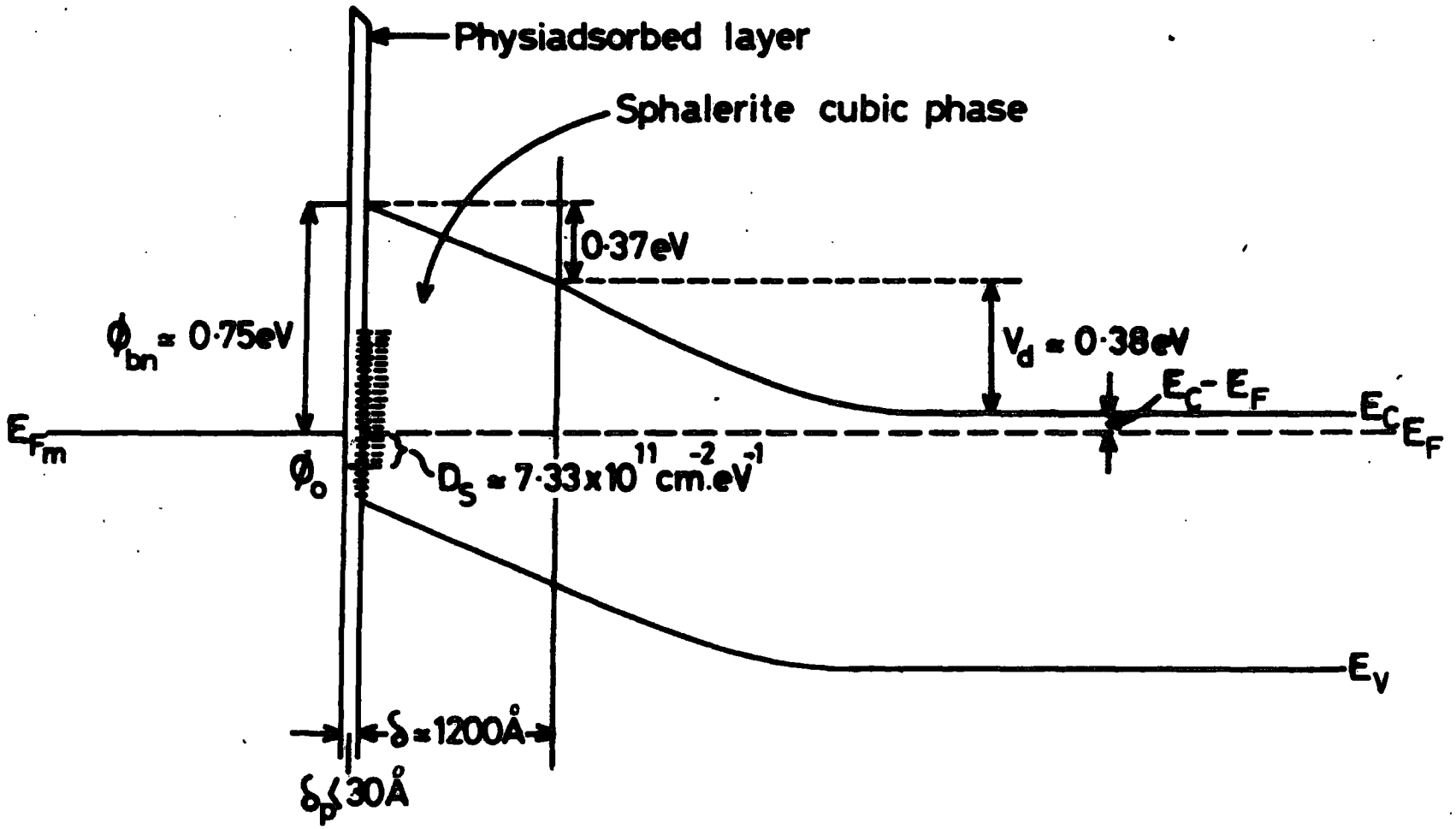

FIGURE 6.4.8 Energy band diagram of a Schottky device prepared on a mechanically polished (sphalerite layer) surface of CdSe

The sphalerite phase of CdSe has previously been produced under a wide range of conditions[35,36], but Daveritz[37] has pointed out that with II-VI compounds in general, there is a strong dependence of the phase formed on the stoichiometry. He concluded that a high Cd excess should favour the hexagonal phase. Since the observation of very low resistivity surfaces is believed to be due to excess Cd, then it was surprising that the surfaces of aged crystals were cubic. In fact it was only after prolonged exposure in O_2 ambient that the cubic phase was observed. It may therefore be concluded that the presence of cubic surface layers is associated with O_2 adsorption.

The reflective nature of the polished surfaces would not permit an estimate of the thickness of the interfacial layer from RHEED observations, but the value of 1200Å obtained from C-V measurements was probably fairly accurate given the particle size of 1/4 μm used for polishing. Since the electron beam penetration depth on these surfaces would be much less than that with etched surfaces because of the surface asperities produced by etching, RHEED would be more sensitive to any additional surface layer. The observation of only the rings due to the sphalerite phase of CdSe in RHEED patterns clearly indicated that such a layer, if present, was negligibly thin. In this case the permittivity of the semiconductor could also be used for the interfacial layer and the calculations became less complicated.

The smaller reverse bias leakage current of the devices made on etched surfaces can be attributed to a higher degree of surface conversion from accumulation to depletion. This conversion would be more pronounced because highly conducting (< 0.1 Ω cm) as-grown CdSe was employed for the substrate material in the preparation of devices

on polished surfaces. The larger potential barrier of these devices can also be attributed to the higher degree of surface conversion, and this would have been less dependent on the metal work function. Following similar arguments in Sec. 6.2.7 and 6.3.6, it may be concluded that the initial higher density of donor like states would accommodate more oxygen and therefore would have given rise to a more resistive and thicker interfacial layer with a correspondingly larger potential barrier.

The fact that oxygen and adsorption appeared to be much enhanced on the polished surfaces provided a convenient way of studying the deep levels associated with oxygen. This was done using space-charge techniques on devices prepared on polished surfaces of CdSe and from the subject matter of the following chapter.

6.5 SCHOTTKY BARRIERS FORMED ON COPPER DOPED SAMPLES

6.5.1 Introduction

The important role of copper as an acceptor impurity in CdSe has already been discussed, and the probable energy levels were obtained from the photoconductivity measurements described in Chap. 5. The main object in preparing Schottky devices on Cu-doped samples was to derive more quantitative information about the parameters of the copper associated centres in CdSe crystals by using space-charge techniques.

The introduction of copper impurity by several methods, and the sample preparation techniques for Schottky devices have been described in Chap.4. Achievement of moderate resistivity (1-1000) Ωcm material by copper doping was found to be even more difficult than by annealing in selenium. Resistivities measured after diffusing in the plated copper impurity were either very high (10^6 -

10^7) Ωcm or very low ($\rho < 10^{-1}$ Ω cm). Of all the methods tried, vacuum deposition of metallic copper gave the most control in obtaining medium resistivity crystals. Because of this difficulty experiments on Schottky diodes could only be carried out on a very limited number (5) of devices.

6.5.2 Electrical Characteristics

The I-V characteristics of a typical copper doped Schottky device in the as-made and aged conditions are given in figure 6.5.1. The relatively small leakage current of the device at the as-made stage was very similar to the sample annealed for one month in Se. After ageing the characteristic improved following the usual pattern found in all the devices made on etched surfaces of CdSe.

The C^{-2}-V plots for Cu-doped CdSe Schottky diode are shown in figure 6.5.2 and the parameters calculated in the usual way are summarized in table 6.5.1.

6.5.3 Measurements of Barrier Height

(a) Photoelectric

Although there was a detectable short-circuit current the barrier height could not be determined because of the non-linear behaviour of the Fowler plots.

(b) Forward I-V Characteristics

The plot of lnJ against V for a typical Cu-doped Schottky barrier is shown in fig. 6.5.3. The calculation of the barrier height using the intercept of the linear section of this plot yielded a value of Φbn_{I-V} = 0.56eV for an aged device.

6.5.4 RHEED Studies

RHEED examination of an aged device formed on a Cu-doped CdSe crystal gave a diffraction pattern similar to that shown in fig.

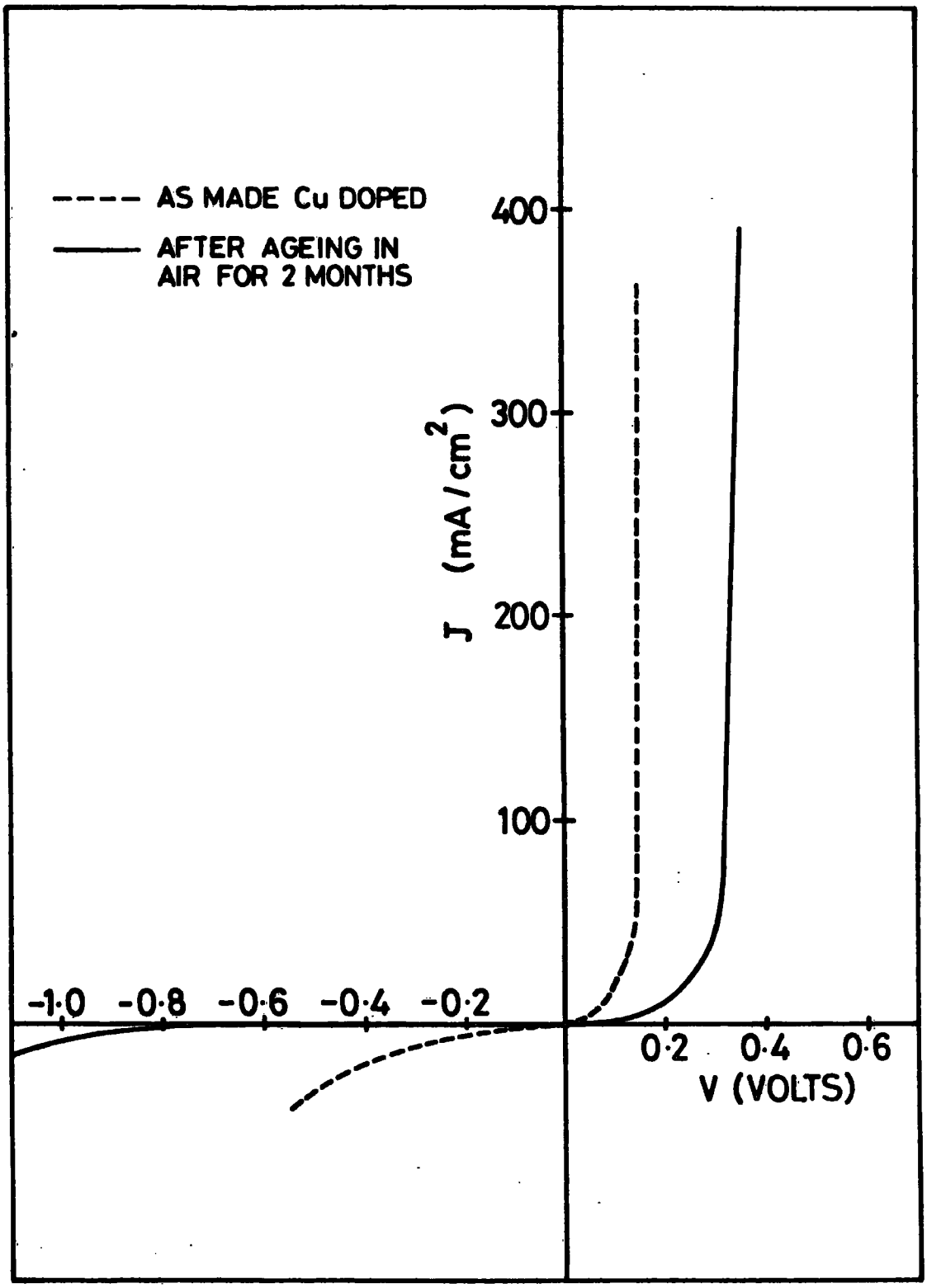

FIGURE 6.5.1 I-V characteristics of a typical Schottky device prepared on Cu-doped CdSe (Before and after ageing)

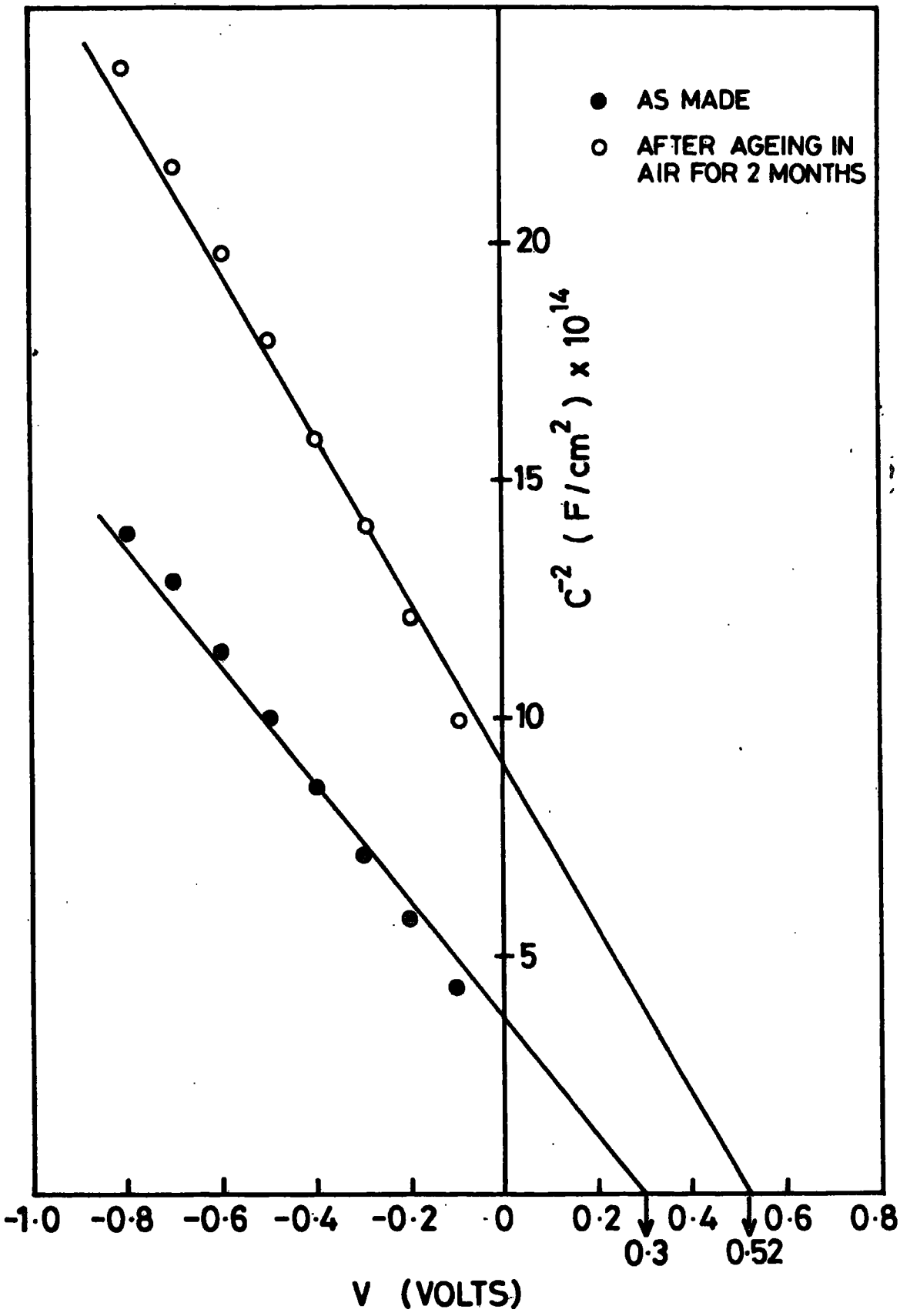

FIGURE 6.5.2 C^{-2}-V characteristics of the same device (fig. 6.5.1) measured before and after ageing

Description of Characteristics	V_{dif}(eV)	N_d (10^{16}) cm^{-3}	(E_C-E_F) eV	$\Phi_{bn_{C-V}}$eV	W_{C-V} μm
As-made	0.25	1.16	0.12	0.37	0.15
After Ageing	0.52	0.82	0.12	0.64	0.26

TABLE 6.5.1 General characteristics of Cu-doped Schottky devices.

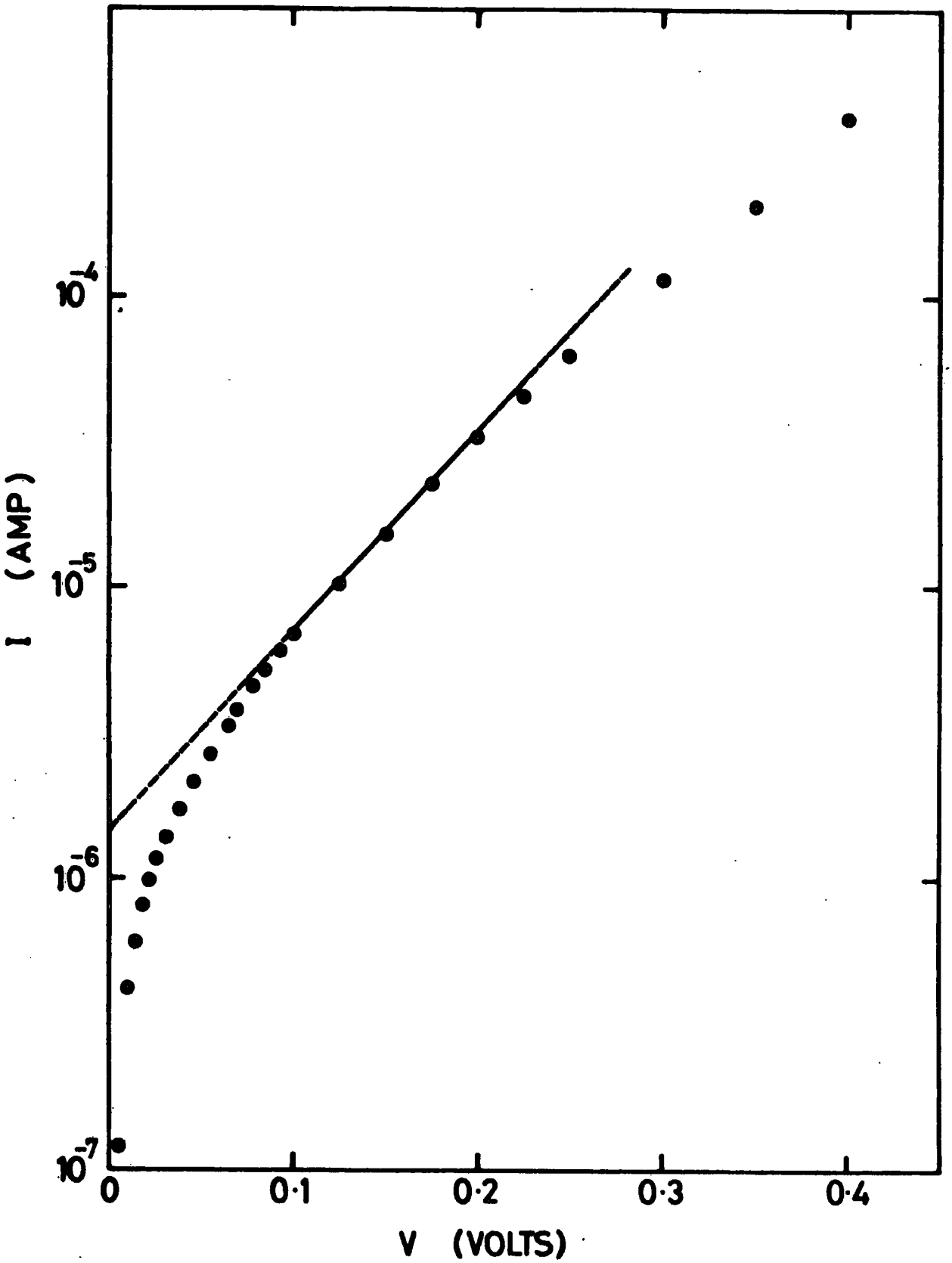

FIGURE 6.5.3 Semilog plot of forward I-V characteristics of an aged Schottky diode prepared on Cu-doped CdSe

6.5.4. The only observable difference from the pattern for Se-annealed devices was a slight decrease in the intensities of the polycrystalline cubic rings and the appearance of an additional weak hexagonal polycrystalline ring corresponding to the $(10\bar{1}3)$ reflection of the wurtzite structure indicated by the arrow in fig. 6.5.4.

6.5.5 Surface Effects

Unfortunately neither of the calculations used for the surface state densities in sec. 6.2.5 and 6.4.5 could be applied because of the non-linearity in the Fowler plot and an absence of saturation in the C-V curves so that C_I could not be estimated. Nevertheless apparent similarities in the electrical characteristics and RHEED observations with those of the Se-annealed devices would be accepted as evidence of the validity of the proposed models on etched surfaces.

6.5.6 Discussion

The reduced net donor concentration in these devices at the as-made stage, is attributed to the copper which acts as an acceptor impurity. The experiment described in chapter 4.4.2 showed that the annealing conditions (650°C 2h) were sufficient to ensure that the copper had diffused uniformly, so that the compensation of the Se-vacancies by copper acceptors would also have been uniform. This was consistent with the linear behaviour of the C^{-2}-V curves.

On the other hand the non-linearities in the Fowler plots may have been due to an increase in the photoexcitation of free carriers from additional interfacial states presumably introduced by copper.

The electrical characteristics of the Cu-doped Schottky diodes were almost identical to those of diodes prepared as CdSe annealed for one month in selenium. This suggests that the copper doped

FIGURE 6.5.4 RHEED pattern of Cu-doped CdSe after ageing

diodes can be treated qualitatively in the same way as discussed in Sec. 6.2.5.

6.6 SUMMARY AND CONCLUSIONS

The common feature of all the Schottky devices was the reduction of reverse bias leakage current with time (i.e. ageing). This is believed to be due to oxygen adsorption and diffusion. This suggestion is supported by parallel RHEED observations.

The adsorption of oxygen was found to be responsible for the phase transformation of CdSe surfaces from hexagonal to sphalerite cubic structure. This surface phase was less conductive than the bulk and behaved as a resistive interfacial layer. Mechanical polishing produced an identical, but thicker cubic structure with similar electrical characteristics.

Estimates of the surface state density and the thickness of the interfacial layer were made from the C-V and photoelectric measurements. These allowed a semi-quantitative analysis to be made which implied a dependence of the barrier height on the parameters of the interfacial layer as well as the metal work function. It can be concluded that oxygen plays a crucial role in controlling the electrical characteristics of Schottky devices, both as a consequence of surface re-construction and of the introduction of associated surface and bulk acceptor-like states.

REFERENCES

1. I. E. Türe, G. J. Russell and J. Woods, J. Cryst. Growth 59 (1982) 223.
2. A. M. Cowley, J. Appl. Phys. 37 (1966) 3024.
3. S. J. Fonash, J. Appl. Phys. 54 (1983) 1966.
4. E. H. Rhoderick, Metal-Semiconductor Contacts, Clarendon Press, Oxford, 1978.
5. S. M. Sze, Physics of Semiconductor Devices, John Wiley & Sons, New York, 1969.
6. C. R. Crowell, W. G. Spitzer, L. E. Howarth and E. E. Labate, Phy. Rev. 127 (1962) 2006.
7. H. C. Card and E. H. Rhoderick, J. Phys. D. 4 (1971) 1589.
8. R. W. Swank, Phy. Rev. 153 (1967) 153.
9. J. Bardeen, Phy. Rev. 71 (1947) 717.
10. L. J. Brillson, Surface Sci. 69 (1977) 62.
11. D. M. Heinz and E. Banks, J. Chem. Phys. 24 (1956) 391.
12. R. H. Bube, J. Chem. Phys. 27 (1957) 496.
13. G. A. Somorjai, J. Phys. Chem. Solids 24 (1963) 175.
14. M. J. Katz and K. J. Haas, Surface Sci. 19 (1970) 380.
15. E. Guesne, C. Sebenne and M. Balkanski, Surface Sci. 24 (1971) 18.
16. M F. Chung and H. E. Farnsworth, Surface Sci. 25 (1972) 321.
17. R. G. Wagner and G. C. Breitweiser, Solid St. Elec. 12 (1969) 229
18. K. Tanaka, Japan J. Appl. Phys. 9 (1970) 1070.
19. A. Y. C. Yu and E. H. Snow, J. Appl. Phys. 39 (1968) 3008.
20. J. M. Shannon, Solid St. Elec. 19 (1976) 537.
21. R. S. Popovic, Solid St. Elec. 21 (1978) 1133.

22. M. P. Lepsetter and S. M. Sze, Bell Syst. Tech. J. 47 (1968) 195.

23. W. G. Spitzer, C. R. Crowell and M. M. Atalla, Phty. Rev. Lett. 8 (1962) 57.

24. B. M. Arora, A. K. Srivastava and S. Guha, J. Appl. Phys. 53 (1982) 1820.

25. C. A. Mead, Appl. Phys. Lett. 6 (1965) 103.

26. R. L. Consigny 111 and J. R. Madigan, Solid St. Commun. 7 (1969) 189.

27. R. L. Consigny 111 and J. R. Madigan, Solid St. Elec. 13 (1970) 113.

28. K. W. Frese, Jr. J. Appl. Phys. 53 (1982) 1571.

29. J. L. Shay and W. E. Spicer, Phys. Rev. 169 (1968) 650.

30. H. Tubota, H. Suzuki and K. Hirakawa, J. Phys. Soc. Japan 15 (1960) 1701.

31. R. A. Burmeister and D. A. Stevenson, Phys. Stat. Sol. 24 (1967) 683.

32. M. P. Hung, N. Ohashi and K. Igaki, Japan J. Appl. Phys. 8 (1969) 652.

33. G. J. Russell, A. T. Fellows, S. Oktik, E. Ture and J. Woods, J. Mat. Sci. Lett. 1 (1982) 176.

34. E. N. Clarke, Phys. Rev. 91 (1953) 756.

35. A. S. Pashirikin and R. A. Sapozhriskov, Soviet Phys-Cryst. 7 (1962) 501.

36. M. Aoki and S. Tanaka, J. Appl. Phys. Japan 24 (1955) 113.

37. L. Dăveritz, J. Cryst. Growth 23 (1974) 307.

38. S. Nagata and K. Agata, J. Phys. Soc. Japan 6 (1951) 523.

39. U. Dolega, Z. Naturforsch 18a (1963) 809.

40. F. Frey, Ann. Phys. (Leipzig) 2 (1948) 147.

41. F. G. Smith and V. G. Hill, Acta. Cryst. 9 (1956) 821.

42. T. Sekine and Y. Kotera, J. Luminescence 13/13 (1976) 929.

CHAPTER 7

DEFECT AND IMPURITY LEVELS MEASURED BY SPACE-CHARGE TECHNIQUES

7.1 INTRODUCTION

This chapter concerns the investigation of defect and impurity levels in single crystal CdSe using various kinds of space-charge techniques, namely steady-state photocapacitance (PHCAP), steady-state infrared quenching of photocapacitance (IRQ-PHCAP), transient photocapacitance (PHCAP-TR), transient infrared quenching of photocapacitance (IRQ-PHCAP-TR), deep level transient spectroscopy (DLTS) and optical DLTS (ODLTS). These junction capacitance and other space-charge methods have been successfully applied to many of the II-VI compounds[1-9] and their advantages are well known. However, the use of such techniques with CdSe has been very limited[10,11], probably for the reasons described in the introductory chapter of this thesis.

The above mentioned junction capacitance methods were carried out on Schottky barriers on crystals annealed in Se-vapour, on crystals, doped with copper or on mechanically polished surfaces of single crystals. The general description of the experimental arrangements and some of the details of these measurements have already been given in Chapter 4. Because of the drastic effect of copper in CdSe, atomic absorption measurements were undertaken to establish copper concentrations in the various types of Schottky device. The results indicated that there was no detectable level of copper impurity in the as-grown crystals or any of the selenium treated samples. The concentration of copper in intentionally doped samples (used for device fabrication) lay in the range of (5-15) ppm.

The steady state measurements were usually made with a very slow monochromator scan rate or occasionally manually (point by point) to ensure correct readings where the time constants associated with the deep levels were very long. The transient measurements were also recorded manually. The intensities of the photon flux used in photo-ionisation cross-section measurements were in the range from 10^{12} - 10^{13} photons $cm^{-2}s^{-1}$.

7.2 MEASUREMENTS ON SCHOTTKY DEVICES PREPARED ON SE-ANNEALED SAMPLES

7.2.1 Introduction.

The electrical characteristics of Schottky devices prepared on both 3-day and 1-month Se-annealed crystals have been described in the previous chapter. Although the electrical characteristics of the two materials were almost identical (i.e. following the artificial ageing process described in section 6.4.2), space-charge measurements revealed a qualitative difference.

In order to present a more comprehensive discussion of deep levels in Se annealed CdSe, a parallel study was made using the space-charge techniques in addition to the photoconductivity measurements (which are concerned with bulk properties) previously described. Therefore more effort was devoted to the 1-month Se-annealed devices, simply because of the stronger similarity in the preparational methods of such devices and the photoconductive samples.

7.2.2 Steady state photocapacitance

The experimental details of the spectral dependence of PHCAP measurements were given in Chapter 4.7.4. Figure 7.2.1 shows PHCAP spectra of a typical Schottky device prepared on a 3-day Se-annealed crystal measured at 90 and 300K, together with the lamp response. In

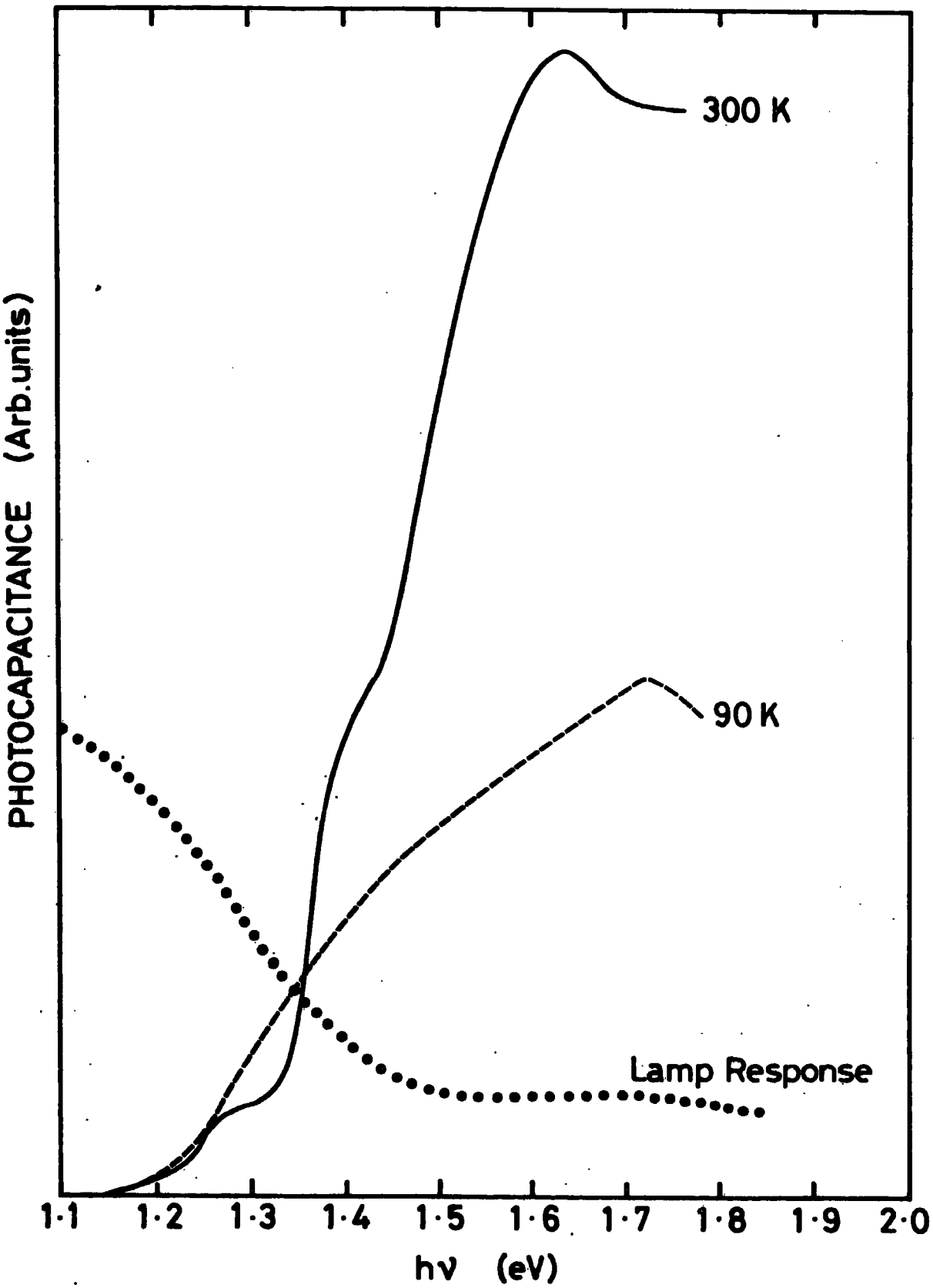

FIGURE 7.2.1 Steady-state PHCAP measurement for 3-day Se-annealed devices at 90 and 300K

the room temperature spectrum the principal threshold occurred at a photon energy of 1.14 eV which indicated that there was an acceptor-like state 0.6eV above the valence band. This assumes that the bandgap was 1.74eV at room temperature. Other positive-going steps were observed in the same spectrum at photon energies of 1.23, 1.32 and 1.46 eV implying that there were three possible acceptor levels at energies of 0.51, 0.42 and 0.28 eV above the valence band edge. The sudden decrease in PHCAP at 1.63 eV suggests the presence of a donor-like level at 0.12 eV below the conduction band.

In the low temperature spectrum the principal threshold was observed at 1.21 eV corresponding to a value of 0.63 eV for the position of the level relative to the valence band. The bandgap has been taken to be 1.84 eV at 90K. Similarly in the room temperature spectrum the decrease in PHCAP at 90K occurred at a photon energy of 1.72 eV, giving a value of 0.11 eV below the conduction band for the donor level. There was an additional, but small threshold at 1.1 eV, indicating, possibly, another acceptor-like level 0.73 eV above the valence band edge. On the other hand the absence of the 0.51, 0.42, and 0.28 eV levels in the low-temperature spectrum was unexpected because normally such detail should be enhanced at lower temperatres, due to the reduction in thermal quenching. Photocapacitance is thermally quenched when the thermal capture and emission rates exceed the optical rates, so that the optical excitation cannot sufficiently alter the steady-state trap occupancy to produce any measurable change in capacitance. However, the disappearance of such detail from the 90K spectrum was probably an artifact of the experimental technique. During the setting up procedure many of these levels would have been

emptied and would have remained so at liquid nitrogen temperatures. Consequently these features would not have been observed during the actual spectral scanning.

PHCAP spectra for a Schottky device prepared on a sample annealed in Se for 1 month are shown in figure 7.2.2. The threshold of the PHCAP spectrum at room temperature occurred at 1.03 eV indicating a level 0.71 eV above the valence band. The additional feature at 1.51eV in the spectrum clearly indicated the existence of a level $\sim$0.23 eV above the valence band. This level also was not well-resolved at low-temperature for the same reasons indicated above.

At 90K the threshold occurred at 1.16eV corresponding to an ionisation energy of 0.68eV of the acceptor level. The magnitude of photocapacitance started to decrease when the photon energy of the incident light was increased above 1.71eV suggesting the presence of a shallow donor level below the conduction band. The absence of a similar decrease in the room temperature spectrum could possibly be due to the thermal quenching.

7.2.3. Steady-State Infrared Quenching of Photocapacitance.

The same experimental system with an additional light source ($1.7eV < h\nu < 1.9eV$) to provide the constant illumination was used to measure the infrared quenching of photocapacitance. The spectra of IRQ-PHCAP for both types of device are shown in figure 7.2.3. For devices on 3-day annealed CdSe two thresholds were observed at secondary illumination energies of 0.58 and 0.71eV, suggesting the presence of two acceptor-like levels at these energies above the valence band. This is in reasonable agreement with the PHCAP spectra which also indicated that there were two closely spaced levels at energies of 0.63 and 0.73eV.

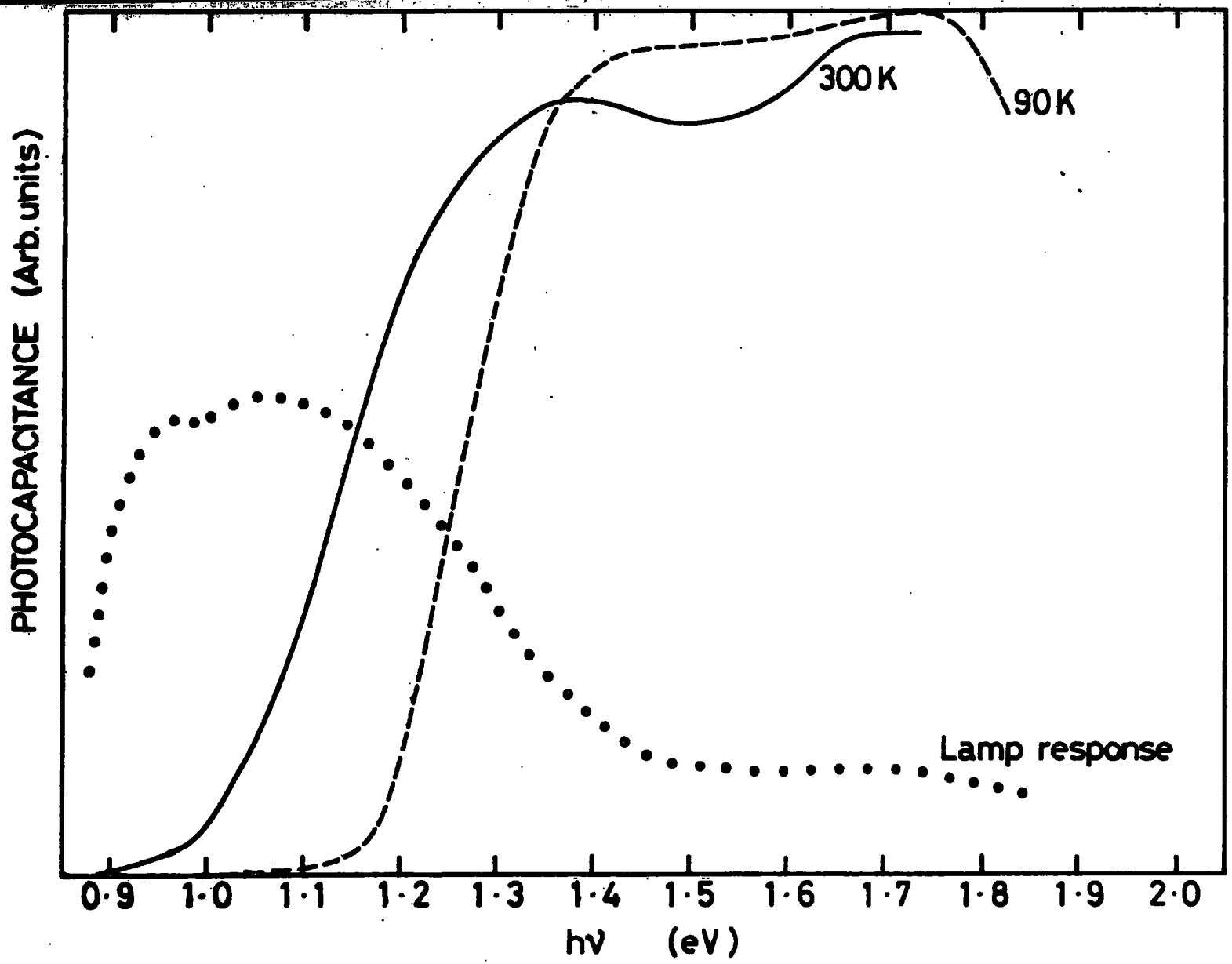

FIGURE 7.2.2 Steady-state PHCAP measurement for 1-month Se-annealed devices at 90 and 300K

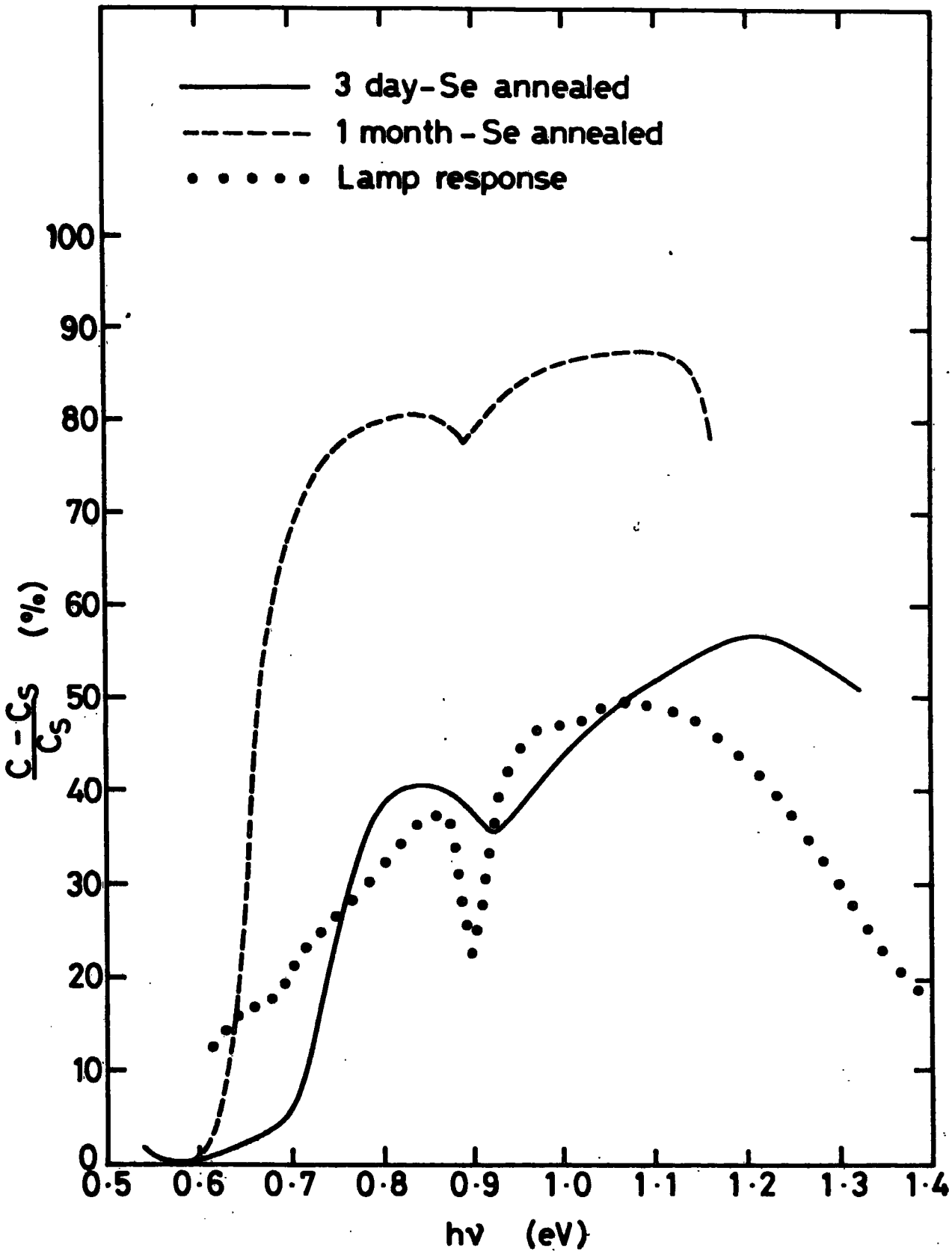

FIGURE 7.2.3 Steady-state IRQ-PHCAP measurements for 3-day and 1-month Se-annealed devives

For devices on one-month annealed CdSe there was only one quenching threshold at 0.62eV with respect to the valence band edge. This is also in good agreement with the PHCAP measurements.

7.2.4 Transient Photocapacitance measurements

The method and the advantages of the transient technique have already been described in Chapter 3.4.3. Here the experimental determinations of the photionisation cross-sections for holes and electrons of the main sensitising centre will be presented, together with the necessary experimental details.

(a) Photoionisation Cross-section of Holes (σ_p^o)

In this particular experiment (IRQ-PHCAP-TR) the reverse biased Schottky diode was first illuminated with a primary light with photon energy $h\nu_1 \simeq 1.62eV$ ($E_c - E_T < h\nu_1 < E_g$) for about 2 minutes at 90K. This would be expected to empty a substantial proportion of the centres as indicated by a rise in photocapacitance. The radiation was then switched off and the new steady state was achieved. Since the thermal emission rates can be neglected at temperatures below freeze out, the change in the occupancy of these centres would be very small after the removal of the primary light. The concentration of the empty centres is

$$P_T(0) = \frac{e_n^o}{e_n^o + e_p^o} N_T \qquad \text{(see Chap. 3.4.3)}$$

and $P_T(0)$ was considered to represent the initial condition for the transient measurements. Because the defect level investigated was in the lower half of the bandgap, the final state could be considered as completely filled ($n_T(\infty) = N_T$) when illuminated by the secondary light of

$$E_c - E_T > h\nu_s > E_T - E_V \quad (e_n^o \simeq 0)$$

According to these boundary conditions equation 3.21 can be written as;

$$\ln [C^2(t) - C^2(\infty)] = \ln K \frac{e_n^o}{e_n^o + e_p^o} N_T - e_p^o t \qquad (7.1)$$

The decay curves arising from the photoexcitation of holes to the valence band or in other words refilling these centres with electrons were recorded for different wavelengths of secondary illumination in the energy range $0.6eV \leq h\nu_s \leq 1.0eV$. When the photocapacitance transients were plotted on a semilog scale (i.e. $\ln (C^2(t) - C^2(\infty)$ versus time), straight lines were obtained (see Fig. 7.2.4). The slopes of these lines gave the inverse of the time constants, (τ^{-1}) and since $e_p^o = \sigma_p^o \phi$ (i.e. eq. 3.73) and $e_p^o = \tau^{-1}$, the absolute values of photionisation cross-section for holes, (σ_p^o) were found. Figure 7.2.5 shows a spectrum of the photoionisation cross-section of holes at 90K for devices on CdSe annealed for 1 month. Here, the experimental points have been fitted to the Lucovsky model[12] using a non-linear least squares curve fitting program. The resulting curve is shown in figure 7.2.5 as the solid line. The threshold energy of 0.615eV obtained from this curve fitting exercise is in good agreement with the steady state measurements.

(b) Photoionisation Cross-Section of Electrons (σ_n^o)

For the photionisation cross-section of electrons (σ_n^o), the diode was first illuminated with a primary light with photon energies of $E_g/2 > h\nu_1' \gtrsim E_T - E_V$ (i.e. $h\nu_1' \gtrsim 0.6eV$) for about 3 minutes at liquid nitrogen temperature. Since $e_n^o \approx 0$ for this excitation, the centres could be considered as completely filled, and this time the initial condition would be $n_T(0) \approx N_T$. Again by neglecting the thermal

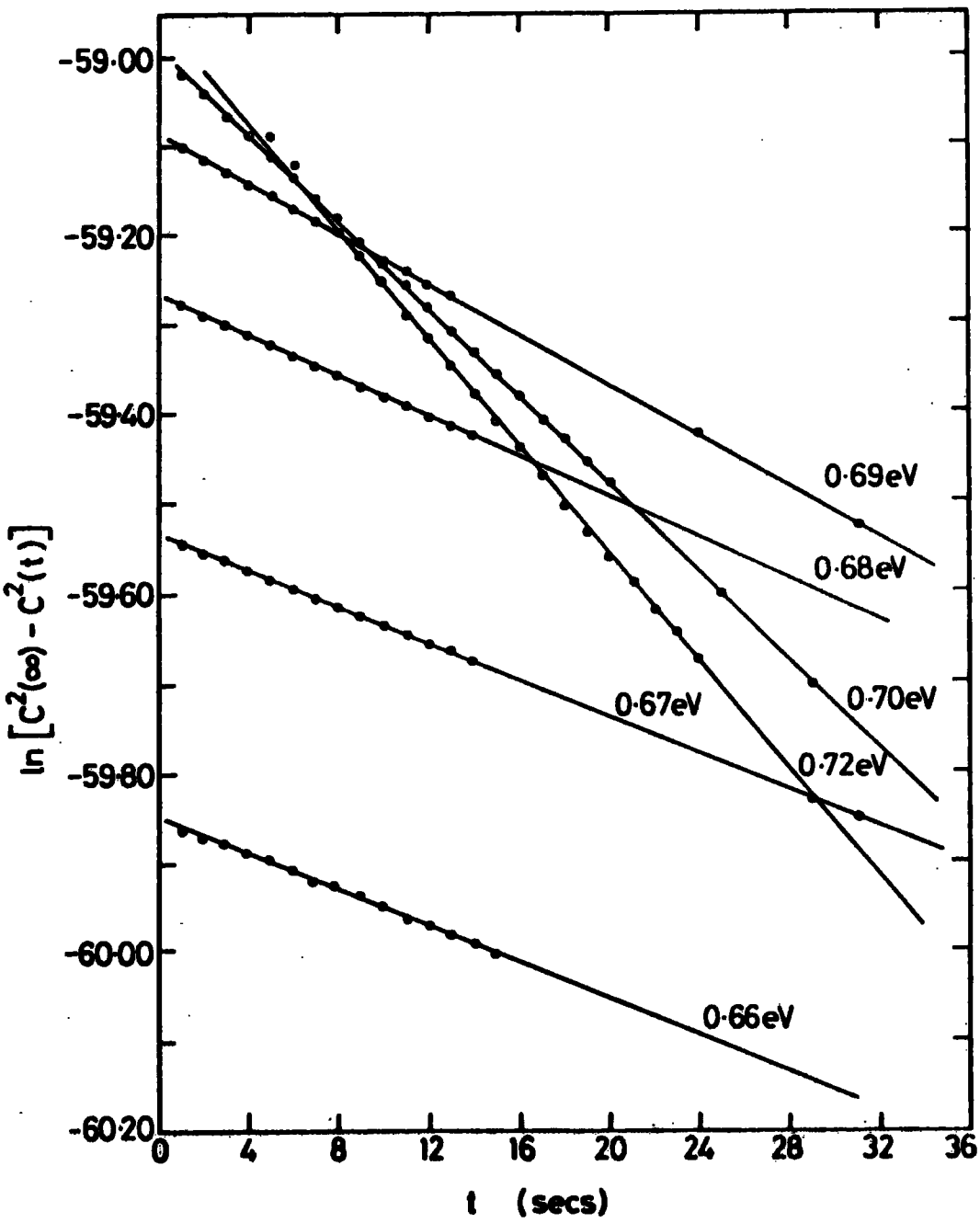

FIGURE 7.2.4 Semilog plots of IRQ-PHCAP transients for different photon energies of secondary illumination

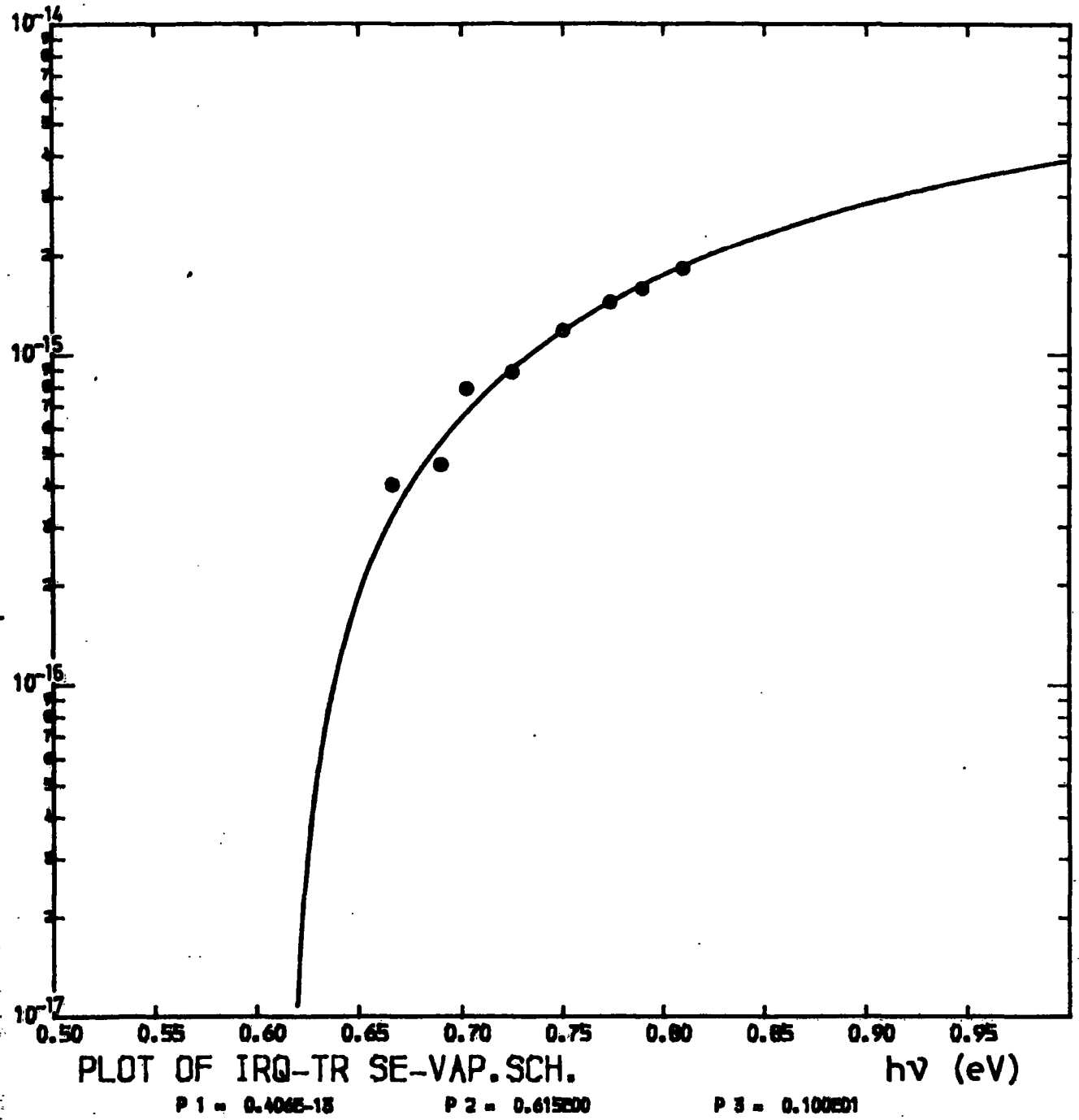

FIGURE 7.2.5 Spectral dependence of photoionisation cross-section of holes (Lucovsky plot) for 1-month Se-annealed devices

emission rates these centres would have remained filled after the ilumination was removed.

When the increases in PHCAP for excitation with light energies in the range $E_g > h\nu_s' > E_c - E_T$ were plotted against time, in the same way as decribed in section (a), the slopes of the resulting straight lines gave the time constants of the transients ($\tau^{-1} = e_n^o + e_p^o$). If the initial ($n_T(0) \simeq N_T$) and final ($n_T(\infty) \simeq \frac{e_p}{e_n^o + e_p^o} N_T$) states of the transients were used in equation 3.71 the relationship

$$\ln[C^2(\infty) - C^2(t)] = \ln K \frac{e_n^o}{e_n^o + e_p^o} N_T - (e_n^o + e_p^o)\, t \qquad (7.2)$$

was obtained. Since $\tau^{-1} = e_n^o + e_p^o$, the intercepts of these lines (see Fig. 7.2.4) can be written as

$$\frac{A^2 \varepsilon_o \varepsilon_s q}{2(V_d + V_R)} \quad \sigma_n^o \phi \tau N_T \qquad (7.3)$$

As the total concentration of the defect centres was not known, the absolute values of σ_n^o could not be determined. Nevertheless the spectrum of σ_n^o could be obtained in relative units. This is shown as a function of $h\nu_s^1$ in figure 7.2.6 together with the best-fit Lucovsky curve (solid line). When the threshold energy of 1.14eV was substracted from the bandgap value, the position of the defect level was found to be $E_T = 0.695$eV above the valence band. This was slightly higher ($\sim$0.08eV) than the value obtained from the measurements of (σ_p^o).

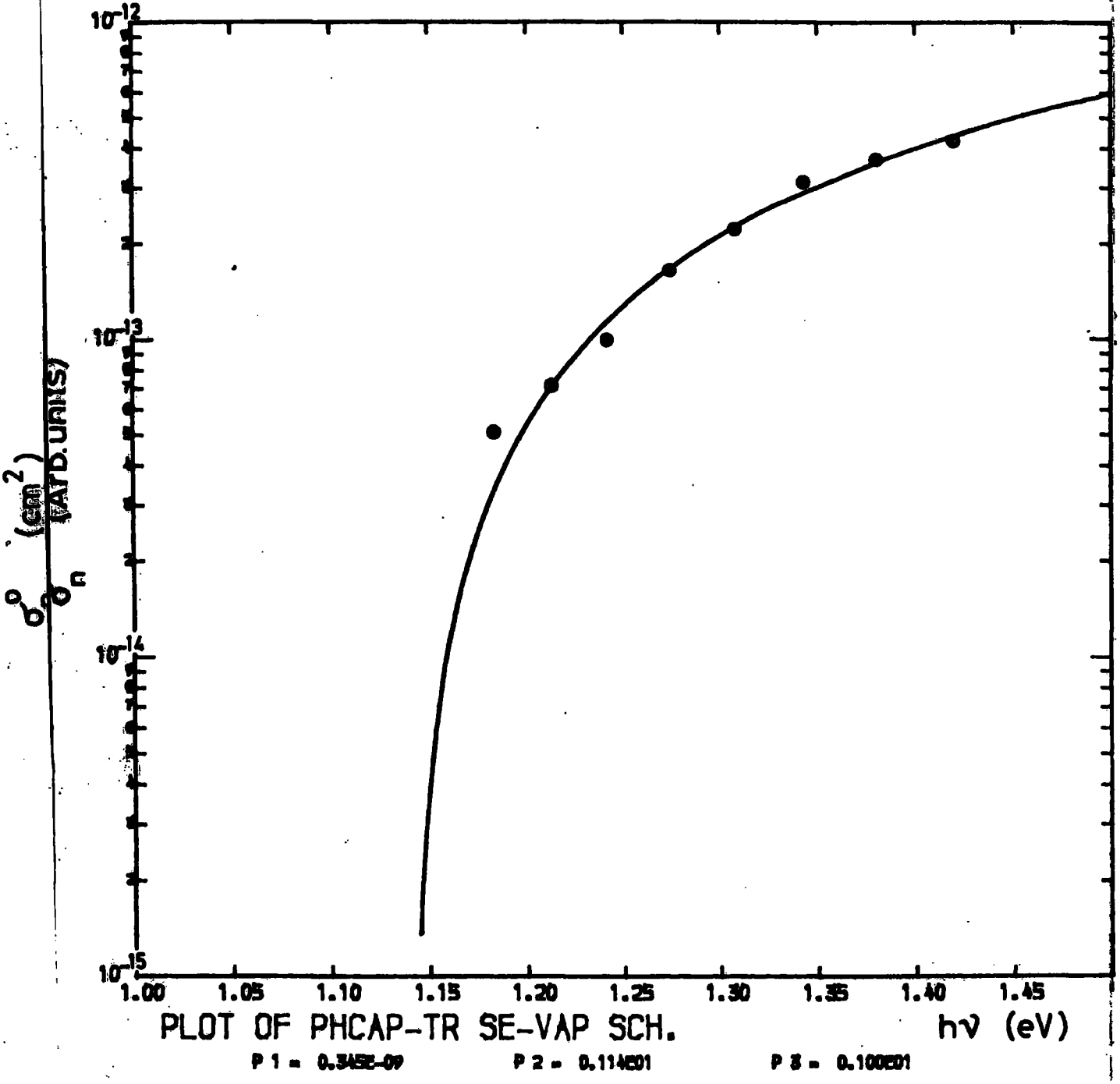

FIGURE 7.2.6 Spectral dependence of photoiionisation cross-section of electrons (Lucovsky plot) for 1-month Se-annealed devices

7.2.5 DLTS and ODLTS Measurements

DLTS and ODLTS measurements were carried out using the double boxcar technique described in Ch. 4.8. The theory of these measurements was reviewed in Chapter 3.4.3. Here, the results on both types of device are presented.

(a) DLTS Measurements for Electron Traps

It is well known that DLTS measurements on Schottky barriers can only provide information on majority carrier traps (electrons in the case of CdSe). The DLTS spectra shown in figure 7.2.7 obtained from the two types of device revealed three electron traps, labelled E_1, E_2 and E_3 for devices on CdSe annealed for 1 month, curve (a) with peaks at temperatures near 135, 250 and 385K respectively, but only the two traps E_1 and E_3 in the CdSe annealed for three days, Curve (b). The time constant for electron emission is given by the expression

$$\tau = (N_c \langle v_n \rangle \sigma_n)^{-1} \exp(\Delta E/kT) \quad \text{(see Chap. 3.4.3.c)}$$

where $N_c = 2\left(\frac{2\pi m_e^* kT}{h^2}\right)^{3/2}$ and $\langle v_n \rangle = \left(\frac{3kT}{m_e^*}\right)^{1/2}$. When $\ln(\tau T^2)$ was plotted against $10^3/T$, straight lines (Arrhenius plots) were obtained. Figure 7.2.8 shows the three Arrhenius plots associated with these electron traps E_1, E_2 and E_3. Ionisation energies of 0.16, 0.46 and 0.94eV and corresponding apparent cross-section ($\sigma_n(\infty)$) of 2.4×10^{-18}, 2.6×10^{-16} and $2.0\ 10^{-13}$ cm^2 at infinite temperature were calculated from the slopes and intercepts of these Arrhenius plots.

(b) ODLTS Measurements for Hole Traps

In this optical variation of the DLTS technique, pulses of sub bandgap light, obtained by filtering ($\lambda > 0.78\mu m$) and chopping the

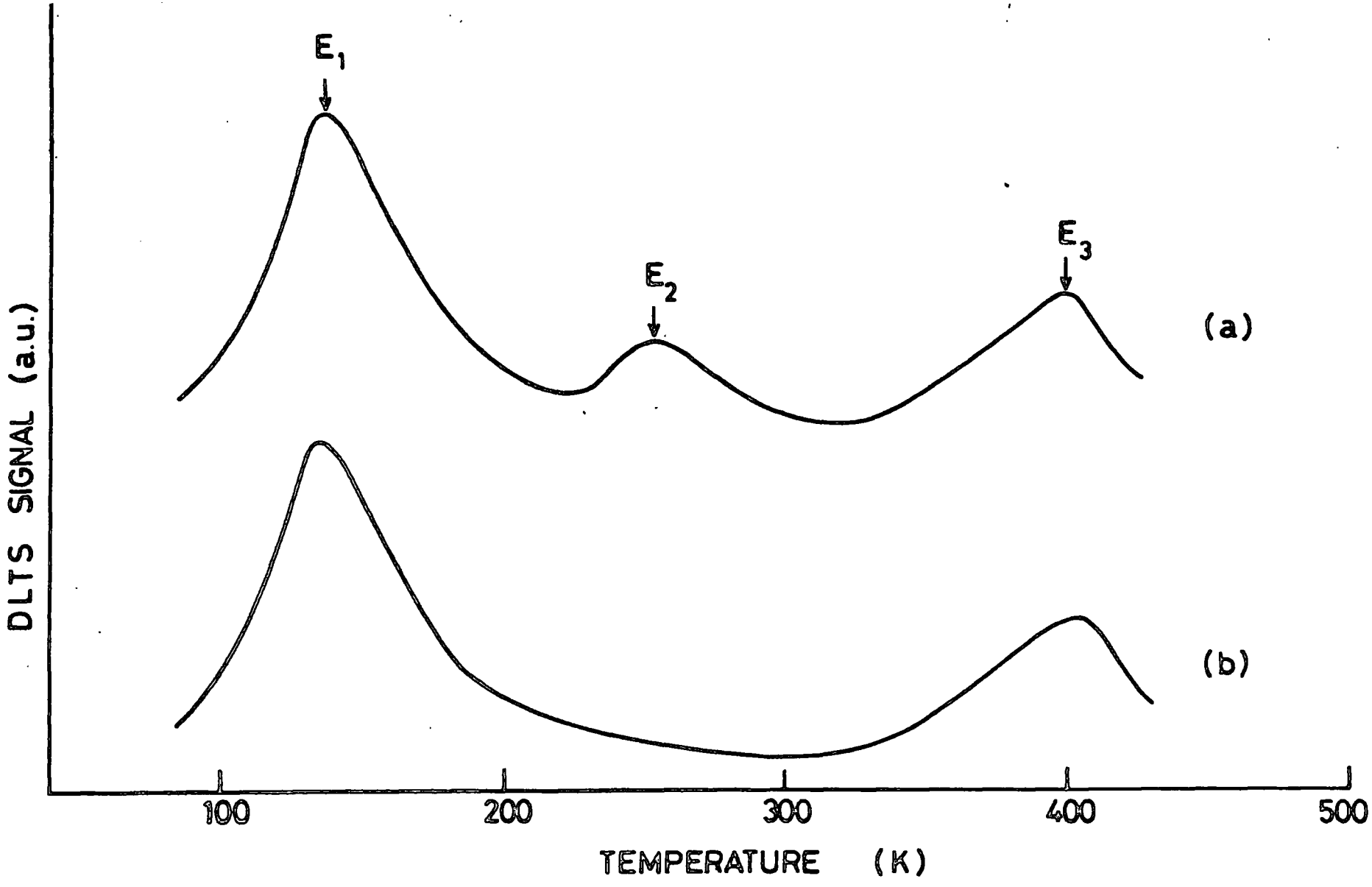

FIGURE 7.2.7 DLTS spectra for 3-day and 1-month Se-annealed devices

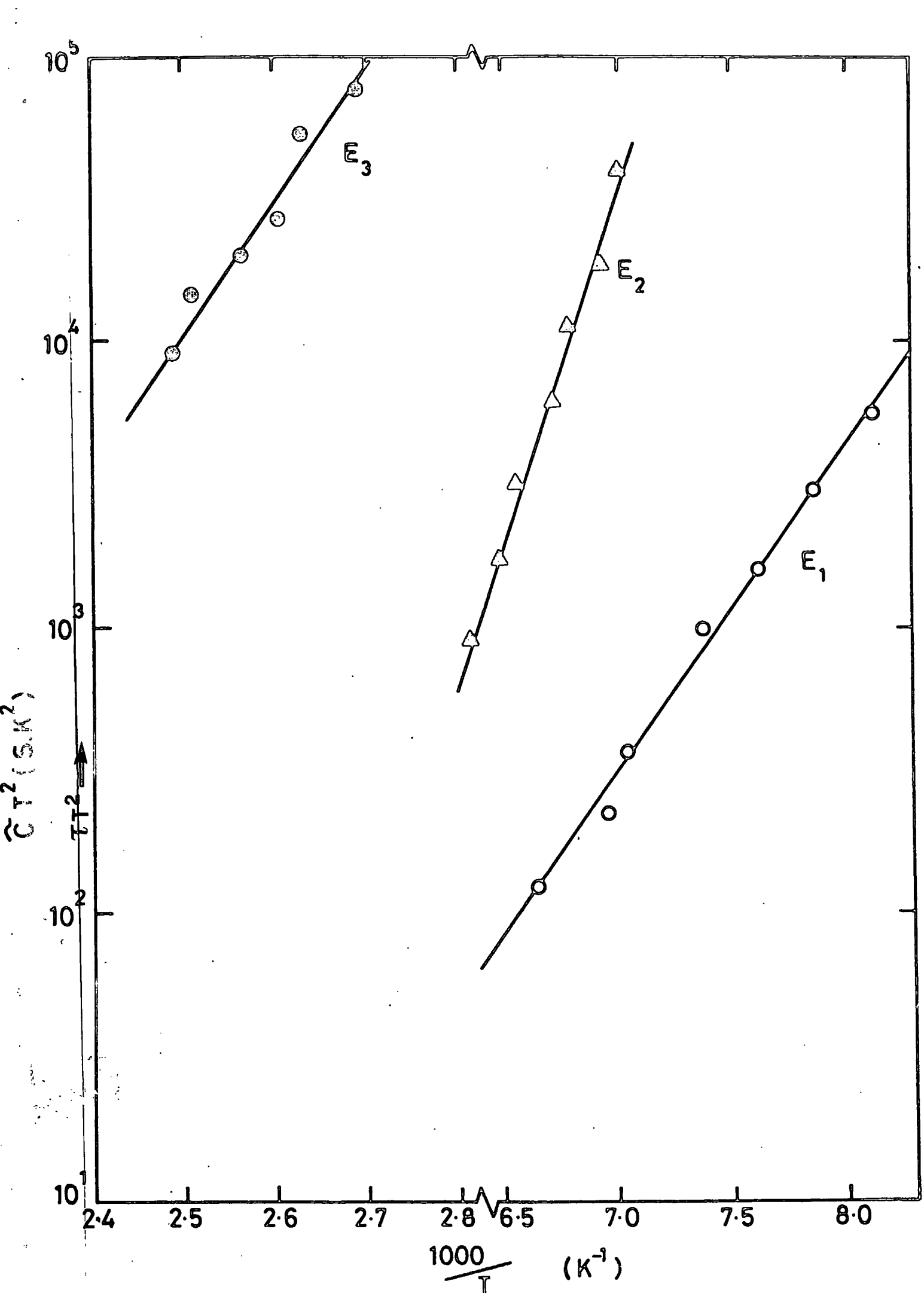

FIGURE 7.2.8 Arrhenius plots for the electron traps (from DLTS)

light from a tungsten filament lamp were used to empty the traps, especially in the lower half of the bandgap. Subsequent refilling produced a characteristic capacitance transient which could be analysed in the same manner as DLTS.

In contrast to the DLTS spectra, the ODLTS spectra of the two types of device were considerably different. Figure 7.2.9 shows typical ODLTS spectra obtained from both types of CdSe sample. The principal feature in the spectra from 3-day annealed material was the double minimum centred around 270K (curve a). Although this feature could not be satisfactorily resolved, it was assumed, on the basis of the PHCAP and IRQ-PHCAP results that it corresponded to two relatively closely spaced hole traps. One of the 3-day Se-annealed devices also exhibited another minimum near 100K indicating (See Fig. 7.2.9) a hole trap H_1 with an ionisation energy of ~ 0.2eV and capture cross-section $\sigma_p(\infty) \simeq 5 \times 10^{-17}$ cm^2. The ODLTS spectra obtained with 1-month annealed CdSe showed a single well defined minimum near 280K corresponding to a hole-trap with an ionisation energy of 0.64eV and capture cross-section of 1×10^{-14} cm^2. The Arrhenius plots for both H_1 and H_2 are shown in figure 7.2.10 and were evaluated assuming a hole effective mass of $0.45\ m_o$ [13].

7.3 DISCUSSION

The advantages of employing a variety of space-charge techniques for the detection of deep levels may be summarized as follows: (a) The limits associated with any particular method or instrumentation, (i.e. temperature, long wavelength threshold of the monochromator etc.) can be extended, (b) more information can be obtained and (c) results from different techniques can be compared and verified.

As an aid to discussion the results in the previous sections have been collected into the form of inferred energy level diagrams.

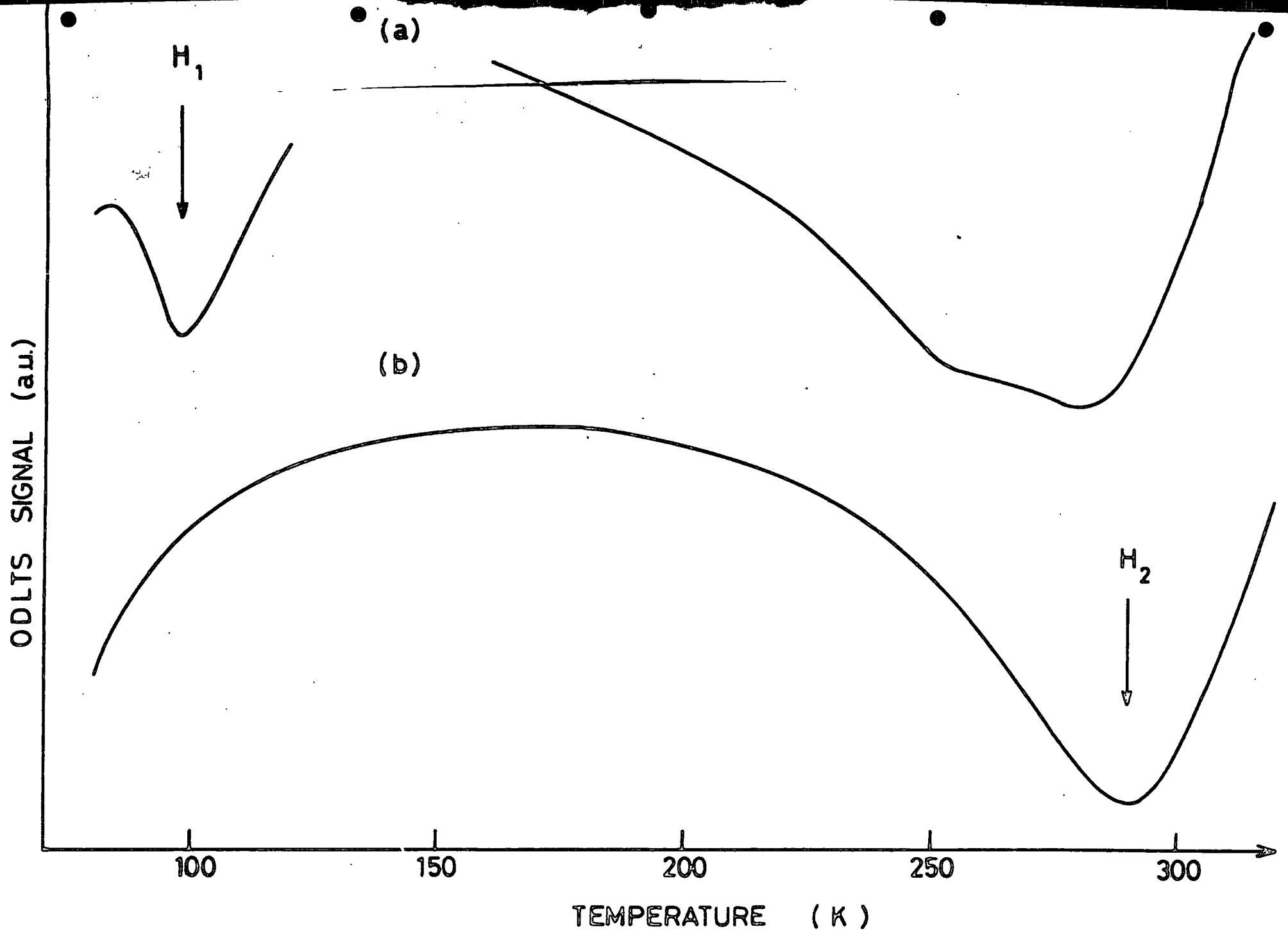

FIGURE 7.2.9 ODLTS spectra for 3-day and 1-month Se-annealed devices

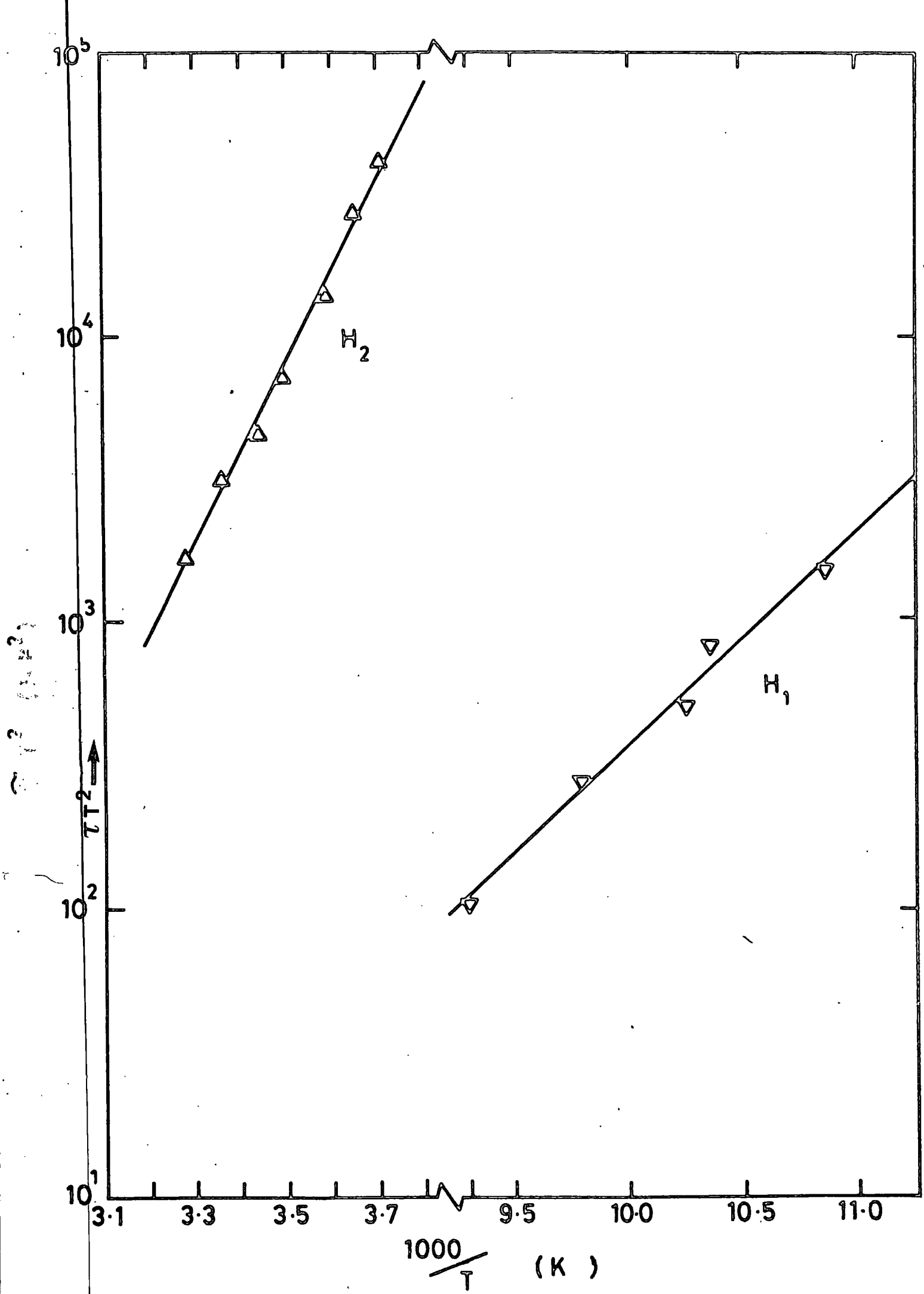

FIGURE 7.2.10 Arrhenius plots for the hole traps (from ODLTS)

Figures 7.3.1 and 7.3.2 show the energy levels for 3-day and 1-month annealed material. Energy levels marked (VB) and (CB) are referred to the valence or conduction bands respectively.

The two electron traps which the DLTS measurements showed to be at 0.46 and 0.90eV below the conduction band were not observed in the PHCAP spectra. With the first level a sharp increase might have been expected in the PHCAP spectrum at around 0.46eV and a decrease at 1.3eV.As indicated earlier 0.46eV was beyond the limit of the long wavelength threshold of the monochromator and the first expected increase could not therefore have been observed. The absence of the second expected change at 1.3eV would probably have been masked by the intense electron emission from the main sensitizing centre ($\sim$0.64eV above valence band) to the conduction band. It is well known that the energy levels in the middle of the bandgap, such as that at 0.9eV, are always difficult to detect in PHCAP because of the competition between the emptying and filling processes[14]. Nevertheless the DLTS measurements did indicate a high value of capture cross-section ($\sigma_n(\infty) \simeq 2 \times 10^{-13} cm^2$) for this 0.90eV electron trap. Such a large cross-section implies that the level in the middle of the bandgap should act as a recombination centre and would therefore exercise an important influence on carrier lifetime.

The electron trap level at about 0.13eV below the conduction band was observed both in DLTS and PHCAP measurements. The slightly higher energy value ($\sim$0.16eV) obtained from DLTS measurements can perhaps be attributed to lattice relaxation. In general the distribution of electron traps in both types of device was very similar except for the absence of the 0.46eV level in the devices on 3-day annealed material. This may be a consequence of the self-compensation mechanisms and cannot be readily explained.

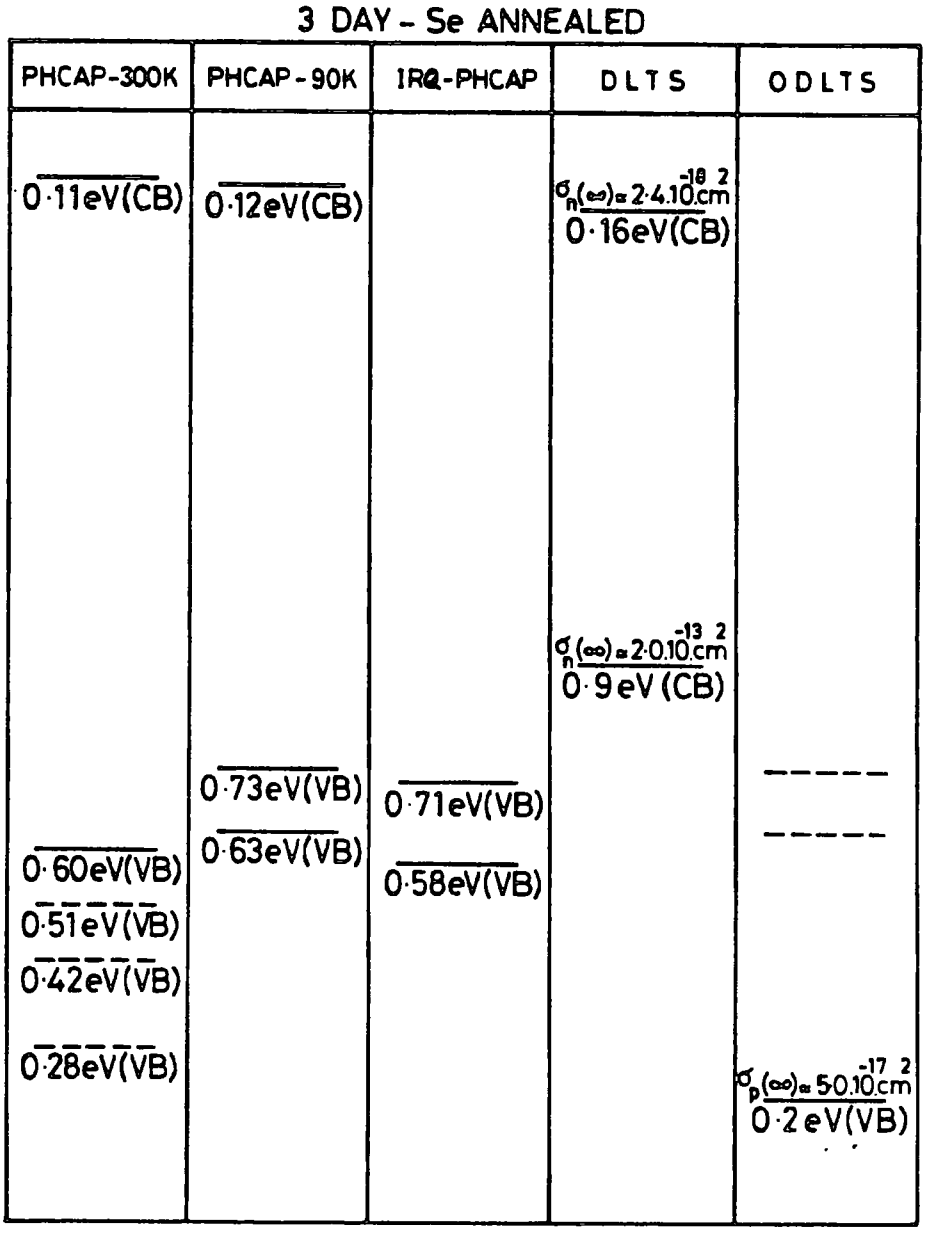

FIGURE 7.3.1 Summary of the inferred energy levels for 3-day Se-annealed material

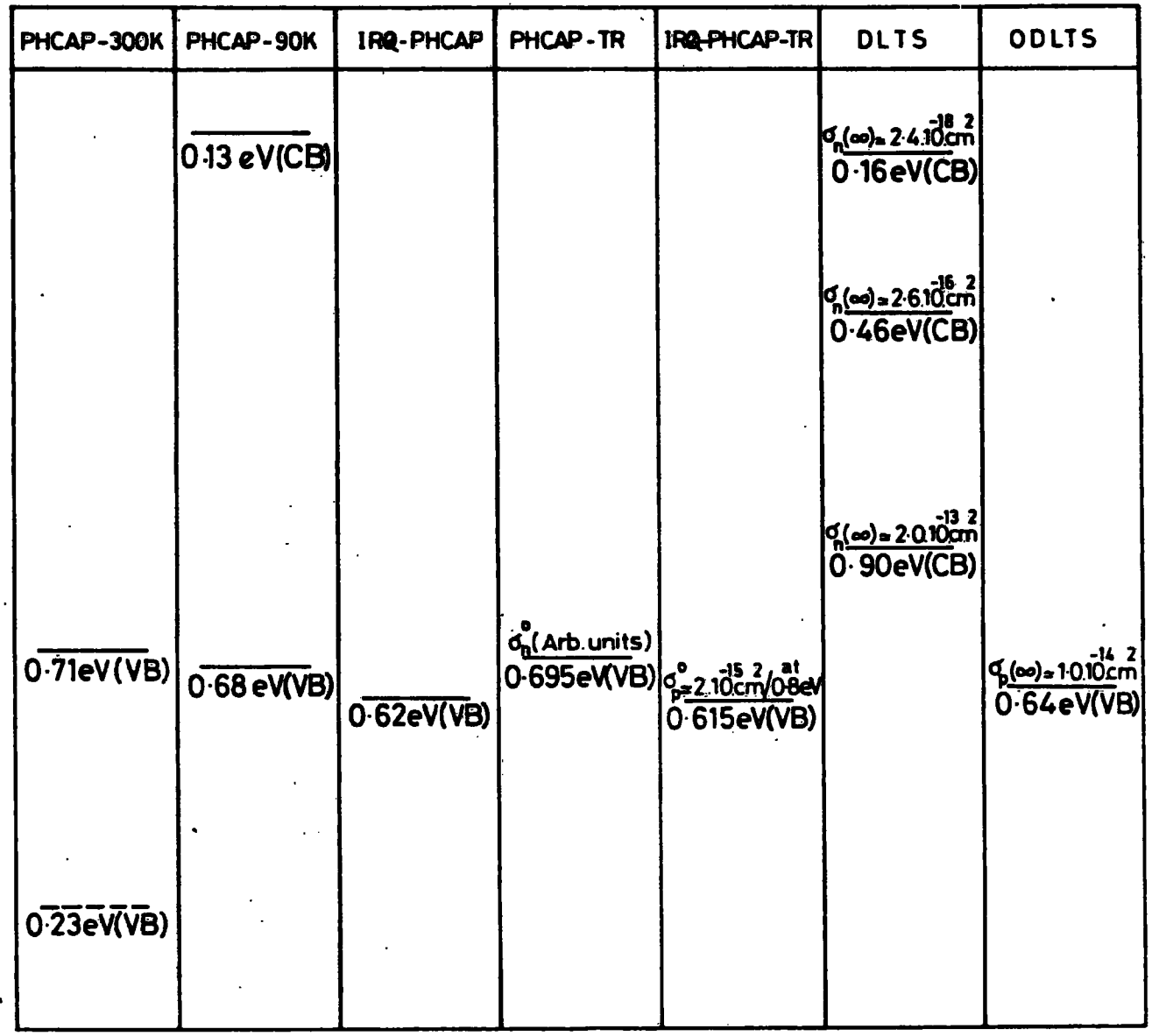

FIGURE 7.3.2 Summary of the inferred energy levels for 1-month Se-annealed material

It can be seen from figures 7.3.1 and 7.3.2 that the results for the hole-traps obtained from PHCAP, IRQ-PHCAP, ODLTS, PHCAP-TR and IRQ-PHCAP-TR measurements are in reasonably good agreement but unlike the electron traps their distribution was markedly different in the two types of device. The two hole traps observed at (0.51-0.58) and (0.71-0.73)eV above the valence band in 3-day annealed materials were apparently absent from 1-month annealed CdSe. Instead there was a well defined acceptor level (0.62-0.64)eV and only a slight indication of the 0.23eV level above the valence band in the latter. This result is particularly important since the 0.64eV level has long been thought to be the main sensitising centre in CdSe[15,16,17].

Robinson and Bube[18] found a similar difference in the distribution of acceptor levels between material annealed in selenium and material heated in vacuum after the selenium treatment. They found several acceptor levels in the range 0.1 to 0.75eV above the valence band after annealing in selenium. However heating in vacuum for 6 h at 500°C, substantially reduced the density of these acceptor levels relative to the concentration of sensitising centres. Robinson and Bube concluded that the introduction of the sensitising centre was a two-stage process involving annealing first in selenium then in vacuum at low temperature, or else by annealing for a long time at room temperature. It would appear that the two-stage process was combined into one in the preparation of Se-annealed devices in the work described in this thesis, i.e. lowering the Se-annealing temperature (550°C) and extending the duration of the process had the same net effect. The implication is that the formation of sensitising centresis primarily dependent on the temperature and therefore probably involves the creation of defect complexes by thermally driven processes of

migration and association. Nevertheless it is not simply a matter of temperature and time alone.

The measurements of the ionisation energy of the sensitising centre fall into two groups, involving either electron emission (PHCAP, PHCAP-TR) or hole emission (IRQ-PHCAP, ODLTS, IRQ-PHCAP-TR). While there was very good agreement within each group, the results obtained from the first group were slightly higher ($\sim$0.07) than for the second. This small but consistent difference might be attributed to phonon broadening[19] of this level.

It is well known that sensitising centres are characterised by large capture cross-sections for holes and small capture cross-sections for electrons. They thus have large hole to electron cross-section ratios σ_p/σ_n. Therefore the large value of $\sigma_p(\infty)$ for holes 1×10^{-14} cm^2 for the 0.64eV level in 1-month annealed CdSe is strong evidence that the level behaves as a sensitising centre. The 0.64eV centre was not observed in DLTS and this places an upper limit on the cross-section for electron capture of $\sigma_n(\infty) \simeq 5 \times 10^{-16}$ cm^2 and hence a lower limit on the cross-section ratio σ_p/σ_n of about 200. This is entirely consistent with the notion that the level is behaving as a sensitising centre. Bube[20] reported a ratio of 2×10^7 for a level at 0.67eV above the valence band. If this were the same level, as the 0.64eV centre then the electron capture cross-section would be $\sigma_n(\infty) \simeq 10^{-21}$ cm^2. Such a small electron capture cross-section would be consistent with Bube's suggestion that the centre is doubly negative charged.

Another hole-trap around (0.20 - 0.28)eV above the valence band with a smaller hole capture cross-section of $\sigma_p(\infty) \simeq 5 \times 10^{-17}$ cm^2 was apparently intrinsic to all CdSe crystals and may be associated with

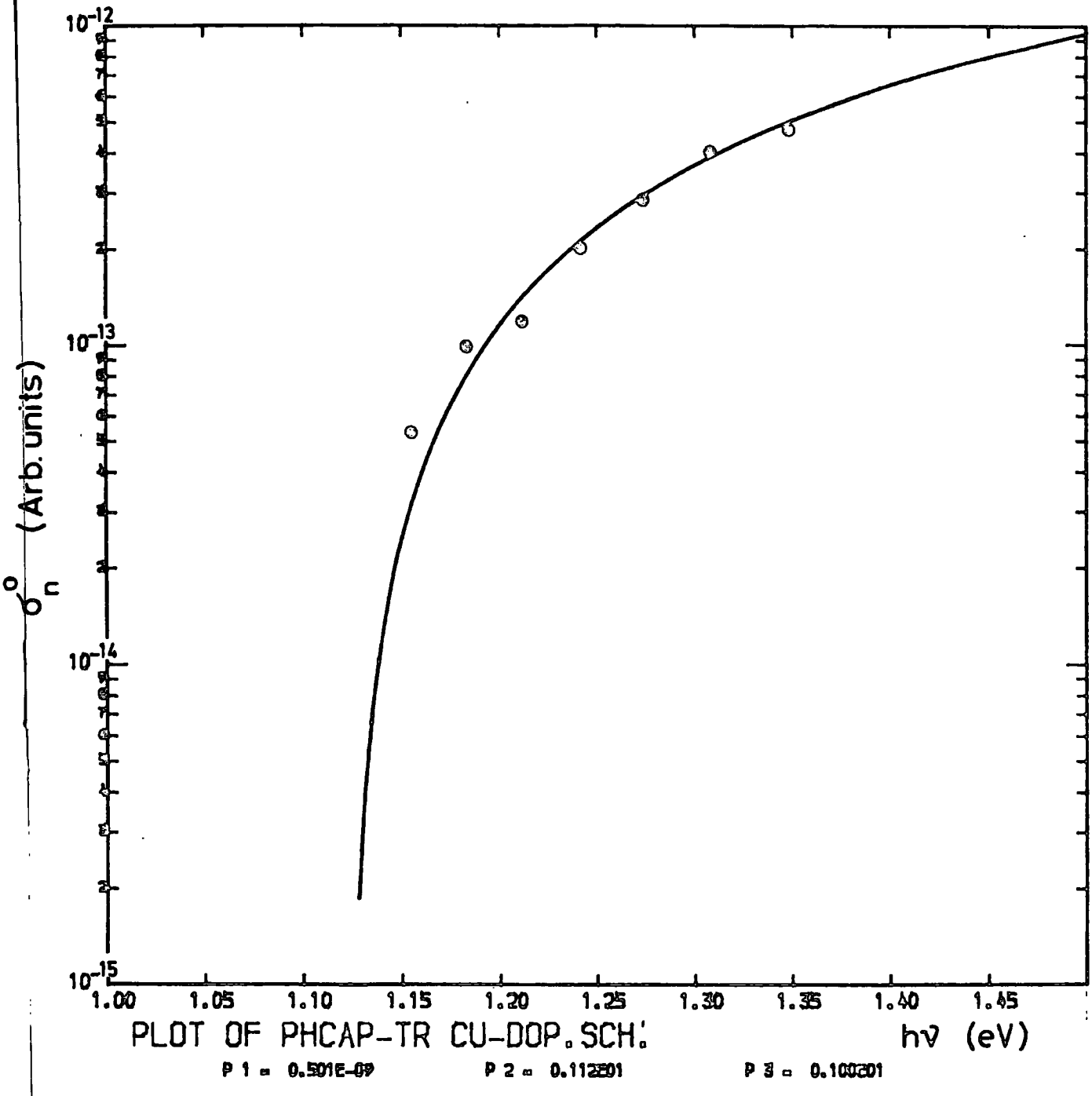

FIGURE 7.4.7 Spectral dependence of photoionisation cross-section of electrons (Lucovsky plot) for Cu-doped devices

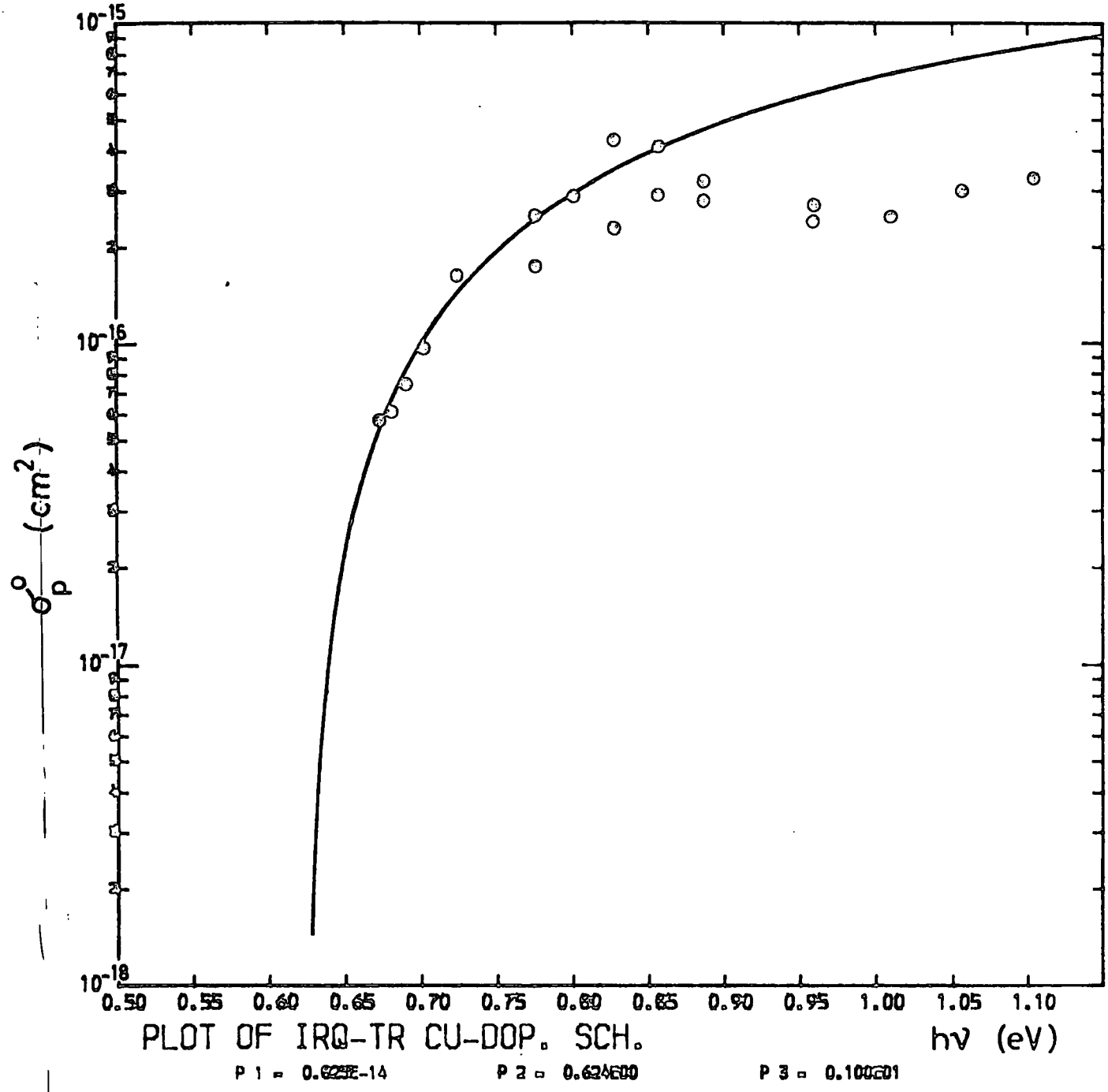

FIGURE 7.4.6 Spectral dependence of photoionisation cross-section of holes (Lucovsky plot) for the same device (fig. 7.4.5) including points from the higher energies of ($h\nu > 0.74$eV) secondary illumination

the singly ionised cadmium vacancy centre[17,21,22]. The absence of this centre in the ODLTS spectra of 1-month annealed CdSe may be due to a reduction in its concentration compared with that in 3-day annealed material. This level was also not well resolved in the PHCAP spectra for 1-month annealed material either, being observed (not conclusively) only in the 300K spectrum.

7.4 SCHOTTKY DEVICES PREPARED ON CU-DOPED SAMPLES

7.4.1 Introduction

Although the importance of copper in all II-VI compounds is well known, its role and physical characterisation has not yet been fully established in CdSe. This section concerns the investigation of native defects and copper related impurity centres in particular in Schottky barrier devices, prepared on intentionally Cu-doped samples, using the space charge capacitance techniques. Details of the copper doping process and the electrical characterisation of this type of Schottky diodes can be found in chapters 4 and 6.

7.4.2 Steady-State PHCAP Measurements

The steady-state PHCAP measurements of a typical Cu-doped Schottky diode at 300 and 90K are shown in figure 7.4.1. The sudden increase in the 300K spectrum at a photon energy of about 0.74eV can be associated with an electron emission process from a level 0.74eV below the conduction band. A sharp decrease in the same spectrum at about 1.26eV may be attributed to a deep donor level lying 0.48eV below the conduction band edge. The 300K PHCAP spectra also revealed a relatively shallow acceptor level 0.22eV above the valence band and a shallow donor 0.12eV below the conduction band, corresponding to photon energies of 1.52 and 1.62eV respectively.

In the low temperature PHCAP spectrum the thresholds were observed at incident photon energies of 0.86 and 1.61eV. Electron emission

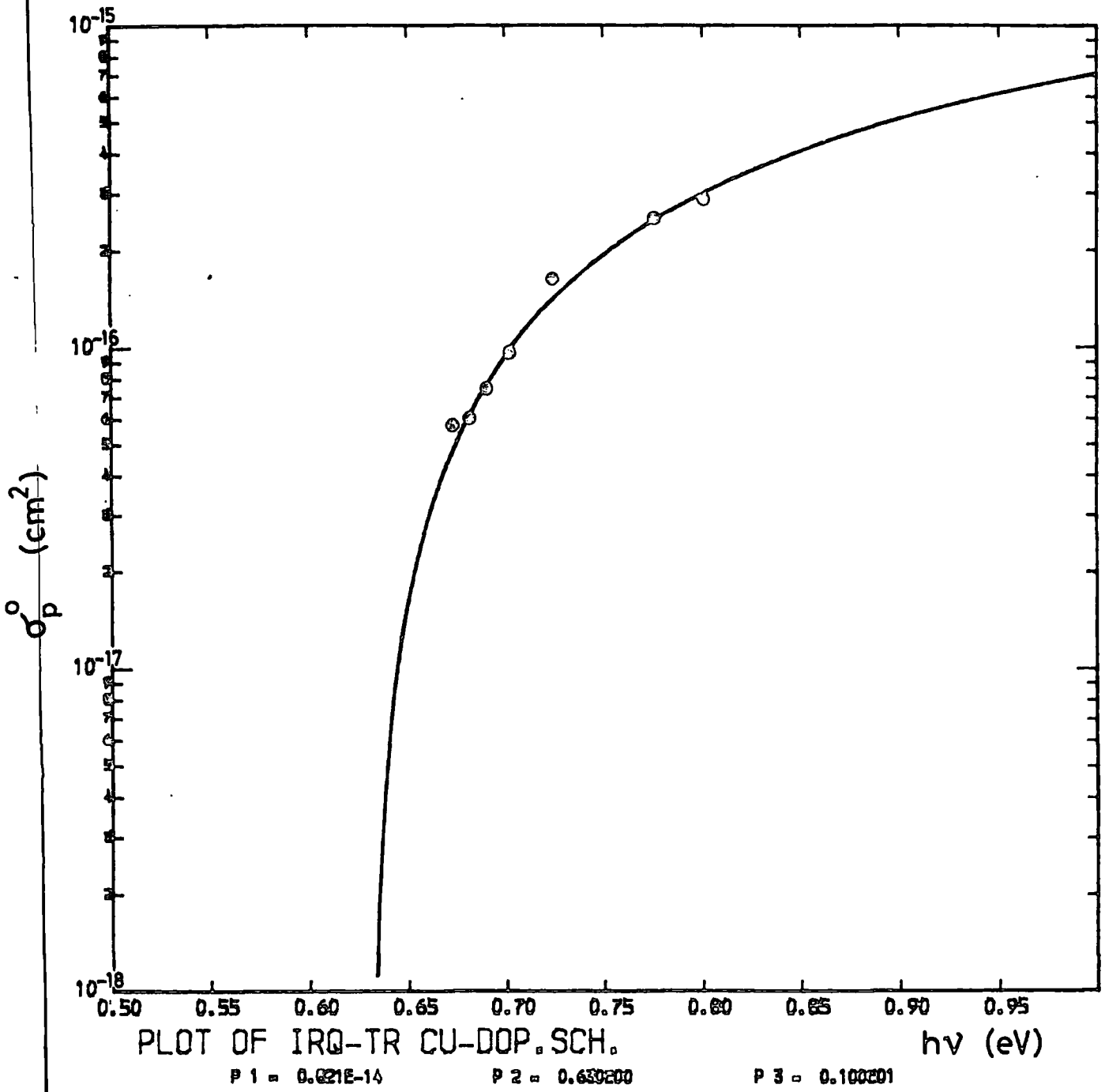

FIGURE 7.4.5 Spectral dependence of photoionisation cross-section of holes (Lucovsky plot) for Cu-doped devices

processes involve transitions to the conduction band and therefore the change in threshold energy from 0.74 to 0.86eV implies that this level is pinned to the valence band i.e. the centre is located at ∿1.0eV above the valence band edge. This conclusion is supported by subsequent experiments as shown below. Similarly the 1.61eV level corresponds to the acceptor level 0.23eV above the valence band. In addition to these two centres, the 90K spectrum indicated another acceptor level at about 0.80eV above the valence band, and two donor levels ∿0.54eV and ∿0.08eV below the conduction band. Although the activation energy of the deep donor (∿0.54eV) level was slightly higher than the 0.48eV observed in the 300K spectrum the 0.12eV level appeared to be shallower (∿0.08eV) in the low-temperature PHCAP spectra.

When an acceptor-like level (high hole cross-section) lies in the upper half of the bandgap, the measurements are complicated by the competition between the emptying and filling processes. Moreover, as already mentioned in the previous section some levels would have remained comparatively empty below the freeze out temperature and hence could not have been detected. In order to overcome some of these difficulties, and to enable additional information to be obtained, PHCAP measurements at 90K were also carried out following illumination with primary light of ∿1.62eV for about 30 mins. This would have ensured that all levels were initially empty. Fig. 7.4.2 shows the PHCAP spectra obtained from this type of measurement. The initial reduction of PHCAP for the low-energy values of incident photon energies clearly demonstrated the refilling process of acceptor centres in the lower half of the bandgap. This spectrum also indicated another acceptor level at about 0.60eV above the valence band which was not observed in the straightforward PHCAP measurements.

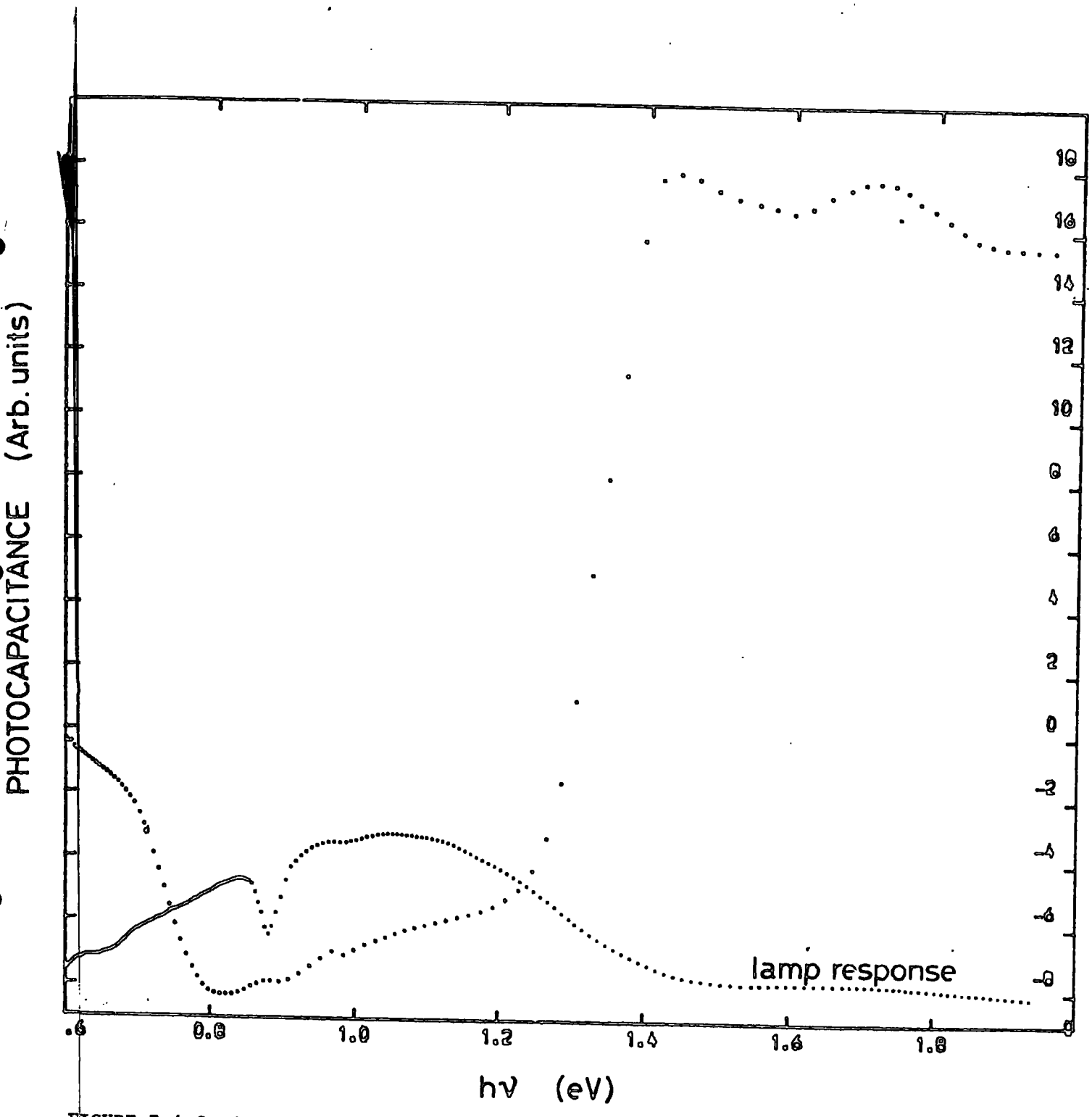

FIGURE 7.4.2 Steady-state PHCAP measurement for Cu-doped devices after pre-illumination

7.4.3 Steady State IRQ-PHCAP Measurements

The details of the spectral dependence of the IRQ-PHCAP measurements have already been given in Chapter 4.7.2. and 7.2.3. The IRQ-PHCAP spectrum for a typical Cu-doped Schottky diode is shown in figure 7.4.3. together with the lamp response. The long wavelength threshold of 0.67eV suggests an acceptor level at this energy above the valence band. More importantly the indication of an additional feature at about 0.99eV provides further evidence for the existence of the 1.0eV acceptor level in the upper half of the bandgap. This level was only observed in intentionally Cu-doped photoconductive CdSe crystals and may therefore be related to the copper centre.

7.4.4 PHCAP and IRQ-PHCAP Transient Measurements

Since the details of these experiments have already been described in a previous section (7.2.4 a and b), only the results will be presented here:

(a) Photoionisation Cross-Sections of Holes (σ_p^o).

The existence of four possible acceptor levels gave rise to some complications as expected and made the interpretation of transient measurements rather difficult. When the PHCAP transients were plotted semi-logarithmically against time, good straight lines with single slope were observed at low energy values of the secondary light(fig. 7.4.4a). From these plots the photoionisation cross-sections were calculated (See Sec. 7.2.4(a)) and plotted against photon energy as in fig. 7.4.5. When the photon energy of the secondary illumination was above ~0.74eV, the semi-log plot developed onto two straight lines and this inevitably led to uncertainty and scattering revealed in fig. 7.4.4 c & d and 7.4.6.

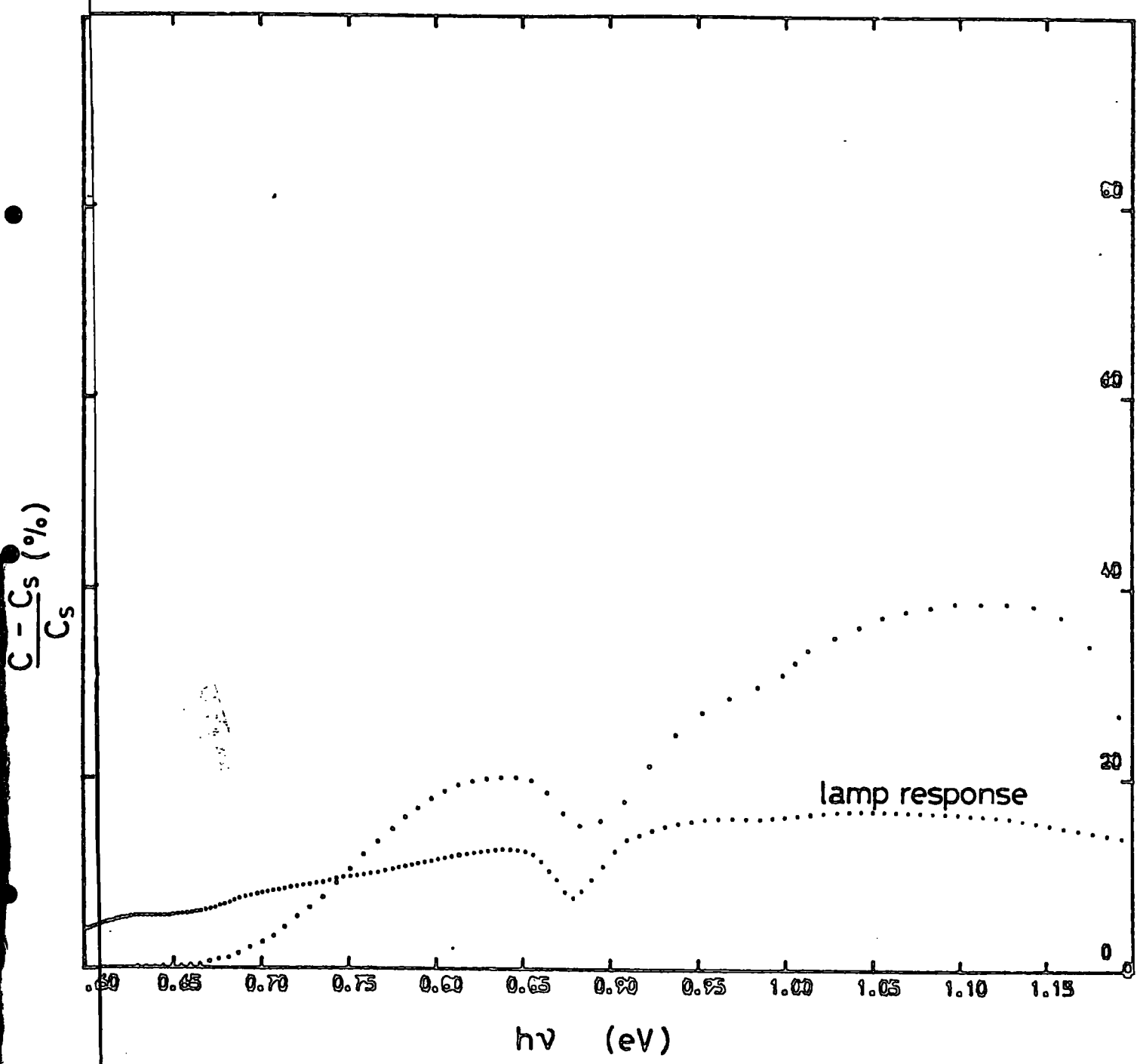

FIGURE 7.4.3 Steady-state IRQ-PHCAP measurement for Cu-doped devices

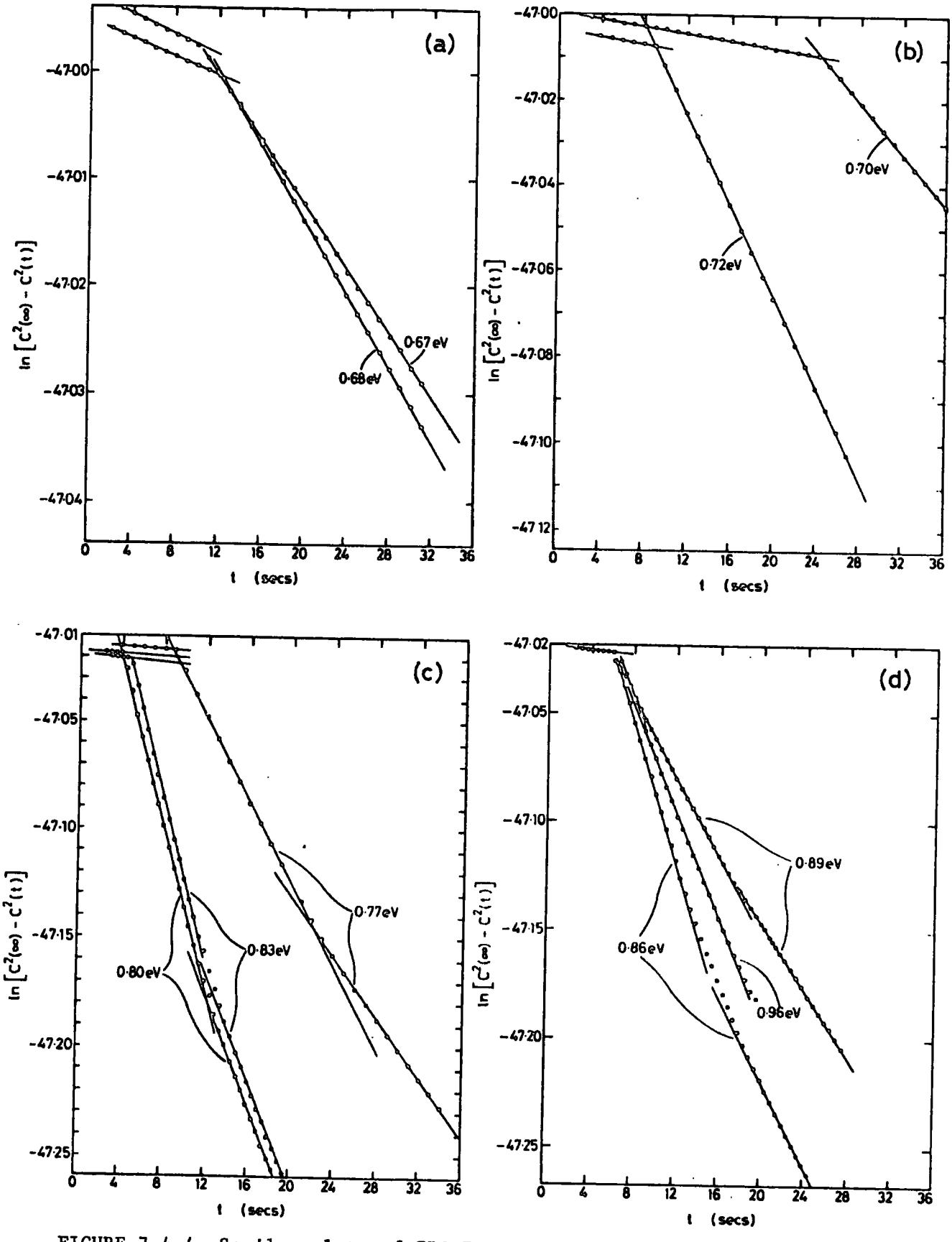

FIGURE 7.4.4 Semilog plots of IRQ-PHCAP transients for different photon energies of secondary illumination (for Cu-doped)

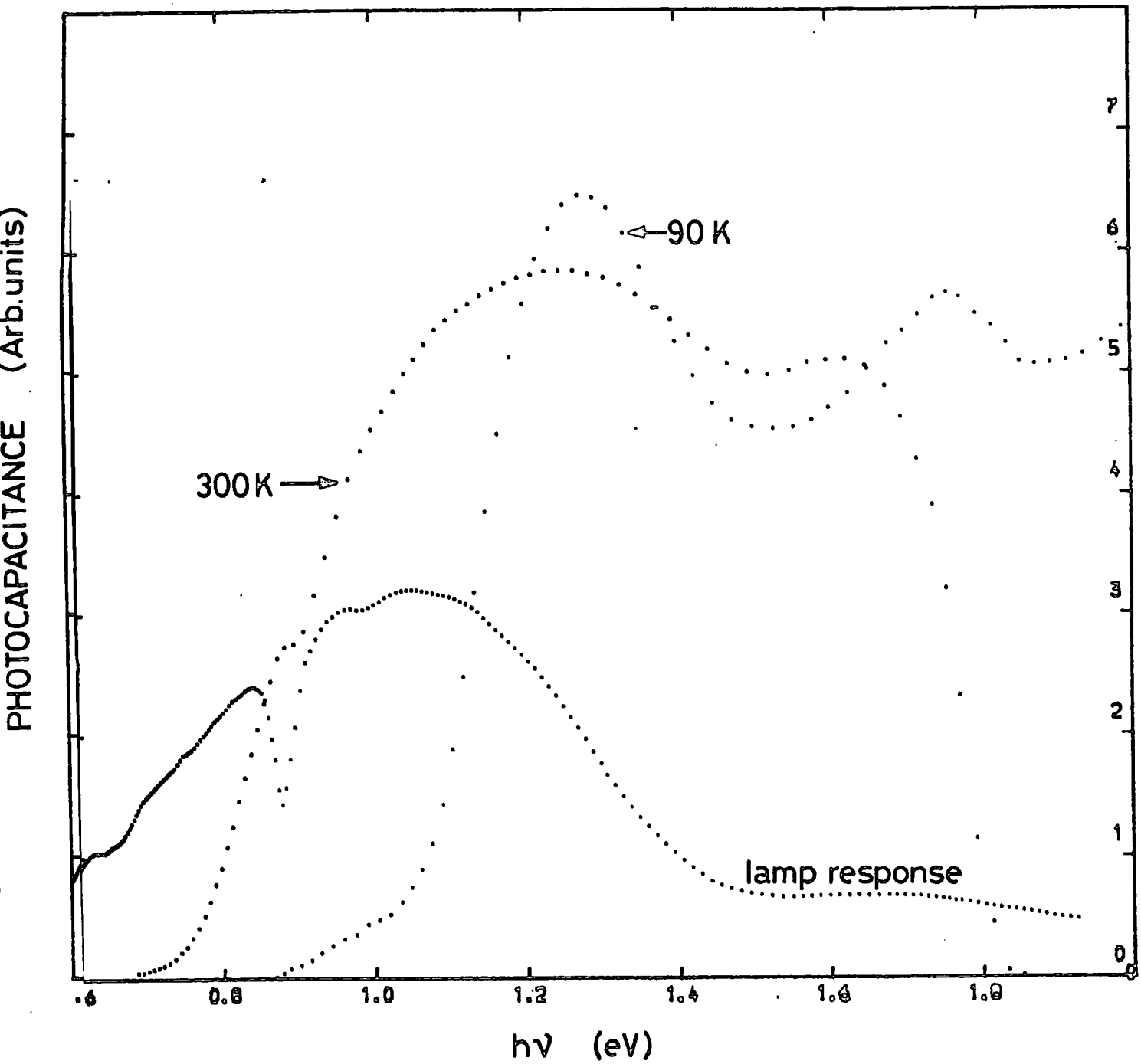

FIGURE 7.4.1 Steady state PHCAP measurement for Cu-doped device at 90 and 300K

Because more than two levels with different electron and hole ionisation energies were involved, the individual cross-section spectra could not be resolved too well. However, the application of a non-linear least squares curve fitting programme for the well defined first five points produced a good fit to the Luicovsky model with a threshold value of 0.63eV which is indeed in good agreement with the other measurements.

(b) Photoionisation Cross-Section of Electrons (σ_n^o)

Because of similar difficulties to those described in the previous section transient experiments for the photoionisation cross-section of electrons were carried out over a limited range of wavelengths only to avoid further complications. Figure 7.4.7 shows a typical spectrum for σ_n^o in relative units as a function of photon energy, together with the best fit Lucovsky curve (solid line). The threshold energy of 1.12eV (CB) obtained from this figure indicates the presence of a deep acceptor level 0.72eV above the valence band.

7.4.5 DLTS and ODLTS Measurements

DLTS and ODLTS measurements on Cu-doped Schottky devices were carried out using a computerised system (See Chap. 4.8). The advantage of this was that the whole transient was recorded, whereas with the double boxcar method, only a single rate-window for each run was used.

In the ODLTS mesurements generally a high intensity "sweet spot" LED with peak output at 820nm was used in conjunction with the 799.5 nm interference filter. In some runs the interference filter was removed in order to detect levels closer to the valence band edge. Light chopping was achieved by simply pulsing the LED which had a response time of 150ns.

Electron Trap	Activation Energy (CB) ΔE(eV)	Apparent Capture Cross-Section at infinite temperature $\sigma_n(\infty)$ Cm^2
E_1'	0.47	1.47×10^{-15} cm^2
E_2'	0.69	7.9×10^{-18} cm^2
E_3'	0.90	2.4×10^{-15} cm^2

TABLE 7.4.1 (DLTS data). Activation energy and apparent capture cross-section at infinite temperature of electron traps in Cu-doped CdSe

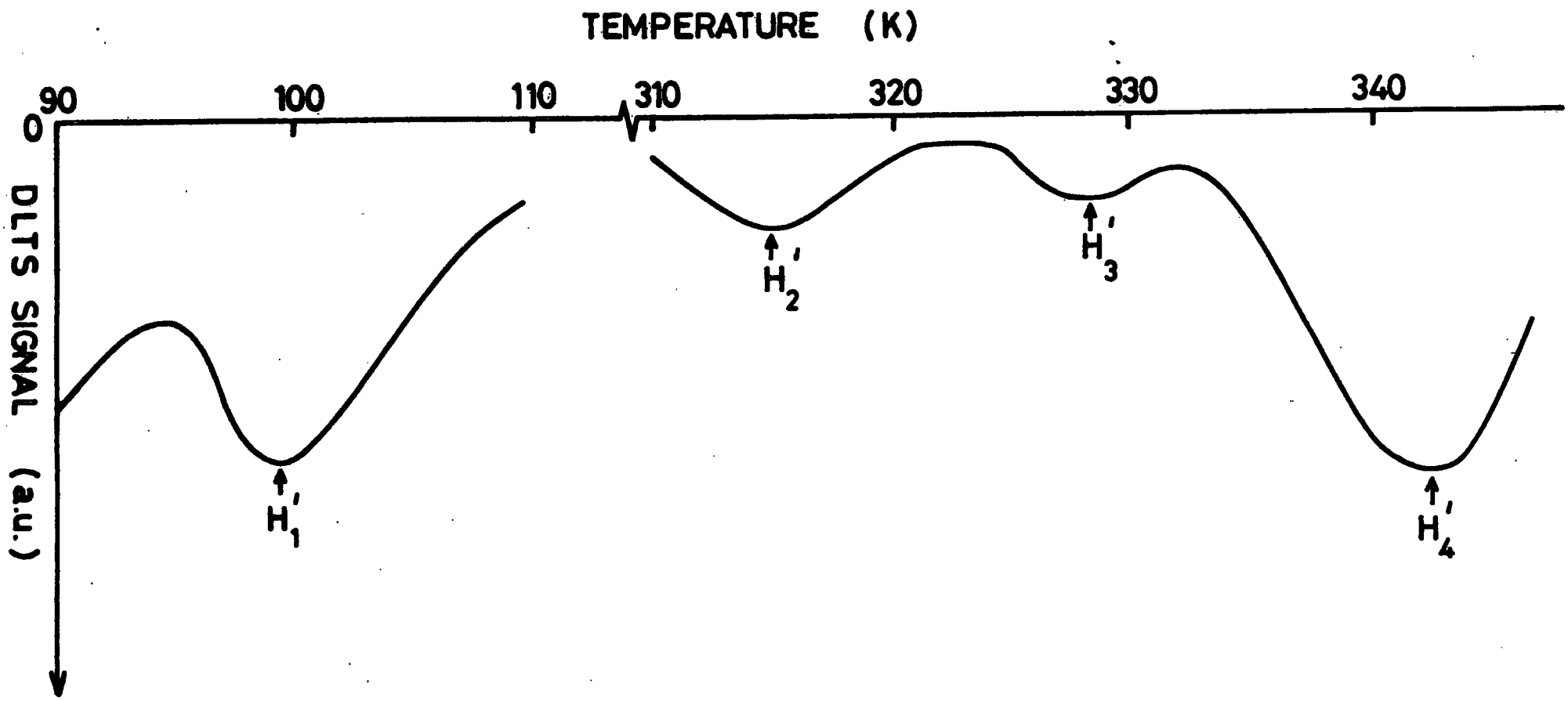

FIGURE 7.4.10 ODLTS spectra for Cu-doped devices

(a) DLTS Measurements

DLTS measurements on Cu-doped Schottky devices revealed three main electron traps E_1', E_2' and E_3' with peaks at about 250, 415, and 450K (figure 7.4.8). The Arrhenius plots for these traps are shown in figure 7.4.9. The corresponding ionisation energies and capture cross-sections are summarised in table 7.4.1.

(b) ODLTS Measurements

The hole traps obtained from the ODLTS measurements led to peaks in the vicinity of 100, 315, 335 and 350K. The ODLTS spectra and the corresponding Arrhenius plots are shown in figures 7.4.10 and 7.4.11 respectively. The ionisation energies and capture cross-sections calculated from these figures are given in table 7.4.2.

7.5 DISCUSSION

The experimental data obtained from the various space-charge techniques applied to the Cu-doped devices generally showed good agreement. The results are summarised in a diagram (Figure 7.5.1) similar to that used in the previous section. As can be seen from this diagram the (0.94 - 1.0)eV acceptor level was the only one which could be conclusively related to the copper impurity centre. This conclusion is supported by the photoconductivity measurements made on Cu-doped samples (see chap. 5.8), and it is also in reasonably good agreement with the 1.05eV (VB) level for copper suggested by Robinson and Bube[18]. The other levels, with the exception of that 0.2eV above the valence band were unambiguously present in unintentionally doped material and are therefore very likely to have been associated with native defects[23,24]. The ~0.2eV (VB) level appeared to be more complicated and will be discussed later.

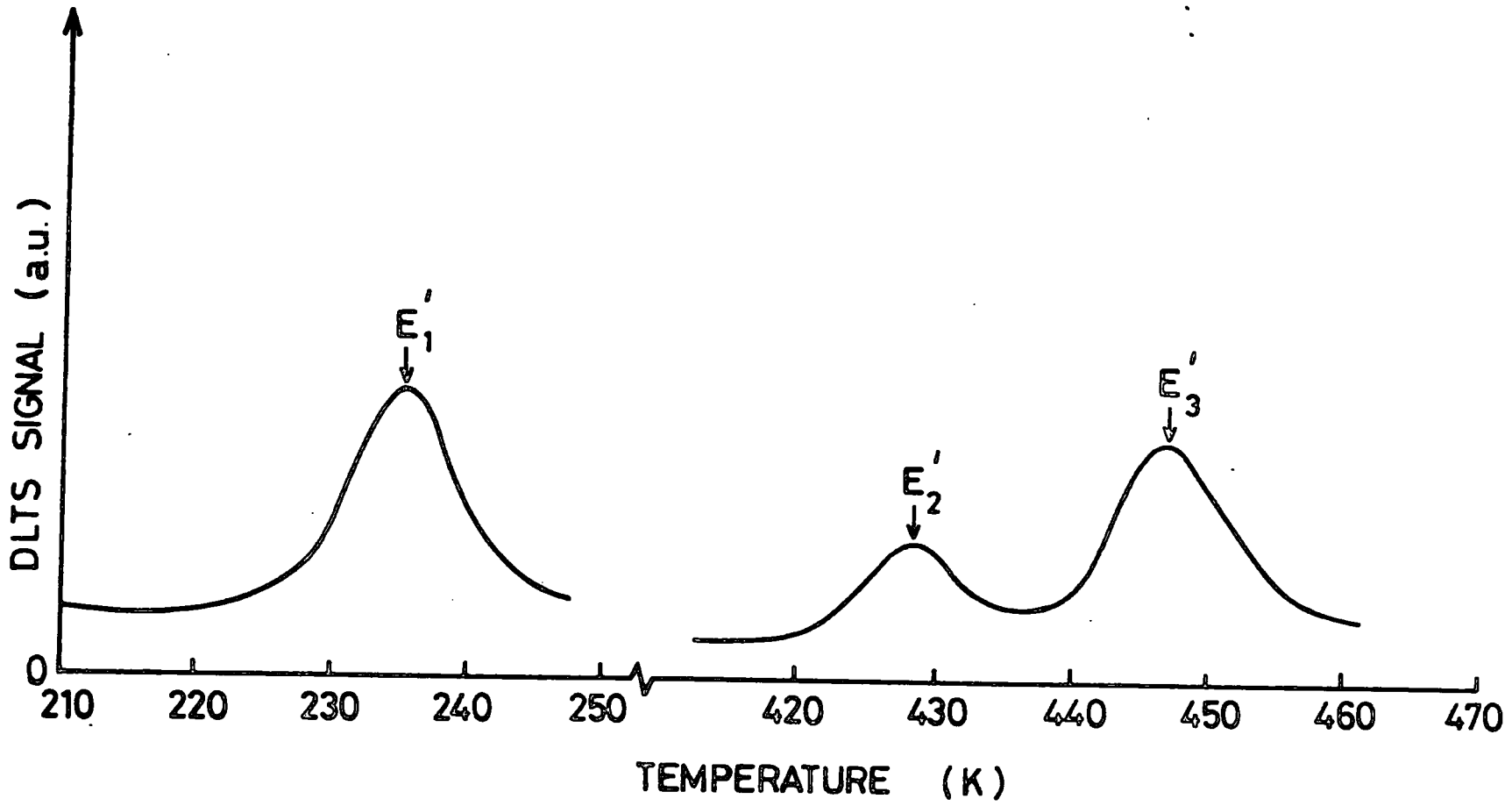

FIGURE 7.4.8 DLTS spectra for Cu-doped devices

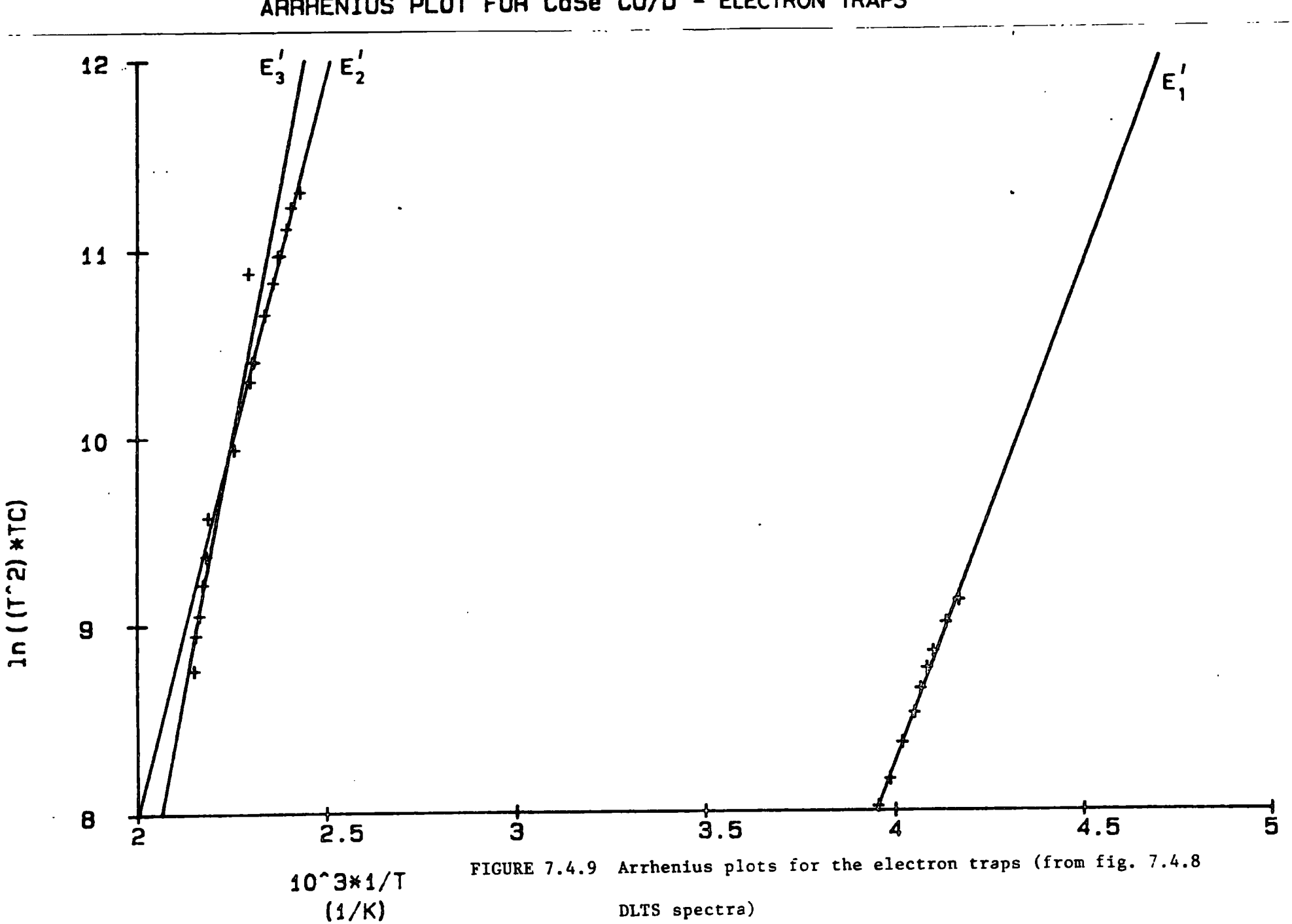

FIGURE 7.4.9 Arrhenius plots for the electron traps (from fig. 7.4.8 DLTS spectra)

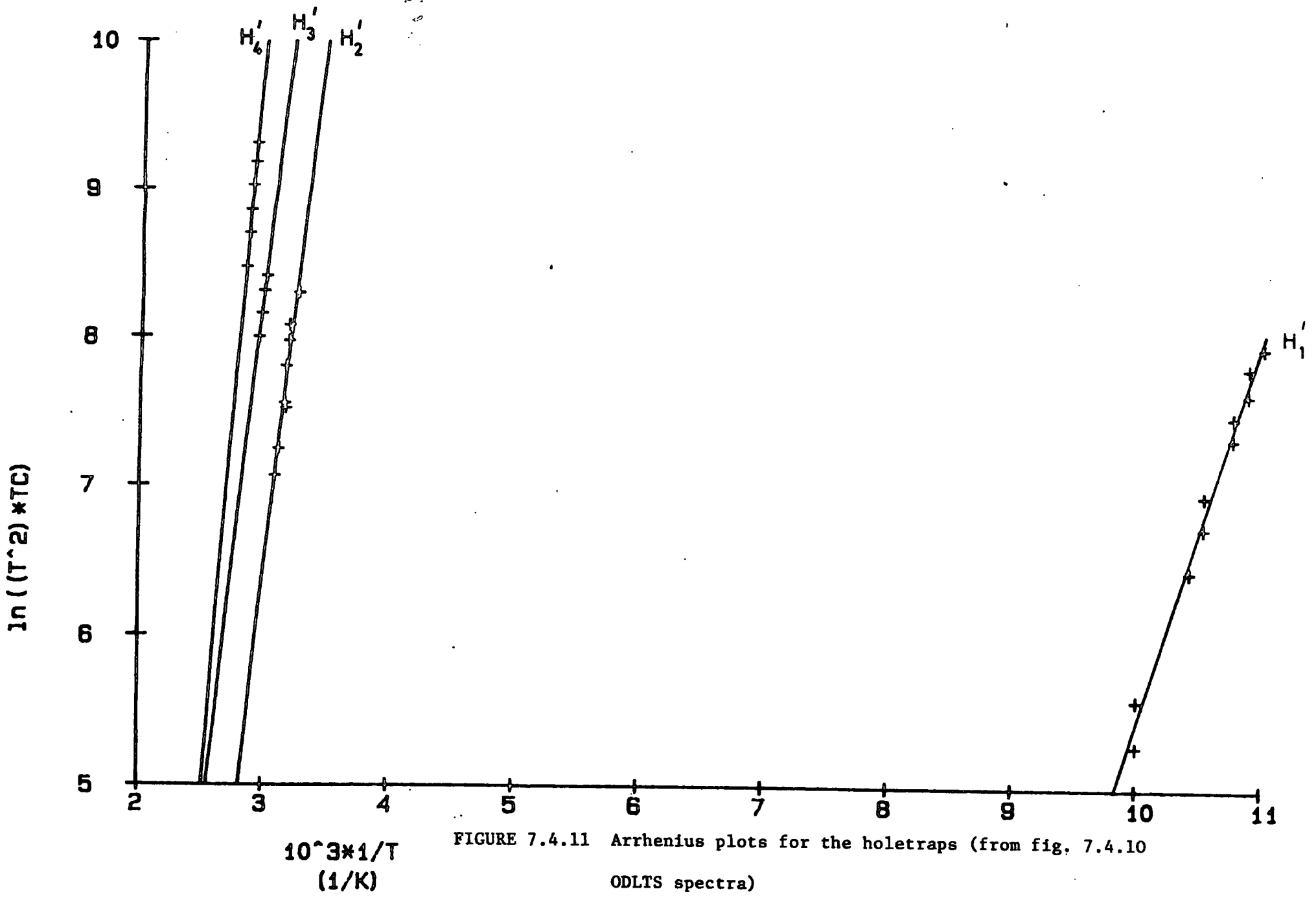

FIGURE 7.4.11 Arrhenius plots for the holetraps (from fig. 7.4.10 ODLTS spectra)

Hole Trap	Activation Energy (VB) ΔE(eV)	Apparent Cross-section at infinite temperature $\sigma_p(\infty)$ cm^2
H_1'	0.22	5.5×10^{-13} cm^2
H_2'	0.67	1.4×10^{-14} cm^2
H_3'	0.78	8×10^{-14} cm^2
H_4'	0.94	4.3×10^{-12} cm^2

TABLE 7.4.2 (ODLTS data)
Activation energy and apparent capture cross-section at infinite temperature of hole traps in Cu-doped CdSe

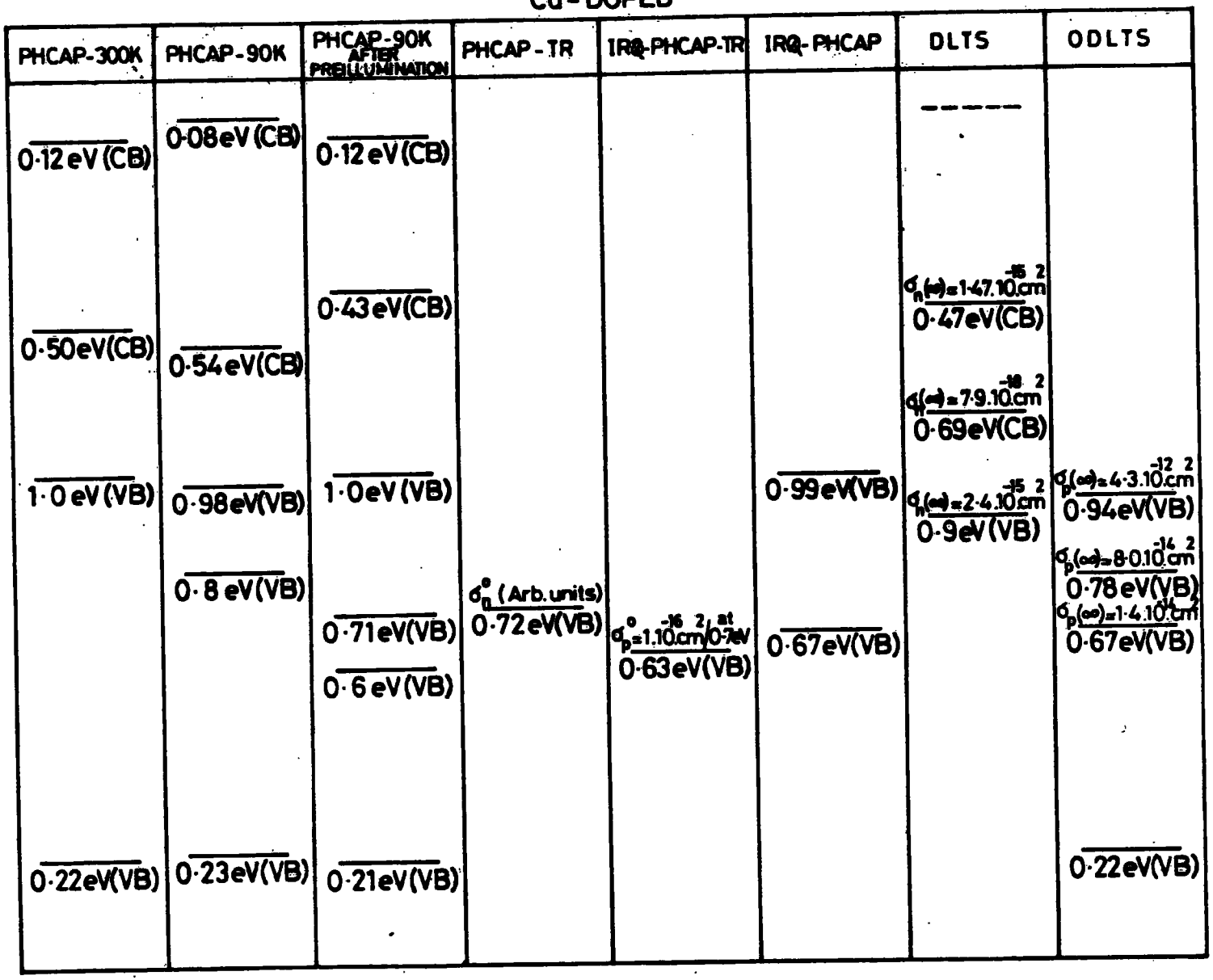

FIGURE 7.5.1 Summary of the inferred energy levels for Cu-doped devices

The electron trap 0.69eV from the conduction band, observed in the DLTS measurements was detected only in intentionally Cu-doped CdSe crystals. A level 0.69eV below the conduction band at about 420K is about 0.97eV above the valence band. If this level is assumed to be pinned to the valence band then it almost exactly coincides with the 0.94eV (VB) level observed in ODLTS measurements. If this were the case, the capture cross-section ratio (σ_p/σ_n) for the level would be $\sim 10^5$. Thus, this Cu-related centre was evidently behaving as a sensitising centre. This result is particularly interesting as it demonstrates the power of space-charge techniques in characterising and understanding the role of defects or impurity centres in semiconductors. That copper should be related to a sensitising centre in CdSe is not greatly surprising as its role in the promotion of sensitizing centres in other II-VI compounds is well known[25] and documented. Although Robinson and Bube[18] came to a contrary conclusion, they were not in fact able to measure the cross-section ratio, and their conclusion was based on observations in crystals dominated by the action of the 0.64eV sensitising centre. Of course the transient capacitance methods used here permit greater discrimination between levels, than do bulk or steady-state techniques.

A (0.20-0.23)eV hole trap found in the Cu-doped devices was also observed in Se-annealed crystals and has been attributed to a native defect. However, the relative response associated with the $\sim$ 0.2eV level was considerably larger in the Cu-doped samples. Moreover, the level was also found to be responsible for a small but continuous decrease during the low-temperature PHCAP measurements (apparently due to the thermal release of holes to the valence band). This decrease was reflected in the PHCAP-TR measurements as a continous temperature related drift in the dark capacitance following primary illumination,

irrespective of the wavelength of secondary illumination. This indicates that the drift was entirely related to thermal effects and suggests that the ~0.2eV level was not completely frozen out at liquid nitrogen temperature. Analysis of the ODLTS minimum at about 95K gave a value for the capture cross-section $\sigma_p(\infty)$ of 5.5 x 10^{-13} cm^2, with related time constants for the transient capacitance decay of less than 1 second. However, the dark capacitance drift observed in the PHCAP transient measurements (see fig. 7.4.4) had a time constant, at 90K, of 2000 seconds, suggesting the possibility of two quite distinct levels at about 0.2eV. Careful analysis of the ODLTS transients confirmed this statement. At about 120K the transient time constants were of the order of 200 m sec. corresponding to a cross-section of (10^{-17} - 10^{-18}) cm^2. This was close to the value obtained for level with similar energy in the Se-annealed crystal, although no dark capacitance drift was observed during PHCAP transient measurements at 90K with this material. This might have been due to a reduced concentration of these centres in the Se-annealed material. The picture that emerges, therefore is one in which two levels exist at similar energies of about 0.2 - 0.25eV in Cu-doped CdSe. One of these levels is characterised by a smaller cross-section of $\sim 10^{-17}$ cm^2, and is also present in Se-annealed CdSe, and is probably a native defect, possibly a singly ionised cadmium vacancy[17]. The other level, with the much larger cross-section of 10^{-13} cm^2, which was only observed in Cu-doped material, is most probably, therefore, copper related presumably, either as an excited state of Cu, by anology with CdS[26], or as some sort of complex. In this context it may be noted that a defect complex of the form $(Cu_i^{+} + V_{Cd}^{--})^{-}$ has been predicted by Varvas and Nirk[27] and Öpik Varvas[28].

The occurrence of a highly effective acceptor-like impurity centre (∿1.0 eV(VB)) in the upper half of the bandgap would cause some complications in the correct detection of other levels, especially acceptor-like ones in the lower half of the bandgap. The slightly higher value of 0.54eV (CB) as measured by normal PHCAP at 90K for the electron trap is likely to have been a consequence of the competing processes of filling and emptying of levels. In fact the value ∿0.43eV (CB) for this level obtained under the more controlled conditions in which pre-illumination with sub bandgap light was employed provided more consistent agreement with the DLTS measurements.

In the mid bandgap region there was also one electron 0.9eV (CB) and one hole-trap 0.78eV (VB) with almost the same magnitudes of capture cross-sections. It is tempting, therefore, to make a similar argument for these levels to that which was used from the copper sensitising centre. If the 0.9eV (CB) level is assumed to have been pinned to the conduction band, then the 0.78eV (VB) hole trap obtained from the ODLTS measurements at about 335K would coincide almost exactly with the 0.9eV electron-trap. This suggests that these two traps are probably the same level and because the capture cross-section ratio is close to unity it would have been expected to behave as a recombination centre, or so called Class I centre.

The level at about 0.64eV above the valence band is well established, and is usually attributed to a doubly ionised cadmium vacancy[15,17]. For this particular centre figure 7.5.1 demonstrates that while the results of ODLTS, IRQ-PHCAP and IRQ-PHCAP-TR measurements were in a very good agreement PHCAP measurements were less so. For example this level was undetected in PHCAP spectra at 300K. This may be attributed to the shadowing effect of the ∿1.0eV (VB)

level. On the other hand the 0.8eV (VB) acceptor-like level obtained from the ordinary 90K PHCAP spectrum (see fig. 7.4.1) could not be easily associated with the main sensitising centre. Instead it could be interpreted in two different ways; (a) it might have been shadowed by the ∿1.0eV (VB) level so that the observed threshold energy of 0.8eV did not reflect the true value or, (b) it might be related to the 0.78eV acceptor-like level which was observed in ODLTS measurements, and taken to be a recombination centre together with the 0.9eV (CB) level. The evidence from the pre-illuminated PHCAP measurements at 90K (see fig. 7.4.2) is in the favour of the second interpretation. Furthermore the 90K spectrum also revealed two closely spaced acceptor-like states which were also seen in the IRQ-PHCAP-TR and PHCAP-TR measurements. Although the level at ∿0.62 eV(VB) was clearly the main sensitising centre, the assignment of the other level(0.72eV) was less certain. It may have been related to the 0.78eV level seen in ODLTS, or it may have been a different centre altogether. However, the situation was reminiscent of that found with the material annealed in Se for 3 days where a similar spread in energy values was observed.

Studies of copper diffusion in CdS and CdSe have shown that copper can act both as an acceptor and as a donor depending on whether it occupies substitutional or interstitial sites in the lattice[26.28]. The acceptor dominant behaviour of Cu arises when the number of copper atoms on cadmium substitutional sites is larger than the number of atoms in interstitial positions. The factors which determine the diffusion of copper and hence the self compensation mechanisms due to the different charge states of the doubly ionised cadmium vacancy and the singly ionised copper are not well understood. However, it is likely that the process would involve either defect complexes and/or thermal regeneration of cadmium vacancies. This would be entirely consistent with the results presented and discussed here.

7.6 SCHOTTKY DEVICES ON MECHANICALLY POLISHED SURFACES

7.6.1 Introduction

The properties of the surface layer produced on CdSe crystals by mechanical polishing have been described in Chapter 5.7, where Schottky devices prepared on such layers have been discussed in Chapter 6.5. It was shown that mechanical polishing has an effect very similar to oxygen adsorption in introducing acceptor type surface states. The particularly striking resemblance between the RHEED patterns obtained from polished surfaces and aged samples which had originally been annealed in selenium vapour for 1-month, together with the strong similarities between the electrical characteristics of the Schottky devices on these two differently prepared surfaces provided further supportive evidence for the above statement.

The steady-state IRQ-PHCAP spectra were almost identical with those for the 1-month annealed material in which the principal level was the 0.64eV sensitising centre (see Sec 7.2.3). Therefore only steady-state PHCAP measurements which showed some dissimilarities will be presented in this section.

7.6.2 Steady-State PHCAP Measurements

The spectral dependence of PHCAP for a typical Schottky device made on a mechanically polished surface of a CdSe crystal is shown in figure 7.6.1. In the 300K spectrum the threshold values occurred at 1.16, 1.36, 1.46 and1.61eV implying that there were three acceptor-like levels some 0.6, 0.38, 0.28eV above the valence band, and a donor level at about 0.13eV below the conduction band.

All the energy levels observed in the 300K spectrum were also observed in the 90K spectrum except for that at 0.28eV (VB). This level was evidently shadowed by the 0.36eV (VB) centre in the low temperature measurements. The (0.36 - 0.38)eV acceptor-like centre

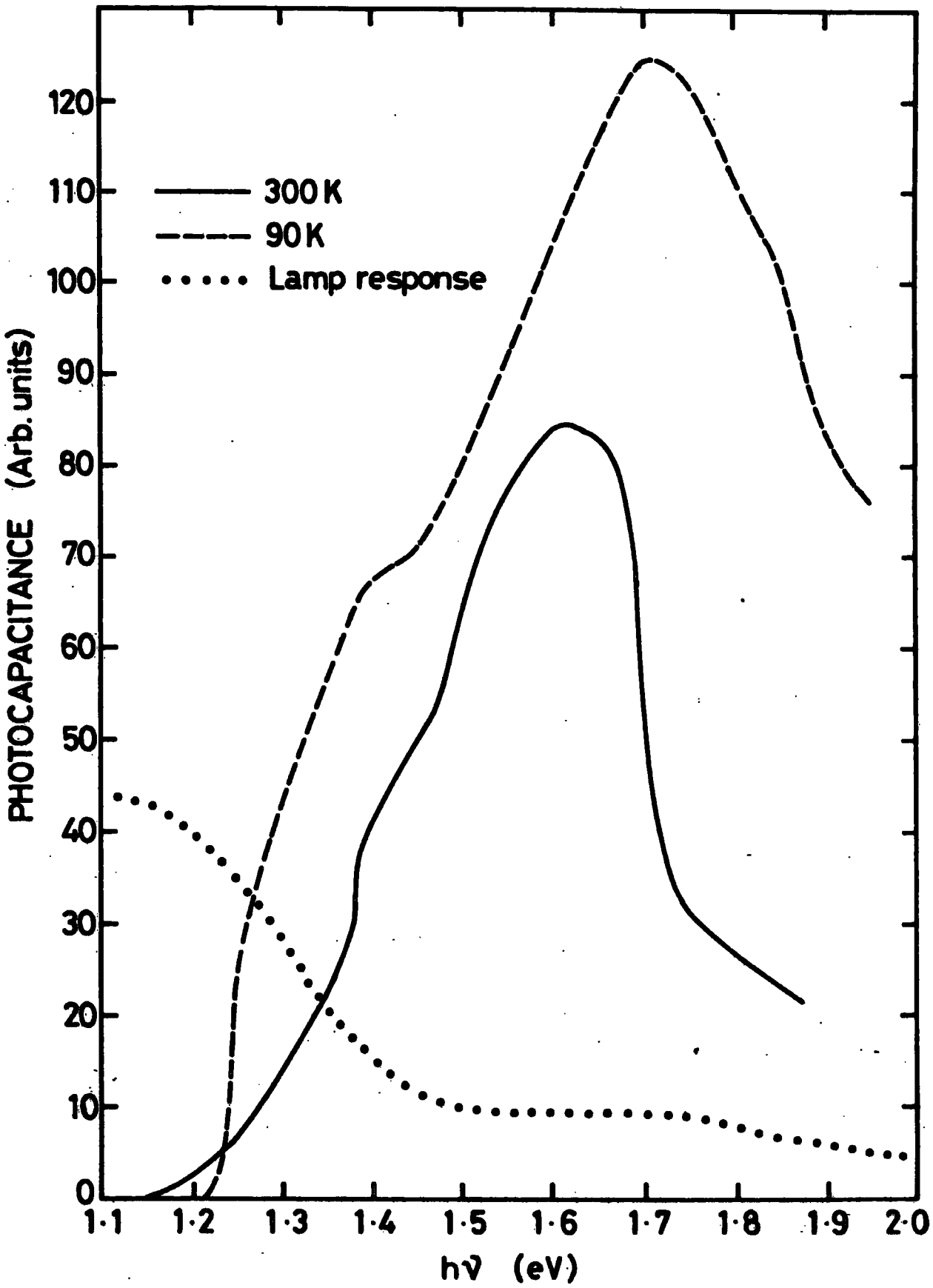

FIGURE 7.6.1 Steady state PHCAP measurement at 90 and 300K for a typical Schottky device made on a mechanically polished CdSe surface

observed in PHCAP was only detected with the mechanically polished (sphalerite phase) CdSe samples which suggests that this centre may be related to oxygen because of the very strong similarities between the oxygen adsorbed and mechanically polished samples. This level was also observed in photoconductivity measurements on mechanically polished samples.

7.7 DISCUSSION

The suggested relation between the (0.36-0.38)eV acceptor level and oxygen is mainly based on the very strong similarity between the oxygen adsorbed and mechanically polished layers. Brillson[29] has reported a level at about exactly this energy in oxygen adsorbed surfaces. Nevertheless, the relationship between mechanical polishing and or adsorption is not fully understood. It would have certainly been very interesting to investigate this relationship by other methods such as Auger spectroscopy, X-ray photoelectric spectroscopy etc. but this was beyond the scope of the present study. Although there is a lack of information in this particular connection, two possible explanations may be offered.

(a) Mechanical polishing may introduce some new defect centres, coincidently, very similar to those introduced by oxygen. However, electro-chemical photocapacitance spectroscopy (EPS) studies by Haak et al[11] on CdSe single crystals in aqueous solutions have shown that the polishing did not introduce any new states but instead enhanced the existing energy levels in the bandgap.

(b) Mechanical polishing may enhance oxygen adsorption via surface defects. Kröger et al[30] have pointed out that O_2 adsorption would be facilitated by the presence of selenium vacancies. The balance of evidence seems to favour the latter interpretation. The

conclusion that polishing enhances O_2 adsorption and that the ∿0.36eV level is O_2 related, was also drawn by Haak and Tench[31] recently. It is interesting to note that they obtained a nearly identical distribution of energy levels.

7.8 SUMMARY AND CONCLUSIONS

It has been shown that the application of the various space-charge techniques clearly provided a better picture of the distribution of defect and impurity levels in CdSe crystals. It has also been concluded that the appearance of the photoconductivity sensitising centre 0.64eV above the valence band was attributable as much to the low temperature used in the Se-annealing process as to the introduction of the excess selenium itself. The large value of hole capture cross-section for this centre is further evidence for describing it as a sensitising centre.

Copper impurity was found to introduce an acceptor level 1.0eV above the valence band. The capture cross-section for both holes and electrons was measured and the ratio(10^5) provided strong evidence that this level was also behaving as a sensitising centre. There appeared to be a second copper related centre ∿0.2eV above the valence band, although the presence of a native defect at the same energy position complicated the situation. However, the large disparity in the measured hole capture cross-sections did imply the existence of two distinct levels. The native defect was probably a singly ionised cadmium vacancy with a small cross-section (10^{-17} cm^2), whereas the larger cross-section was possibly associated with a copper-defect complex or with an excited state of copper.

REFERENCES

1. Y. Marfaing, J. Lascaray and R. Triboulet, Inst. Phys. Conf. Ser. 22 (1974) 201.
2. P. F.Lindquist and R. H. Bube, J. Appl. Phys. 43 (1972) 2839.
3. T. Suda and S. Kurita, J. Appl. Phys. 50 (1979) 483.
4. T. Suda, K. Matsuzaki and S. Kurita, J. Appl. Phys. 50 (1979) 3638.
5. H. G. Grimmeiss, N. Kullendorf and R. Broser, J. Appl. Phys. 52 (1981) 3405.
6. H. G. Grimmeiss, C. Ovren and J. W. Allen, J. Appl. Phys. 47 (1976) 1103.
7. T. Suda and R. H. Bube, J. Appl. Phys. 52 (1981) 6218.
8. H. R. Szawelska and J. W. Allen, J. Phys. C. 10 (1977) 2115.
9. H. G. Grimmeiss, C. Ovren, W. Ludwig, and R. Mach, J. Appl. Phys. 48 (1977) 5122.
10. I. E. Türe, F. Poulin, A. W. Brinkman, and J. Woods, Phys. Stat. Sol (a) 77 (1983) 535.
11. R. Haak, C. Ogden, and D. Tench, J. Electrochem. Sco. 129 (1982) 891.
12. G. Lucovsky, Solid State Commun. 3 (1965) 299.
13. R. G. Wheeler and J. O. Dimmock, Phys. Rev. 125 (1962) 1805.
14. H. G. Grimmeiss, Ann. Rev. Mat. Sci. 7 (1977) 341.
15. R. H. Bube, J. Appl. Phys. 35 (1964) 586.
16. R. H. Bube and L. A. Barton, J. Chem. Phys. 29 (1958) 128.
17. C. Manfredotti, R. Murri, E. Pepe, and D. Semisa, Phys. Stat. Sol (a) 20 (1973) 477.
18. A. L. Robinson and R. H. Bube, J. Appl. Phys. 42 (1971) 5280.
19. H. Kukimoto, C. H. Henry and F. R. Meritt, Phys. Rev. B 7 (1973) 2486.
20. R. H. Bube, J. Appl. Phys. 32 (1961) 1707.

21. G. L. Belenkii, A. V. Lyubchenko and M. K. Sheinkman, Soviet Phys. Semicond. 2 (1968) 445.

22. R. H. Bube, J. Chem. Phys. 30 (1959) 266.

23. L. Kindleysides and J. Woods, J. Phys. D3 (1970) 451.

24. C. Manfredotti, A. Rizzo, L. Vasanelli, S. Galassini, and L. Ruggiero, J. Appl. Phys. 44 (1973) 5463.

25. B. Ray, II-VI Compounds, Pergamon Press Ltd. 1969.

26. H. G. Grimmeiss, and N. Kullendorf, J. Appl. Phys. 52 (1981) 3405.

27. J. Varvas and T. Nirk, Phys. Stat. Sol (a) 33 (1976) 75.

28. A. I. Opik and J. A. Varvas, Phys. Stat. Sol (a) 74 (1982) 467.

29. G. A. Sullivan, Phys. Rev. 184 (1969) 796.

30. L. J. Brillson, Surface Sci. 69 (1977)62.

31. F. A. Kröger, H. J. Vink and I. Van der Boomgard, Z. Physik. Chem. 203 (1954) 1.

32. R. Haak and D. Tench. J. Electrochem. Soc. 131 (1984) 275.

CHAPTER 8

CONCLUSIONS

8.1 SUMMARY OF RESULTS

8.1.1 Material Preparation

In an attempt to characterise the native defect and impurity centres in CdSe the main emphasis in this work has been placed on space-charge capacitance techniques which yield more quantitative information, and which had not previously been extensively applied to CdSe. This required the use of Schottky barriers as the junction devices for the application of these techniques. The devices therefore had first to be fabricated and then investigated in order to establish their electrical characteristics. Although high resistivity photoconductive CdSe samples could easily be obtained from the very low resistive as-grown material, using different annealing and impurity doping processes, the optimum resistivity required for Schottky diode fabrication proved difficult to achieve. However, it appeared that annealing CdSe crystals in a very low vapour pressure of selenium (6.10^{-3} Atm) at 550°C for long periods of time (several weeks) was one of the possible ways of achieving the appropriate resistivity for devices. Another satisfactory solution involved the incorporation of Cu-impurity by evaporating a very small amount of metallic copper onto the surface of the material then heating at 650°C for few hours to diffuse it in uniformly.

8.1.2 Schottky Barriers

The electrical characteristics of Schottky barriers prepared using either of these optimum resistivity substrate materials changed

dramatically during ageing in air. This was attributed to a change in the role of the ever present oxygen layer following its transition from being initially physically adsorbed to chemically adsorbed with time. Using measurements of I-V and C-V characteristics both before and after ageing, and utilising the theoretical work of Cowley[1], Fonash[2], Crowell and Sze[3], and Card and Rhoderick[4], it has been shown that the Schottky barrier height is determined by a combination of the thickness of the interfacial layer, the occupancy of surface states and the metal work function. The barrier height in CdSe Schottky diodes has frequently been reported to be independent of the metal work function (Mead[5] and Consigny et al)[6]. They suggested that the minimum required number of surface states to explain such an observation should be $> 10^{13}$ cm^{-3} eV^{-1}. This density of surface states had not been obtained in the studies of Consigny et al[6] and Brillson[7] to provide evidence for the metal work function independent Schottky barrier height. This difficulty is resolved by the model proposed in the present work where an increase in band bending occurs with the diffusion of increasing amounts of oxygen introducing acceptor like surface states. It has been clearly demonstrated that the calculated number of (2-6) 10^{12} cm^{-2} eV^{-1} surface states is entirely adequate to explain the situation we have found in which the barrier height is not completely independent of the metal work function.

As Somorjai[8] and other workers[9] have shown the non-stoichiometric behaviour of CdSe crystal becomes even more pronounced at the surface. Hence more oxygen may be adsorbed when the surface concentration of Se-vacancies is high. In fact the RHEED investigation of the surface structure showed conclusively that there was a phase transformation from hexagonal to a polycrystalline

sphalerite cubic layer at the surface as a consequence of the oxygen adsorption. Control experiments in different ambients such as dry or wet nitrogen, carbon dioxide or argon indicated that a cubic layer could only be produced in an ambient containing oxygen. When the extremely sensitive nature of the CdSe surface is considered this behaviour does not seem unusual. Mark and Creighton[10] have reported that changes in several surface parameters of representative semiconductors exposed to oxygen scale logarithmically with the Pauling electronegativity difference of the semiconductor constituents. Application of this scaling curve to the Pauling electronegativity difference for CdSe and for CdS for example, revealed that the bonding of oxygen on CdSe is more than 5 times as strong as it is on CdS. On the other hand extensive studies on thin films of CdSe, have shown that the hexagonal phase is favoured when the metallic component is in excess and the cubic phase when the non-metallic component is in excess. An investigation of the transformation mechanism is beyond the scope of the present work but by drawing an analogy between Se-interstitials and oxygen (both of which introduce acceptor-like levels), it is not unreasonable that an excess of oxygen should give rise to the cubic phase.

It has also been shown that mechanical polishing of the CdSe crystal with alumina powder with a particle size less than 3 μm promotes an identical phase transformation. Such polished layers had much higher resistivities than the underlying hexagonal base material, and they give rise to photoconductive effects. The parallel behaviour between the mechanical polished and oxygen adsorbed surfaces was striking, as indicated by:

(1) identical RHEED patterns from both aged (oxygen adsorbed) and mechanically polished surfaces.

(ii) almost identical electrical characteristics for devices made on either mechanically polished surfaces or etched surfaces measured after ageing.

(iii) very strong resemblance in PHCAP spectra of Schottky diodes on the two substrates.

Similar studies by Haak and Tench[11] have led to the conclusion that the polishing does not introduce new levels, but enhances existing ones. Furthermore, according to Kroger et al[12], oxygen adsorption would be facilitated by the presence of surface defects such as Se-vacancies and hence the mechanical polishing would promote adsorption via the resulting increase in surface defects.

The application of space-charge capacitance techniques to Schottky diodes prepared on mechanically polished surfaces of CdSe, and the photoconductivity measurements on the same surfaces indicated an acceptor level (0.36–0.38)eV above the valence band. In view of the similar effects of oxygen adsorption and mechanical polishing, it is suggested that this level is related to oxygen. This suggestion is strongly supported by the extensive studies of Brillson[7] on CdSe surfaces exposed to air, and the more recent study of Haak and Tench[13] on mechanically polished surfaces of CdSe. These have demonstrated the existence of the same energy level (in excellent agreement with the present study) and it is notable that they reached the same conclusion that this level is related to oxygen.

8.1.3 Deep Levels

The studies of deep levels both by photoconductivity (the bulk method) and with space-charge techniques on almost all the crystals available have shown conclusively that a level of (0.61–0.65)eV above the valence band is the major acceptor level in CdSe. The large hole

capture cross-section of $\sim 1.10^{-14}$ cm^2 for this level and the measurements of the IRQ-photoconductivity, provide strong evidence that this level acts as a photoconductivity sensitising centre. This conclusion is in very good agreement with the work of Robinson and Bube[14], and Manfredotti et al[15]. Using the reported capture cross-section ratio of $\sim 10^7$ for a similar level, the electron capture cross-section would be of the order of $\sim 10^{-21}$ cm^2. Such a small cross-section would be consistent with Bube's suggestion that the centre is a doubly ionised cadmium vacancy.

Another acceptor level with an ionisation energy of 0.20-0.22eV was also invariably present which suggests that this is also a native defect. The smaller hole cross-section of $\sim 5.10^{-17}$ cm^2 for this centre implied that it is probably a singly ionised Cd vacancy as suggested by Bube[16], Manfredotti et al[15], and Balenkii et al[17].

A relatively shallow electron trap (0.11-0.16)eV level below the conduction band with an electron capture cross-section of $\sim 2.10^{-18}$ cm^2 was also found to be intrinsic to CdSe and can probably be attributed to singly ionised Se-vacancy donors. This would be also in good agreement with the suggestions of Bube and Barton[18] and Kindleysides and Woods[19]. Apart from these important and well established levels, evidence was also found in other less well defined levels, and these have been discussed in the relevant parts of this thesis.

More importantly, measurements on Cu-doped CdSe revealed that an acceptor level ~ 1.0eV above the valence band edge was associated with this impurity. The corresponding hole capture cross-section of 4.10^{-12} cm^2 and the relatively small electron capture cross-section (7.10^{-18} cm^2) clearly demonstrated that, with a capture cross-section ratio for 10^5, this particular impurity acts as a sensitising centre. Although

this conclusion is in good agreement with the role of copper impurity in most of the II-VI compounds, Robinson and Bube[14] were in fact unable to confirm that Cu acts as a sensitising centre in CdSe. Nevertheless, their estimate of 1.05eV for the activation energy of the centre is in excellent agreement with our measurements.

8.2 SUGGESTIONS FOR FUTURE WORK

Because CdSe is a less well researched member of the family of the II-VI compounds, many interesting projects which go well beyond the scope of this thesis could be proposed. Several possible areas for future work following on from the present work are:

(a) It would be interesting to introduce a fundamental change in the method of crystal growth in an attempt to produce more stoichiometric CdSe single crystals.

(b) Photoconductivity studies should be carried out using the constant photocurrent technique because of its easier interpretation and better resolution. Similarly, the same technique could be applied to infrared quenching measurements, by using an infrared source together with different filters particularly in the far infrared region.

(c) In view of the success of the DLTS and ODLTS measurements it would be interesting to extend the study of similar devices to investigation by the deep level optical spectrocopy (DLOS) technique. This would enable trap levels to be determined with a higher degree of accuracy.

(d) Since CdSe has been found to be a promising material in the fabrication of MIS and Cu_2Se/CdSe heterojunction type of solar cells, the device characterisation described in this thesis could be extended to these devices.

(e) Solar cells might be fabricated with thin films of this material to provide large area devices at lower cost.

REFERENCES - CHAPTER 8

1. A. M. Cowley, J. Appl. Phys. 37 (1966) 3024.
2. S. J. Fonash, J. Appl. Phys. 54 (1983) 1966.
3. C. R. Crowell and S. M. Sze, Solid-St. Elec. 9 (1966) 1035.
4. H. C. Card and E. H. Rhoderick, J. Phys. D.4 (1971) 1589.
5. C. A. Mead, Appl. Phys. Lett. 6 (1965) 103.
6. R. L. Consigny III and J. R. Madigan, Solid-St.Elec. 13 (1970) 113.
7. L. J. Brillson, Surface Sci. 69 (1977) 62.
8. G. A. Somorjai, J. Phys. Chem. Solids, 24 (1963) 175.
9. M. F. Chung and H. E. Farnsworth, Surface Sci. 25 (1972) 321.
10. P. Mark and W. F. Creighton, Appl. Phys. Lett. 27 (1975) 400.
11. R. Haak, C. Ogden and D. Tench, Proc. Electrochem. Soc. Sym. Oct. 1981. Denver, Co.
12. F. A. Kröger, H. J. Vink and J. Vanden Boomgard, Z. Phys. Chem. 203 (1954) 1.
13. R. Haak and D. Tench, J. Electrochem. Soc. 131 (1984) 275.
14. A. L. Robinson and R. H. Bube, J. Appl. Phys. 42(1971) 5280.
15. C. Manfredotti, R. Murri, E. Pepe and D. Semisa, Phys. Stat. Sol. (a) 20 (1973) 477.
16. R. H. Bube, J. Phys. Chem. 30 (1959) 266.
17. G. L. Belenkii, A. V. Lyubchenko, and M. K. Sheinkman, Sovie Phys. Semicond. 2 (1968) 445.
18. R. H. Bube and L. A. Barton, J. Chem. Phys. 29 (1958) 128.
19. L. Kindleysides and J. Woods, J. Phys. D.3 (1970) 451.